

University of Central Florida

STARS

Electronic Theses and Dissertations, 2020-

2023

Developing Cost-Effective Specialty Adsorbents to Meet the Emerging Challenges of Pollutant Removal in Surface Water Systems

Diana Ordonez
University of Central Florida



Part of the [Environmental Engineering Commons](#), and the [Water Resource Management Commons](#)

Find similar works at: <https://stars.library.ucf.edu/etd2020>

University of Central Florida Libraries <http://library.ucf.edu>

This Doctoral Dissertation (Open Access) is brought to you for free and open access by STARS. It has been accepted for inclusion in Electronic Theses and Dissertations, 2020- by an authorized administrator of STARS. For more information, please contact STARS@ucf.edu.

STARS Citation

Ordonez, Diana, "Developing Cost-Effective Specialty Adsorbents to Meet the Emerging Challenges of Pollutant Removal in Surface Water Systems" (2023). *Electronic Theses and Dissertations, 2020-*. 1628. <https://stars.library.ucf.edu/etd2020/1628>

DEVELOPING COST-EFFECTIVE SPECIALTY ADSORBENTS TO MEET
EMERGING CHALLENGES OF POLLUTANT REMOVAL IN SURFACE
WATER SYSTEMS

by

DIANA L ORDONEZ

M.S. Environmental Engineering, University of Central Florida, 2019

A dissertation submitted in partial fulfillment of the requirements
for the degree of Doctor of Philosophy
in the Department of Civil, Environmental, and Construction Engineering
in the College of Engineering and Computer Science
at the University of Central Florida
Orlando, Florida

Spring Term
2023

Major Professor: Ni-Bin Chang

© 2023 Diana Ordonez

ABSTRACT

The production of clean water is emphasized under the United Nations goals for sustainable development (SDGs), enlightening the acute need of developing new sustainable technologies in all disciplines. SDGs have urged all engineers in the 21st century to mitigate pollution of drinking water sources and prevent all receiving waterbodies from the impact of agriculture discharge, wastewater effluent, and stormwater runoff. Current water matrix constituents of concern include traditional pollutants (i.e., total nitrogen and total phosphate), natural organic matters (i.e., total organic carbon (TOC), tannic acid), heavy metals (i.e., copper, calcium), and harmful algae toxins (i.e., microcystin), as well as contaminants of emerging concern (i.e., Per- and polyfluoroalkyl substances (PFAS), pharmaceuticals, endocrine disrupting chemicals, personal care products). This study presents the most recent development of a suite of *in situ* cost-effective, scalable, and fit-for-purpose specialty adsorbents to simultaneously remove PFAS, TOC, total nitrogen, total phosphate, and microcystin through synergistic effect of different specialty ingredients. It is also aimed to clarify physiochemical removal mechanisms for the removal of color (tannic acid), nutrients (phosphate and nitrate), contaminants of emerging concern (PFAS) and algal toxins (Microcystin LR). The originality of these specialty adsorbents with chemical, molecular, and even microbial insights falls within the sustainable nature of specialty ingredients and wide availability tailored for scalable applications in any landscape.

To my family and friends for all their support

ACKNOWLEDGMENTS

I would like to express my deepest appreciation to my advisor and mentor Dr. Ni-bin Chang for all his support, help and feedback during this journey. His dedication and genuine interest in helping his students has been crucial to the success of this work. I am especially thankful for sharing his knowledge, experience, meticulous scrutiny, and amiability. I'd also like to extend my gratitude to my committee members Dr. Andrew Randall, Dr. A H M Anwar Samdani, Dr, Jiannan Chen and Dr. Jonathan Caranto for their valuable advice and constructive comments. I am grateful to my friend and colleague Dr. Andrea Valencia for all her help and collaboration. I would be remiss not to mention the personnel at the College of Engineering and Computer Science for all their assistance.

Finally, special thanks to my parents Patricio and Martha Ordonez for their unmeasurable love and support during this process. To my husband and stepson Alvaro and Stefan Mongrutt for their profound belief in my abilities. To my siblings Byron and Julie Ordonez and Paul and Gabriela Yanza and to my nephew and niece Axel and Natalia Yanza for being by my side, their emotional support greatly impacted this journey.

TABLE OF CONTENTS

LIST OF FIGURES	xii
LIST OF TABLES	xvi
LIST OF ACRONYMS (or) ABBREVIATIONS	xix
CHAPTER 1: INTRODUCTION	1
1.1. Background	1
1.1.1. Color contamination.....	1
1.1.2. Algal Toxin	2
1.1.3. Nutrient Pollution.....	3
1.1.4. Per-and polyfluoroalkyl substances (PFAS).....	4
1.1.5. Health Concerns and Regulations	5
1.1.6. Meta-analysis of publications for color, microcystin, phosphate, and PFAS and water treatment.	8
1.2. Study Objectives	11
CHAPTER 2: COLOR REMOVAL FOR LARGE-SCALE INTERBASIN WATER TRANSFER: EXPERIMENTAL COMPARISON OF FIVE SORPTION MEDIA	14
2.1. Introduction.....	14
2.2. Material and Methods	17
2.2.1. Study region	17

2.2.2. Composition and characterization of sorption media	19
2.2.3. Experimental set-up for the column study	22
2.2.4. Water parameter analysis	22
2.2.5. Dynamic adsorption models	23
2.2.6. Life expectancy	24
2.3. Results and Discussion	26
2.3.1. Material Characterization.....	26
2.3.2. Color Removal Efficiency	31
2.3.3. Removal Mechanism	36
2.3.4. Dynamic Adsorption Modeling	38
2.3.5. Comparison of ZIPGEM with other adsorbents	40
2.3.6. Application potential.....	40
2.3.7. Risk assessment	43
2.4. Chapter Conclusion.....	44
 CHAPTER 3: EXPLORING SIMULTANEOUS REMOVAL OF MICROCYSTIN AND PHOSPHORUS VIA SPECIALTY ABSORBENTS FOR EUTROPHIC WATER TREATMENT	 46
3.1. Introduction.....	46
3.2. Material and Methods	50

3.2.1. Media characterization.....	50
3.2.2. Chemicals.....	51
3.2.3. Isotherm study.....	52
3.2.4. Equilibrium isotherm	55
3.2.5. Statistical analysis.....	56
3.2.6. Columns study	57
3.2.7. Media characteristics	59
3.3. Results and Discussion	60
3.3.1. Isotherm results.....	63
3.3.2. Removal mechanism.....	69
3.3.3. Competing effect between phosphate and MC-LR removal.....	72
3.3.4. Dynamic removal efficiency with canal water	73
3.4. Chapter Conclusion.....	77
CHAPTER 4: SENSITIVITY ANALYSIS OF PHOSPHATE ADSORPTION UNDER VARYING WATER MATRIX CONSTITUENTS AND SPECIALTY INGREDIENTS.....	79
4.1. Introduction.....	79
4.2. Methodology	82
4.2.1. Media characterization.....	82
4.2.2. Isotherm experiments.....	84

5.2.5. Statistical Analysis.....	113
5.3. Results and Discussion	114
5.3.1. Background PFOS and PFOA concentrations and water quality parameters.....	114
5.3.2. Media characterization.....	116
5.3.3. PFOS and PFOA removals by the filtration media.....	122
5.3.4. Removal mechanisms of PFOS and PFOA using filtration media.....	123
5.3.5. PFOA breakthrough.....	126
5.3.6. PFOA dynamic adsorption analysis.....	128
5.3.7. Statistical analysis.....	129
5.3.8. Influence of water matrix on PFOS and PFOA adsorption by the media.....	130
5.3.9. Recycle and disposal of filtration media.....	131
5.4. Chapter Conclusion.....	131
CHAPTER 6: COMPARING FATE AND TRANSFORMATION OF LONG AND SHORT CHAIN PER- AND POLYFLUOROALKYL SUBSTANCES (PFAS) VIA TWO SPECIALTY ADSORBENTS	133
6.1. Introduction.....	133
6.2. Material and Methods	138
6.2.1. Preparation and characterization of specialty adsorbents	138
6.2.2. Isotherm Kinetic Study	139

6.2.3. Fixed-Bed Column Study and Dynamic Models	141
6.2.4. Water Characterization	143
6.3. Results and Discussion	144
6.3.1. Specialty adsorbents and water characteristics	144
6.3.2. Performance of PFOS and PFOA Removal.....	147
6.3.3. Real-World Applications and Limitations	158
6.4. Chapter Conclusion.....	161
CHAPTER 7: CONCLUSION	163
APPENDIX A: COMPLEMENTARY INFORMATION ON CHAPTER 4.....	169
APPENDIX B: COMPLEMENTARY INFORMATION ON CHAPTER 5	173
APPENDIX C: COMPLEMENTARY INFORMATION ON CHAPTER 6.....	176
REFERENCES	179

LIST OF FIGURES

Figure 1. Visualization co-occurrence map for the literature search on (a) color and water treatment, (b) microcystin and water treatment, (c) Microcystin and water treatment and (d) Phosphate and water treatment [Produced on VOS viewer]. Size of the circles are related with the co-occurrence of the keyword.....	11
Figure 2. Sample collection site a) image of the location of Black Creek Tributary, b) sample collection site, c) image of raw water and d) chemical structure of tannic acid.....	18
Figure 3. Gradation curves of sorption media (*x-axis is in logarithmic scale).....	28
Figure 4. Photography and SEM images of sorption media (a) CTS, (b) IFGEM-1, (c) IFGEM-4, (d) CPS and (e) ZIPGEM.....	30
Figure 5. Photography and SEM images of composition of media materials where (a) is sand, (b) is clay, (c) is perlite and (d) is ZVI.	31
Figure 6. The dynamic color removal efficiency curves and breakthrough curves for (a) and (b) of CTS, (c) and (d) of IFGEM-1, (e) and (f) of IFGEM-4, (g) and (h) of CPS, and (i) and (j) of ZIPGEM, respectively	35
Figure 7. Graphical summary of the removal mechanisms in ZIPGEM	38
Figure 8. Life expectancy curves for volume of water expected to be treated by various masses of ZIPGEM for $C_0=175 \pm 10$ units Pt-Co	42
Figure 9. Rhodamine tracer study for ZIPGEM based on 1-ft long 3” diameter column (1,200 ml of media) with influent flow rate of $4 \text{ ml}\cdot\text{min}^{-1}$	42
Figure 10. (a) MC-LR chemical structure [modified from Cayman Chemical, accessed: 2/2/2023], and (b) 3-D structure of the MC-LR [modified from MolView.org, accessed: 2/2/2023].	52

Figure 11. Experimental setup of this study	60
Figure 12. Percentage removal obtained by CPS, ZIPGEM, and BIPGEM under different initial conditions (Control, Condition 1, Condition 2, Condition 3, Condition 4, and Condition 5) and cases where (a) is Case 1 (MC-LR), (b) is Case 2 (MC-LR and PO_4^{3-}), and (c) is Case 3 (MC-LR and Ca^{2+}).	66
Figure 13. Image of biochar at magnification of (a) 65X and (b) 1 KX. (Imagens were taken via Zeiss Ultra-55 SEM)	71
Figure 14. Dynamic MC-LR removal curves for (a) CPS, (b) ZIPGEM, and (c) BIPGEM from a fixed bed column study with real canal water spiked to $70 \mu\text{g}\cdot\text{L}^{-1}$ MC-LR as influent conditions.	74
Figure 15. Location of PZC for CPS, ZIPGEM and BIPGEM.....	84
Figure 16. Adsorption capacity of (a) CPS, (b) ZIPGEM and (c) BIPGEM for nitrate varies at different water matrices.	94
Figure 17. Simultaneous (a) NO_3^- and (b) PO_4^{3-} removal efficiency of CPS, ZIPGEM and BIPGEM using canal water spiked with phosphate to a concentration of 0, 0.7, 2, 3, 4, 5, 15, 30, 60, 120, and $240 \text{ mg}\cdot\text{L}^{-1}$ PO_4^{3-} while maintaining a constant NO_3^- concentration of $2 \text{ mg}\cdot\text{L}^{-1}$, denoted as influent 1, 2, 3, 4, 5, 6, 7, 8, 9, 10 and 11, respectively.	95
Figure 18. Dynamic PO_4^{3-} removal efficiency of ZIPGEM via a column study	99
Figure 19. Location of C-23 and water sample collection points for PFAS background study for determining removal using filtration media (Source: Google Earth – Canal 23, 2021).	108
Figure 20. Experimental set up of the fixed-bed column study (in triplicate).	111

Figure 21. Initial pH vs. Δ pH plots for determining the pH_{PZC} for (a) CTS and (b) IFGEM (Color lines represent triplicates).	117
Figure 22. XPS spectra of (a) C1s, (b) O1s, (c) Si2p and (d) Al2p for filtration media CTS [x-axis for all figures correspond to the binding energy (eV)]	120
Figure 23. XPS spectra of (a) C1s, (b) O1s, (c) Si2p, (d) Al2p (e) Fe2p for filtration media IFGEM [x-axis for all figures correspond to the binding energy (eV)].	121
Figure 24. Media performances based on samples collected from the columns in triplicate: (a) PFOS and PFOA percentage removals when using CTS and (b) when using IFGEM [Error bars represent standard deviations of the column runs in triplicate]	122
Figure 25. SEM images for (a) CTS raw media, (b) CTS exhausted media, (c) IFGEM raw media, and (d) IFGEM exhausted media (yellow circles highlight the “clustering” of media particles upon exhaustion).	126
Figure 26. PFOA breakthrough curve for (a) CTS and (b) IFGEM [Error bars represent standard deviations of the column runs in triplicate]	127
Figure 27. Thomas model linear regression for (a) CTS and (b) IFGEM.	129
Figure 28. Point of Zero Charge for ZIPGEM and CPS (Each error bar represents one standard deviation above or below the mean of triplicate analyses).	145
Figure 29. XRD spectra for raw and exhausted CPS (a) and ZIPGEM (b) collected from the top section of the column.	147
Figure 30. Long-chain and short-chain PFAS removal by (a) CPS and (b) ZIPGEM based on column study.	152

Figure 31. Breakthrough curve for PFOA and PFAS adsorption by (a) CPS and (b) ZIPGEM. (Red line signifies the equilibrium point where $C_t/C_0=1$) 153

Figure 32. Total concentrations of long and short-chain PFAS for (a) CPS and (b) ZIPGEM based on column study..... 157

LIST OF TABLES

Table 1. Human health effects caused by the exposure to different contaminants.....	7
Table 2. United State Environmental Protection Agency (US EPA) and the World Health Organization (WHO) regulations for current and emerging water pollutants.....	8
Table 3. Media matrix and composition	20
Table 4. Summarize description of dynamic adsorption models with the definitions of parameters	24
Table 5. Sorption media matrix in percent by volume and physical characteristics.....	27
Table 6. Chemical composition analysis of sorption media mixes from XRF analysis	29
Table 7. Summary of dynamic performance in column studies	35
Table 8. Parameters estimated from the linear regression of Thomas, MDR and Yoon Nelson dynamic modes for the sorption media CTS, IFGEM-1, IFGEM-4, CPS and ZIPGEM.	39
Table 9. Summary and confirmation of adsorption capacity in literature and in this study	40
Table 10. Effluent concentrations of dissolved iron and aluminum ions in the effluent given the influent concentration listed at the third row.	44
Table 11. Summary of the different influent conditions and cases examined in batch tests.	54
Table 12. Summary of green sorption media characteristics of CPS, ZIPGEM, and BIPGEM... ..	61
Table 13. XRF chemical elemental composition for sand, clay, perlite, ZVI, and biochar (elements found at tracer level have been excluded from the table).	62
Table 14. XRF chemical elemental composition for CPS, ZIPGEM, and BIPGEM (values in parentheses are for the standard deviation calculated from 3 samples; elements found at tracer level have been excluded from the table).	62

Table 15. Langmuir isotherm parameter retrieved from the regression plot of $Ceqe$ vs. Ce for the different influent conditions.....	68
Table 16. Freundlich isotherm parameter retrieved from the regression plot of $\ln(q_e)$ vs. $\ln(C_e)$ at 3 different influent conditions.....	68
Table 17. Summary of previous isotherm studies for MC-LR removal	69
Table 18. Results from the dynamic modeling of the MC-LR adsorption in a fixed bed column study.....	76
Table 19. Summary of previous column studies and the current one for MC-LR removal and adsorption capacity	76
Table 20. Media matrices in percent by volume and media characterization.....	84
Table 21. Chemical element composition of CPS, ZIPGEM and BIPGEM raw media obtained via the XRF (elements detected at tracer level were excluded).....	89
Table 22. Summary of Langmuir isotherm parameter values.....	96
Table 23. Freundlich isotherm parameters for media	96
Table 24. Comparative phosphate adsorption capacities of different adsorbents/media estimated via isotherm studies.....	97
Table 25. Comparative phosphate adsorption capacities of different functionalized adsorbents/media estimated via isotherm studies.	98
Table 26. Adsorption capacity of new sorption media in comparison to different adsorbents in the literature.	99
Table 27. Media matrix and characterization of filtration media.	116

Table 28. Elemental composition of raw filtration media CTS and IFGEM based on XRF analysis.	118
Table 29. Chemical oxide composition of raw filtration media CTS and IFGEM based on XRF analysis.....	118
Table 30. Correlation coefficient and model parameters in dynamic PFOA adsorption modeling analyses.	129
Table 31. Selected properties and background concentrations of selected PFAS in C-23 surface water.....	144
Table 32. Media characterization.....	145
Table 33. Summary of rate model results for green sorption media investigated for PFAS removal.	150
Table 34. PFAS removal efficiencies during the first 9 h column run time (unit: %).	155

LIST OF ACRONYMS (or) ABBREVIATIONS

AC	Activated Carbon
AMPAC	Advanced Materials Processing and Analysis Center
BIPGEM	Biochar, Zero-Valent Iron, Perlite Green Environmental Media
BMPs	Best Management Practice
CECs	Compounds of Emerging Concern
CPS	Clay, Perlite and Sand
CTS	Clay, Tire crumb and Sand
DBPs	Disinfectants by Products
DI	Deionized
FDEP	Florida Department of Environmental Protection
GAC	Granulated Activated Carbon
HABs	Harmful Algal Blooms
IFGEM	Iron-Filing Green Environmental Media
IRL	Indian River Lagoon
LC-MS/MS	Liquid Chromatography with Tandem Mass Spectrometry
MC	Microcystin

MCLR	Microcystin LR
MMPB	2-methyl-3-methoxy-4-phenylbutyric acid
N	Nitrogen
P	Phosphorus
PAC	Powder Activated Carbon
PFAS	Per-polyfluoroalkyl Substances
PFOS	Perfluorooctanesulfonic Acid
PFOA	Perfluorooctanoic Acid
PFNA	Perfluorononanoic Acid
PFH _x S	Perfluorohexanesulfonic Acid
PFHpA	Perfluoroheptanoic Acid
PFBS	Perfluorobutanesulfonic Acid
PPCPs	Pharmaceutical and Personal Care Products
PZC or pH _{PZC}	Point of Zero Charge
SEM	Scanning Electron Microscopy
TP	Total Phosphorus
TN	Total Nitrogen

UCF	University of Central Florida
USEPA	United States Environmental Protection Agency
UN	United Nations
WHO	World Health Organization
ZIPGEM	Zero-valent Iron, Perlite Green Environmental Media
BIPGEM	Biochar-zero-valent Iron, Perlite Green Environmental Media
XPS	X-ray Photoelectron Spectroscopy
XRF	X-ray Fluorescence
ZVI	Zero-Valent Iron

CHAPTER 1: INTRODUCTION

1.1. Background

According to the United Nations, the world population reached 8 billion in mid-November 2022, and it is anticipated that the world's population will reach 9.7 billion by 2050 (UN, 2022). Current trend of population growth has created diverse sustainability issues including food and water scarcity (Gundersen and Ziliak, 2015), deforestation (Barbier and Burgess, 2001), climate change (Melillo et al., 2014), soil erosion (Borrelli et al., 2020), air and water pollution (Chaudhry and Malik, 2017; Manisalidis et al., 2020) among other environmental and economic issues (Talibi et al.). Water pollution is an important environmental issue as it directly impacts human health (Lin et al., 2022), biodiversity (Jain et al., 2010), potable water sources (Atikul Islam et al., 2013), and food supply chain (Toussaint et al., 2019). Water pollutants include excess nutrients, heavy metals, pharmaceuticals, oils, organic matter, and algal toxins (Wurtsbaugh et al., 2019; Ukaogo et al., 2020). This chapter describes current and emerging challenges of water pollution including color, algal toxins, excess nutrients, and per- and polyfluoroalkyl substances (PFAS), and their related health concerns and current regulations from which some of the research niches can be identified.

1.1.1. Color contamination

Color in water can be a representation of the dissolved organic compounds present in the water system. For example, dissolved organic matter (i.e., humic, fulvic, and tannic acids) results in a brownish or yellowish color in water. Iron in water produces a reddish color, while phytoplankton and other algae can make the water appear greenish (USGS, 2018). Fluorescent colors in water systems are usually linked with the effluent from textile industry (Lee et al., 2021).

Water with high concentration of color can be detrimental for aquatic life, as it can limit the penetration of light, leading to long-term damage of the aquatic system due to lack of dissolved oxygen. While color is not harmful to human health, per se, when subjected to chlorination it can result in Disinfectant by Products (DBPs). DBPs (i.e., Trihalomethanes) are produced from the interaction of chlorine and bromine with natural organic matter and DBPs are linked as carcinogenic in humans (Diana et al., 2019). The removal of color from water can be achieved via membrane filtration, ultrafiltration, coagulation, adsorption, chemical oxidation, ozone, Fenton processes among the most popular.

1.1.2. Algal Toxin

High concentrations of nutrients in water systems lead to the potential occurrence of algal blooms which could end up with eutrophication (Khan and Mohammad, 2014; Soro et al., 2023). Eutrophication leads to stress and deterioration of the water quality, while further depleting the dissolved oxygen in a water system. Microcystin (MC) is a hepatotoxin produced naturally by cyanobacteria, commonly known as “blue-green algae”. The concentration of phosphorus is the main element regulating cyanobacterial biomass, yet the nitrogen concentration can influence the overall toxicity of the algal blooms (Davis et al., 2015; Heath et al., 2016). The U.S. Environmental Protection Agency (USEPA) has recently re-evaluated microcystin in the Contaminants of Emerging Concern (CECs) program given the human health effects of microcystin. MC are cyclic heptapeptides with seven amino acids, the excessive presence of it on water systems contributes to the reduction of survival, decline of swimming movements, and reduction of fecundity in aquatic life (Thostrup and Christoffersen, 1999; Landsberg, 2002). The most studied specie of MC is Microcystin-LR (MC-LR) where L stands for leucine and R for argentine amino acids.

One of the most popular sorbents for microcystin toxins are activated carbons (AC) due to its high adsorption capacity. The adsorption of microcystin onto AC is a factor of the functional group of the carbon surface and surface charge (Huang et al., 2007). For instance, Huang et al. (2007) found that a higher number of carboxylic groups in the surface of the AC promotes MC adsorption. Moreover, electrostatic interactions between the positive or negative adsorbent surface charge and the MC molecules play an important role in the adsorption process, resulting in attraction or repulsion of the negatively charged molecule (Ampiauw et al., 2019). Efficient degradation of the microcystin LR toxin by biologically active slow sand filters was presented by Bourne et al. (2006). Yet, the removal of microcystin toxin by metals modified sorbent including Cu²⁺ immobilized nanoparticles (Gao et al., 2007) and iron-activated biochar (Zeng and Kan, 2021) have also been reported, where the degradation of microcystin LR by metals is viable by oxidation processes (Sharma et al., 2012).

1.1.3. Nutrient Pollution

Nutrients are essential in aquatic ecosystems for continuous growth, survival, and decomposition of organisms. The two most important nutrients for the survival of an aquatic ecosystem are phosphorus (P) and nitrogen (N). However, overabundance of P and N are the leading factors promoting eutrophication (Boyd and Boyd, 2020). Human-induced eutrophication caused by an increase of nutrient laden effluent discharged into receiving waterbodies can possibly lead to the occurrence of harmful algal blooms (HABs) with higher frequency and greater intensity that could be further exacerbated by global warming impact (Padmakumar et al., 2012; Xiao et al., 2019). When eutrophication occurs, abundant growth of algae arises in an aquatic ecosystem resulting in HABs, dead zones, and fish kills (Dorgham, 2014).

To mitigate the effect of excessive nutrients, it is important to prevent nutrients from reaching the receiving waterbodies. Phosphate removal can be achieved via physiochemical and biological methods. Physiochemical removal for phosphate includes precipitation, sorption, and ion exchange. The sorption process for the removal of phosphate exhibits various advantages including cost-effectiveness at varying level of phosphate concentrations and lower operational complexity. The sorption mechanism of the phosphate to different sorbents depends on the surface characteristics of the sorbent. The main phosphate sorption mechanisms include ligand exchange (Awual et al., 2014), hydrogen bonding (Wu et al., 2019), surface precipitation (Ler and Stanforth, 2003), diffusion (Das et al., 2021), and ion exchange (Loganathan et al., 2014; Bektaş et al., 2021). Moreover, given that phosphate is essential for agriculture, its recovery is an important aspect, making green sorption media excel in terms of sustainability due to the possibility of nutrient recovery in the end (Loganathan et al., 2014; Ordonez et al., 2020b).

1.1.4. Per-and polyfluoroalkyl substances (PFAS)

Contaminants of Emergency Concern (CECs) describe chemicals and compounds whose concentrations were previously at low level or where not detected in water systems but exhibit profound health impact (Sauvé and Desrosiers, 2014). These CECs are unregulated or newly regulated contaminants such as pharmaceutical and personal care products (PPCPs), plasticizers, food additives, laundry detergents, disinfection by-products (DBPs) and per- and polyfluoroalkyl substances (PFAS). One group of CECs that have captured significant attention are the group of manmade chemicals known as per-and polyfluoroalkyl substances (PFAS). PFAS are known as forever chemical due to its resistance to degradation, attributed to the existence of the C-F bond in its structure, where the C-F bond is the strongest covalent bond in organic chemistry. The concern

with PFAS lays on its elevated concern with human health (Sauvé and Desrosiers, 2014) and negative effect on aquatic ecosystems as it can cause a decrease in biological diversity and reduction of aquatic population for fishery (Panieri et al., 2022). PFAS can be found on different daily use products (i.e., water resistant fabrics, grease-resistant paper, nonstick cookware, cleaning products) ending up in the air, soil, and water systems.

The USEPA has recommended four types of treatment systems for the removal of PFAS from drinking water, including granulated activated carbon (GAC) (Cantoni et al., 2021), powdered activated carbon (PAC) (Murray et al., 2019), ion exchange resins and high-pressure membranes (nanofiltration or reverse osmosis) (Xiong et al., 2021). Among these technologies the most popular is the sorption of PFAS to AC due to its high removal efficiency. The main mechanism of adsorption of PFAS to AC counts on electrostatic interactions and chemical interactions between the positively charged surface of AC and the PFAS molecules (Pauletto and Bandosz, 2022). Furthermore, different studies have identified the adsorption of PFAS to other materials and metals including sand (McGregor and Zhao, 2021), clay (McGregor and Zhao, 2021), iron (Hori et al., 2007), and aluminum (Lin et al., 2015). The sorption of PFAS to different sorbents is dependent of the chain length of the PFAS and the physiochemical characteristics of the sorbent, where longer chain PFAS and sulfonate PFAS tend to have higher adsorption (Darlington et al., 2018; Liu et al., 2019).

1.1.5. Health Concerns and Regulations

One of the main concerns of water pollution is its effect on human health. For instance, the consumption of water with high concentrations of nitrates can cause methemoglobinemia in babies, commonly known as blue baby syndrome (Fan and Steinberg, 1996). While phosphate at

average levels is not harmful for human health, per se, if found at high concentration in water it can promote the occurrence of HABs, resulting in the possible presence of algal toxins (Khan and Mohammad, 2014; Soro et al., 2023). Algal toxins include microcystin and nodularin, and they can harm the liver and promote tumor growth. Similarly, the cyanotoxin cylindrospermopsin can generate tissue injuries, while damaging the gastrointestinal lining, liver, and kidneys (Falconer, 1998). Moreover, DBPs and PFAS can act as endocrine disruptors in humans, signifying that it can alter the functions of hormones impairing the reproductive, immune, and metabolic systems (Ghisari et al., 2014a; Sunderland et al., 2019). A detailed summary of the human health effects caused by different contaminants is presented in Table 1.

Table 1. Human health effects caused by the exposure to different contaminants.

Contaminant	Health Effect	Source of contaminant	Reference
Nitrates	<ul style="list-style-type: none"> - Affects children under the age of six months and can result in methemoglobinemia. - Can result in spontaneous miscarriages, thyroid disorders, and birth defects. 	Fertilizer, animal waste and septic tanks.	Greer and Shannon. (2005)
Phosphate	<ul style="list-style-type: none"> - Phosphate at very high levels can cause diarrhea, while also causing calcification of organs and soft tissue. - Indirectly affects human health by contribution to eutrophication and thus, to the occurrence of algae toxins. 	Fertilizers, phosphate mining	Nieder et al. (2018)
PFASs	<ul style="list-style-type: none"> - PFOA increases the risk of kidney, testicular and prostate cancer. - Increases the risk of hyperuricemia. - Affects the metabolic system, and can result in diseases including diabetes, obesity, thyroid. - It can affect body weight and cause dyslipidemia. - Result in low infant birth weights - It can trigger the junction in the brain endothelial cell and raise the permeability of the blood brain cell. - Can cause attention-deficit, hyperactivity disorder (ADHD), and behavior problems. 	Household use products including food packaging, cookware, furniture carper among others. PFASs are one of the main components of aqueous film forming foams (AFFF).	Lopez-Espinosa et al. (2012); Barry et al. (2013); Ghisari et al. (2014b); Sunderland et al. (2019)
DBPs	<ul style="list-style-type: none"> - Birth defects and spontaneous abortion. - Lower speed and mobility of sperm. - Carcinogenic and/or poisonous to kidney. - Associated with tumors in kidneys, uterus, and spleen. - Bladder and renal cancer. 	Resultant of chlorination of water. Includes trihalomethanes: dichloromethylhydroxyfuranone, potassium bromates, chloroform, bromodichloromethane, bromoform, dichloromethane and dibromomethane.	Morris et al. (1992); Larson et al. (1994); Hooth et al. (2002)
Microcystin-LR	<ul style="list-style-type: none"> - Possible carcinogenic to humans. - Tumor promoter. - Affect the nervous system, kidney, liver, and skin. 	Eutrophic water systems.	Fujiki and Suganuma (2011)
E. Coli	<ul style="list-style-type: none"> - Diarrhea and hemolytic-uremic syndrome - Kidney failure, neurologic damage. 	Animal and/or human feces.	Rasko et al. (2011)

With the effort to minimize the environment and health impact of current and emerging contaminant the World Health Organization (WHO) and the USEPA have generated a set of regulation to establish the maximum concentrations and recommended allowed concentration in drinking water, reclaimed wastewater, and lakes, rivers, and reservoirs. The regulations according to the WHO and USEPA for the pollutants of interest in this dissertation are presented in Table 2.

Table 2. United State Environmental Protection Agency (US EPA) and the World Health Organization (WHO) regulations for current and emerging water pollutants.

Contaminant	Water matrix	Regulation (USA EPA)	Regulation (WHO)	Refence
Nitrate	Drinking Water	10 mg·L ⁻¹	50 mg·L ⁻¹	EPA, (2017a); WHO, (2017)
Nitrite	Drinking Water	1 mg·L ⁻¹	3 mg·L ⁻¹	EPA, (2017b); WHO, (2017)
Total Nitrogen	Streams and rivers	<0.3 mg·L ⁻¹	--	EPA, (2002)
	Lakes and reservoirs	<0.1 mg·L ⁻¹	--	EPA, (2002)
Total Phosphates	Streams entering lakes	0.05 mg·L ⁻¹	--	EPA, (1986)
Total Phosphorus	Flowing waters	0.1 mg·L ⁻¹	--	EPA, (1986)
PFAO	Drinking Water	4 ppt	100 ppt	Rizzuto, (2022); EPA, (2023a)
PFOS	Drinking Water	4 ppt	100 ppt	EPA, (2023a)
GenX	Drinking Water	10 ppt	--	EPA, (2023a)
PFBS	Drinking Water	2,000 ppt	--	EPA, (2023a)
Microcystin-LR	Drinking Water	--	1 ug·L ⁻¹	WHO, (2003)
	Water bodies in including Ohio, New Jersey, Rhode Island, and Utah	<1.6 ug·L ⁻¹	--	Yeager and Carpenter (2019)
	Total daily consumption	--	0.04 μg·kg ⁻¹ ·day ⁻¹	WHO, (2003, 2017)
Cyanotoxins microcystin	Recreational Water	8 mg·L ⁻¹	--	USEPA, (2019)
	Drinking Water	1 mg·L ⁻¹	--	
Color	Drinking Water	15 color units	--	EPA, (2023c)

1.1.6. Meta-analysis of publications for color, microcystin, phosphate, and PFAS and water treatment.

To position the current statues of understanding for the pollutants covered in this dissertation (i.e., color, microcystin, phosphate, and PFAS), a metadata analysis was conducted using the Web of Science database. The results for the search of the words “Color” and “water treatment” in Web of Science resulted on 2,790 documents. The results of the search were transformed into a map of the most co-occurrence Keywords (Figure 1(a)). Color in water is mostly caused by the present of minerals, organic matter, and dyes (Team, 2009). From In Figure 1(a) it can be observed that natural organic matter, methylene blue and dye are the most studied relating to color in water. Moreover, it can be observed that the most common types of color removal

treatment are flocculation, photocatalysis, adsorption, electrocoagulation, ozonation, ultrafiltration and nanofiltration.

By searching the word “Microcystin” in the Web of Science database the number of documents found were limited to 6,930, of which, 561 were related to “water treatment”. Figure 1(b) was produced to visualize the co-occurrence (limited to a co-occurrence of over 14 times) of the keywords from the database retrieved from the search of Microcystin and water treatment. In Figure 1(b) it can be observed that Microcystin LR is the main Microcystin specie studied, and that is commonly explored with geosmin (a metabolite from cyanobacteria (Cerón-Vivas et al., 2023) and cylindrospermopsin (a cyanotoxin produced by freshwater cyanobacteria (Kinnear, 2010). Moreover, the removal treatment technologies for Microcystin are distributed between adsorption, biodegradation, ozone oxidation, photocatalytic degradation, and coagulation.

By searching the name phosphate, the number of publications that appeared were 469,279. By further limiting the search to water treatment related document the resultant documents were 3,532. A visualization map of the co-occurrence of the keywords in the data base retrieved from the combination of the word “phosphate” and “water treatment” was proceed by VOS viewer, limiting the co-occurrence to over 30 times (Figure 1.(c)). Figure 1(c) indicates that adsorption is the most studied phosphate treatment removal with biochar being one of the most studied adsorbents. Moreover, the regeneration of adsorbents stands out in Figure 1(c), pointing at its importance from an economical and sustainable perspective (Kulkarni and Kaware, 2014). Other phosphate removal treatments that stand out are precipitation, electrocoagulation, and coagulation. Furthermore, phosphate is known to be present in wastewater with other nutrients, especially nitrogen with constructed wetland being connected given its efficiency for biophysiochemical

nutrient removal (Vymazal, 2010). Phosphate recovery from wastewater in the form of struvite seems to also be another topic of interest, perhaps linked with the need to meet current and future phosphate demand for agriculture (Li et al., 2016a) and to minimize the impact of phosphate mining (Beavers et al., 2013). Finally, the linkage between eutrophication and phosphate in Figure 1(c) supports the important role that phosphate plays in eutrophication and the significance on phosphate removal to mitigate eutrophication (Schindler, 1974).

Similarly, the number of studies found by searching “PFAS” was 4,108 and by limiting to “water treatment” related studied the number of documents decreased to 291. The visualization of the co-occurrence of keywords (limited to a co-occurrence of over 6 times) of these studies is presented Figure 1(d). From Figure 1(d) can be concluded that PFOA and PFOS are the main PFAS species of concern (Cordner et al., 2019). Moreover, the adsorption of PFAS by activated carbon and granulated activated carbon appears to be a highly studied topic, followed by reverse osmosis, nanofiltration and photocatalysis. The concern of bioaccumulation of PFAS is also show case in Figure 1(d) (Yun et al., 2023).

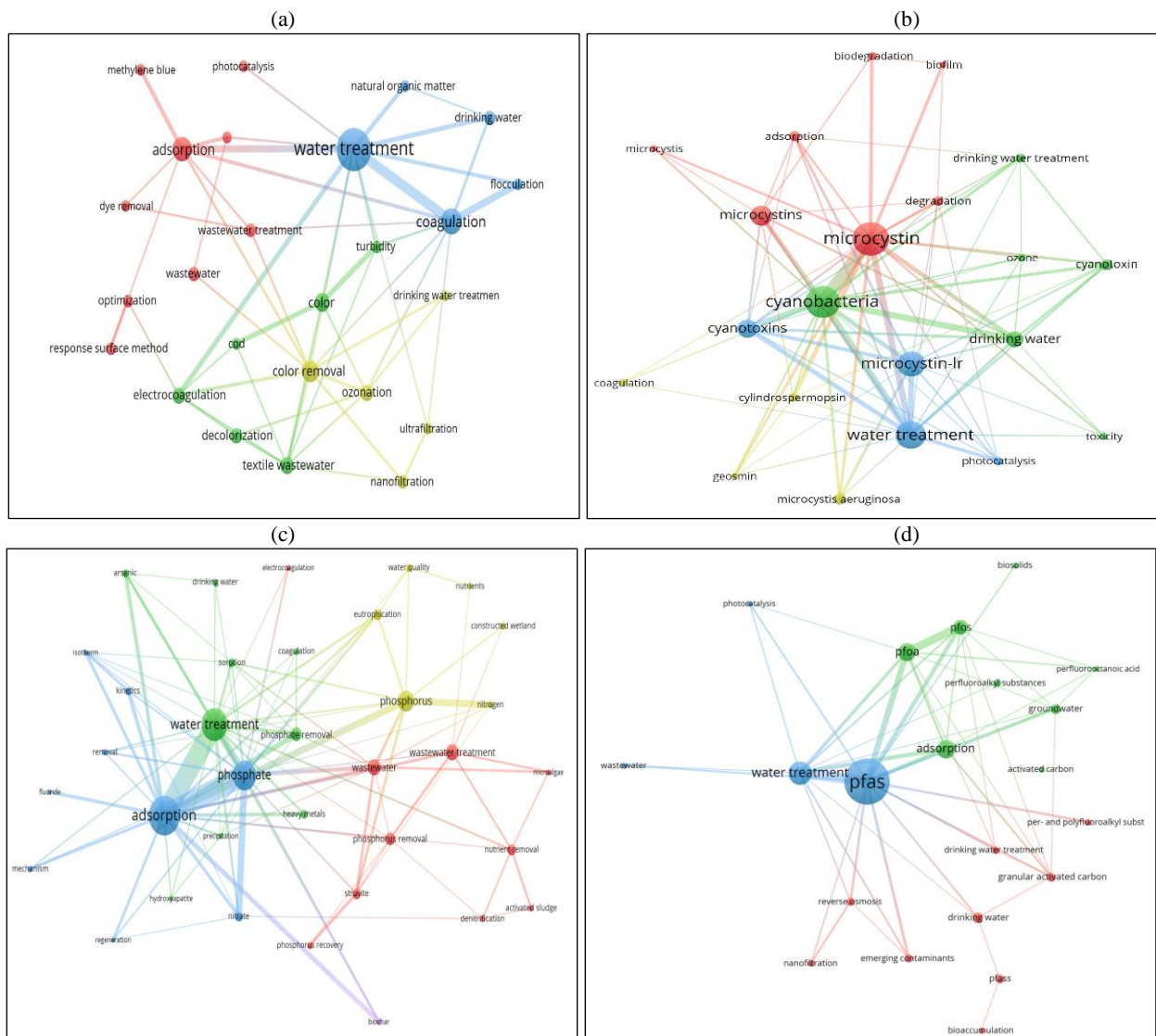


Figure 1. Visualization co-occurrence map for the literature search on (a) color and water treatment, (b) microcystin and water treatment, (c) Microcystin and water treatment and (d) Phosphate and water treatment [Produced on VOS viewer]. Size of the circles are related with the co-occurrence of the keyword.

1.2. Study Objectives

To mitigate the environmental impacts caused by emerging challenges in water pollution new sustainable technologies are being developed and implemented. Best Management Practices (BMPs) are technologies developed to improve water quality and control water quantity (Li et al., 2023). One of the popular BMPs are green sorption media due to its cost-effectiveness, easy to

operate, scalable and adaptable, fast reactions, null production of sludges, and the possibility for reuse (Crini et al., 2018). Despite the multiple advantages of the green sorption media, it is important to understand the removal mechanism, operational efficiency, and life expectancy for different contaminants given different water matrices. In this dissertation, several green sorption media were investigated for its potential to treat color (from tannic acid), microcystin, phosphate, and PFAS individually or collectively under different conditions.

In Chapter two, a few green sorption media including Clay-Tire crumb and Sand sorption media (denoted CTS, hereafter), Iron-Filings Green Environmental Media 1 and 4 (denoted IFGEM-1 and IFGEM-4, hereafter, respectively), Clay-Perlite and Sand sorption media (denoted CPS, hereafter) and Zero-valent Iron and Perlite Green Environmental Media (denoted as ZIPGEM) were studied for its color removal potential and physiochemical color removal mechanism. This experiment encompasses the need to recharge Lake Brooklyn near Keystone Heights to maintain recreational activities while replenishing the Upper Floridian aquifer with appropriate water quantity and quality. Water collected from Black Creek South Prong, a tributary of the Lake Brooklyn, impaired with high concentration of tannic acid was selected as the influent condition.

In Chapter three, three green sorption media including CPS, ZIPGEM and a newly developed media known as Biochar-Zero-valent-Iron and Perlite Based Green Environmental Media (denoted BIPGEM, hereafter) were studied for its potential to removing algal toxin (i.e., MC-LR). A series of isotherms were performed to study the effects on the adsorption capacity of the green sorption media due to the presence of Ca^{2+} and PO_4^{3-} . The incorporation of both chemicals is significant given that they can coexist with MC-LR in Florida environments. Finally,

the removal efficiency and adsorption mechanism of the green sorption media with real canal water was studied to maximize the understanding of the interaction (i.e., competition or collaboration) between the different constituents of the water matrix. For this study, canal water from the C-23 located in Martin County was used as the influent condition. C-23 is a tributary of St. Lucie River and has been identified as an impaired waterbody due to high concentration of nutrients.

In Chapter four, three green sorption media including CPS, ZIPGEM, and BIPGEM were evaluated for understanding phosphate adsorption capacity and mechanism partaking in phosphate removal. To assess the phosphate removal feasibility facing different aquatic environments, the green sorption media mentioned above were evaluated at different pHs (i.e., 4 and 10). Moreover, kinetic studies of green sorption media and their life expectancy were evaluated to support large scale application. Finally, the reuse of the media as a possible soil amendment was discussed as an alternative for artificial fertilizers to save the cost of spent media disposal.

Lastly, since St. Lucie River has been impaired with CECs including PFAS, Chapter 5 intends to investigate PFAS adsorption capacity of four green sorption media including Iron-Filings Green Environmental Media 7 (denoted IFGEM-7, hereafter), CTS, CPS, and ZIPGEM. A series of column studies with water from canal C-23 as influent condition were conducted to understand the adsorption behavior via different green sorption media facing different water quality constituents. Finally, this study also evaluated the adsorption kinetic of each green sorption media mix to further characterize its removal mechanism. With this progress, we are empowered to present a holistic understanding of the adsorption capacity of the tested green sorption media, transitioning from color to algal toxins, to nutrients, to the current most worrisome CEC, which is PFAS.

CHAPTER 2: ¹COLOR REMOVAL FOR LARGE-SCALE INTERBASIN WATER TRANSFER: EXPERIMENTAL COMPARISON OF FIVE SORPTION MEDIA

2.1. Introduction

Natural or manmade color present in aquatic systems includes dyes from domestic or industrial wastewater (Tara et al., 2020), dissolved natural organic matter (NOM) from plant species (Kutser et al., 2005), and algae (Shengguang et al., 1991). NOM including humic, fulvic, and tannic acids (Darko et al., 2014) can result in a yellow, red, brown and/or gray color in aquatic system. Humic and fulvic acids are the final products from the natural decay of plants and animals while tannin acid mostly occurs from leaching of twigs and swelling of certain trees including chestnut and oak trees. While these organic acids are beneficial to soil for agricultural processes, they can cause color contamination in water bodies. Therefore, they can affect the ability of these water bodies to be used as drinking water sources as they are precursors to disinfectant by-products (DBPs) after drinking water treatment (EPA, 2012; Ahamed et al., 2019). For this reason, the US Environmental Protection Agency (EPA) has regulated color concentration in drinking water to 15 Pt-Co units (visual color on the Platinum-Cobalt Scale) under the secondary drinking water standards (Dietrich and Burlingame, 2015).

DBPs are unintentional by-products resulting from the interaction of disinfectants like chlorine with NOM (Tak and Vellanki, 2018). Trihalomethanes, haloacetic acids, formaldehyde, and acetaldehyde are some of the commonly found DBPs (Palmstrom et al., 1988; Krasner et al., 1989). The occurrence of DBPs in drinking water can cause adverse effects on human health

¹ Ordonez, D., Valencia, A., Pereira, B., and Chang, N. B. (2022): Color removal for large-scale interbasin water transfer: Experimental comparison of five sorption media, *Environmental Research*, <https://doi.org/10.1016/j.envres.2022.113208>.

(Fawell et al., 1997) including increasing risk of bladder cancer (Li and Mitch, 2018), and can influence reproduction and result in birth defects (Wigle, 1998). The removal of DBP precursors (i.e., NOM) within drinking water treatment facilities typically requires coagulation, microfiltration (Bottino et al., 2001) or adsorption (Gora and Andrews, 2017; Sun et al., 2017). Given such complicated treatment processes, the removal of color from the natural aquatic sources utilized as drinking water is of importance as it can lower the treatment cost and minimize the emergence of DBPs.

In pretreatment, adsorption processes are cost-effective to treat DBP precursors. Activated carbon (AC) is one of the most frequently utilized filtration materials for the removal of color due to its simplicity and regeneration potential (Rao and Krishnaiah, 1994; Singh et al., 2003; Zhou et al., 2021b). Innovative agricultural waste materials are also utilized to synthesize AC for dye removal including rice husk (Vadivelan and Kumar, 2005), waste metal hydroxide sludge (Santos et al., 2008), palm kernel shell (El-Sayed, 2011), banana and orange peels (Mane and Bhusari, 2012), coconut shell (Aljeboree et al., 2017), mango peels (Jawad et al., 2017), and coffee waste (Wong et al., 2020). Prema et al. (2011) reported maximum color removal efficiency of 90.72% with Fe⁰ synthesized nanoparticles of size 16.64 nm. Moreover, Ma et al. (2019) successfully designed a polysilicate aluminum magnesium and cationic polyacrylamide flocculant and was able to obtain turbidity and color removal above 98% at optimum in drinking water. The use of membranes to remove color and dyes have also been investigated. Rambabu et al. (2019) studied the dye rejection potential of a polyethersulfone nanoporous membrane modified with calcium chloride. A 95% rejection of Congo Red dye with the polyethersulfone nanoporous membrane was observed. Perlite is a soil amendment derived from volcanic rock usually formed from siliceous

lava or ash. Natural perlite is usually grey, but it can also be green, red, blue, or brown; yet after heating it usually takes on a white color. The chemical formula of perlite is $\text{Al}_2\text{CaFe}_2\text{K}_2\text{MgNa}_2\text{O}_{12}\text{Si}$ and the molecular weight is $574.29 \text{ g}\cdot\text{mol}^{-1}$; hence it is natural sodium-potassium-aluminum-silicate. The presence of aluminum, silica, and iron in the ingredients deserves further investigation. The use of perlite and volcanic rock has also been studied for the removal of dyes from aqueous solutions (Rossatto et al., 2021). Doğan et al. (2000) examined the adsorption of methylene blue from aqueous solutions to unexpanded and expanded perlite samples activated by H_2SO_4 and NaCl solutions to remove cationic dyes. Their results indicated that perlite can be used for removal of methylene; a better removal efficacy was observed from unexpanded perlite. Meesuk and Seammai (2010) suggested that expanded perlite can be used to remove dark color from spent palm oil via physical mechanism and can also remove benzo(a)pyrene from the palm oil. Although the adsorption of tannic acid onto perlite has not been broadly explored, the adsorption efficiency of humic substances onto expanded perlite was investigated by Chassapis et al. (2010). Chassapis et al. (2010) indicated that the adsorption of humic substance stems involved Coulombic attraction forces related to the positively charged humic substances and negative sites of the perlite (i.e., alumino-silicate).

In the study reported herein, five sorption media, including Clay-Tire crumb and Sand sorption media (denoted CTS, hereafter), Iron-Filings Green Environmental media 1 and 4 (denoted IFGEM-1 and IFGEM-4, hereafter, respectively), Clay-Perlite and Sand sorption media (denoted CPS, hereafter) and Zero-valent Iron and Perlite Green Environmental Media (denoted as ZIPGEM), were tested to evaluate their effectiveness to remove color from a source water collected from a water canal polluted with tannic acid. The tannic acid in this canal is high given

the abundant in cypress forests within the study area. Among these sorption media, CTS and IFGEM-1 were previously studied for nutrient and metal removal (Chang et al., 2019a; Chang et al., 2019b; Valencia et al., 2019; Wen et al., 2018, 2020a). IFGEM-4, CPS and ZIPGEM were developed for this study, due to the potential contribution of coupled perlite and zero-valent iron (ZVI) on the top of traditional sand and clay to the removal of color. The research objective and novelty in this study is associated with exploring and comparing the effectiveness of five sorption media (made from recycled materials) which are cheaper than activated carbon to treat water with high concentration of color and to examine whether they can meet the regulatory requirement (i.e., 40 Pt-Co color unit) in the St. Johns River Water Management District for source water pretreatment (SJRWDM, 2021.). The research questions to be answered were: (1) Is there any incremental effect on color removal from the sequential use of recycled iron filings and perlite? (2) What is the removal mechanism of color the proposed media recipe ingredients of recycled iron filings, clay, and perlite? (3) Which media mix of the five used can achieve the best color removal efficiency?

2.2. Material and Methods

2.2.1. Study region

Lake Brooklyn near Keystone Heights in Clay County, Florida, the United States (US) is facing a problem with low water level which is affecting recreational use and nearby shallow aquifer drinking water wells. Some wells have gone dry due to aquifer overuse, and hence Lake Brooklyn is in acute need of replenishment. A state project to pump water from the Black Creek South Prong, a tributary of the St. Johns River, to Lake Brooklyn to recharge the semi-confined Upper Floridian aquifer at Keystone Heights has moved forward with the recent land acquisition

needed for the roughly 27-km pipeline through southwest Clay County. The Floridan aquifer is one of the main sources of groundwater in the US and it is mainly composed of limestone and dolomite beds. The Floridan aquifer has confined, unconfined, and semiconfined areas, where the areas in the St. Johns River Management District are mostly semiconfined (Katz, 1992). This is the first attempt in Northeast Florida for a project of this magnitude and will take up to 37,000 metric tons per day (10 million gallons per day) from Black Creek. However, the interbasin water transfer project is hampered by the excessive concentration of color in Black Creek. Brown reddish color in this creek is the product of the high amount of tannic acid reaching the water body from cypress trees surrounding this area (Figure 2).

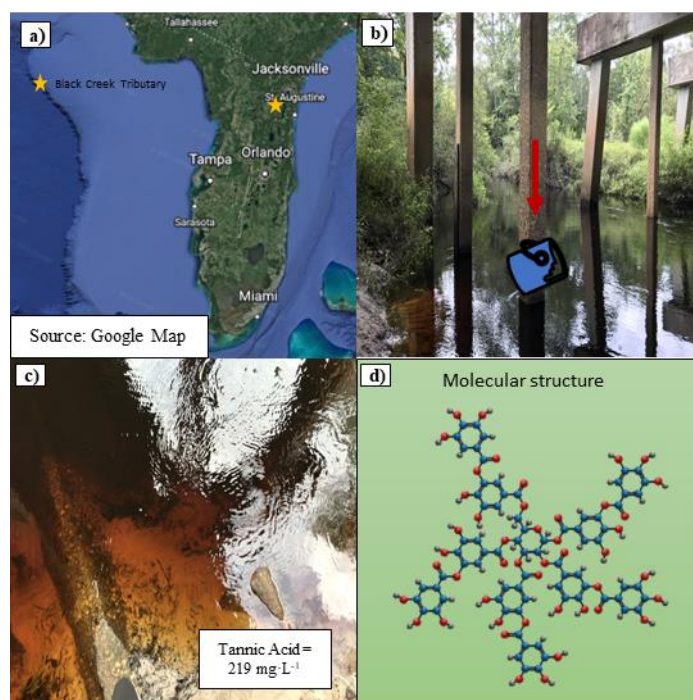


Figure 2. Sample collection site a) image of the location of Black Creek Tributary, b) sample collection site, c) image of raw water and d) chemical structure of tannic acid.

Before water can be transferred to the Upper Floridan aquifer, the water from Black Creek needs to be treated for color removal *in situ*. Current concentrations in this region range from 170

to 325 Pt-Co color units. However, the St. John River Management District standard for drinking source water is less than 40 color units Pt-Co (SJRWDM, 2021) before the interbasin transfer is allowed. Given the low cost associated with adsorption processes, and low maintenance requirements for filtration facilities, column studies to compare the application of sorption media were conducted to find the most appropriate design. Water collected from Black Creek was used as the influent for the column studies and was collected in $18.9 \times 10^{-3} \text{ m}^3$ plastic buckets and stored at the University of Central Florida (UCF) in a walk-in refrigerator set at a temperature of $-17.8 \text{ }^\circ\text{C}$.

2.2.2. Composition and characterization of sorption media

In this study, five sorption media recipes were tested systematically for their potential to remove color from Black Creek water. The composition and matrix of the sorption media studied are summarized in Table 3. To further explore the effect on zero valent iron (ZVI) (e.g., iron filings) as component of the media, new iron-sand based sorption media mixes, known as IFGEM-1 and IFGEM-4, were developed. Furthermore, the utilization of perlite for the removal of contaminants (i.e., metals, dyes, and nutrients) is a novel development (Alkan and Dogan, 2001; Moussavi and Bagheri, 2012; Hosseini and Toghroli, 2021). Dogan and Alkan (2003) suggested that perlite has considerable potential to remove methyl violet dye from aquatic solutions, and its efficiency improves with increasing temperature and pH. Such studies substantiate the inclusion of perlite in two newly developed sorption media denoted as Clay-Perlite and Sand media (denoted as CPS, hereafter) and Zero-valent Iron and Perlite Green Environmental Media (denoted as ZIPGEM, hereafter). The media recipes in this study followed previous ones (Valencia et al., 2021). In the current study (Table 3), CTS media mix was used as control to compare against iron-

based media mixes, including IFGEM-1 and IFGEM-4, as well as perlite-based media mixes, including CPS and ZIPGEM.

Table 3. Media matrix and composition

Media name	Media Matrix (% by volume)	Sources
CTS	85 % sand, 5% clay, 10% tire crumb	Wen et al. (2018)
IFGEM-1	96.2 % sand and 3.8% ZVI	Chang et al. (2019b)
IFGEM-4	90% sand and 10% ZVI	Ordonez et al. (2022b)
CPS	92% sand, 5% clay and 3% perlite	Ordonez et al. (2022b)
ZIPGEM	85% sand, 5% clay, 6% ZVI and 4% perlite	Ordonez et al. (2022b)

These five-sorption media were characterized by hydraulic conductivity ($\text{m}\cdot\text{sec}^{-1}$), BET surface area ($\text{m}^2\cdot\text{g}^{-1}$), porosity (%), bulk density ($\text{g}\cdot\text{cm}^{-3}$), and chemical composition (% per element). Media samples were delivered to the laboratories of EMSL Analytical, Inc. in Orange City, Florida for the measurement of grain size distribution, bulk density, and BET surface area. The methods ASTM D422, ASTM D854 and ASTM B922 for particle size analysis for soils, specific gravity of soils and standard test methods for metal powder specific surface area by physical adsorption, respectively, were followed.

The hydraulic conductivity (or intrinsic permeability) was determined in a standard permeameter following the protocol for Constant Head Permeability test in the Geotechnical Laboratory at UCF. The porosity and the hydraulic retention time (HRT) of the sorption media were measured at UCF. The porosity was determined by measuring the volume of water needed to fill the pores of a dry media sample. The HRT was determined via a tracer study with Rhodamine dye (CAS Number 37299-86-8). Rhodamine dye was selected for this study due to low cost, easy operation and detection via a fluorometer, low natural background, limited toxicity level, and nonreactivity (Richardson et al., 2004). For the tracer study, about 1 ml of Rhodamine dye was

injected at the top of the column, subsequently effluent samples were collected at 5-10 min intervals and measured by an AquafloTM (Turner Designs 998-0851) handheld fluorometer until the rhodamine dye breakthrough was observed and completed.

The chemical compositions of the different media were analyzed via an X-Ray Fluorescence Spectrophotometer (XRF) PANalytical Epsilon at the Materials Characterization Facility (MCF) at UCF (Dewi et al., 2018). Textural characterization of the media was obtained at the MCF at UCF with a Scanning Electron Microscopy (SEM) Jeol JSM -6480 SEM instrument. The Jeol SEM allows a variable pressure mode of operation allowing microscopy of non-conductive, oily, and damp samples.

The results of the sieve analyses were plotted to obtain the grain size distribution curves or gradation curves from each sorption media mix. These results were used to evaluate whether these sorption media were poorly or well graded. To do so, the coefficient of uniformity (C_u) and the coefficient of gradation (C_c), which are the common measures of soil gradation, were calculated based on Eq. 1 and Eq. 2 for these media mixes. Within this context, D_{60} , D_{30} and D_{10} is the grain diameter at 60%, 30% and 10% finer, respectively. The higher the C_u value the higher the range of particle size. If the C_u is greater than 4 and less than 6 then the media mix is classified as well graded, but, if the C_u is less than 4 then the media mix is classified as poorly graded. However, for a media mix to be well graded, the C_c value must range between 1 and 3.

$$C_u = \frac{D_{60}}{D_{10}} \quad (1)$$

$$C_c = \frac{D_{30}^2}{D_{60}D_{10}} \quad (2)$$

2.2.3. Experimental set-up for the column study

A series of experiments with fixed bed columns was performed for the purpose of exploring the color removal efficiency and life expectancy of these selected sorption media. Columns 30.48 cm (12 in) in depth and 7.62 cm (3 in) diameter were filled with 1200 ml of the selected sorption media (i.e., CTS, IFGEM-1, CPS, IFGEM-4 and ZIPGEM) and a 5.08 cm (2-in) free space was left above the media in case of overflow. Each column set-up included a filter and a layer of pebbles at the bottom to prevent clogging, while a layer of pebbles was placed at the top of each column to aid in water distribution.

All column experiments were operated with a downward flow, simulating the planned implementation at field scale. Before the experiment, each column was flushed with de-ionized water (DI) at a flowrate of $8 \text{ ml}\cdot\text{min}^{-1}$ for approximately 3 bed volumes and left to drain for >10 hours to remove any pre-existing contaminants in the sorption media. Subsequently, water collected from the Black Creek tributary of the St. Johns River (Section 2.2.1) (denoted as influent, hereafter) was supplied to each column via a peristaltic pump at a fixed flowrate of $4 \text{ ml}\cdot\text{min}^{-1}$. The color concentration of the influent was modified to 175 ± 10 Pt-Co units by adding DI water if necessary to maintain the same influent color concentration for all the column experiments. For the column studies the hydraulic loading rate maintained was $1.26 \text{ (m}^3\cdot\text{day}^{-1}\cdot\text{m}^{-2}\text{)}$.

2.2.4. Water parameter analysis

Water samples from the influent and effluent at distinct time intervals were collected, analyzed, and catalogued to obtain information on color removal. All water samples were analyzed for color within 24 hours of collection to prevent any biological and chemical processes from altering color concentrations. All water sample analysis was performed at the Environmental

Engineering Laboratories at UCF. True color of each water sample was measured using a Hach Method 8025 spectrophotometer. First, water samples were filtered through a Millipore Sigma MF-Millipore Cellulose Ester membrane with 0.45- μm pore size. Subsequently, 10 ml of filter samples were used to fill a 465 nm cell and placed in the DR-5000 Hach Spectrophotometer meter to measure and catalogue true color concentrations.

2.2.5. Dynamic adsorption models

Dynamic modeling of the breakthrough curves allows the understanding of the sorption behavior of color to the sorption media. In this study, Thomas, Modified Dose Response (MDR), and Yoon-Nelson models were selected to characterize the dynamic sorption mechanism. The Thomas model is derived from the Langmuir adsorption isotherm to describe the equilibrium between adsorbate and adsorbent where diffusion is neglected (Mustafa and Ebrahim, 2010; Ghasemi et al., 2011). The MDR model is an empirical model, appropriate for applications in breakthrough curves that have an asymmetric behavior (Chang et al., 2016). The Yoon-Nelson model is the simplest dynamic adsorption model as it does not require information on the adsorbent, adsorbate, or the physical characteristics of the sorption bed (Ghribi and Chlendi, 2011). The linear forms of these dynamic adsorption models with the definitions of parameters are presented in Table 4.

Table 4. Summarize description of dynamic adsorption models with the definitions of parameters

Model name	Linear Form	Parameters	Reference
Thomas	$\ln\left[\left(\frac{C_0}{C_t}\right) - 1\right] = \frac{k_T q_0 m}{Q} - k_T C_0 t$	k_T = Thomas rate constant (L·mg of Pt-Co ⁻¹ ·min ⁻¹) q_0 = media equilibrium uptake (mg of Pt-Co·g ⁻¹) m = mass of media in the column (g) Q = flow rate (L·min ⁻¹)	Ghasemi et al. (2011)
MDR	$\ln\left(\frac{C_t}{C_0 - C_t}\right) = a_{mdr} \ln(C_0 Q t) - a_{mdr} \ln(q_0 m)$	a_{mdr} = MDR rate constant q_0 = media equilibrium uptake (mg·g ⁻¹) Q = flow rate (L·min ⁻¹) m = mass of media in the column (g)	Chang et al. (2016)
Yoon-Nelson	$\ln\left(\frac{C_t}{C_0 - C_t}\right) = k_{YN} t - \tau k_{YN}$	τ = half time (min) k_{YN} = Yoon Nelson rate constant (min ⁻¹)	Ghribi and Chlendi (2011)

* C_0 corresponds to the influent concentration (in color unit Pt-Co), C_t corresponds to the effluent concentration at time t (in color unit Pt-Co) and t stands for time (in minutes).

To improve the goodness of fit of the dynamic adsorption models, a method for outlier detection and removal was performed. Detection of outliers from the data sets was accomplished by drawing 95% confidence intervals (CI) around the scatter plots of the effluent concentration (in color units) vs. time (minutes). Outliers outside of the 95% CI were removed from the data sets. Moreover, these steps were performed multiple times after the removal of outliers until all data points were within the 95% CI (Uusipaikka, 2008).

2.2.6. Life expectancy

For field implementation, it is important to determine the frequency of media replacement after treatment capacity has been exhausted. This can be achieved by formulating life expectancy curves for a range of removal efficiencies (e.g., 40-90%) to treat a volume of color impacted water. To estimate the media's replacement frequency, first the media usage rate (Eq. 3) is determined according to the target removal efficiency (R). The usage rate (g·L⁻¹) specifies the mass of media

in grams that can treat 1 L of water based on the desired effluent concentration. As a result, each removal efficiency will have its corresponding usage rate and thus corresponding life expectancy curve. The determination of usage rate employs the influent concentration C_0 ($\text{mg}\cdot\text{L}^{-1}$), the average target effluent concentration C_1 ($\text{mg}\cdot\text{L}^{-1}$) (where $C_1 = C_0(1 - R)$), and the maximum adsorption capacity q_0 ($\text{mg}\cdot\text{g}^{-1}$) selected from the appropriate dynamic adsorption model that can best describe the experimental data collected from column studies. The modeled R is dependent on the reasonable range of color removal obtained from the column study. To produce the life expectancy curves, a range of volume of treated water $V_{\text{water treated}}$ (L) is selected to calculate the corresponding range of mass of media required for treatment $\text{mass}_{\text{media}}$ (g) according to Eq. 4. Since the determination of the media's replacement frequency is dependent on the flow rate specified, the design flow rate (Q in $\text{L}\cdot\text{h}^{-1}$) needs to be first selected by taking into account the maximum flow rate ($Q_{\text{threshold}}$ in $\text{L}\cdot\text{h}^{-1}$) considered as the design threshold and it is preferred for Q to be less than $Q_{\text{threshold}}$. Having an understanding of the $Q_{\text{threshold}}$ is crucial to prevent possible ponding effect. In this case, gravity is assumed to dominate the flow path contributing to vertical flow as the filter depth is small (i.e., 0.3-0.6 m). Hence the laboratory HRT determined from the column tracer study is utilized to determine the $Q_{\text{threshold}}$ (Eq.6) to be representative when scaling from a laboratory study up to a field application. To estimate the life expectancy, the void volume or pore space (V_{void} in m^3) corresponding to the available water retention capacity in the media is first determined from Eq.5, using the media mass, media porosity ϕ , and density (ρ_{media} in $\text{kg}\cdot\text{m}^{-3}$). Once the design flow rate (Q) is selected, the surface area of the filter cell is determined from the hydraulic loading rate (HLR in $\text{m}^3/\text{m}^2 \text{d}^{-1}$) based on the experimental column-study conditions following Eq. 7. The volume of the cell V_{cell} (m^3) representing the volume occupied by the media is determined

according to the area $area_{design}$ (m^2) and the depth of cell $depth_{filter}$ (m) (Eq.8). Hence, the $mass_{media}$ $_{design}$ corresponding to the filter cell dimensions and the density of media, can be calculated according to Eq. 9. Lastly, the life expectancy is calculated from Eq. 10, for a specified media mass ($mass_{media}$ $_{design}$) corresponding to filter design and the design flow rate (Q). A design chart can be generated accordingly with a few turning lines to link the target removal efficiency curve with the treated water in volume and the selected mass of media.

$$\text{Usage Rate} = \frac{C_0 - C_1}{q_0} \quad (3)$$

$$V_{\text{water treated}} = \frac{mass_{media}}{usage\ rate} \quad (4)$$

$$V_{\text{void}} = mass_{media} (\emptyset) \left(\frac{1}{\rho_{media}} \right) \quad (5)$$

$$Q_{\text{threshold}} = \frac{V_{\text{void}} * \text{conversion factor} \left(\frac{1000\ L}{1\ m^3} \right)}{HRT} \quad (6)$$

$$area_{\text{surface}} = \frac{Q * \left(\frac{1\ m^3}{1000\ L} \right)}{HLR} \quad (7)$$

$$V_{\text{cell}} = area_{\text{surface}} * depth_{\text{cell}} \quad (8)$$

$$mass_{media\ design} = V_{\text{cell}} * \rho_{media} \quad (9)$$

$$\text{Life Expectancy} = V_{\text{design water treated}} \left(\frac{1}{Q} \right) * \text{conversion factor} \left(\frac{d}{24\ h} \right) \quad (10)$$

2.3. Results and Discussion

2.3.1. Material Characterization

The physical characteristics of the five selected sorption media in this study (i.e., CTS, IFGEM-1, IFGEM-4, CPS, and ZIPGEM) are summarized in Table 5. Among the selected sorption media, ZIPGEM has the largest surface area ($2.55\ m^2 \cdot g^{-1}$) followed by IFGEM-4, CPS, CTS, and IFGEM-1. Larger surface area can lead to have better adsorption potential (Wang, et al., 2014). In terms of porosity CTS has the highest porosity (40.10%) followed by IFGEM-1, ZIPGEM, CPS,

and finally IFGEM-4. The saturated hydraulic conductivity for all media is within the typical range for sand (10^{-3} to 10^{-5} m·sec⁻¹) (Reddi and Inyang, 2000), indicating appropriateness for field implementation. Finally, the inclusion of ZVI in the sorption media can be associated with the resultant higher density and larger surface area in ZIPGEM contributing to better color removal.

Table 5. Sorption media matrix in percent by volume and physical characteristics

Media name	BET Surface Area (m ² ·g ⁻¹)	Porosity (%)	Density (g·cm ⁻³)	Saturated Hydraulic Conductivity (m·sec ⁻¹)	Source
CTS	0.86	40.10	2.40	$2.6 \cdot (10^{-4})$	Wen et al. (2018)
IFGEM-1	0.31	36.16	2.73	$2.8 \cdot (10^{-4})$	Chang et al. (2019b)
IFGEM-4	2.33	25.97	3.01	$1.7 \cdot (10^{-4})$	Ordonez et al. (2022b)
CPS	1.08	26.48	2.61	$1.7 \cdot (10^{-4})$	Ordonez et al. (2022b)
ZIPGEM	2.25	29.04	2.80	$2.8 \cdot (10^{-4})$	Ordonez et al. (2022b)

The gradation curves or particle size distribution curves of each sorption media in this study are presented in Figure 3. The uniformity coefficient (C_u) and the coefficient of gradation (C_c) are the measures of soil property sand are presented in Figure 3. For the media mix to be well graded, the value of C_c must range between 1 and 3. The value of C_c of IFGEM-4 is slightly larger than others while all of them are smaller than 2. This implies all five media mixes are poorly graded. Higher value of C_u indicates that the media mix consists of media particles with different size distributions. All the C_u values are below 4 signifying that all sorption media are poorly graded. But CTS has the highest C_u value among the five media mixes. What followed CTS are IFGEM-4, IFGEM-1, ZIPGEM, and CPS.

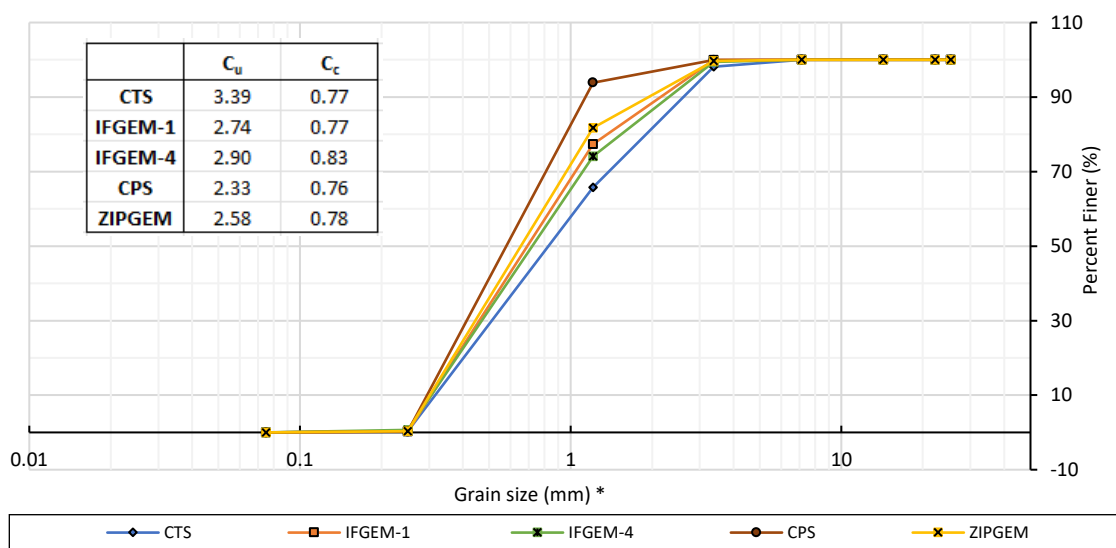


Figure 3. Gradation curves of sorption media (*x-axis is in logarithmic scale)

In addition to physical characterization of the media mixes, samples were evaluated via an XRF analysis to describe the chemical composition of the media mixes (Table 6). The main chemical element in all mixes was silica (Si), corresponding to >83.4% of the chemical composition (Table 6). As shown by Wang et al.(2010), amino-functionalized magnetic mesoporous silica can remove tannic acid from aqueous solution by adsorption. The second most abundant chemical components for all sorption media mixes, excluding IFGEM-1 is aluminum (Al). The presence of Al as a chemical component in the sorption media mixes can be explained by the inclusion of clay as key ingredient of the mixes (Nayak and Sing, 2007). Al is utilized for removal of diverse contaminants including nutrients, metals, and contaminants of emerging concern (Nouri et al., 2010; Ordonez et al., 2020a; Zaied et al., 2020). The inclusion of recycled ZVI (95.6% Fe) as an ingredient of the sorption media for the removal of contaminants is highly promising given its reactivity, large surface area, lower cost, and environmentally friendly nature (Khuntia et al., 2019). Furthermore, K and Ca (1-2.5% and 0.7-1%) are also part of the chemical

composition of the sorption media mixes, and thus, to some extent their presence can aid in a synergistic effect that can be helpful for the removal of contaminants.

Table 6. Chemical composition analysis of sorption media mixes from XRF analysis

Compound	CTS	IFGEM-1	IFGEM-4	CPS	ZIPGEM
Al (%)	8.6	10.1	2.4	9.8	9.3
Si (%)	86.0	81.7	90.4	84.6	83.4
P (%)	1.8	1.8	1.6	1.8	1.7
K (%)	2.2	1.0	1.8	2.4	2.5
Ca (%)	1.0	0.7	0.7	1.0	0.8
Fe (%)	0.3	4.8	3.1	0.5	2.4

Images of the media mixtures attained from SEM analysis are presented in Figure 4; these images complement the physical characteristics in providing a visualization of the media mixes at the microscale. The most salient change among the selected sorption media is the color, as the darkish brown tone increases with the increasing concentration of ZVI. Moreover, the media morphology indicates that ZIPGEM particles are the most heterogenous in size and shape which may provide 3-dimensional morphological structures with a higher hydraulic conductivity at the microscale to promote molecular diffusion in a multi-layer structure during an adsorption process. Poorly graded materials with morphological structures would have higher potential to allow dispersion and molecular diffusion to occur in layer-by-layer films during the adsorption process. As Crittenden et al. (1986) mentioned, such a unique process can be formed by the following four steps: (1) mass transfer in a liquid phase via convective mass transfer followed by molecular diffusion; (2) interface diffusion via film diffusion between the liquid phase and the exterior surface of the adsorbent; (3) intrapellet mass transfer through surface diffusion and pore diffusion; and (4) the adsorption-desorption reaction before and after equilibrium. On the other hand,

IFGEM-4 had the higher number of larger particles along with a larger surface area and lower hydraulic conductivity given its higher content of ZVI and better gradation, all prone to form a monolayer structure in an adsorption process.

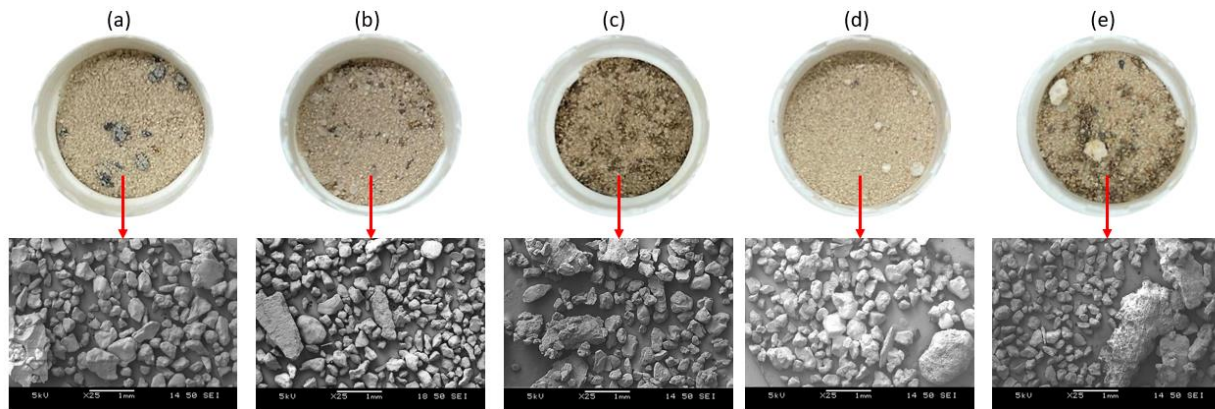


Figure 4. Photography and SEM images of sorption media (a) CTS, (b) IFGEM-1, (c) IFGEM-4, (d) CPS and (e) ZIPGEM.

To further visualize the physical difference of the sorption media and analyze material morphology, and structure of the key elements of the media materials, SEM images of sand, clay, ZVI, and perlite are presented in Figure 5. When compared to sand and clay in general, ZVI and perlite have greater morphological structure variability. As shown in Figure 5(c) and 5(d), perlite exhibits *more* morphological alterations in nuclei, vacuoles, and shapes suggesting sophisticated surface areas for intraparticle diffusive processes during adsorption. ZVI has surface structural, morphological, and chemical attributes that can aid in oxidation and adsorption by increasing the available contact spaces for water and oxygen. The clay particles exhibit a crystalline structure. Moreover, the smaller particle sizes of clay can overpower the benefits of clay richness in Al if the content of clay in the sorption media is too high, as it can create possible clogging issues due to blockage of the pore spaces of the media. The richness of perlite and sand in Si and Al can provide

larger particle size and reduce clogging issues in sorption media. Hence a suitable media mix is critical to further support sorption and adsorption for color removal.

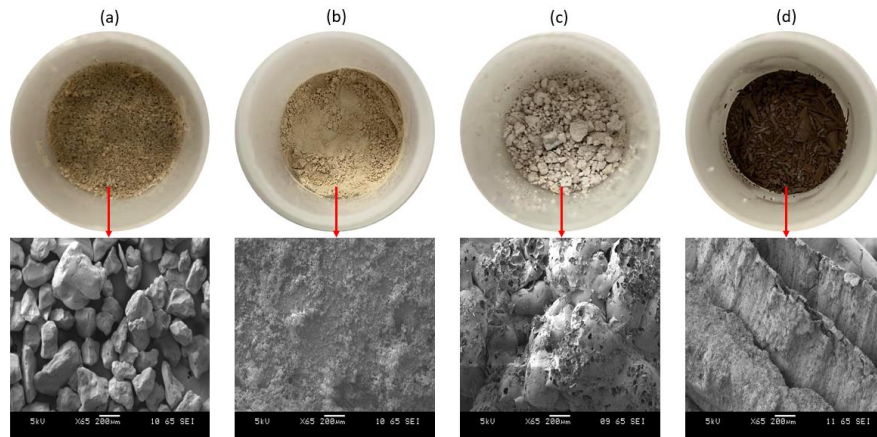


Figure 5. Photography and SEM images of composition of media materials where (a) is sand, (b) is clay, (c) is perlite and (d) is ZVI.

2.3.2. Color Removal Efficiency

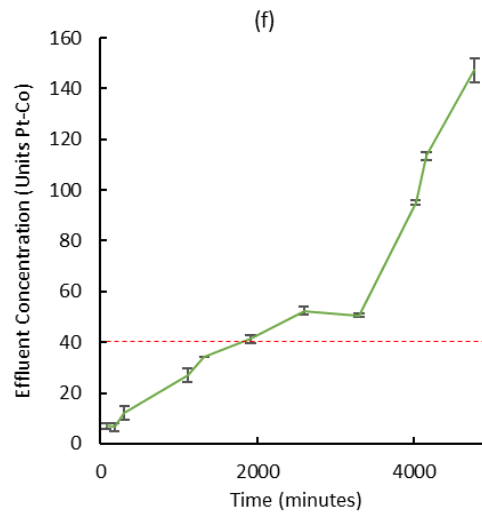
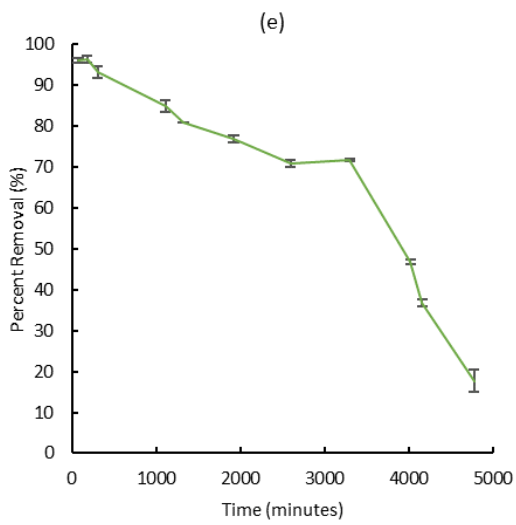
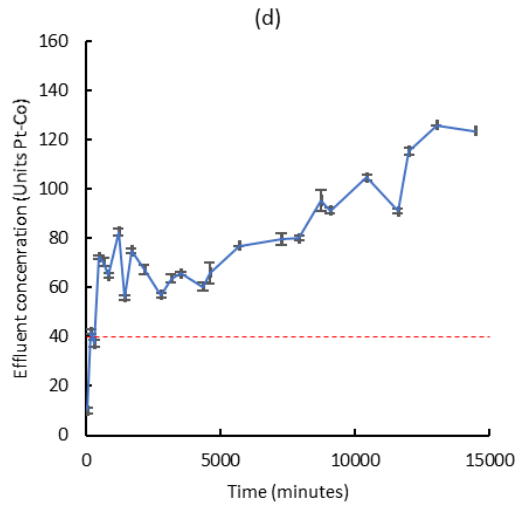
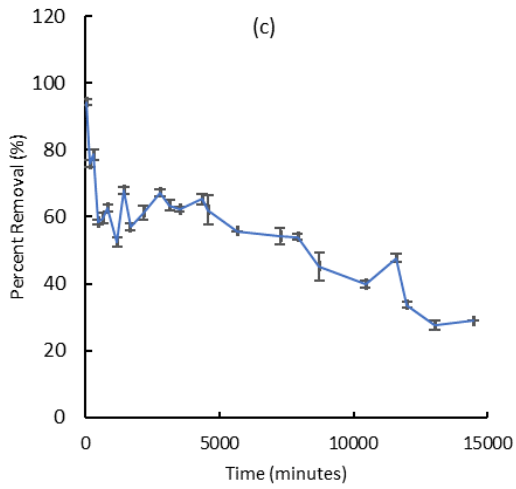
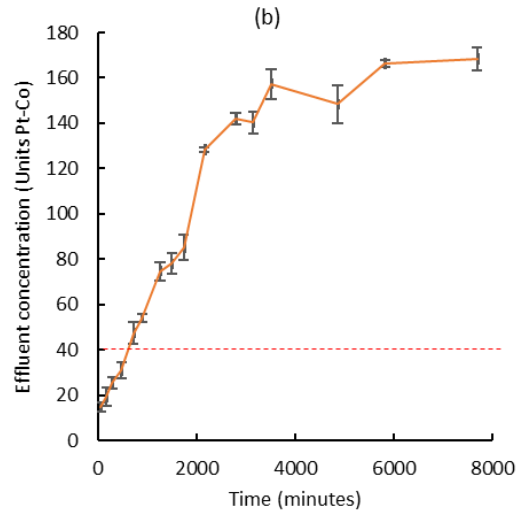
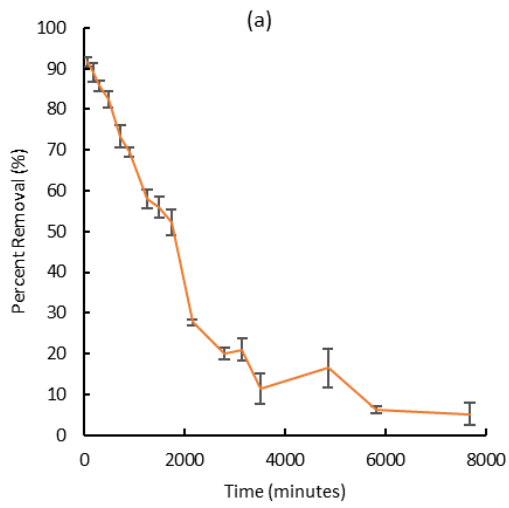
To meet the requirement imposed by the St. John River Management District for source water, color concentration of source water must be less than 40 Pt-Co color units. As the influent water influent concentration is 175 ± 10 Pt-Co units the media needs to achieve about 77% color removal. The results of the columns study in terms of time (minutes) vs. color removal efficiency (%) are presented in Figure 6, and the times when the media removal efficiency drop below 77% and the terminal time point of the five media reaching the regulatory limit in this column study are summarized in Table 7. When comparing the results, it is observed that the color removal efficiency for IFGEM-1 was the first one to drop below 77% after 200 minutes, resulting in effluent concentration above the standard (40 Pt-Co color units). Following IFGEM-1 in ascending order is CPS, CTS, IFGEM-4, and ZIPGEM which maintained appropriate color removal for the first 325, 600, 1,500 and 14,080 minutes respectively (Table 7). While IFGEM-1 was the first one to

drop below 77% removal efficiency, it reached terminal time point later than CTS (2,652 minutes) and CPS (5,820 minutes). The extended breakthrough curve for IFGEM-1 can be associated with the presence of ZVI, which can contribute to color removal by ionic interactions. The benefit of ZVI in some media mixes can be further observed by the results of IFGEM-4 (Figure 6(c)), obtaining color removals above 77% for about 1,500 minutes. In this study, some of the media reached terminal time point due to ponding issues before the end of the life cycle of media, indicating that the ZVI content in the media might be too high.

The sorption media ZIPGEM, a media mix of ZVI, perlite, clay, and sand stood out at the final stage for the color removal. As presented in Figure 6(e), ZIPGEM had the best performance among all the media recipes in this study, as effluent concentrations below 40-unit Pt-Co were observed for prolonged times. Additionally, a possible recovery of the adsorption capacity of ZIPGEM around 40,000 minutes was observed when the color removal efficiency increased to ~74.5%. Such phenomenon might be due to the synergetic effects among several different ingredients of ZVI, clay, sand, and perlites. However, ZIPGEM shows ponding and clogging issues at time 52,480 minutes (875 hours), before the media reached the ending point of life cycle.

Clogging and ponding may be associated with the ZVI particles undergoing oxidization, resulting in iron oxide clogging of the pore space in the media mix and affecting the infiltration negatively. Given that some Al and Fe can be dissolved in water the major tannic acid removal mechanism could be chemical precipitation driven by the formation of solid organometallic complexes, the emergence of Al-tannate can also contribute to clogging issues. The higher the content of ZVI, the larger the chance to have a ponding effect due to accumulation of aluminum and iron salts on the surface of Si (found in sand). The ZVI and sand ratio were calculated for

IFGEM-1, IFGEM-4 and ZIPGEM based on the media matrix (Table 3) resulting in 0.04, 0.11 and 0.071 (ZVI/Sand percent by volume), with these results it can be recommended that, to avoid ponding issues, the ZVI to sand ratio should be less than 0.071. However, since the clogging issue in ZIPGEM occurred long after the media stopped efficiently treating the influent when the color exceeded 40-unit Pt-Co, this issue is not an immediate concern. The strong performance of ZIPGEM can be attributed to a larger surface area and hydraulic conductivity, high porosity, and better morphological structure among the media mixes in this study, with stronger ionic interactions, van der Waals forces, and hydrogen bonding effect.



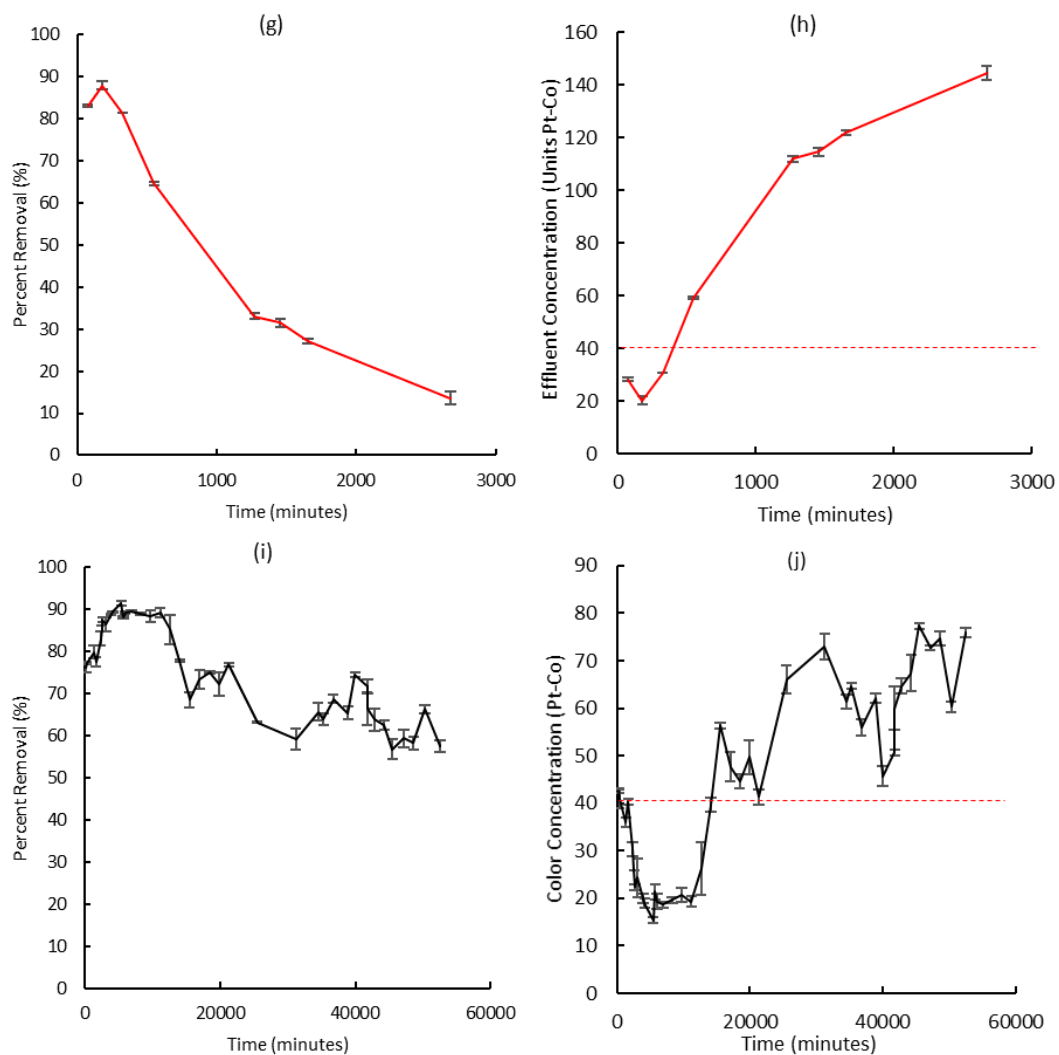


Figure 6. The dynamic color removal efficiency curves and breakthrough curves for (a) and (b) of CTS, (c) and (d) of IFGEM-1, (e) and (f) of IFGEM-4, (g) and (h) of CPS, and (i) and (j) of ZIPGEM, respectively

Table 7. Summary of dynamic performance in column studies

Media name	Mass of media (kg)	Time for the effluent to be <40 Pt-Co (minutes)	Terminal time point (minutes)
CTS	1.60	600	5820
IFGEM-1	1.44	200	11460
IFGEM-4	1.84	1,500	*4602
CPS	1.28	325	2675
ZIPGEM	1.64	14,080	*52,480

*Terminal time points were reached due to clogging issues.

2.3.3. Removal Mechanism

Tannic acid has a tendency to spontaneously adsorb to different surfaces to yield a hydrophilic coating (Ball and Meyer, 2016). Kaal et al. (2005) suggested the interactions between soil minerals and tannins result in adsorption. Wang, et al. (Wang et al., 2010) discovered that the adsorption mechanism is heterogeneous, and dependent on pH and ionic strength. Ball, et al. (Ball and Meyer, 2016) indicated that the adsorption of tannic acid to silicate is completed after about 15 minutes revealing that it produces a thin layer on SiO₂. The removal of tannic acids with clay is also related to adsorption. Attapulgite/CoFe₂O₄ was developed by Teng, et al. (Teng et al., 2019) for tannic acid removal, and the main mechanism responsible for the sorption was hydrogen bonding and surface complexation. As mentioned by Amari et al. (2021), however, attapulgite clay coated with chitosan was found to adsorb 95.3 mg g⁻¹ of tannic acid driven by electrostatic interactions, hydrogen bonding, and Van der Waals forces (Deng et al., 2012b). Furthermore, since the anionic functional groups of tannic acid include hydroxyl and carboxyl groups it can adsorb on oxide surfaces (Zhang et al., 2009). Tannic acid is negatively charged, hence Ca²⁺ can aid to bind negatively charged surfaces such as species of tannic acid (Perez-Benito, 2003; Zhang et al., 2009).

Besides, an Al ion has the possibility of interacting with multiple tannic acid molecules and the formation of insoluble complexes resulting from aluminum compounds such as Al-OH at low and high pH. While at pH between 5-6, when Al(OH)₃ is the predominant form, complex formation is replaced by adsorption onto Al(OH)₃ surface (Georgantas and Grigoropoulou, 2006). The coprecipitation of tannic acid with Al(OH)₃ occurs in the presence of hydrous aluminum oxide (e.g., Al(OH)₃) leading to soluble colloidal hydroxy-Al-tannate complexes (Omoike, 1999).

In the case of humic substances, Al-humic complexes are formed, and charge neutralization occurs (Georgantas and Grigoropoulou, 2006). Similarly, since tannic acid is a polymeric molecule, it can chelate with Fe^{3+} ions, producing an insoluble complex where the structure is contingent on the solution pH (Al-Mayouf, 1997).

Given the composition of NOM present in natural water, the color removal mechanism encompasses the process of precipitation, charge neutralization, entrapment, adsorption, and complexation with coagulant metal ions into insoluble particles. The reduction in tannic acid in water can also be attained by precipitation leading to the formation of solid complexes which can be separated in processes like coagulation and sedimentation. Omoike (1999) examined the effect of tannic acid on phosphate and organism matter removal during wastewater treatment. Inorganic salts of aluminum or iron are primary coagulants in natural or engineered systems that can hydrolyze to generate insoluble precipitates and entrap particles, neutralizing the charge on the particles. As mentioned in Section 2.3.3, accumulation of positively charged aluminum and iron salts (i.e., coagulating metal ions) on the surface of Si given the suitable pH values in water, could also attract negatively charged particles. NOM removal with ferric salts has been reported in a range for 29-70% (Uyak and Toroz, 2007) and NOM can also react with polyvalent metal cations producing soluble metal-NOM complexes (Li et al., 2016b).

Interactions among components in media mixes are possible (Figure 7). For instance, Fe and sand interactions in Feoxide coated quartz (Qtz) sand were explored by Kaal et al. (2005) for tannic acid retention given the potential for tannin-Fe oxide binding. The interactions among the main ingredients (i.e., perlite, clay, sand, and ZVI) of ZIPGEM thus promote efficient color removal. Sand and perlite can work together via the retention of the precipitates (Al-tannin and

Fe-tannin complexes) in the porous space while aiding in adsorption. It should be noted that sand, clay, and perlite may share removal mechanisms pertaining to Al and Al-Si bonds given their chemical composition. The unique media morphology of ZIPGEM (Figure 4(e)) helps diffusion and dispersion. Dissolved Al comes from clay and perlite when pH values are appropriate.

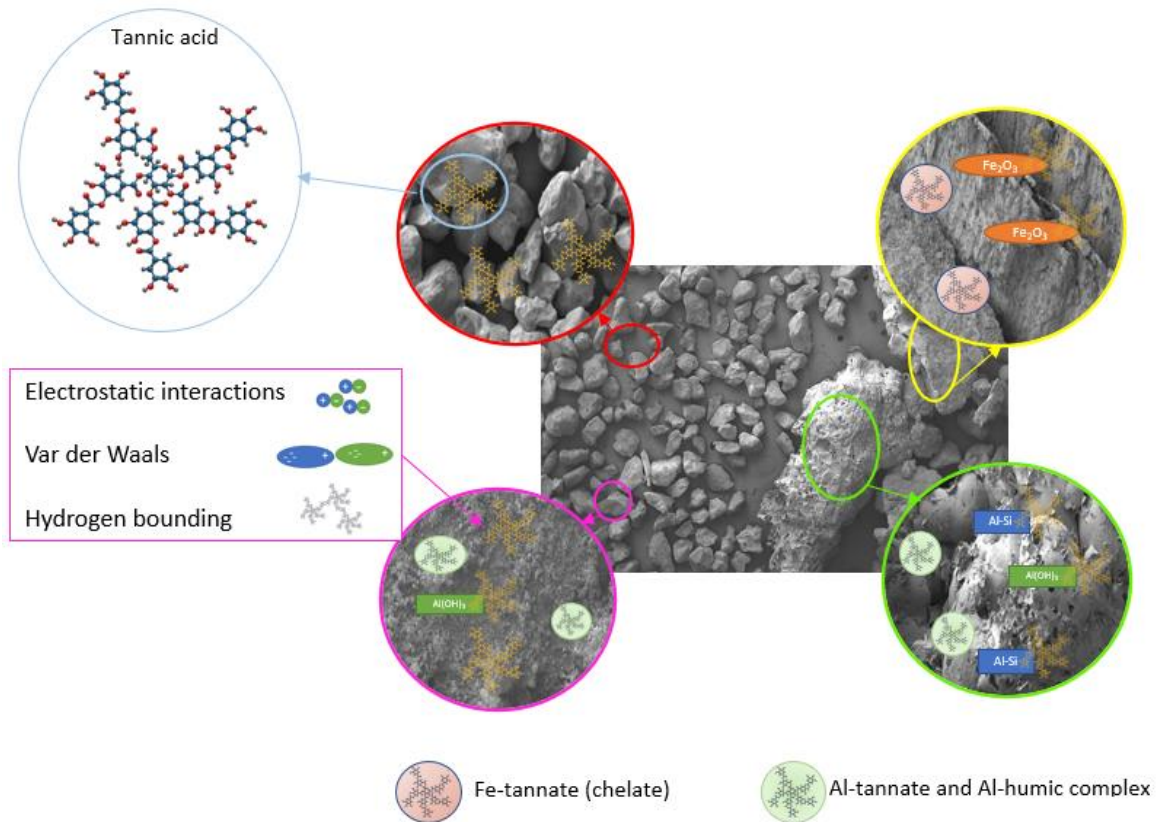


Figure 7. Graphical summary of the removal mechanisms in ZIPGEM

2.3.4. Dynamic Adsorption Modeling

The Yoon Nelson model is a kinetic empirical model that allows the estimation of the time needed for the media to reach 50% breakthrough (τ) ($C_t/C_0 = 50\%$). For CTS, IFGEM-1, IFGEM-4, CPS, and ZIPGEM this value was estimated as 2,152, 9,840, 3,382, 1,151 and 62,023 minutes, respectively. Alternatively, Thomas model parameters were selected for comparison as their

predictions were consistent having an appropriate r-squared value for all media ($R^2 > 0.6$). By comparing the q_0 it can be observed that ZIPGEM has the highest adsorption capacity (27.1 mg of Pt-Co·g⁻¹) among the tested sorption media. Thus, the efficiency of the media can be categorized in descending order based on the adsorption capacities (q_0) as ZIPGEM < IFGEM-1 < IFGEM-4 < CTS < CPS. Furthermore, in comparison to the Thomas model which predictions of q_0 for all the media were consistent, the MDR model showed an inconsistent prediction in q_0 for ZIPGEM ($q_0 = 421.52$ mg of Pt-Co·g⁻¹). Thus, despite the high r-squared value for MDR model, it was not selected as the preferred model to estimate the dynamic adsorption capacity (Figure 8).

Table 8. Parameters estimated from the linear regression of Thomas, MDR and Yoon Nelson dynamic modes for the sorption media CTS, IFGEM-1, IFGEM-4, CPS and ZIPGEM.

Media	Model	R ²	Parameter
CTS	Thomas	0.858	$k_T = 3.94 (10)^{-6}$ L·mg of Pt-Co ⁻¹ ·min ⁻¹ $q_0 = 1$ mg of Pt-Co·g ⁻¹
	MDR	0.898	$a_{mdr} = 1.22$ $q_0 = 0.494$ mg of Pt-Co·g ⁻¹
	Yoon-Nelson	0.858	$k_{YN} = 7(10)^{-4}$ min ⁻¹ $\tau = 2,151.57$ min (1.49 day)
IFGEM-1	Thomas	0.606	$k_T = 6 (10)^{-7}$ L·mg of Pt-Co ⁻¹ ·min ⁻¹ $q_0 = 4.80$ mg of Pt-Co·g ⁻¹
	MDR	0.731	$a_{mdr} = 0.44$ $q_0 = 2.66$ mg of Pt-Co·g ⁻¹
	Yoon-Nelson	0.606	$k_{YN} = 1.5(10)^{-3}$ min ⁻¹ $\tau = 9,840$ min (6.83 day)
IFGEM-4	Thomas	0.939	$k_T = 5.03 (10)^{-6}$ L·mg of Pt-Co ⁻¹ ·min ⁻¹ $q_0 = 1.31$ mg of Pt-Co·g ⁻¹
	MDR	0.960	$a_{mdr} = 1.40$ $q_0 = 0.03$ mg of Pt-Co·g ⁻¹
	Yoon-Nelson	0.939	$k_{YN} = 9(10)^{-4}$ min ⁻¹ $\tau = 3,382.33$ min (2.35 day)
CPS	Thomas	0.928	$k_T = 8.38 (10)^{-6}$ L·mg of Pt-Co ⁻¹ ·min ⁻¹ $q_0 = 0.64$ mg of Pt-Co·g ⁻¹
	MDR	0.885	$a_{mdr} = 1.09$ $q_0 = 0.37$ mg of Pt-Co·g ⁻¹
	Yoon-Nelson	0.928	$k_{YN} = 1.5(10)^{-3}$ min ⁻¹ $\tau = 1150.73$ min (0.8 day)
ZIPGEM	Thomas	0.676	$k_T = 1.67(10)^{-7}$ L·mg of Pt-Co ⁻¹ ·min ⁻¹ $q_0 = 27.1$ mg of Pt-Co·g ⁻¹
	MDR	0.354	$a_{mdr} = 0.27$ $q_0 = 421.52$ mg of Pt-Co·g ⁻¹
	Yoon-Nelson	0.676	$k_{YN} = 3(10)^{-5}$ min ⁻¹ $\tau = 62,023.3$ min (43 day)

2.3.5. Comparison of ZIPGEM with other adsorbents

The advantages of low cost, feasible field application and easy maintenance motivated innovation of different adsorbents, including agricultural waste, activated carbon, activated alumina, and zero-valent iron among the most popular. In their study, the color removal using the activated sand showed an efficacy of 70% in the first 3 minutes while the non-modified sand had an efficacy of 40%. More comparisons of different adsorbents for color removal are summarized in Table 9.

Table 9. Summary and confirmation of adsorption capacity in literature and in this study

Adsorbent	Adsorbent capacity	Description	References
Activated clay	153 and 28.3 mg·g ⁻¹	Tannic acid and humic acid	Chang and Juang. (2004)
Amino-functionalized magnetic mesoporous silica	510.2 mg·g ⁻¹	Tannic acid	Wang et al. (2010)
Sunflower stalks	105 and 317 mg·g ⁻¹	Methylene and basic red 9	Sun and Xu. (1997)
Orange Peel	19.88 mg·g ⁻¹	Aid Violet	Sivaraj et al. (2001)
Citrullus Lanatus rind	11.9 mg·g ⁻¹	Crystal Violet	Bharathi and Ramesh. (2013)
Iron based sludge	625, 833.34 and 333.34 mg·g ⁻¹	Direct blue 71, acid blue 40 and basic violet blue 16.	Kayranli. (2011)
Spherical Fe ₃ O ₄ nanoparticles	630 mg·g ⁻¹	Congo red dye	Chatterjee et al. (2020)
ZIPGEM	27.1 mg of Pt-Co·g ⁻¹	Color	Ordonez et al. (2022b)

2.3.6. Application potential

Different electrochemical, physicochemical, and photocatalytic methods allow for the removal of dyes for industrial wastewater treatment. In the traditional technology hub, microfiltration, ultrafiltration, and nanofiltration for removal of humic substances have shown potential and can remove 90 % of humic acids in water treatment plants (Lowe and Hossain, 2008). The removal of NOM (i.e., tannic and humic acid) by photocatalytic methods is an effective method too. An example is the degradation of dyes, detergents, and organic acids by TiO₂ nanofilms (Albu et al., 2007) with the aid of UV light due to their photocatalytic activity (occurring

at UV absorbance at the range of 254 nm ~ 370 nm) (Quan et al., 2005; Qaseem et al., 2020). In addition, the removal of tannic acid from wastewater by electrochemical oxidation was confirmed by Govindaraj et al.(2010). However, most of these existing technologies are costly and operationally complex due to regeneration and/or final disposal of sorbents while ZIPGEM can be used as daily coverage at landfills. It is helpful to estimate the replacement frequency upon the exhaustion of all adsorption capacity or reach the threshold (e.g., regulatory limit) to maintain reliable treatment. The life expectancy assessment curves based on a set of prescribed removal efficiency can be derived (Figure 8) to predict the volume of water treated over the media's usage life corresponding to the quantity of media selected. For demonstration, the life expectancy calculation is presented for an application of ZIPGEM in color removal in Lake Brooklyn, FL given the influent condition of 179 color units Pt-Co (e.g., C_o). Aiming for a target effluent color concentration at or below 40 color units Pt-Co per SJRWMD requirements (SJRWMD, 2021.), the removal efficiency R of 80% is selected for demonstration in this water pretreatment case based on the removal ranges (57-91% color removal as shown) and HRT (Figure 9). By employing the laboratory HRT of 3.7 h for ZIPGEM and the corresponding laboratory HLR of 31.06 gpd/ft² (1.27 m³/(m² d⁻¹)) (Table 2), the maximum flow rate ($Q_{\text{threshold}}$) and surface area $area_{\text{surface}}$ for the filter cell can be determined. Hence, the maximum flow rate $Q_{\text{threshold}}$ of 4.88 (10)³ L·d⁻¹ (0.0013 MGD) for a V_{void} of 0.75 m³ was calculated. Reducing the $Q_{\text{threshold}}$ by 20% to avoid unexpected flooding or ponding in water treatment filter, a controlled pumping flow rate or design flow rate (Q) of 3.91(10)³ L·d⁻¹ (0.0010 MGD) was selected for life expectancy estimation. Based on this controlled pumping flow rate (Q), the corresponding $area_{\text{surface}}$ of 3.09 m² (33.26 ft²) was determined. Note that the selected Q (design flow rate) is a function in terms of HRT, removal efficiency, and adsorption capacity of the adsorbent. For a design filter depth of approximately

0.30 m, a cell volume of 0.88 m^3 (31 ft^3) was required which corresponds to a design media mass of $2.46(10)^3 \text{ kg}$ in a treatment cell. The turning-line method in Figure 8 following the life expectancy curves can showcase the volume of water treated ($V_{\text{water treated}}$) over the media useful life corresponding to the quantity of media needed ($\text{mass}_{\text{media}}$) in a treatment cell. The value to treat a specific volume of water was determined as 0.47 ML (0.12 MG) in such a filter cell from which the estimated life expectancy corresponding to this $V_{\text{design water treated}}$ is 119.21 d (0.33 y) based on approximately 2.5 tons of ZIPGEM.

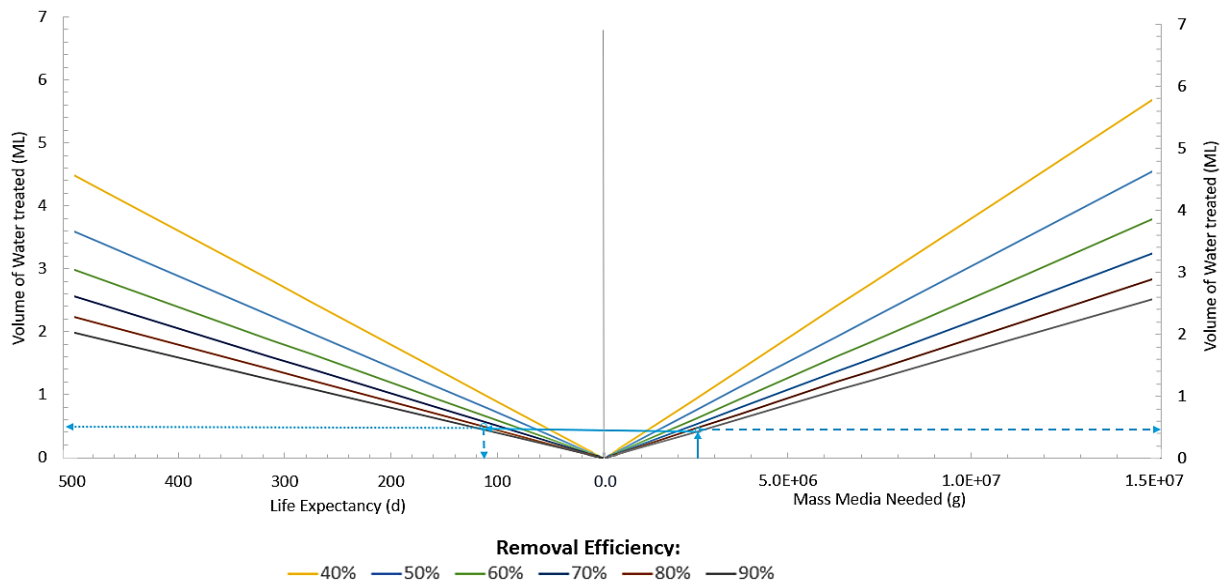


Figure 8. Life expectancy curves for volume of water expected to be treated by various masses of ZIPGEM for $C_0=175 \pm 10$ units Pt-Co

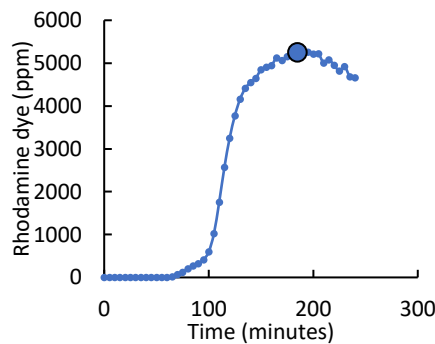


Figure 9. Rhodamine tracer study for ZIPGEM based on 1-ft long 3'' diameter column (1,200 ml of media) with influent flow rate of $4 \text{ ml}\cdot\text{min}^{-1}$

2.3.7. Risk assessment

It is important to ensure that implementation of the sorption media as a pretreatment system does not have any side effect that can have any negative health or environmental impact. For instance, long-term human exposure to aluminum can cause encephalopathy, anemia, and bone disease in dialyzed patients (Colomina and Peris-Sampedro, 2017). Moreover, iron is an essential element for living organisms as it contributes to oxygen transportation and electron transport. Yet, if the iron intake is excessive, it can lead to tissue damage (Abbaspour et al., 2014). The EPA in the US has established standards for iron and aluminum ion concentration under the secondary drinking water standards. Under these standards, the EPA has recommended that the concentration of aluminum and iron in drinking water should not exceed the concentrations of 0.2 and 0.3 mg·L⁻¹, respectively. Moreover, the World Health Organization indicated that the aluminum levels in drinking water facilities using aluminum sulfate coagulation ranges from 0.1 to 2.7 mg·L⁻¹.

Therefore, effluent samples from each column were analyzed in terms of dissolved aluminum and dissolved iron ion concentration to confirm that there was no harmful leachate with these metals from the sorption media. The results from CTS and CPS (Table 10) indicate some increase in the dissolved aluminum ion concentration, yet the results did not exceed the concentration of aluminum found previously in drinking waters treated with aluminum sulfate coagulate. On the contrary, IFGEM-1, IFGEM-4 and ZIPGEM effluents did not contain dissolved aluminum, on the contrary, they provided aluminum removal. Removal was observed in terms of dissolved iron in the ZIPGEM column. In IFGEM-4, iron concentration increase was observed after 69 hours potentially driven by clogging in the column as dissolved iron increased in the effluent.

Table 10. Effluent concentrations of dissolved iron and aluminum ions in the effluent given the influent concentration listed at the third row.

CTS		IFGEM-1			IFGEM-4			CPS		ZIPGEM		
Time (hour)	Dissolved Aluminum ions (mg/L)	Time (hour)	Dissolved Iron ions (mg/L)	Dissolved Aluminum ions (mg/L)	Time (hour)	Dissolved Iron ions (mg/L)	Dissolved Aluminum ions (mg/L)	Time (hour)	Dissolved Aluminum ions (mg/L)	Time (hour)	Dissolved Iron ions (mg/L)	Dissolved Aluminum ions (mg/L)
Inf	0.3	Inf	0.0	0.3	Inf	1.1	0.3	Inf	0.6	Inf	1.1	0.3
37	0.4	3	0.0	0.9	5	0.6	0.0	5	0.5	3	0.1	0.0
81	0.4	53	0.0	0.0	32	1.1	0.1	28	0.8	22	0.5	0.0
128	0.4	151	0.0	0.0	69	3.1	0.0	--	--	115	0.5	0.0

*Inf stand for Influent

2.4. Chapter Conclusion

The source water to be utilized for drinking water supply is oftentimes troubled by the presence of NOM (i.e., tannic and humic acid). Adsorption is still one of the most cost-effective treatment methods for the removal of color for drinking water treatment. This study proposed a low maintenance alternative for any *in-situ* pretreatment of drinking water sources. Five low-cost sorption media were produced and tested by fixed bed column studies to determine the color removal efficiency. Given the influent condition of 175 ± 10 Pt-Co units, the adsorption capacity can be ranked in terms of how long the proposed media sustained the color removal of ~77% or greater. ZIPGEM was ranked the first followed by IFGEM-1, IFGEM-4, CTS, and CPS. ZIPGEM maintained the effluent below 40 Pt-Co units for about 14,000 minutes based on the media mix of 1,200 ml by volume and the prescribed adsorption capacity. Such performance can be attributed to the inclusion of both perlite and ZVI and synergetic effects between clay and sand. With the predicted Thomas model parameter, the adsorption capacity of ZIPGEM ($27.1 \text{ mg of Pt-Co} \cdot \text{g}^{-1}$) was superior to the adsorption capacity of the rest of four sorption media in this study. Moreover, observed morphology of ZIPGEM shown by SEM indicated a heterogenous surface further

supporting the longer duration of color removal observed. Such synergistic interactions among the four ingredients with unique morphological structure promoted color removal by improving physicochemical interactions via better dispersion and diffusion. Future work can be emphasized by the in-situ applications of ZIPGEM to either pretreat source water to be utilized for drinking water supply or treat wastewater with high color content (e.g., dye content in textile wastewater).

CHAPTER 3: EXPLORING SIMULTANEOUS REMOVAL OF MICROCYSTIN AND PHOSPHORUS VIA SPECIALTY ABSORBENTS FOR EUTROPHIC WATER TREATMENT

3.1. Introduction

Global economic development, rapid population growth, and deforestation have deeply impacted natural resources management and called for more environmental pollution control owing to disrupted nutrient cycle (Setoguchi et al., 2022). The presence of HABs driven by eutrophication not only leads to detrimental effects on aquatic ecosystems, but also exhibits an impact on human health. HABs contain cyanobacteria, which can uptake the oxygen and nutrients in an aquatic system. Moreover, cyanobacteria produce cyanotoxins, which greatly affect the ecosystem's health in an aquatic environment (Sultana et al., 2022). The cyanotoxins include microcystins (MCs), cylindrospermopsin, and anatoxin-a group, where MCs' toxins are often dominant (Filatova, 2021, Su et al., 2017). MCs are cyclic heptapeptide toxics and are categorized as the most toxic cyanotoxin species. Microcystin-LR (MC-LR), a type of MC, is the most common and toxic algae toxin with a median lethal dose (LD50) of $50 \mu\text{g}\cdot\text{kg}^{-1}$ of body weight (Bláha et al., 2009). According to the United States Environmental Protection Agency (USEPA), MC-LR has acute human health effects including abdominal pain, headache, sore throat, vomiting and nausea, diarrhea, blistering, and pneumonia (EPA, 2021). Moreover, the International Agency for Research on Cancer has associated MC-LR with a possible human carcinogen (Lone et al., 2015), and some epidemiological researchers have proposed a correlation between liver cancer and MCs (Rao and Bhattacharya, 1996; Žegura et al., 2003). To mitigate the effects of MCs on human health, both the World Health Organization (WHO) and the USEPA have passed regulations to control the concentration of MCs in drinking and recreational waters. For instance,

the WHO has set provisional guidelines for drinking water and recreational water concentrations not to exceed $1 \mu\text{g}\cdot\text{L}^{-1}$ and $24 \mu\text{g}\cdot\text{L}^{-1}$, respectively (WHO, 2020). Moreover, the USEPA has set the drinking water health advisory (average of 10th days) to $1.6 \mu\text{g}\cdot\text{L}^{-1}$ and a criterion of $8 \mu\text{g}\cdot\text{L}^{-1}$ of MCs for recreational water (USEPA, 2015).

Considering the drinking water guidelines and health advisory concentrations, efforts to treat MC in drinking water have been intensified. Current technologies applied for removing MCs from water include nanofiltration (Selezneva et al., 2021; Teixeira and Rosa, 2005), ultrafiltration (Lee and Walker, 2008; Zhan and Hong, 2022), and reverse osmosis (Neumann and Weckesser, 1998; Zhan and Hong, 2022), yet these technologies are applicable mostly to drinking water treatment. Other technologies such as chlorination (Zhang et al., 2019) and ozonation (Shawwa and Smith, 2001) have also demonstrated efficient removals of MCs; however, these technologies can result in disinfectant by-products if not properly dosed (Hu et al., 1999). Other separation and purification techniques such as photolysis (Almuhtaram et al., 2021), microbial degradation (Dziga et al., 2013), and Fenton reaction (Lopes et al., 2017) have been employed albeit costly.

Because MCs tend to be adsorbed in organic substances, granulated activated carbon (GAC), and powdered activated carbon (PAC) have been widely employed for adsorption of MCs (Lopes et al., 2017). Lambert et al. (1996) studied the performance of GAC and PAC in a drinking water treatment system and concluded that 80% of MCs was removed from raw water, meeting the guidance level for drinking water set by Health Canada. Meanwhile, the removal of 4 MCs (MC-LR, MC-LY, MC-LW, MC-LF) onto PAC under the presence of natural organic matter (NOM) was explored along with the effect of ionic strength. It was concluded that the presence of Ca^{2+} improved adsorption (Campinas and Rosa, 2006). Pavagadhi et al. (2013) indicated that high

adsorption capacity was observed by graphene oxide for MC-LR ($1,699.7 \mu\text{g}\cdot\text{g}^{-1}$) and Microcystin-RR (MC-RR) ($1,877.8 \mu\text{g}\cdot\text{g}^{-1}$). Furthermore, Pavagadhi et al. (2013) explored the effect that different anions and cations (e.g., normal environmental pollutants such as phosphate, nitrate, and heavy metals) have on the MC-LR and MC-RR adsorption capacity of graphene oxide and concluded that some environmental pollutants might reduce the adsorption capacity of graphene oxide for MC-LR but not for MC-RR. Other researchers found that kaolinite, illite, and montmorillonite can also affect adsorption of MC-LR (Liu et al., 2019b). For example, Morris et al. (2000) discovered that kaolinitic and montmorillonitic clay materials can remove MC-LR from water, achieving a removal rate of up to 81%. The high adsorption capacity of sediments is suggested from the interaction between surface-bound NOM in the material that binds to the hydrophobic β -(2S, 3S, 8S, 9S)-3-amino-9-methoxy-2, 6, 8-trimethyl-10-phenyldeca-4,6-dienoic acid (Adda) group of MC-LR via hydrophobic bonding (Liu et al., 2019b). Moreover, other researchers found better MC-LR adsorption to iron oxide nanoparticles at lower fulvic acid concentrations by enhancing the hydrophobic attraction of the MC-LR (Lee and Walker, 2011). It was observed that the negative net charge of MC-LR molecules can be adsorbed by kaolinite at varying pH values from 2.19 to 12.48 (de Maagd et al., 1999).

The physical and chemical characteristics of the waterbody can affect MC production. For instance, Baldia et al. (2003) indicated that the production of MCs was higher when the transparency and the conductivity of water were high, with a production rate of $88.6 \mu\text{g}$ per 100 mg of dried cell, while PO_4^{3-} acted as a limiting constraint. Li et al. (2012) suggested that MC-LR biodegradation by winter biofilm was inhibited in the presence of phosphate because its complete degradation was extended from 7 days to 10 days. Moreover, Yuan et al. (2014) presented a

threshold below $570 \mu\text{g}\cdot\text{L}^{-1}$ of TN and $37 \mu\text{g}\cdot\text{L}^{-1}$ of chlorophyll-a or $1,100 \mu\text{g}\cdot\text{L}^{-1}$ of TN and $3 \mu\text{g}\cdot\text{L}^{-1}$ of chlorophyll-a to maintain the concentration of MC below $1 \mu\text{g}\cdot\text{L}^{-1}$. Much of Florida's landscape consists of a karst limestone environment, and thus Florida's aquifer supplies more than 8 billion gallons of water each day, providing 90% of the state's drinking water. Therefore, the understanding of the biogeochemical processes in these environments is imperative because these environments are prone to contamination given their morphology (i.e., cracks and crevasses). Karst environments are rich in Ca^{2+} ; however, they are low on metals availability and biodegradation efficiency. Karst environments are usually high on permeability and have short hydraulic residence time; for this reason, denitrification potential is very low, while nitrification is high. The presence of cyanotoxins in the cave passages at Mammoth National Park was investigated by Byl et al. (2021), and the concentration in 10 caves of MCs ranged from $0.154\text{--}2.59 \mu\text{g}\cdot\text{L}^{-1}$. Florida's ecosystems have been highly affected by HABs, partially owing to the presence of abundant phosphate; for instance, Philips et al. (2011) reported the presence of 24 HAB species, of which 16 were toxin producers, in the Indian River Lagoon. HABs also cause economic impacts, for instance, the Indian River Lagoon, located in Florida, reported an economic impact of $\sim\$197\text{M}$ loss/year between 2011 and 2013 (Lapointe et al., 2015).

Thus, the motivation of this study is to develop a low-cost green sorption media capable of removing MC-LR *in-situ* over different landscapes during the emergency events, while maintaining environmental sustainability by an easier way through rapid deployment on an as-needed basis anywhere. Three green sorption media known as Clay-Perlite and Sand (CPS), Zero-valent-Iron- and Perlite-based Green Environmental Media (ZIPGEM), and Biochar-zero-valent-Iron- and Perlite-based Green Environmental Media (BIPGEM) were selected for a series of

isotherm studies with distilled (DI) water to first quantify the adsorption capacity of these green sorption media. Subsequently, a fixed-bed column study with water collected from a canal (C-23) close to the Indian River Lagoon was utilized as an influent to investigate the MC-LR removal rates and removal mechanisms. The research questions to be answered include: 1) What is the role of iron filings in ZIPGEM for the adsorption of MC-LR? 2) What is the differential effect of having biochar in BIPGEM on top of other common ingredients in ZIPGEM for MC-LR removal? 3) What is the effect of the coexistence of phosphate or calcium on the MC-LR removal efficiency of CPS, ZIPGEM, and BIPGEM? 4) How does the nature of local water matrix affect the removal efficiency of the sorption media?

3.2. Material and Methods

3.2.1. Media characterization

The adsorption capacities and removal mechanism of MC-LR of the three selected green sorption media were explored in this study. The sorption media CPS is composed of 92% sand, 5% clay, and 3% perlite in percentage by volume and was selected as control for the effectiveness of ZVI and biochar sequentially to investigate the differential effect due to the inclusion of zero valent iron (ZVI) and biochar as media component in sequence within ZIPGEM and BIPGEM. ZIPGEM is composed of 85% sand, 5% clay, 5% ZVI, and 5% perlite, and BIPGEM is composed of 80% sand, 5% clay, 5% ZVI, 5% perlite, and 5% biochar in percentage by volume. The physical and chemical characteristics of the media were investigated for a better interpretation of the media removal mechanism. The density and Brunauer-Emmett-Teller (BET) surface area were analyzed by EMSL Analytical Laboratory. The saturated hydraulic conductivity and porosity were determined in a geotechnical laboratory at the University of Central Florida (UCF). The point of

zero charge (PZC) was measured at a chemical laboratory at UCF following the salt addition method (Bakatula et al., 2018; Mahmood et al., 2011). The methodology followed in this study was presented in detail by Ordonez et al. (2022a). Finally, the chemical composition of the media and the individual components was measured at the Advanced Materials Processing and Analysis Center at UCF via an X-ray fluorescence (XRF) analysis.

3.2.2. Chemicals

The MC-LR standard solution utilized for the isotherm studies was acquired from Sigma-Aldrich in liquid form with a concentration of 2.5 mM. The MC-LR standard for the column studies was obtained from Cayman chemical in a solid form. The MC-LR standard was first dissolved in methanol in accordance with its solubility point of 10 mg·ml⁻¹. The formal name for the MC-LR is cyclo[2,3-didehydro-N-methylalanyl-D-alanyl-L-leucyl-(3S)-3-methyl-D-β-aspartyl-L-arginyl-(2S,3S,4E,6E,8S,9S)-3-amino-9-methoxy-2,6,8-trimethyl-10-phenyl-4,6-decadienoyl-D-γ-glutamyl], and its molecular form is C₄₉H₇₄N₁₀O₁₂ (Figure 10).

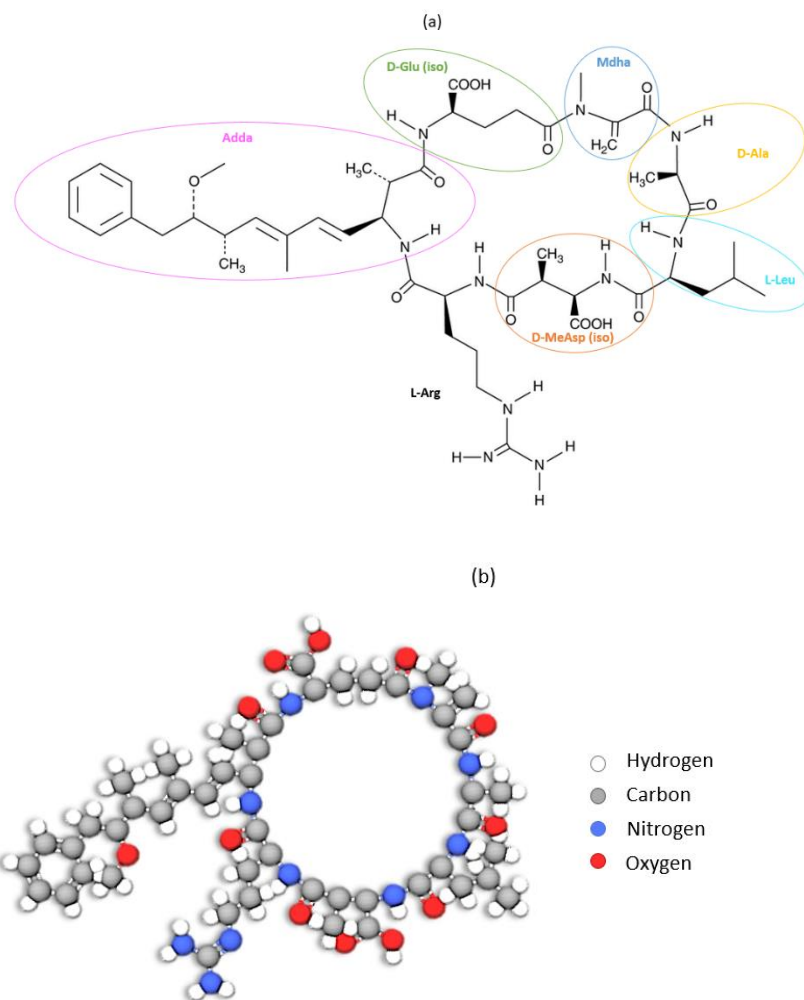


Figure 10. (a) MC-LR chemical structure [modified from Cayman Chemical, accessed: 2/2/2023], and (b) 3-D structure of the MC-LR [modified from MolView.org, accessed: 2/2/2023].

3.2.3. Isotherm study

A series of equilibrium isotherms (i.e., stepped isotherms) were performed on the sorption media (i.e., CPS, ZIPGEM, and BIPGEM) to determine its MC-LR adsorption capacity and the effect the coexistence of phosphate (PO_4^{3-}) or calcium (Ca^{2+}) has on the MC-LR removal potential. In the first equilibrium isotherm (denoted as Case 1 hereafter), 5 aliquant on Erlenmeyer Flask were set with 10 g of media and 250 ml of DI water spiked with MC-LR to different initial concentrations ranging from 5–350 $\mu\text{g}\cdot\text{L}^{-1}$ (5, 35, 50, 100, and 350 $\mu\text{g}\cdot\text{L}^{-1}$ denoted as Condition 1,

Condition 2, Condition 3, Condition 4, and Condition 5, respectively). In the second and third isotherm studies (denoted as Case 2 and Case 3, respectively, hereafter) the same protocol was followed; however, the initial conditions were modified by including PO_4^{3-} to a concentration of $20 \text{ mg}\cdot\text{L}^{-1}$ (i.e., Case 2) or Ca^{2+} to a concentration of $30 \text{ mg}\cdot\text{L}^{-1}$ (i.e., Case 3) across all influent conditions (Table 1) to mimic the real-world situation in a karst environment with nutrient contamination (i.e., South Florida environment). The resultant solutions were shaken in a shaking platform for 24 hours at 160 rpm. At the conclusion of the shaking time the solutions were left to settle for 1 hour. Subsequently, duplicate water samples with 100 ml of the resultant solutions were collected in a plastic bottle to be delivered to an external lab (i.e., Green Water laboratories) for MC-LR analysis.

Guo et al. (2017) compared the analysis of MCs in drinking water by enzyme-linked immunoassay (ELISA) and LC-MS/MS method, finding that the LC-MS/MS results were more reliable than those from ELISA. Hence, water samples in this study delivered to Green Water laboratory in Palatka, Florida were analyzed for total MC with a Liquid Chromatography – Mass Spectrometry/Mass Spectrometry (LC-MS/MS) following the MMPB (2R-methyl-3S-methoxy-4-phenylbutanoic acid) method (Foss et al., 2020). An extra set of samples was collected and analyzed for PO_4^{3-} or Ca^{2+} concentration via in-house Hach measuring kits. The Hach product TNT844 was utilized to analyze the samples for PO_4^{3-} , and the Hach product TNT869 was utilized to analyze the samples for Ca^{2+} concentrations. Water samples analyzed for PO_4^{3-} or Ca^{2+} were previously filtered via a $0.45 \mu\text{m}$ membrane filter. To minimize the risk of the MC-LR adsorbing to the Erlenmeyer flask or sampling bottles, each of the flask and sampling bottles was rinsed 3 times with the spiked solution or the corresponding water sample prior to sample storage.

Table 11. Summary of the different influent conditions and cases examined in batch tests.

	Case 1	Case 2	Case 3
Control		20 mg·L ⁻¹ PO ₄ ³⁻	30 mg·L ⁻¹ Ca ²⁺
Condition 1	5 µg·L ⁻¹	5 µg·L ⁻¹ + 20 mg·L ⁻¹ PO ₄ ³⁻	5 µg·L ⁻¹ + 30 mg·L ⁻¹ Ca ²⁺
Condition 2	35 µg·L ⁻¹	35 µg·L ⁻¹ + 20 mg·L ⁻¹ PO ₄ ³⁻	35 µg·L ⁻¹ + 30 mg·L ⁻¹ Ca ²⁺
Condition 3	50 µg·L ⁻¹	50 µg·L ⁻¹ + 20 mg·L ⁻¹ PO ₄ ³⁻	50 µg·L ⁻¹ + 30 mg·L ⁻¹ Ca ²⁺
Condition 4	100 µg·L ⁻¹	100 µg·L ⁻¹ + 20 mg·L ⁻¹ PO ₄ ³⁻	100 µg·L ⁻¹ + 30 mg·L ⁻¹ Ca ²⁺
Condition 5	350 µg·L ⁻¹	350 µg·L ⁻¹ + 20 mg·L ⁻¹ PO ₄ ³⁻	350 µg·L ⁻¹ + 30 mg·L ⁻¹ Ca ²⁺

The different concentrations in this study were selected given the wide range of concentrations at which MC-LR is found in different environments. For instance, the presence of MC-LR has been found in different drinking water sources or public reservoirs. In Sao Paulo, Brazil, concentrations ranging from 0.5–100 µg·L⁻¹ were found in a public reservoir (Nobre, 1997), while concentrations up to 1.25 µg·L⁻¹ were detected in Pará, in the Brazilian Amazonia (Vieira et al., 2005). Different aquatic systems have also been affected with high concentrations of MC; for instance, the concentrations of MC-LR in the Indian River Lagoon in the state of Florida ranged from 0.01–85.70 µg·L⁻¹ between 2018 and 2019, with higher concentration detected during the wet season (May to October) (Laureano-Rosario et al., 2021). Moreover, Billam et al. (2006) reported MC-LR concentration in 2 lakes in Texas with concentrations ranging from 0.096–4.914 µg·L⁻¹ in Buffalo Spring Lake and 0.2–5.83 µg·L⁻¹ in Lake Ransom Canyon, and in both lakes higher concentrations were observed during the spring season. The issue with high concentrations of MC extends outside of the USA; for instance, in Beira Lake in Sri Lanka, MC-LR concentrations varied from 11,450–25,230 µg·L⁻¹, with higher concentration targeted within the rainy season (Piyathilaka and Manage 2017).

3.2.4. Equilibrium isotherm

Data collected for MC-LR concentration at different influent conditions were analyzed in terms of percentage removal as well as for its absorption capacity by the Langmuir and Freundlich isotherm models. The Langmuir isotherm has been widely used to explore the adsorption capacity of different sorption materials in the past few decades (Ho and Chiang, 2001). Different linearization of the Langmuir model can be found in literature; however, Guo and Wang (2019) suggested that the linear form presented in Eq. 12 can better estimate the Langmuir parameters. In this equation the parameter q_e is the amount of sorbate adsorbed per unit weight ($\mu\text{g}\cdot\text{g}^{-1}$) of the sorption media, and it can be calculated following Eq. 12. In Eq. 12, m is the mass of the sorption media in grams, C_o is the initial concentration on the solution in $\mu\text{g}\cdot\text{L}^{-1}$, C_e is the concentration of the solution at equilibrium in $\mu\text{g}\cdot\text{L}^{-1}$, and V is the volume of the solution in L. Moreover, the Langmuir parameters K_L and q_m correspond to the Langmuir equilibrium constant ($\text{L}\cdot\mu\text{g}^{-1}$) and the maximum adsorption capacity of the absorbent ($\mu\text{g}\cdot\text{g}^{-1}$), respectively, and are retrieved from the regression plot of $\frac{C_e}{q_e}$ vs. C_e .

$$q_e = \frac{q_m b C_e}{1 + b C_e} \quad (11)$$

$$\frac{C_e}{q_e} = \frac{1}{q_m} C_e + \frac{1}{K_L q_m} \quad (12)$$

$$q_e = \frac{(C_o - C_e)V}{m} \quad (13)$$

The Freundlich isotherm model is an empirical equation, and its nonlinear form is presented in Eq. 14, while one of the most common linear forms is presented in Eq. 15 (Appel, 1973). The linear form of the Freundlich equation is obtained from the linear regression $\ln q_e$ vs. $\ln C_e$, where the slope of the line is $1/n$ and the K_F is calculated from the x-interception. The $1/n$

parameter indicates the adsorption intensity where the adsorption is favorable if $1/n$ is between 0 and 1 ($0 < 1/n < 1$), yet if $1/n$ is greater than 1 ($1/n > 1$) then the adsorption is unfavorable.

$$q_e = K_F C_e^{\frac{1}{n}} \quad (14)$$

$$\ln q_e = \frac{1}{n} \ln C_e + \ln K_F \quad (15)$$

3.2.5. Statistical analysis

Data obtained from the isotherm studies were subjected to a 1-way and a 2-way Analysis of Variance (ANOVA) test without replication with the data analysis module in Microsoft Excel. The 1-way ANOVA is utilized to test if there is any statistically significant difference between the means of different groups (Ross et al., 2017). Three assumptions are considered in 1-way ANOVA including normal population distribution, equal variance, and data independence. In this study the one-way ANOVA was taken to verify if the differences in removal efficiency among the different sorption media (i.e., CPS, ZIPGEM, and BIPGEM) at the various influent cases were significant under a 95% confidence interval. The null hypothesis (H_0) and alternative hypotheses (H_a) to be tested are as follows.

H_0 : There is not a significant difference in the means of removal rates among the three selected different green sorption media.

H_a : There is a significant difference in the means of removal rates among the three selected green sorption media.

The 2-way ANOVA is utilized to compare the means of different groups related to different factors. The assumption considered by the 2-way ANOVA includes the homogeneity of variance, independence of observations, and normally distributed dependent variables, and the data should not have significant outliers (Knežević and Žmuk, 2021). The 2-way ANOVA test was applied to

the removal efficiency of each media at different influent conditions and cases to verify if the differences in removal efficiency are significant under a 95% confidence interval. The 2-null hypotheses (H_{01} , H_{02}) and 2 alternative hypotheses (H_{a1} , H_{a2}) to be tested are presented as follows.

H_{01} : There is not a significant difference in the average removal efficiencies among the different initial influent MC-LR concentrations (i.e., Conditions 1–5) for CPS, ZIPGEM, and BIPGEM. (H_{a1} : There is a significant difference in the average removal efficiencies among the different initial influent MC-LR concentrations (i.e., Conditions 1–5) for CPS, ZIPGEM, and BIPGEM.)

H_{02} : There is not a significant difference in the average removal efficiencies among the different cases (i.e., Cases 1, 2, and 3) for CPS, ZIPGEM, and BIPGEM. (H_{a2} : There is a significant difference in the average removal efficiencies among the different cases (i.e., Cases 1, 2, and 3) for CPS, ZIPGEM, and BIPGEM.)

The acceptance or rejection of the null hypotheses was determined by comparison of the F and F_{crit} values. If the F value was greater than the F_{crit} value, then the null hypothesis was rejected and the alternative hypothesis was chosen.

3.2.6. Columns study

A fixed-bed column study for CPS, ZIPGEM, and BIPGEM was performed to collect information on its removal efficiency and adsorption capacity for MC-LR treatment in a dynamic environment. The experimental setup consisted of a polyvinyl chloride column of 12.7 cm depth (5 inches) and 10.2 cm (4 inches) diameter in triplicate for each sorption media. Each column contained a filter and layer of pebbles at the bottom to prevent clogging, followed by 1,300 mL of media (i.e., CPS, ZIPGEM, and BIPGEM) and topped with a layer of pebbles to aid in water

distribution at the surface of the column. The column was operated in a downflow manner with peristaltic pump to provide a constant flowrate of $14 \text{ mL}\cdot\text{min}^{-1}$. Each column has 1,300 ml of media. The hydraulic loading rate is $2,517 \text{ L}\cdot\text{day}^{-1}\cdot\text{m}^{-2}$ ($8.146 \text{ ft}^3\cdot\text{day}^{-1}\cdot\text{ft}^{-2}$). The influent consisted of spiked surface water at a concentration of $70 \mu\text{g}\cdot\text{L}^{-1}$ of MC-LR that reflects the typical high range of MC-LR concentrations in natural environments. The media reach 50% breakthrough at 40 hours (50% removals were obtained at this point).

Water samples were collected at different times to capture the breakthrough curve of CPS, ZIPGEM, and BIPGEM for MC-LR adsorption. The collected water samples were delivered to Green Water laboratory for analysis for total MC with a LC-MS/MS. Moreover, a set of triplicate samples collected from surface water was sent to Eurofins Flowers Chemical Laboratories, Inc. for analysis of basic water parameters (i.e., dissolved iron, dissolved aluminum, nitrogen kjeldahl, nitrate, nitrite, total nitrogen, total phosphorus, and chlorophyll-a). A separate set of triplicate water samples was sent to ALS testing laboratories to test the concentration of tannic acid in the water.

Information on the breakthrough curve for all sorption media (i.e., CPS, ZIPGEM, and BIPGEM) was imputed into 2 dynamic models, namely Thomas and Modified Dose-Response (MDR) model (Thomas 1944, Yan et al., 2001). The Thomas model is commonly used to produce a general analysis of the adsorption process in a fixed bed column. The Thomas model was developed based on the Langmuir isotherm equilibrium and second-order reversible kinetics (González-López et al., 2021). The linear form of the Thomas model is presented in Eq. 16 and can be obtained from the linear regression of $\ln\left(\frac{C_0}{C_t} - 1\right)$ vs. t , where t is time in minutes; C_0 and C_t are the influent MC-LR concentration and the effluent concentration at time t in $\mu\text{g}\cdot\text{L}^{-1}$,

respectively; m is the mass of media along the fixed bead in grams; Q is the influent flow rate in $L \cdot \text{min}^{-1}$; K_T is the Thomas constant in $L \cdot \text{minutes}^{-1} \cdot \text{ug}^{-1}$; and q_0 is the maximum adsorption capacity of the media in $\text{ug} \cdot L^{-1}$.

$$\ln \left(\frac{C_o}{C_t} - 1 \right) = \frac{K_T q_o m}{Q} - K_T C_o t \quad (16)$$

The MDR model is an empirical model, which is more suitable for asymmetric breakthrough curves and thus minimizes the error from the Thomas model (Thomas 1944, Song et al., 2011). The linear form of the MDR model (Yan et al., 2001) is presented in Eq. 17; from this equation the constants C_t , C_o , Q , m , q_o , and t keep the same meaning and units as in the Thomas model, however, the constant a_{mdr} corresponds to the MDR constant (unitless). Figure 2 summarizes the whole experimental setup in this study.

$$\ln \left(\frac{C_t}{C_o - C_t} \right) = a_{mdr} \ln(C_o Q t) - a_{mdr} \ln(q_o m) \quad (17)$$

3.2.7. Media characteristics

The characteristics of the sorption media CPS, ZIPGEM, and BIPGEM are summarized in Table 12. The results indicate that the sorption media ZIPGEM has a higher density, porosity, and BET surface area, followed by BIPGEM and CPS. ZIPGEM has the highest saturated hydraulic conductivity followed by CPS and finally BIPGEM. The difference in the physical characteristics among CPS, ZIPGEM, and BIPGEM can be attributed to the inclusion of ZVI or ZVI and biochar as media components and the different media matrices. A larger surface area and higher porosity can be beneficial for adsorption processes because it can provide more active sites (Bhatnagar and Jain, 2005; Rong et al., 2017; Subramaniam et al., 2017), while a lower saturated hydraulic conductivity can be beneficial for adsorption process because it extends the contact time of the

media and the adsorbate. However, a lower density can be beneficial for application purposes given the inverse relationship between density and volume (pore space).

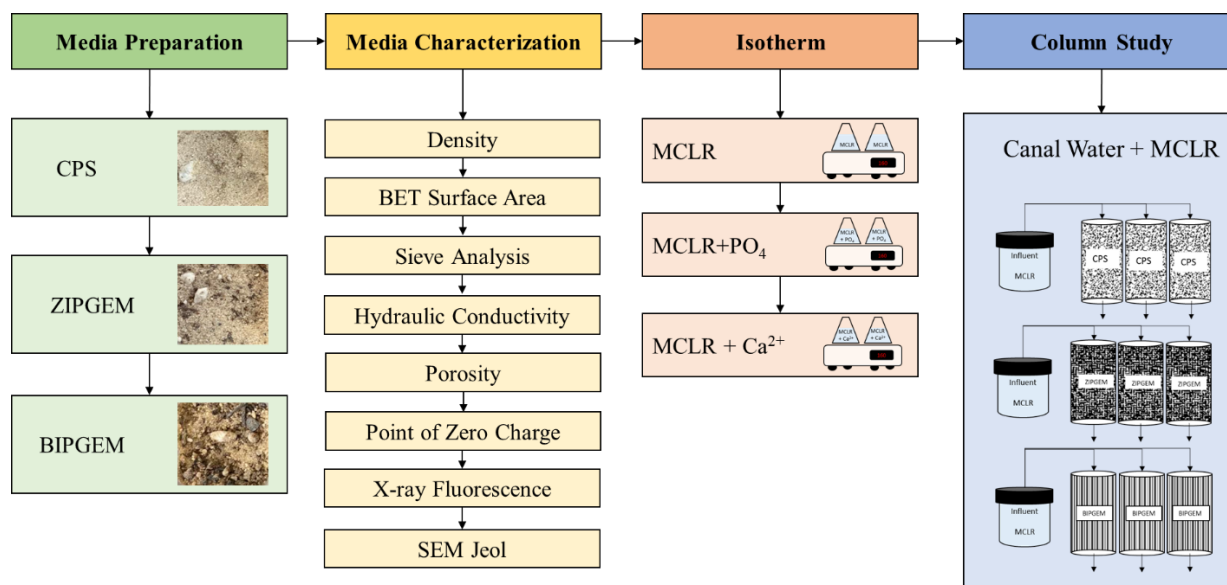


Figure 11. Experimental setup of this study

3.3. Results and Discussion

The location of the PZC for the media can also impact the removal mechanisms. The PZC for CPS, ZIPGEM, and BIPGEM occurs at pH of 5.6, 9.2, and 9.6, respectively, meaning that at this pH the charge at the surface of the sorption media is zero. However, when the pH drops below the PZC the surface charge is positively charged, whereas when the pH is above the PZC the charge in the surface of the media is negatively charged (Bhatnagar and Jain, 2005). The location of the PZC for ZIPGEM can be attributed to the presence of ZVI because the PZC for iron hydroxides ranges from 7–9 (Wu et al., 2017). However, the higher location of the PZC in BIPGEM can be attributed to the presence of biochar, given that the PZC for biochar (in this study) is located at a pH of 10.6 (Table 12).

Table 12. Summary of green sorption media characteristics of CPS, ZIPGEM, and BIPGEM

Name	Density (g·cm ³)	BET Surface Area (m ² ·g ⁻¹)	Porosity (%)	Saturated Hydraulic Conductivity (m·sec ⁻¹)	PZC (±Stdev)
CPS	2.61	1.08	26	1.7(10 ⁻⁴)	5.6±0.22
ZIPGEM	2.78	1.50	33	2.8(10 ⁻⁴)	9.2±0.33
BIPGEM	2.59	1.35	30	1.2(10 ⁻⁴)	9.6±0.06
Biochar	1.18	371.11	--	--	10.6±0.01

The chemical elemental composition of the different components of the media matrix were explored by an XRF analyzer to explore how each material can contribute to the removal mechanism of the sorption media (Table 13). The main component of these green sorption media is sand, followed by clay and perlite, whereas ZVI is a component of ZIPGEM and BIPGEM and biochar is a component of BIPGEM alone. Sand (the main component of all media in this study) is made of ~91% Si, and clay (the second main component in the all-media matrix) is made of ~38% and ~52% Al and Si, respectively. The composition of perlite is mainly a mixture of Si, K, and Al, accounting for ~57%, ~19%, and ~9%, respectively. ZVI is composed of ~95% of Fe, while the main components of biochar are Ca and K, accounting for ~50.9% and ~23.8% respectively.

In Table 13 and Table 14, the elemental composition for CPS, ZIPGEM, and BIPGEM is presented. The major difference in the elemental composition among the three green sorption media is the presence of Fe in ZIPGEM and Fe and biochar in BIPGEM in comparison to CPS (i.e., control) that implies the differential effect in material morphology can be realized via such observations. In ZIPGEM and BIPGEM, Fe accounts for ~12% and ~12.8% respectively of the media's chemical elemental composition, in comparison to CPS, in which Fe only accounts for ~0.4% of its elemental composition. With the increased Fe percentage in ZIPGEM, the percentage of Si decreases as evidence of the lower content of sand in ZIPGEM and BIPGEM.

Table 13. XRF chemical elemental composition for sand, clay, perlite, ZVI, and biochar (elements found at tracer level have been excluded from the table).

Element	Sand		Clay		Perlite		ZVI		Biochar	
	Conc	Unit	Conc	Unit	Conc	Unit	Conc	Unit	Conc	Unit
Al	2.3±(0.4)	%	37.7±(0.1)	%	9.3±(0.5)	%	0.4±(0.3)	%	--	%
Si	90.9±(3.2)	%	51.6±(0.1)	%	57.0±(1.7)	%	0.7	%	2.7	%
P	2.0±(0.1)	%	1.5	%	2.2±(0.1)	%	0.5	%	1.9	%
S	0.4±(0.3)	%	0.5	%	1.3±(0.2)	%	--	%	0.9	%
Cl	1.6±(1.1)	%	1.5	%	1.7±(0.1)	%	0.5	%	2.3	%
K	2.1±(0.2)	%	0.8	%	19.3±(1.4)	%	--	%	23.8	%
Ca	0.9±(0)	%	1	%	6.1±(0.1)	%	0.3	%	50.9	%
Ti	0.9±(0.6)	%	1.7	%	0.2	%	--	%	1.6	%
Fe	0.3±(0.1)	%	3.6	%	2.4±(0.1)	%	95.6±(0.2)	%	13	%
Cr	--	--	--	--	--	--	0.3	%	0.1	%
Mn	--	--	--	--	0.3	%	0.5	%	2.1	%
Ni	--	--	--	--	--	--	0.4	%	--	%
Cu	--	--	--	--	--	--	0.5	%	0.4	%
Zn	--	--	--	--	--	--	0.3	%	0.2	%
Sr	--	--	--	--	--	--	--	--	0.1	%

Table 14. XRF chemical elemental composition for CPS, ZIPGEM, and BIPGEM (values in parentheses are for the standard deviation calculated from 3 samples; elements found at tracer level have been excluded from the table).

CPS			ZIPGEM			BIPGEM		
Compound	Conc	Unit	Compound	Conc	Unit	Compound	Conc	Unit
Al	10.5±(0.7)	%	Al	8.4±(0.9)	%	Al	11.5±(0.1)	%
Si	80.1±(1.6)	%	Si	70.3±(2)	%	Si	70.4±(0.2)	%
P	2.1±(0.2)	%	P	1.9±(0.1)	%	P	1.4±(0)	%
S	0.6±(0.1)	%	S	--	%	S	--	%
Cl	1.8±(0.2)	%	Cl	2.0±(0.2)	%	Cl	1.3±(0)	%
K	2.9±(0.8)	%	K	2.8±(0.4)	%	K	0.6±(0)	%
Ca	1.1±(0.2)	%	Ca	1.0±(0.1)	%	Ca	1.1±(0)	%
Ti	0.4±(0.1)	%	Ti	1.3±(0.2)	%	Ti	0.7±(0.2)	%
Fe	0.4±(0.1)	%	Fe	12.1±(1.2)	%	Fe	12.8±(0.2)	%

3.3.1. Isotherm results

A series of stepped isotherm studies were performed to understand the removal efficiency and the effect that different influent concentrations have on the MC-LR removal by the different sorption media (i.e., CPS, ZIPGEM, and BIPGEM). Additionally, 3 different cases were selected to investigate the effect that the coexistence of PO_4^{3-} and Ca^{2+} has on the MC-LR removal efficiency of sorption media. In Case 1, MC-LR alone was spiked in the influent at different concentrations, while in Case 2, PO_4^{3-} at a constant concentration was spiked in the influent with varying MC-LR concentrations and in Case 3, Ca^{2+} at a constant concentration was included along the spiked influents with different MC-LR concentrations. The different influent concentrations ranged from 5–360 $\mu\text{g}\cdot\text{L}^{-1}$ and are denoted as Condition 1–5 as explained in Table 11. In general, in Case 1 and Case 3 (Figure 12 (a) and Figure 12 (c)), a trend can be observed with decreasing removal efficiency as the concentration of MC-LR in the influent increases. Moreover, in Case 2 (Figure 12 (b)), such a trend is not as perceptible. The highest MCLR removal efficiencies were obtained by BIPGEM, followed by ZIPGEM and CPS. For instance, in Case 1 the removal efficiencies of BIPGEM ranged from 44.6–82.9%, while in Case 2 and Case 3 the removal efficiencies ranged from 29.5–91.7% and 63–100%, respectively. For ZIPGEM and CPS the removal efficiencies were lower. In Case 1 the removal efficiencies of ZIPGEM and CPS ranged between 9% and 35% and 6.1% and 26.7%, respectively. In Case 2, the removal efficiencies ranged between 0% and 22% for ZIPGEM and between 0% and 14.6% for CPS. Finally, in Case 3 the removal efficiencies attained by ZIPGEM and CPS ranged from 20.6–28.6% and 6–27.7%, respectively.

In Case 2, the simultaneous removal of phosphorus was studied, and it was observed that ZIPGEM outperformed the other two green sorption media in terms of phosphate removal rates, with removals ranging from 49.4–60.6%. The PO_4^{3-} removal by BIPGEM ranged from 33.7–43.13%, while PO_4^{3-} removal by CPS ranged from 10.3–20.6%. Hence, CPS is the least efficient media to treat PO_4^{3-} . In Case 3, occurrence of Ca^{2+} was studied, and no significant change in the effluent concentration, in comparison to the influent concentration, was observed among the 3 different sorption media.

The MC-LR percentage removals obtained by each sorption media in each case were subject to a 1-way ANOVA at a 95% critical interval. By comparing the resultant F and F_{crit} values, it was concluded that there is a significant difference among the mean values of these removal efficiencies across the three selected green sorption media. This conclusion was attained via the acceptance of the alternative hypothesis. Furthermore, the percentage removals across the 3 different cases (i.e., Cases 1, 2, and 3) and conditions (i.e., Conditions 1, 2, and 3) within each media were further compared by a 2-way ANOVA test with a 95% critical interval. The test was performed to determine if there was a significant difference among the MC-LR percentage removals attained at the different cases and conditions within each media. The acceptance or rejection of the null hypothesis was determined based on the comparison of the F and F_{crit} value. For both ZIPGEM and CPS, both null hypotheses (H_{01} and H_{02}) were accepted, leading to the conclusion that there were not significant differences in the MC-LR percentage removals obtained among the different MC-LR influent concentrations and cases. On the contrary, for BIPGEM the first null hypothesis was rejected (H_{01}), allowing for acceptance of the first alternative hypothesis, leading to the conclusion that there were significant differences across MC-LR percentage

removals attained by the different influent MC-LR conditions. Moreover, for BIPGEM, the second null hypothesis was accepted, generating the conclusion that there were not significant differences in the MC-LR removals across the different cases.

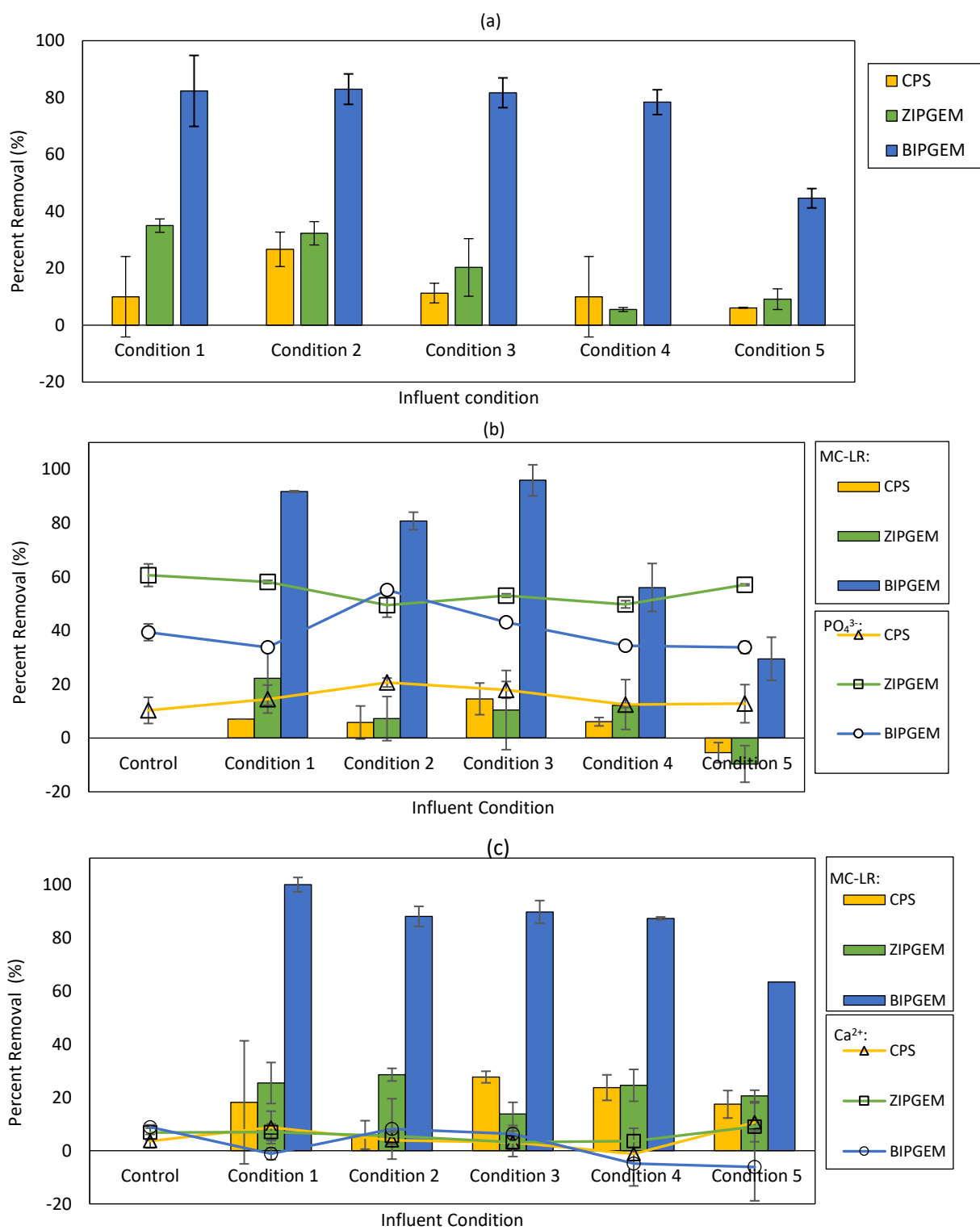


Figure 12. Percentage removal obtained by CPS, ZIPGEM, and BIPGEM under different initial conditions (Control, Condition 1, Condition 2, Condition 3, Condition 4, and Condition 5) and cases where (a) is Case 1 (MC-LR), (b) is Case 2 (MC-LR and PO₄³⁻), and (c) is Case 3 (MC-LR and Ca²⁺).

To further characterize the MC-LR adsorption capacity of CPS, ZIPGEM, and BIPGEM, the isotherm results were imputed into the Langmuir and Freundlich isotherm models, and the results are presented in Table 15 and Table 16. High correlation efficiencies (R^2) were obtained for all media (i.e., CPS, ZIPGEM, and BIPGEM) from the linear regression following the Freundlich isotherm. However, for the Langmuir isotherm model, high value of R^2 was only obtained from the linear regression of BIPGEM and CPS Case 1, and an acceptable R^2 was obtained for ZIPGEM case 1. The low R^2 for CPS and ZIPGEM Case 2 and Case 3 can be explained by the first and second assumption of the Langmuir isotherm that states that the adsorption is entirely of a monolayer at the surface and that only one adsorbed molecule can be adsorbed at each site. Considering these results, it can be concluded that for CPS and ZIPGEM the adsorption is monolayer on homogeneous sites when MC-LR is alone in the influent, whereas, when MC-LR coexists with other contaminants (i.e., PO_4^{3-} and Ca^{2+}), the adsorption is multilayer on heterogeneous sites according to the assumption of the Freundlich isotherm model. Such a conclusion cannot be made for BIPGEM, given the high R^2 attained for both Langmuir and Freundlich models, which is possible due to its high adsorption capacity in comparison to CPS and ZIPGEM.

The adsorption capacities in Case 1 for CPS, ZIPGEM, and BIPGEM obtained by the Langmuir model are $0.74 \mu\text{g}\cdot\text{g}^{-1}$, $1 \mu\text{g}\cdot\text{g}^{-1}$, and $4.63 \mu\text{g}\cdot\text{g}^{-1}$, respectively. BIPGEM had the higher adsorption capacity followed by ZIPGEM and CPS. Moreover, the n value derived from the Freundlich isotherm model indicates whether the adsorption is favorable or unfavorable. Based on the n values from CPS, the adsorption for Case 1 and Case 3 is favorable, while the adsorption in Case 2 is not favorable. On the contrary, for ZIPGEM and BIPGEM the adsorption is favorable

for all cases (Case 1, Case 2, and Case 3). The adsorption capacity of BIPGEM was compared to different adsorbents in the literature and is summarized in Table 17.

Table 15. Langmuir isotherm parameter retrieved from the regression plot of $\frac{C_e}{q_e}$ vs. C_e for the different influent conditions.

<i>Media</i>	<i>Condition</i>	<i>R²</i>	<i>Equation</i>	<i>Parameter</i>
CPS	Case 1	0.841	$y = 1.348x + 155.9$	$K_T = 0.009$ $q_m = 0.74 \mu\text{g}\cdot\text{g}^{-1}$
	Case 2	0.005	$y = -0.363x + 498.08$	$K_T = -0.0007$ $q_m = -2.75 \mu\text{g}\cdot\text{g}^{-1}$
	Case 3	0.045	$y = -0.433x + 341.65$	$K_T = -0.433$ $q_m = -2.31 \mu\text{g}\cdot\text{g}^{-1}$
ZIPGEM	Case 1	0.239	$y = 0.999x + 183.03$	$K_T = 0.005$ $q_m = 1.00 \mu\text{g}\cdot\text{g}^{-1}$
	Case 2	0.070	$y = 1.301x + 269.77$	$K_T = 0.0048$ $q_m = 0.77 \mu\text{g}\cdot\text{g}^{-1}$
	Case 3	0.017	$y = 0.062x + 136.56$	$K_T = 0.0005$ $q_m = 16.13 \mu\text{g}\cdot\text{g}^{-1}$
BIPGEM	Case 1	0.999	$y = 0.216x + 7.35$	$K_T = 0.0294$ $q_m = 4.63 \mu\text{g}\cdot\text{g}^{-1}$
	Case 2	0.854	$y = 0.1473x + 7.10$	$K_T = 0.0207$ $q_m = 6.79 \mu\text{g}\cdot\text{g}^{-1}$
	Case 3	0.951	$y = 0.1356x + 3.29$	$K_T = 0.041$ $q_m = 7.38 \mu\text{g}\cdot\text{g}^{-1}$

Table 16. Freundlich isotherm parameter retrieved from the regression plot of $\ln(q_e)$ vs. $\ln(C_e)$ at 3 different influent conditions.

<i>Media</i>	<i>Condition</i>	<i>R²</i>	<i>Equation</i>	<i>Parameter</i>
CPS	Case 1	0.893	$y = 0.795x - 4.748$	$K_F = 0.009$ $n = 1.258$
	Case 2	0.900	$y = 1.066x - 6.3315$	$K_F = 0.002$ $n = 0.938$
	Case 3	0.802	$y = 0.987x - 5.423$	$K_F = 0.004$ $n = 1.013$
ZIPGEM	Case 1	0.771	$y = 0.5852x - 3.7661$	$K_F = 0.023$ $n = 1.709$
	Case 2	0.864	$y = 0.694x - 4.679$	$K_F = 0.009$ $n = 1.442$
	Case 3	0.950	$y = 0.9722x - 4.699$	$K_F = 0.009$ $n = 1.061$
BIPGEM	Case 1	0.917	$y = 0.6332x - 1.6424$	$K_F = 0.194$ $n = 1.579$
	Case 2	0.852	$y = 0.4782x - 0.977$	$K_F = 0.376$ $n = 2.091$
	Case 3	0.964	$y = 0.5836x - 0.984$	$K_F = 0.374$ $n = 1.713$

Table 17. Summary of previous isotherm studies for MC-LR removal

<i>Media</i>	<i>Adsorption capacity</i>	<i>Experimental setup</i>	<i>Reference</i>
Coconut shell	16.1 mg·g ⁻¹	<ul style="list-style-type: none"> • Varying amount of carbon • Initial concentration 250 µg·L⁻¹ 	Huang et al. (2007)
Bituminous coal	17.5 mg·g ⁻¹	<ul style="list-style-type: none"> • pH of 7.5 and Temp. 25 °C • DI water • Langmuir 	
Wood	83.3 mg·g ⁻¹	<ul style="list-style-type: none"> • Langmuir 	
Peat	0.255 mg·g ⁻¹	<ul style="list-style-type: none"> • Varying initial concentration • Concentration range 100–1000 µg·L⁻¹ • pH of 3 • DI water • Langmuir 	Sathishkumar et al. (2010)
Iron oxide nanoparticles	0.594 mg·g ⁻¹	<ul style="list-style-type: none"> • Adsorbent dose = 0.1, 1, 2, 3, and 4 mg·L⁻¹ • Initial concentration 250 µg·L⁻¹ • pH of 7 and Temp. 25 °C • DI water • Langmuir 	Gao et al. (2012)
Wood-based GAC	26 mg·g ⁻¹	<ul style="list-style-type: none"> • Adsorbent dose = 0, 1, 5, and 11 mg·L⁻¹ • Initial concentration: 50 µg·L⁻¹ • DI water 	Villars et al. (2020)
Activated carbon	0.357 mg·g ⁻¹	<ul style="list-style-type: none"> • Varying amount of carbon: 0.01–0.05 g • Concentration range: 5–65 µg·L⁻¹ • pH of 3–9 • DI water • Langmuir 	Mashile et al. (2018)
BIPGEM	0.007 mg·g ⁻¹	<ul style="list-style-type: none"> • Varying initial concentration • Concentration range: 5–360 µg·L⁻¹ • pH of 7 • DI water spiked with Ca²⁺ • Langmuir 	This study

3.3.2. Removal mechanism

MC-LR in water at most pH (3<pH<12) is mostly negatively charged because of the deprotonation of the carboxyl group (Lawton et al., 2003; Lee and Walker, 2006). On the contrary, the surface charge of CPS, ZIPGEM, and BIPGEM is positively charged at pH below 5.6, 9.2, and 9.6 according to its PZC, respectively (Table 12). The location of the PZC in ZIPGEM and BIPGEM can be attributed to the presence of ZVI and ZVI and biochar as part of the sorption media matrix. This is because the location of PZC for iron hydroxide usually lies between 7 and 9 (Wu et al., 2017) and at pH of 10.6 for biochar (in this study). By considering the force of attraction between oppositely charged particles or Coulombic attraction, the higher adsorption capacity

based on the Langmuir isotherm model for ZIPGEM and BIPGEM in comparison to CPS can be justified (Table 15). Previous researchers have explained the interactions between MC-LR and iron particles. For instance, the removal of MC-LR onto iron oxide nanoparticles was examined by Lee and Walker (2011), who concluded that pH strongly affected the adsorption of MC-LR, indicating that the adsorption of MC-LR increased with decreasing pH, thus contributing to the adsorption of MC-LR to iron oxide particles (maghemite) mainly via electrostatic interactions. Moreover, Gao et al. (2012) suggested that the adsorption of MC-LR to iron oxide nanoparticles was spontaneous and endothermic. Additionally, the presence of clay can further aid in the MC-LR adsorption capacity of the sorption media.

The removal efficiency and adsorption capacity of BIPGEM was the highest among all 3-sorption media, and such improvement can be attributed to the inclusion of biochar in the media. The adsorption of MC-LR to biochar was studied by Li et al. (2014), who found that the carboxylic and guanidino groups in the MC-LR structure can be responsible for the adsorption of MC-LR to biochar. Moreover, Li et al. (2014) also suggested that the adsorption of MC-LR to biochar is mainly attributed to the columbic attractions and the hydrogen bonding within the MC-LR and biochar surface. Liu et al. (2018) further indicated that the adsorption of MC-LR to biochar is the result of electrostatic attraction, pore filling, H bonding, and π - π interactions. In this study, biochar was characterized in terms of surface morphology and pH_{PZC} . The surface morphology of biochar is presented in Figure 13(a) and (b). In Figure 13 (a), it can be observed that the surface of biochar is porous. By zooming in, the pore size is characterized, resulting in diameters ranging from 0.49–5.2 μm . The morphology of biochar can support the improved MC-LR adsorption of BIPGEM

explained by the incorporation of pore-filling adsorption by biochar in the synergetic adsorption mechanism of BIPGEM.

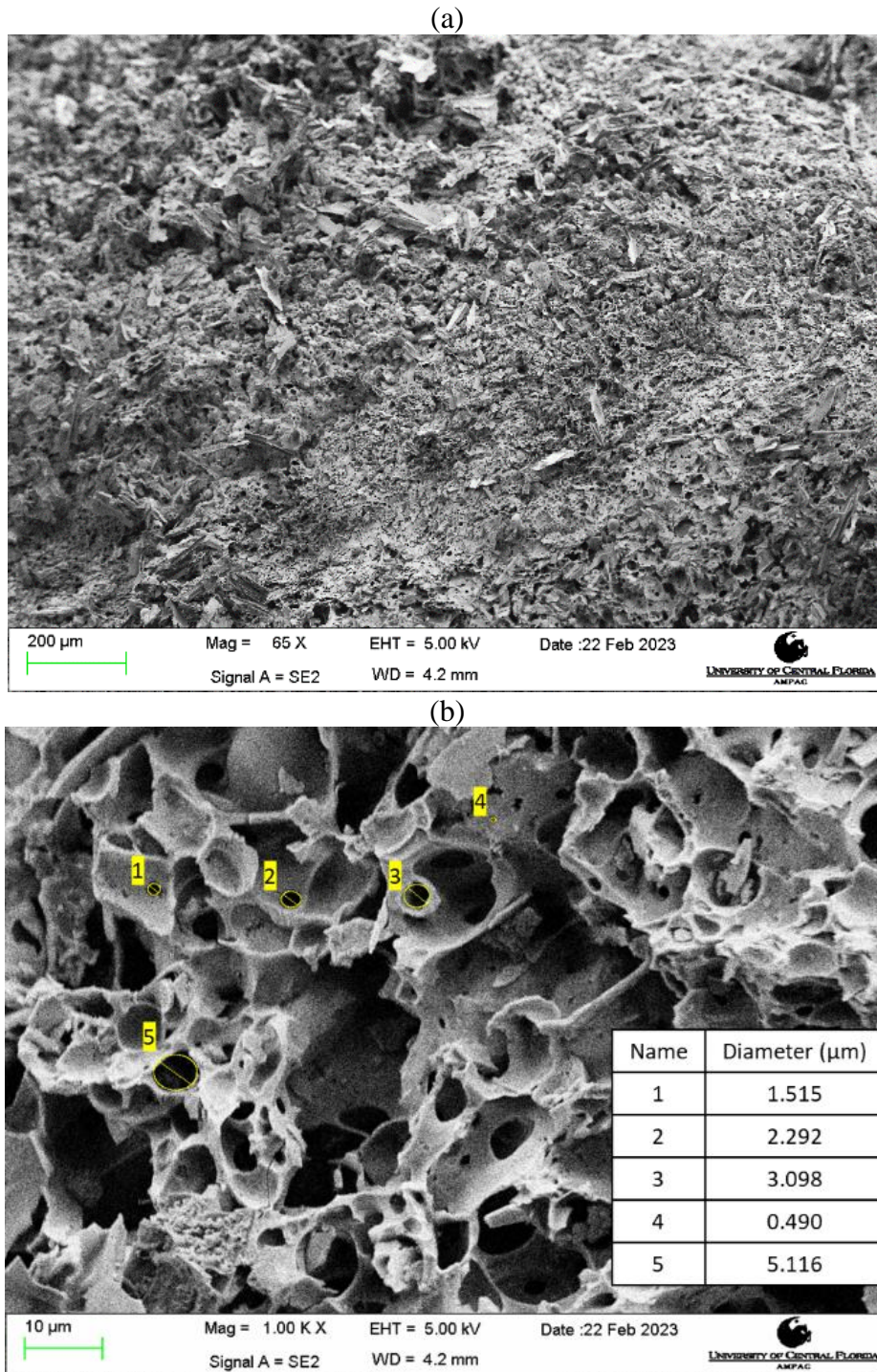


Figure 13. Image of biochar at magnification of (a) 65X and (b) 1 KX. (Imagens were taken via Zeiss Ultra-55 SEM)

3.3.3. Competing effect between phosphate and MC-LR removal

In nature, MC-LR is commonly presented with other compounds including PO_4^{3-} and Ca^{2+} ; for this reason, it is important to understand how its presence can affect the removal efficiency of the sorption media. Based on the fitting of the Langmuir isotherm model, it can be assumed that when MC-LR is alone (Case 1) the adsorption of MC-LR in ZIPGEM and CPS is monolayer, whereas when MC-LR is present with other components (e.g., phosphate and calcium ions), the adsorption is multilayer. Moreover, based on the Freundlich equation, the major effect on the adsorption capacity was observed under the presence of PO_4^{3-} for CPS because the n value indicated that the adsorption was not favorable. The larger PZC and better physical and chemical characteristics of ZIPGEM and BIPGEM can explain whether in accordance with the Freundlich model, the adsorption was maintained as favorable in the presence of PO_4^{3-} . By comparing the percentage removal, in these different conditions prescribed, a decrease in the MC-LR removal rates in Case 2 for all sorption media (i.e., CPS, ZIPGEM, and BIPGEM) can be observed. Such a decrease in removal efficiency of different adsorbents has been previously observed, and it can be attributed to a competition effect of PO_4^{3-} and MC-LR for the available positive adsorption sites (Li et al., 2014). However, the removal of PO_4^{3-} was not affected by the presence of MC-LR, suggesting that the interaction in the surface media will favor PO_4^{3-} .

That said, the presence of cations in the water matrix can enhance the removal of MC-LR, which was observed by comparing the removal efficiencies in Case 3 with the removals in Case 1 for all sorption media. In Case 2, the Ca^{2+} removal was null, and the concentration maintained constant throughout the isotherm studies, regardless of the influent condition. Gao et al. (2012) suggested that calcium ions slightly enhanced the MC-LR adsorption capacity of the iron oxide

nanoparticle. Meanwhile, Liu et al. (2019a) found that metal cation (i.e., Ca^{2+}) on clay surface altered MC-LR adsorption by strengthening the ligand exchange and electrostatic interactions favoring MC-LR adsorption onto surface of kaolinite at lower pH.

Whereas a decrease in the MC-LR removal efficiency of the sorption media is seen in the presence of PO_4^{3-} , an increase in the MC-LR removal efficiency when Ca^{2+} is present in water can be observed. However, its difference is not statistically significant within 95% critical interval in accordance with a 2-way ANOVA. These results support the application of the sorption media in a field scale, especially with BIPGEM due to its high simultaneous removal efficiency of MC-LR and PO_4^{3-} .

3.3.4. Dynamic removal efficiency with canal water

The dynamic removal efficiency of sorption media with canal water as influent condition was investigated to simulate the adsorption behavior on a field scale. The results of the MC-LR percentage removal by the sorption media CPS, ZIPGEM, and BIPGEM are presented in Figure 14 (a), 14 (b), and 14 (c), respectively. The sorption media BIPGEM achieved better MC-LR removal followed by ZIPGEM and CPS. BIPGEM removed over 90% of MC-LR from the influent water for the first 8 hours; in the subsequent hours, its removal efficiency decreased, reaching ~50% after ~40 hours. On the contrary, ZIPGEM media only achieved ~38% MC-LR removal within the first hour, reaching its exhaustion point (no removal efficiency) after 32 hours. As the control in this study, CPS media only achieved 20% MC-LR removal in the first hour, reaching exhaustion after only 2 hours.

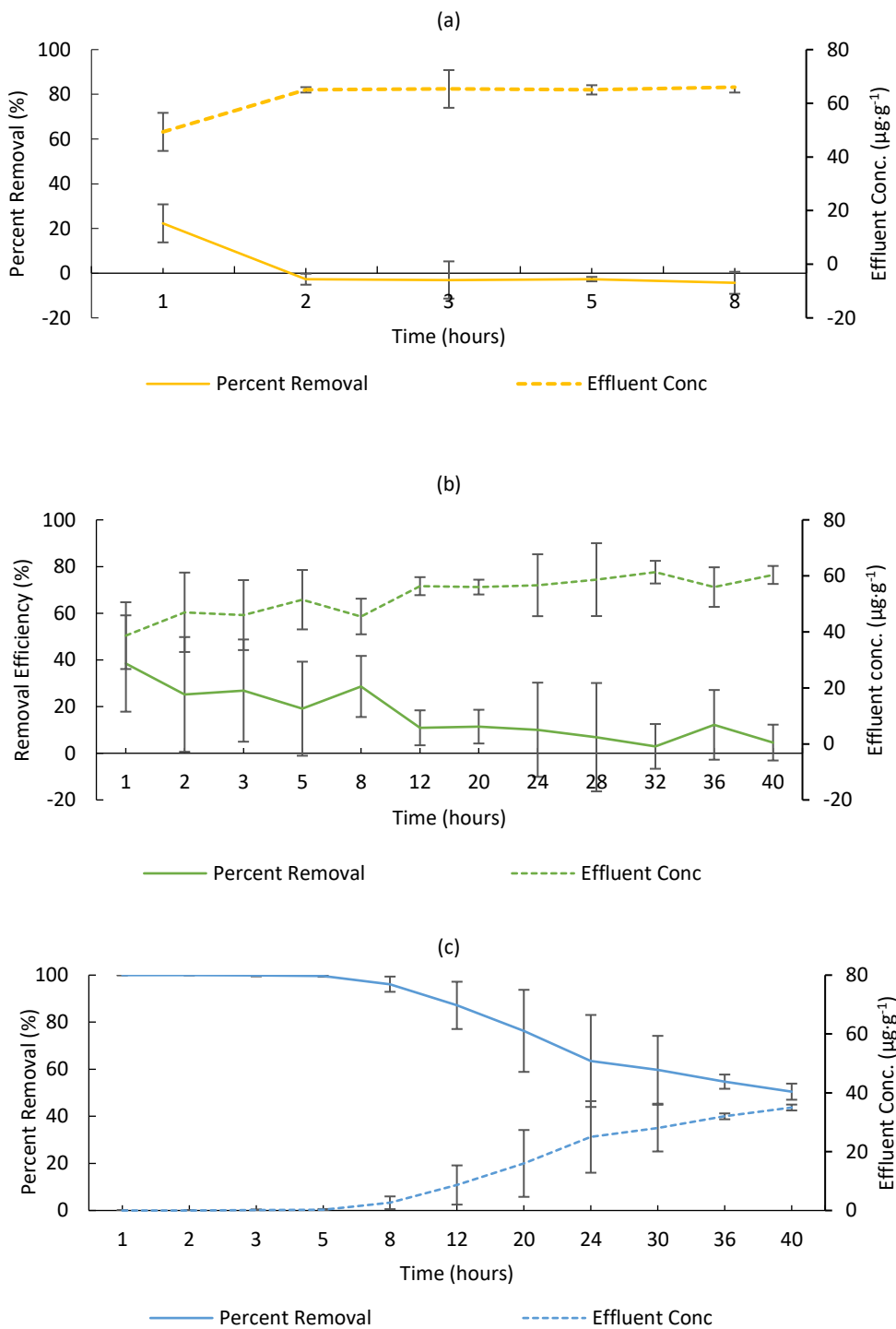


Figure 14. Dynamic MC-LR removal curves for (a) CPS, (b) ZIPGEM, and (c) BIPGEM from a fixed bed column study with real canal water spiked to 70 µg·L⁻¹ MC-LR as influent conditions.

The results from the dynamic column studies for CPS, ZIPGEM, and BIPGEM were imputed into the Thomas and MDR dynamic models, and the results are presented in Table 18. Given the short removal time for CPS, the MDR dynamic model was not applicable. Conversely, the adsorption capacity (q_0) of CPS predicted by the Thomas model was $0.15 \text{ ug}\cdot\text{g}^{-1}$; however, given that the Thomas model is based on the Langmuir model, the R^2 obtained from the linear regression was low (0.35). For ZIPGEM, the Thomas and MDR models were applied, obtaining R^2 of 0.651 and 0.776, respectively. The q_0 value predicted for ZIPGEM by the Thomas model was $0.97 \text{ }\mu\text{g}\cdot\text{g}^{-1}$ and by the MDR model was $0.016 \text{ }\mu\text{g}\cdot\text{g}^{-1}$. The R^2 for BIPGEM obtained by the Thomas and MDR models were 0.417 and 0.965, and the predicted q_0 values were 1.04 and $1.19 \text{ }\mu\text{g}\cdot\text{g}^{-1}$, respectively. The lower R^2 from the Thomas model fitting can be associated with the assumption of monolayer adsorption in the Langmuir isotherm, which, based on the results of the isotherm study, is not a valid assumption when there are other elements in the water matrix.

By comparing the q_0 from the dynamic models and the q_m predicted from the Langmuir equilibrium isotherms, it can be observed that the adsorption capacities obtained in a dynamic condition are lower (Table 15 and Table 18). The water matrix characterization used as influent condition in the dynamic column study was performed by the research team. The decrease in the adsorption capacity of the sorption media can be explained by the presence of other contaminants in the influent water matrix because it can result in competition for the available sites between the adsorbents and the adsorbates. For instance, Gao et al. (2012) studied the removal efficiency of MC-LR to iron oxide nanoparticles and concluded that there is a competitive adsorption effect with other compounds, especially compounds containing carboxyl groups (i.e., citric acid, benzoic acid, and oxalic acid) with the effect increasing with a rising number of carboxyl groups.

Moreover, Li et al. (2014) and Xiao et al. (2012) indicated that the presence of dissolved organic matter, especially tannic acid, inhibits the MC-LR adsorption capacity of biochar because they can compete for the available mesopore or macropore regions. Furthermore, Dixit et al. (2019) showed that inorganic ions (i.e., nitrate, bicarbonate, and sulphate) compete with MC-LR for the available sites in ionic exchange removal mechanisms, resulting in a reduction of MC-LR removal efficiency. Finally, in this study (Section 3.3.3), the negative effect that the presence of phosphate has in the MCLR removal efficiency of CPS, ZIPGEM, and BIPGEM was further explained.

Table 18. Results from the dynamic modeling of the MC-LR adsorption in a fixed bed column study.

<i>Media</i>	<i>Dynamic Model</i>	<i>R²</i>	<i>Equation</i>	<i>Parameters</i>
CPS	Thomas	0.350	$y = -0.005x + 0.1463$	$q_0 = 0.15 \mu\text{g}\cdot\text{g}^{-1}$ $K_T = 7.9 \text{ E}^{-6} \text{ L}\cdot\mu\text{g}^{-1}\cdot\text{min}^{-1}$
	MDR	---	---	---
ZIPGEM	Thomas	0.651	$y = -0.0002x + 0.4027$	$q_0 = 0.97 \mu\text{g}\cdot\text{g}^{-1}$ $K_T = 3.16 \text{ E}^{-6} \text{ L}\cdot\mu\text{g}^{-1}\cdot\text{min}^{-1}$
	MDR	0.776	$y = 0.6586x - 2.2615$	$a_{\text{mdr}} = 0.632$ $q_0 = 0.016 \mu\text{g}\cdot\text{g}^{-1}$
BIPGEM	Thomas	0.417	$y = -0.1497x + 272.75$	$q_0 = 1.04 \mu\text{g}\cdot\text{g}^{-1}$ $K_T = 0.002 \text{ L}\cdot\mu\text{g}^{-1}\cdot\text{min}^{-1}$
	MDR	0.965	$y = 2.532x - 19.318$	$a_{\text{mdr}} = 2.53$ $q_0 = 1.19 \mu\text{g}\cdot\text{g}^{-1}$

Table 19. Summary of previous column studies and the current one for MC-LR removal and adsorption capacity

<i>Media</i>	<i>Adsorption capacity</i>	<i>Experimental setup</i>	<i>Reference</i>
Graphene oxide-coated sand	$10.4 \mu\text{g}\cdot\text{g}^{-1}$	<ul style="list-style-type: none"> Concentration range: 5, 20, 50 $\mu\text{g}\cdot\text{L}^{-1}$ Lake water Biofilm cultivation 	Kumar et al. (2020)
*GAC 1	$1.85 \mu\text{g}\cdot\text{g}^{-1}$	<ul style="list-style-type: none"> Initial concentration: 18.77 $\mu\text{g}\cdot\text{L}^{-1}$ Reservoir water 	Lopes et al. (2017)
GAC2	$4.15 \mu\text{g}\cdot\text{g}^{-1}$		
BIPGEM	$1.19 \mu\text{g}\cdot\text{g}^{-1}$	<ul style="list-style-type: none"> Surface canal water Influent concentration: 70 $\mu\text{g}\cdot\text{L}^{-1}$ 	This study

* Granulated Activated Carbon

3.4. Chapter Conclusion

To respond to the increasing drinking water demand and changing water quality, it is crucial to develop proper treatment for surface water affected by nutrients, metals, and algal blooms. In this study, the MC-LR removal efficiencies, and adsorption capacities of 3 sorption media denoted as CPS, ZIPGEM, and BIPGEM for MC-LR at different water matrices were presented. The first advantage of these green sorption media is the low cost of operation and sustainable nature due to the use of recycled materials (e.g., ZVI and biochar). Additionally, these green sorption media have been proven to treat different pollutants simultaneously.

In terms of MC-LR adsorption capacity, the sorption media BIPGEM outperformed ZIPGEM and CPS. The MC-LR adsorption capacity of BIPGEM, based on the Langmuir isotherm in Case 1, Case 2, and Case 3, was 4.63, 6.79, and 7.38 $\mu\text{g}\cdot\text{g}^{-1}$, respectively, and 1.19 $\mu\text{g}\cdot\text{g}^{-1}$ based on the MDR dynamic model. The adsorption capacity of BIPGEM in a dynamic environment is comparable with other adsorbents in literature. For example, in Table 19, it can be observed that the adsorption capacity of BIPGEM is comparable with the adsorption capacity of GAC studied in a dynamic environment. The best performance of BIPGEM for the MC-LR removal can be attributed to a large BET surface area, lower saturated hydraulic conductivity, high porosity, and the location of the PZC. Moreover, the inclusion of biochar in the media mix increases the MC-LR removal efficiency by its pore structure.

However, in a dynamic environment facing a real water matrix, the adsorption capacity of CPS, ZIPGEM, and BIPGEM could be compromised given the presence of dissolved organic matter and inorganic ions, causing a competition for the available adsorption sites. Such an occurrence was also observed in the isotherm studies, indicating that the presence of PO_4^{3-}

decreases the MCLR removal efficiency of the sorption media. However, the presence of Ca^{2+} resulted in an increase in the MC-LR removal efficiency. Although these trends were represented by the observed change in the percentage removals, the application of a 2-way ANOVA test concluded that these changes are not significant under a 95% confidence interval, further supporting the application of the sorption media in different environments.

The removal of PO_4^{3-} was not affected by the presence of MC-LR, and in terms of PO_4^{3-} removal the sorption media ZIPGEM outperformed BIPGEM and CPS. The removal efficiency of ZIPGEM ranged from 55–60%. Although this researcher slightly studied the PO_4^{3-} removal efficiency of the sorption media, its efficiency to treat PO_4^{3-} suggests further research to find the adsorption capacity of ZIPGEM and BIPGEM. Finally, it can be concluded that the sorption media ZIPGEM and BIPGEM are a good alternative to treat MC-LR and phosphate in-situ. Given the results, the water matrix needs to be studied before deciding on the appropriate sorption media. For instance, in water with high concentrations of PO_4^{3-} but low concentrations of algal toxin, the sorption media ZIPGEM may be more appropriate. But, in water with high concentration of algal toxins and DOM but lower PO_4^{3-} concentration, the filtration media BIPGEM may be more appropriate. Finally, given the poor MC-LR removal efficiency of CPS in a dynamic condition by physiochemical means, it can be recommended to further study the biophysiochemical removal of MC-LR, given that the CPS can be a good environment for microbial ecology growth.

CHAPTER 4: SENSITIVITY ANALYSIS OF PHOSPHATE ADSORPTION UNDER VARYING WATER MATRIX CONSTITUENTS AND SPECIALTY INGREDIENTS

4.1. Introduction

The nutrient cycle is imperative for the life and health of the ecosystem. Continuous population growth has interrupted the natural nutrient cycle, resulting in environmental externalities owing to the deterioration of ecosystem integrity caused by marine dumping, wastewater effluent, agricultural discharge, and urban stormwater runoff. These anthropogenic activities have caused unexpected accumulation of excess quantities of nutrients (i.e., Total Nitrogen (TN) and Total Phosphorus (TP)) in aquatic ecosystems. For instance, TP is necessary in natural water to prompt the growth of photosynthetic algae if TP is found at concentration below $0.03 \text{ mg}\cdot\text{L}^{-1}$. Otherwise, excess phosphorus might result in eutrophication and harmful algal bloom (Wetzel, 2001). Eutrophication causes a rapid growth of algal mass that might further result in hypoxia, polluted drinking water sources, death of aquatic organisms, and less recreational opportunities (Dorgham, 2014). While phosphate does not affect human health directly, it can promote the apparition of algal bloom which can further result in algae toxins such as microcystin. Human exposure to algae toxins can have mild effects including vomiting, diarrhea, skin, eyes, and throat irritation, yet most severe effects include gastrointestinal illness and liver damage (Falconer, 1983).

The significance of clean water and food is visible in the agenda of the United Nations Sustainable Development Goals (SDGs). The significance is expressed in SDG 2.4 and 6.3 which relate to clean water and food, respectively. SDG 2.4 targets sustainable and resilient food production and practices that help improve land and soil quality (United Nations, 2023a) whereas

one of the main points of SGD 6.3 is for pollution reduction for better water quality to increment safe water reuse and recycling (United Nations, 2023b). Thus, to prevent the excessive concentration of TP and TN in natural water a set of in-situ fit-for-purpose filtration technologies that intend to improve the quality and flow control of stormwater before it reaches the downstream waterbody have been developed and tested as the Best Management Practices (BMPs) as various Low Impact Development (LID) technologies (Urbonas and Stahre, 1993; Dietz, 2007; Chang et al., 2014; Chang et al., 2015; Eckart et al., 2017). These LID practices include bioretention cells (Peng et al., 2022), rain gardens (Davis, 2005), grassed swale (Bedan and Clausen, 2009), green roof (Shafique et al., 2018), detention basins (Emerson et al., 2005), retention ponds (Winston et al., 2013), wetlands (Kadlec, 2016) (Kadlec, 2016). Among different stormwater BMPs, filtration media (i.e., cost-effective specialty adsorbents), such as zeolites (Stocker and Ellersdorfer, 2022), coconut shell (Din et al., 2009), woodchips (Wen et al., 2018), and zero valent iron (ZVI) (Valencia et al., 2020), coated sand (Bello et al., 2013), stand out due to simple operation, relatively low cost, and high performance (Sadegh and Ali, 2021). The removal mechanism of phosphate by metal oxides (e.g., Fe, Zn and Al) are linked to chemophysical interactions including electrostatic forces and ion exchange (Li et al., 2016). The utilization of ZVI to remove phosphate has been widely explored owing to its high removal efficiency. Almeelbi and Bezbaruah (2012) reported phosphate removal with nanoscale ZVI from 96 to 100% in a batch study. Moreover, Valencia et al (2019) indicated TP removal of up to 92% with a ZVI-sand base filtration media in a column study. The removal of phosphate is also possible by precipitation with other materials including Ca and Al (Barca, et al, 2012; Ferguson and King, 1977). Natural and synthetic zeolites have also been well studied for phosphate removal owing to their low cost and high removal efficiency. Alshameri et al. (2014) in a batch study found phosphate removals of nearly 100% with a novel TiO₂/Zeolite

when the influent concentrations were below 150 mg L^{-1} . Hamdi and Srasra (2012) indicated based on an isotherm study that a synthetic zeolite from purified clay can uptake phosphate at a rate of $52.9 \text{ mg}\cdot\text{g}^{-1}$. Moreover, biochar has become a specialty adsorbent due to its low cost in production, and large specific surface area (Leng et al., 2021). In the study by Liu et al. (2019), the adsorption capacity of a CaO-biochar made from eggshells and rice straw was $231 \text{ mg}\cdot\text{g}^{-1}$ in accordance with the Langmuir isotherm. While Mor et al. (2016) presented the adsorption capacity based on the Langmuir isotherm of activated rice husk ash to be $0.736 \text{ mg}\cdot\text{g}^{-1}$ at pH of 6. This rice husk ash was recommended as a low-cost adsorbent for wastewater treatment.

As the issue with nutrient laden stormwater runoff persists, new studies have focused on innovating sorption amendments as new specialty adsorbents that can be better suited for removal of various water matrix constituents (i.e., nutrients, microcystin, metals) (Jedla et al., 2022; Liu et al., 2023). They are aimed to achieve simultaneous removals of multiple water pollutants at lower cost, providing a longer service life, and enabling the removal of nutrients. For instance, perlite is an organic soil amendment applied to improve drainage and aeration in soil. While studies on the utilization of perlite for water treatment can be found since 1996 (Sokolovic & Sokolovic, 1996), its use for water treatment has gained new focus in recent years such as the removal of metals (i.e., Copper (II), cadmium) (Alkan and Doğan, 2001; Mathialagan and Viraraghavan, 2002), treatment of leachate (Ozel et al., 2012), and suspended solids from urban runoff (Gironás et al., 2008); yet the information on TP removal via perlite-based filtration media is limited still. Let alone the synergistic effect among perlite, clay, and ZVI under varying influent conditions.

The objective of this study is to test the sensitivity of phosphate adsorption capacity of three newly developed green sorption media (i.e., specialty adsorbents) under different influent conditions and specialty ingredients. The three new media mixes include Clay-Perlite and Sand

(denoted as CPS, hereafter), and Perlite-based Green Environmental Media (denoted as ZIPGEM, hereafter), and Biochar, Zero-Valent Iron, and Perlite-based Green Environmental Media (denoted as BIPGEM, hereafter). The three specialty adsorbents were subjected to a series of isotherm tests to determine the adsorption capacity at varying environments (e.g., pH values) and specialty ingredients. The specialty ingredient difference between ZIPGEM and BIPGEM signifies the differential effect of biochar whereas the specialty ingredient difference between ZIPGEM and CPS magnifies the differential effect of perlite in the media matrix. The most promising sorption media mix among the three was selected for a fixed-bed column study to determine the adsorption capacity and its potential to be utilized as a soil amendment. The novelty of this study surrounds the exploration of the synergistic effects between (1) perlite-ZVI and (2) perlite-ZVI-biochar providing insight for the removal mechanisms that contribute to the adsorption of nutrients (i.e., phosphate) from polluted water. The research questions to be answered are: (1) Is there any difference of nutrient removal rate under varying influent conditions among CPS, ZIPGEM, and BIPGEM and which factor mostly triggers such difference? (2) What is the dominant mechanism of physiochemical nutrient removal in CPS, ZIPGEM and BIPGEM? (3) Can pH affect the PO_4^{3-} removal mechanism of the media mixes? and (4) Does the presence of NO_3^- in the influent water matrix affect the PO_4^{3-} removal of the media mixes?

4.2. Methodology

4.2.1. Media characterization

Three specialty adsorbents were studied to understand its potential to remove phosphate via physiochemical interactions. These media mixes include CPS, ZIPGEM, and BIPGEM. CPS, ZIPGEM and BIPGEM were previously investigated for their potential to treat algal toxins (i.e.,

Microcystin LR) with or without the presence of PO_4^{3-} (unpublished work). While ZIPGEM and BIPGEM presented good PO_4^{3-} removals, its adsorption capacity was not measured alone, and the effect that different environments have on the removal efficiency of the media was also disregarded. The lack of independent information on the PO_4^{3-} removal mechanism and adsorption capacity reveal the importance of the current work.

The components and media matrix in percent by volume for each sorption media are presented in Table 20. The physical characteristics of the media (i.e., CPS, ZIPGEM and BIPGEM) was also included in Table 20, to aid in the explanation of phosphate removal mechanisms. The Zero-Valent Iron (ZVI) utilized for this study was obtained from Connelly-GPM, Inc. Iron Aggregate, with descriptive name ETI CC-1004 (-8+50). The ZVI composition is 87-93% metallic iron. Moreover, the perlite used in this study is from Miracle-Go® and its description indicated that it contains 99.44% perlite. The biochar used is from Plantonix and it is derived from soft wood and tree trimmings. The physical characteristics including BET surface area and density were performed at the EMSL Analytical, Inc laboratories. Density and BET surface area were measured following methods ASTM D854 and ASTM B922. Moreover, the saturated hydraulic conductivity was measured at the University of Central Florida (UCF) Geotechnical laboratories following the constant head permeability test. The Point of Zero Charge (PZC) for each media was also measured by the salt addition method (Mahmood et al., 2011) at UCF. The salt addition method determines the pH where the surface of the adsorbent is at ionic equilibrium, and it is the condition when the number of H^+ and OH^- at the surface of the particle are equal. The protocols followed in this study is presented in detail in Ordonez et al. (2022a) utilizing 0.2 M NaNO_3 solution and adding NaOH or HNO_3 for pH adjustment. The results are presented on Figure 15.

Table 20. Media matrices in percent by volume and media characterization

Name	Media Matrix	Density (g·cm ³)	BET Surface Area (m ² ·g ⁻¹)	Saturated Hydraulic Conductivity (m·sec ⁻¹)	Porosity (%)
CPS	92% sand, 5% clay, 3 % perlite	2.61	1.08	1.7(10 ⁻⁴)	26
ZIPGEM	85% sand, 5% clay, 5% perlite and 5% ZVI	2.78	1.50	2.8(10 ⁻⁴)	33
BIPGEM	80% sand, 5% clay, 5% perlite, 5% ZVI and 5% biochar	2.59	1.35	1.2(10 ⁻⁴)	30

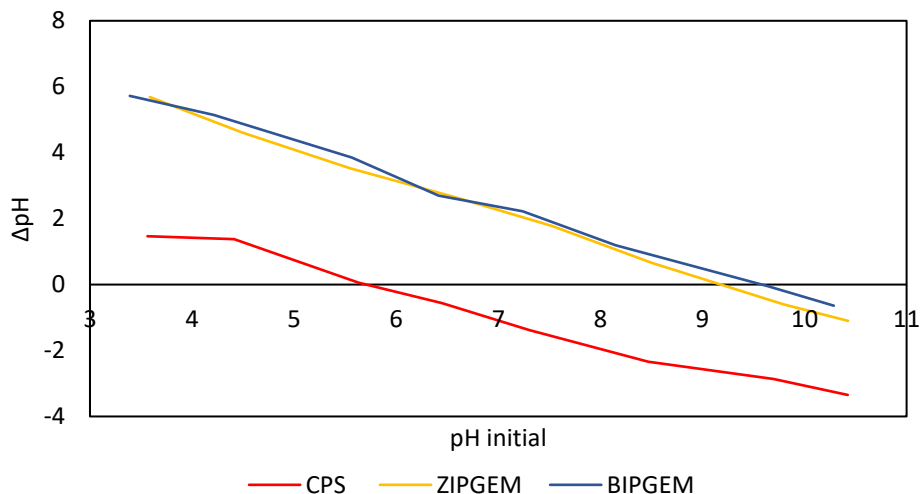


Figure 15. Location of PZC for CPS, ZIPGEM and BIPGEM

4.2.2. Isotherm experiments

A series of isotherm tests were performed to obtain information on the adsorption capacity of the different green sorption media under different pH conditions. In the beginning, the selected green sorption media including CPS, ZIPGEM, and BIPGEM were washed with DI water (3 Bed Volumes (BV)) and then dried for 24 hours at a temperature of 78°C. Subsequently, aliquots of 5 grams of media with 40 ml of DI water spiked to different concentrations (i.e., 0, 0.7, 2, 3, 4, 5, 15, 30, 60, 120, and 240 mg·L⁻¹ PO₄³⁻) were prepared. The aliquots were then shaken for 6 hours on a shaker at 180 rpms and at room temperature. The procedure was repeated at three different pH conditions (i.e., pH of 4, 7 and 10) adjusted with NaOH or HNO₃. At the completion of the shaking time, each aliquot was left to rest for 30 min and the supernatant was extracted, filtered

via a membrane filter with pore size 0.45 μm and analyzed for phosphate concentrations in triplicate. An additional isotherm was performed following the same protocol but substituting the influent with surface canal water spiked with NO_3^- to a concentration of $2 \text{ mg}\cdot\text{L}^{-1}$ while the canal water was still spiked to different concentrations (i.e., 0, 0.7, 2, 3, 4, 5, 15, 30, 60, 120, and 240 $\text{mg}\cdot\text{L}^{-1} \text{PO}_4^{3-}$) to explore the competing effect between nitrate and phosphate.

Collected water samples were analyzed for TP using the Hach TNT 843, 844 and 845 analyze kit, which follows the Ascorbic Acid method (EPA method 365.1) at different detection ranges. Water samples were analyzed for Nitrate using the TNT 835 Hach kit, based on the Dimethylphenol method (EPA method 40 CFR 141). All samples were measured within 24 hours of collection. Additional information on the TNT kits measuring protocols can be found at Hach (2021) and Hach (2022)

4.2.3. Isotherm equilibrium models

Isotherm studies allow the estimation of the adsorption capacity of a sorbent (i.e., sorption media) in an equilibrium condition. For this study, the four linear forms of the Langmuir isotherm model, and Freundlich linear models were applied to the isotherm data to obtain information of the adsorption capacity of the selected green sorption media. The amount of phosphate adsorbed per unit weight of the sorption media (q_e) was calculated in accordance with Eq. 18. Where m is the mass of the sorption media in grams, C_o is the initial concentration on the solution in $\text{mg}\cdot\text{L}^{-1}$, C_e is the adsorbate concentration of the solution at equilibrium in $\text{mg}\cdot\text{L}^{-1}$ and V is the volume of the solution in L.

$$q_e = \frac{(C_o - C_e)V}{m} \quad (18)$$

Langmuir isotherm model assumptions include monolayer adsorption onto a surface with finite number of adsorption sites (Hameed et al., 2007). The Langmuir nonlinear equation follows Eq. 19, where K_L corresponds the Langmuir equilibrium constant or affinity constant ($L \cdot mg^{-1}$) and q_m is the maximum adsorption capacity of the adsorbent ($mg \cdot g^{-1}$) (Guo and Wang, 2019). Four different linear forms of the Langmuir isotherm can be found in the literature and are presented in Eq. 20 (denoted as Langmuir 1, hereafter), Eq. 21 (denoted as Langmuir 2, hereafter), Eq. 22 (denoted as Langmuir 3, hereafter) and Eq. 23 (denoted as Langmuir 4, hereafter).

$$q_e = \frac{q_m K_L C_e}{1 + K_L C_e} \quad (19)$$

$$\frac{C_e}{q_e} = \frac{1}{q_m} C_e + \frac{1}{K_L q_m} \quad (20)$$

$$\frac{1}{q_e} = \left(\frac{1}{K_L q_m} \right) \frac{1}{C_e} + \frac{1}{q_m} \quad (21)$$

$$q_e = q_m - \left(\frac{1}{K_L} \right) \frac{q_e}{C_e} \quad (22)$$

$$\frac{q_e}{C_e} = K_L q_m - K_L q_e \quad (23)$$

The Freundlich model is an empirical model, its linear and nonlinear forms are presented in Eq. 24 and Eq. 25, respectively. In both equations, the constant K_F relates to the adsorption capacity, while the constant n relates to the adsorption intensity. If the n is greater than 1 then the adsorption is favorable (Campbell and Davies, 1995; Dada et al., 2012; Desta, 2013)

$$q_e = K_F C_e^{1/n} \quad (24)$$

$$\ln K_F = \ln K_F - \frac{1}{n} \ln C_e \quad (25)$$

4.2.4. Fixed bed column study

A triplicate set of columns of 5 inches (12.7 cm) in depth and 4 inches (10.2 cm) in diameter filled with 700 ml of sorption media with equivalent weight of gram of 1,000 grams of ZIPGEM

media were set up to understand the dynamic removal of ZIPGEM. A filter and layer of pebbles were placed at the bottom of each media mix to prevent clogging, while a layer of pebbles was placed at the top of each column to aid in water distribution. Prior to the column study, each column was flushed with DI water for 3 BV and left to drain for about 8 hours. The dynamic column study consisted of feeding each column in downward flow with DI water spiked with phosphate standard solution to a concentration of $4 \text{ mg}\cdot\text{L}^{-1} \text{ PO}_4^{3-}$ until the media reached saturation. Water samples were collected from the effluent at different time intervals after 23 hours until the media reached exhaustion. Water samples were analyzed for TP using the Hach TNT 843.

Data obtained from the dynamic column study was applied to Thomas (Eq. 26 and Eq. 27) and Yoon-Nelson (Eq. 28 and Eq. 29) dynamic model. The dynamic Thomas model is one of the most popular models to predict the adsorption behavior of the adsorbent (green sorption media in this study) (Nwabanne et al., 2022). The non-linear form of the Thomas model is presented in Eq. 26, while the linearized form is presented in Eq. 27. Its constant (K_t , unitless) and media maximum adsorption capacity (q_o , $\text{mg}\cdot\text{g}^{-1}$) are retrieved from the linear regression of $\ln \left[\frac{C_o}{C_t} - 1 \right]$ vs. t where C_o is the influent concentration (in $\text{mg}\cdot\text{L}^{-1}$), C_t is the effluent concentration at time t (in $\text{mg}\cdot\text{L}^{-1}$), and t is time in minutes.

$$\frac{C_t}{C_o} = \frac{1}{1 + \exp \left[\left(\frac{K_t}{Q} \right) (q_o m - C_o Q t) \right]} \quad (26)$$

$$\ln \left[\frac{C_o}{C_t} - 1 \right] = \frac{K_t q_o m}{Q} - K_t C_o t \quad (27)$$

Yoon Nelson model is one of the simplest dynamic models as it neglects the information of the physical characteristics of the physical bed and the adsorbent. The non-linear form of the Yoon-Nelson model is presented in Eq. 28 and the linear form of the model is presented in Eq. 29.

The parameters K_{YN} and τ correspond to the Yoon-Nelson constant (in min^{-1}) and the time required for the adsorbent to reach 50% breakthrough (in min) (Nwabanne et al., 2022).

$$\frac{C_t}{C_0} - C_t = \exp(K_{YN}t - K_{YN}\tau) \quad (28)$$

$$\ln\left(\frac{C_t}{C_0 - C_t}\right) = K_{YN}t - \tau K_{YN} \quad (29)$$

4.3. Results

4.3.1. Media characterization

A larger BET surface area and higher porosity can be good indicators of more available adsorbent sites resulting in better adsorption (Gupta et al., 2013). In this study, ZIPGEM has the larger BET surface area and higher porosity followed by BIPGEM and finally by CPS. Moreover, the saturated hydraulic conductivity of ZIPGEM was the highest among the three specialty adsorbents, followed by CPS and BIPGEM, respectively. The saturated hydraulic conductivity is an important factor for appropriate scale-up of the system, as it can indicate the required contact time of the sorption media and adsorbate to obtain good removal efficiency.

Aside from the physical properties of the media, it is crucial to determine the chemical properties to obtain a holistic understanding of removal mechanisms of these specialty adsorbents. The PZC provides an insight on the surface charge of the media at different pH levels. This is, at pH levels below the PZC the surface of the media is positively charged, while at points above the PZC the surface of the media is negatively charged. The location of the PZC for CPS, ZIPGEM, and BIPGEM is located at pH of ~5.6, ~9.2 and ~9.5, respectively (Figure 15).

The chemical composition of the three selected green sorption media mixes (i.e., CPS, ZIPGEM, and BIPGEM) were determined based on the X-ray Fluorescence (XRF) instrument in

this study. In Table 21, the results indicate that Si is the major element on the media matrix of the three sorption media mixes. For CPS, ZIPGEM, and BIPGEM, the percent content of Al is 10.5%, 8.4%, and 11.5%, respectively, being the second major element in the media matrix for CPS and the third major element for ZIPGEM and BIPGEM. The major difference among the chemical element composition is the presence of Fe in ZIPGEM and BIPGEM in comparison to CPS. The Fe percent content in ZIPGEM and BIPGEM is 12.1% and 12.8%, while it is only 0.4% in CPS. Another element that stands out in the chemical element composition of the media is Ca, as it can partake in the removal mechanism of PO_4^{3-} via the different sorption media mixes.

Table 21. Chemical element composition of CPS, ZIPGEM and BIPGEM raw media obtained via the XRF (elements detected at tracer level were excluded).

Element	CPS	ZIPGEM	BIPGEM	Unit
Al	10.5	8.4	11.5	%
Si	80.1	70.3	70.4	%
P	2.1	1.9	1.4	%
S	0.6	0.0	0.0	%
Cl	1.8	2.0	1.3	%
K	2.9	2.8	0.6	%
Ca	1.1	1.0	1.1	%
Ti	0.4	1.3	0.7	%
Fe	0.4	12.1	12.8	%

4.3.2. Phosphate removal mechanism

The different specialty ingredients (i.e., media components) contribute to the overall physicochemical characteristics of each media mix in a synergistic way. Each specialty ingredient was carefully selected to obtain a sorption media mix capable of excelling in the removal of one or more contaminants (i.e., phosphate vs. nitrate) from different water matrices with cost-effective, scalable, and sustainable nature. For instance, silicate sand that has a low cost can maintain an

appropriated flow rate (Table 20). Silicate sand is plentiful while providing an appropriate environment for microbial ecology to thrive, and it is simple to maintain and operate (Valencia et al., 2020). The adsorption of phosphorus to sand is mainly dependent on the Ca^{+2} content of the sand (Brix et al., 2001), as the negatively charged phosphorus is attracted to the positively charged Ca^{+2} (Eq. 30) (Deng et al., 2018, Lei et al., 2018). In the case of CPS, ZIPGEM, and BIPGEM, the percent content of Ca^{+2} is 1.1, 1.0, and 1.1% of the media in terms of element composition, respectively, suggesting that only some phosphorus removal can be associated with the electrochemical interaction of Ca^{2+} and phosphorus.



Nayak and Singh (2007) performed a XRF characterization on clay indicating that SiO_3 and Al_2O_3 are present in major quantities in clay (48.12% and 34.54%, respectively), justifying the high content of Al in the sorption media (i.e., CPS, ZIPGEM and BIPGEM). Furthermore, the adsorption of phosphate to clay is the combination of physiochemical interactions because of ligand exchange and electrostatic attraction (Wang et al., 2018). Phosphate adsorption can also be associated with the results of the interaction between aluminum ion from the dissolution of clay that results on the chemical precipitation of aluminum phosphate following Eq. 31 and 32 (Edzwald et al., 1976).



Moreover, the percentage of Fe in ZIPGEM and BIPGEM is much higher than in CPS, owing to the inclusion of ZVI as specialty ingredient of the sorption media matrices. ZVI can be oxidized by oxygen in the presence of water to form ferrous iron (Eq. 33) which can further be oxidized to ferric iron with oxygen (Stumm & Lee, 1961) (Eq. 34). Subsequently, phosphate can

precipitate with ferrous [Fe(II)] or ferric [Fe(III)] iron in accordance with Eq. 35 and 36, further contributing to phosphate removal.



The removal of phosphate by perlite in literature is disputable; for instance, Ma et al. (2011) concluded that the removal of orthophosphate via perlite is negligible with an adsorption capacity of only 0.01 mg·g⁻¹ found via a Langmuir isotherm test. Similarly, Williams et al. (2000) studied a peat-perlite medium and found that there is no phosphate adsorption. However, a study by Ozel et al. (2012) found that expanded perlite as an *in-situ* landfill liner system has a PO₄³⁻ removal efficiency of 91% from leachate. But Pradhan et al. (2020) treated greywater with perlite via a column study, and only achieved phosphate removals of up to 15%. The use of biochar for nutrient removal has increased due to its sustainable nature. The removal of phosphate by biochar is attributed to the large surface area, location of the PZC, and metal compounds (i.e., Al, Ca, Mg), supporting the main mechanism of removal (Almanassra et al., 2021, Veni et al., 2017, Yao et al., 2011).

4.3.3. Effect of water matrix on PO₄³⁻ adsorption

The effect that different pH values have on the adsorption capacity of CPS, ZIPGEM and BIPGEM was realized via a series of isotherm experiments (Figure 15). The isotherm results reflected that the adsorption capacity of ZIPGEM and BIPGEM are superior to the adsorption capacity of CPS. The better performance of ZIPGEM and BIPGEM can be attributed to the

inclusion of ZVI in the specialty ingredients, aiding the adsorption of PO_4^{3-} by electrostatic interaction in response to the varying the location of the PZC in the media and increasing PO_4^{3-} precipitation with Fe in accordance with Eq. 33-36.

In general, higher PO_4^{3-} adsorption was attained for all media mixes at lower pH (pH = 4); however, when the pH increased to pH of 7 and 10 the adsorption capacity decreased, being the lowest at pH of 10 (Figure 16). The inverse relationship between pH and adsorption capacity has been observed in previous studies. For instance, Liu et al. (2008) concluded that the PO_4^{3-} adsorption capacity of mesoporous ZrO_2 doubled by decreasing the pH in the solution with varying pH values from 10.18 to 2.82. Liu et al. (2008) also suggested that as the pH increases, the surface become less positive owing to the presence of more OH^- in the solution, resulting in a lower PO_4^{3-} adsorption as the negatively charged PO_4^{3-} competes with the OH^- for the positively charged surface, while concurrently, increasing the repulsion between the increasing negatively surface site and PO_4^{3-} . The pattern of variation in PO_4^{3-} adsorption at different pH values was closer between BIPGEM and ZIPGEM. The lower adsorption of ZIPGEM at higher pH (pH of 10) and higher PO_4^{3-} concentrations (above $130 \text{ mg}\cdot\text{L}^{-1}$) further support the competition of PO_4^{3-} and OH^- for the positively charge sites in the media surface, which decreases with increasing pH (Figure 16(b)).

An isotherm test utilizing surface water collected from a canal water system in Florida, USA spiked with NO_3^- to a concentration of 2 mg L^{-1} was performed on CPS, ZIPGEM and BIPGEM to explore the adsorption capacity and the removal mechanism based on real-world water matrices. Remarkably, the adsorption capacity of phosphate in the CPS increased by 8 times its capacity when using canal water in comparison to DI water. This can be related to the presence of calcium ($79.03 \text{ mg}\cdot\text{L}^{-1}$) and magnesium ($14.10 \text{ mg}\cdot\text{L}^{-1}$) in the canal water (Table 1A in Appendix A) which promoted PO_4^{3-} precipitation (Eq. 30). However, no effect in the NO_3^- removal efficiency

of CPS was observed by the presence of PO_4^{3-} at different influent concentrations (i.e., 0, 0.7, 2, 3, 4, 5, 15, 30, 60, 120, and 240 $\text{mg}\cdot\text{L}^{-1}$ PO_4^{3-}). The removal of NO_3^- by CPS was the lowest as compared to other media mixes ranging between 3.55 to 10.8%; The increase in PO_4^{3-} adsorption capacity by ZIPGEM and BIPGEM was only noticeable at high PO_4^{3-} concentrations. However, such change was not salient in comparison to CPS. Furthermore, higher NO_3^- removal was obtained by ZIPGEM with removal efficiency ranging from 27.9 to 39.58%, followed by BIPGEM with removals ranging from 27.45 to 34.44%. In contrast to CPS, a slight decrease in the NO_3^- and PO_4^{3-} removal efficiency of ZIPGEM and BIPGEM at high PO_4^{3-} concentrations was observed (Figure 16). This can be explained by a competition between NO_3^- and PO_4^{3-} for the available positively charged surface which only occurs at high PO_4^{3-} concentrations (Chang et al., 2019). However, for ZIPGEM and BIPGEM, the PO_4^{3-} removal efficiency attained were between 92% and 99%, respectively, regardless of the presence of NO_3^- in the water matrix. Moreover, the PO_4^{3-} removals for ZIPGEM were above 90% when the initial PO_4^{3-} concentration was below 60 $\text{mg}\cdot\text{L}^{-1}$ regardless of pH variation (pH of 4, 7 or 10).

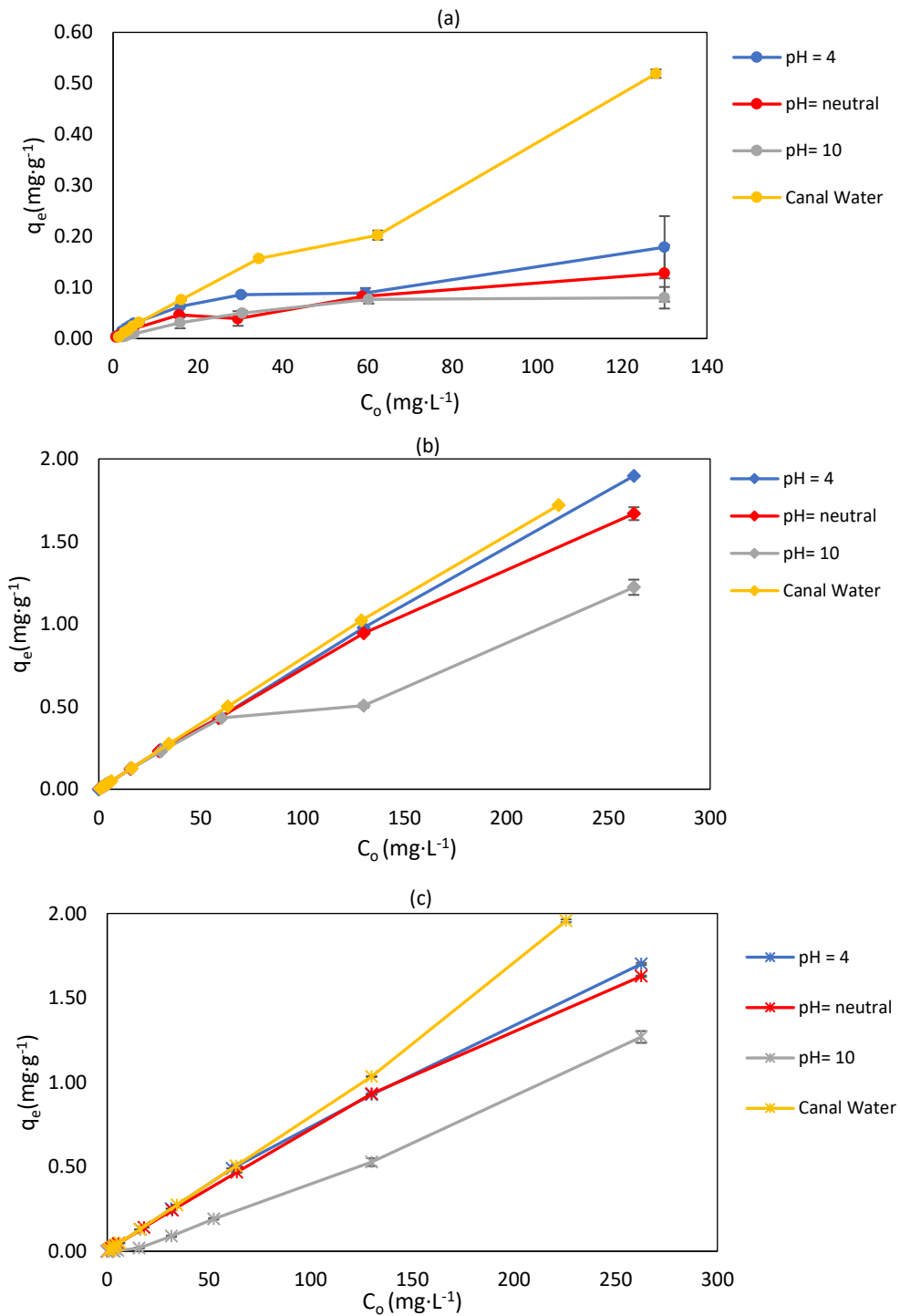


Figure 16. Adsorption capacity of (a) CPS, (b) ZIPGEM and (c) BIPGEM for nitrate varies at different water matrices.

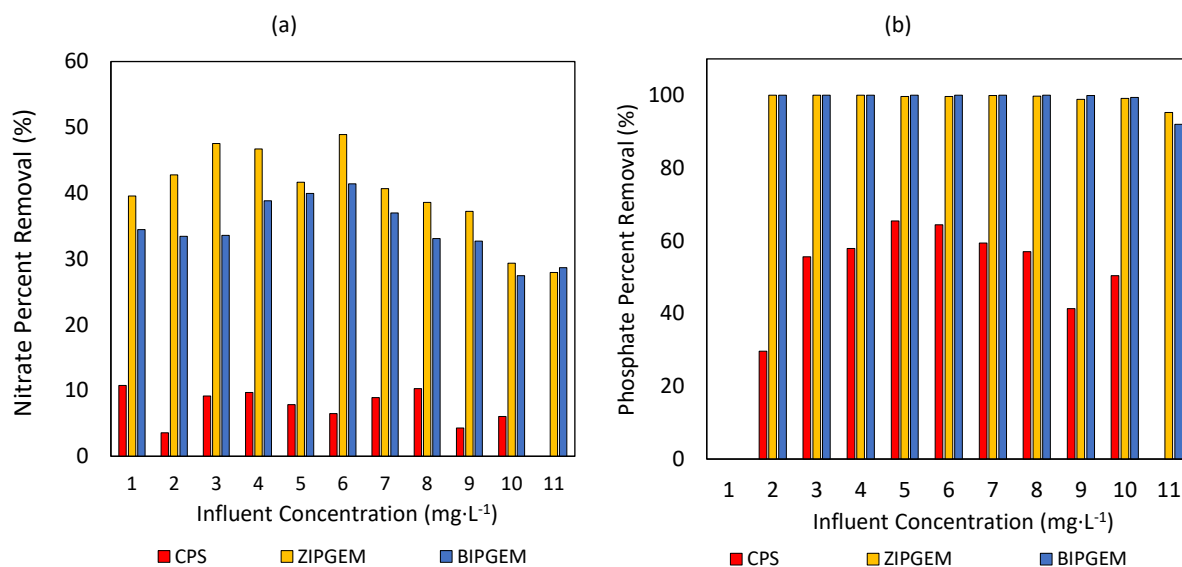


Figure 17. Simultaneous (a) NO_3^- and (b) PO_4^{3-} removal efficiency of CPS, ZIPGEM and BIPGEM using canal water spiked with phosphate to a concentration of 0, 0.7, 2, 3, 4, 5, 15, 30, 60, 120, and 240 $\text{mg}\cdot\text{L}^{-1}$ PO_4^{3-} while maintaining a constant NO_3^- concentration of 2 $\text{mg}\cdot\text{L}^{-1}$, denoted as influent 1, 2, 3, 4, 5, 6, 7, 8, 9, 10 and 11, respectively.

The Langmuir isotherm model is widely utilized for predicting the adsorption capacity of adsorbents. In this study, the data obtained from the isotherm studies were imputed into four different linear forms of the Langmuir isotherm (Figure 1A, 2A and 3A in Appendix A). By comparing the experimental data and the simulated data obtained from the different forms of the linear Langmuir isotherm, it can be concluded that linear form present in Eq. 20 (Langmuir 1) is the most appropriate to predict the adsorption capacity of the media, followed by the linear form in Eq. 23 (Langmuir 4). These results are consistent with the findings by Guo and Wang (2019). The different parameters simulated by the Langmuir and Freundlich equation are summarized in Table 22. The q_m values obtained for CPS at different water matrices ranged from 0.114 to 0.938 $\text{mg}\cdot\text{g}^{-1}$. The q_m obtained for BIPGEM and ZIPGEM were close in range with each other, but over 10 times higher than that for CPS. The q_m values for ZIPGEM ranged from 0.946 to 1.832 and for BIPGEM the q_m ranged from -0.131 to 1.824. The negative adsorption capacity obtained for q_m value for BIPGEM at pH of 10 is the result of an inappropriate fitting of the Langmuir model

(Figure A3 in Appendix A). Hence, it cannot be considered as an adequate model for estimating the q_m value. The n value results obtained from the Freundlich model further support the results obtained from the Langmuir isotherm model, suggesting that pH is inversely correlated with the media's adsorption capacity and adsorption favorability (Table 22). The adsorption capacities of different low and high-cost adsorbent found in literature were included in Table 24 and Table 24, respectively. The adsorption capacity of the green sorption media of ZIPGEM and BIPGEM are comparable to adsorption capacities of the natural adsorbents (Table 24) such as Chitin and Chitosan.

Table 22. Summary of Langmuir isotherm parameter values

	Parameters	pH=4	pH=7	pH=10	Canal Water
CPS	R^2	0.869	0.838	0.925	0.457
	$K_a(L \cdot mg^{-1})$	0.102	0.042	0.024	0.012
	$q_m(mg \cdot g^{-1})$	0.168	0.140	0.114	0.938
ZIPGEM	R^2	0.734	0.942	0.7802	0.973
	$K_a(L \cdot mg^{-1})$	0.377	0.165	0.154	2.072
	$q_m(mg \cdot g^{-1})$	1.832	1.796	0.947	1.778
BIPGEM	R^2	0.932	0.926	0.469	0.999
	$K_a(L \cdot mg^{-1})$	0.172	0.198	-0.011	3.399
	$q_m(mg \cdot g^{-1})$	1.824	1.703	-0.131	1.687

Table 23. Freundlich isotherm parameters for media

	Parameters	pH=4	pH=7	pH=10	Canal Water
CPS	R^2	0.928	0.928	0.942	0.957
	K_f	0.026	0.008	0.003	0.014
	n	2.744	1.696	1.275	1.228
ZIPGEM	R^2	0.966	0.952	0.896	0.864
	K_f	3.002	0.171	0.102	0.658
	n	2.257	1.504	1.811	1.950
BIPGEM	R^2	0.898	0.949	0.848	0.973
	K_f	0.734	0.188	0.0001	0.977
	n	5.865	1.818	0.4876	4.973

Table 24. Comparative phosphate adsorption capacities of different specialty adsorbents/media estimated via isotherm studies.

Adsorbent	Phosphate adsorption capacity	Description	Reference
CPS	0.140 mg·g ⁻¹	<ul style="list-style-type: none"> • Variation of initial concentration • Concentration range (0 to 240 mg·L⁻¹) • DI water at pH of 7 • Langmuir model 	This study
ZIPGEM	1.796 mg·g ⁻¹		
BIPGEM	1.703 mg·g ⁻¹		
IFGEM*-2	0.019 mg·g ⁻¹	<ul style="list-style-type: none"> • Variation of adsorbent mass • Influent concentration of 1 mg·L⁻¹ • DI water at a pH of 7 • Langmuir model 	Chang et al. (2019)
Iron-coated sand	0.693 mg·g ⁻¹	<ul style="list-style-type: none"> • Variation of adsorbent dosage • Adsorbent range from 0.1 to 1 g • pH of 7 and constant ionic strength • Langmuir model 	Huang et al. (2014)
Iron-manganese coated sand	0.590 mg·g ⁻¹		
Chitosan	6.64 mg·g ⁻¹	<ul style="list-style-type: none"> • Variation of initial concentration • Concentrations range (3 to 25 mg·L⁻¹) • Langmuir model 	Szymczyk et al. (2016)
Chitin	2.09 mg·g ⁻¹		
Sponge iron	1.11 mg·g ⁻¹	<ul style="list-style-type: none"> • Variation of initial concentration • Concentrations range (3 to 40 mg·L⁻¹) • Langmuir model 	Jiang et al. (2013)
Zeolite	0.303 mg·g ⁻¹		
Sugar cane bagasse biochar	2.95 to 13.21** mg·g ⁻¹	<ul style="list-style-type: none"> • Variation of initial concentration • Concentrations range (25 to 400 mg·L⁻¹) • pH of 7 • Langmuir model 	Trazzi et al. (2016)
Miscanthus giganteus biochar	3.75 to 16.10** mg·g ⁻¹		
Kaolinite	0.491 mg·g ⁻¹	<ul style="list-style-type: none"> • Variation of initial concentration • Concentrations range (25 to 400 mg·L⁻¹) • pH of 6.5±0.5 • Langmuir model 	Fang et al. (2017)
Montmorillonite	0.228 mg·g ⁻¹		
Hematite	0.064 mg·g ⁻¹		

*IFGEM stands for Iron fillings-based green environmental media

**Difference in the adsorption capacity is dependent of the pyrolysis and residence time utilized for the preparation of the biochar

Table 25. Comparative phosphate adsorption capacities of different functionalized adsorbents/media estimated via isotherm studies.

Functionalized Adsorbent	Phosphate adsorption capacity	Description	Reference
Functionalized sand with Mg-Fe layered double hydroxide	69.47 mg·g ⁻¹	<ul style="list-style-type: none"> • Variation of initial concentration • Temperature of 25 °C • Langmuir model 	Abdolmaleki et al. (2021)
Functionalized sand with Ni-Fe layered double hydroxide	66.64 mg·g ⁻¹		
Mesoporous zirconium oxide	29.71g·g ⁻¹	<ul style="list-style-type: none"> • Variation of initial concentration • Langmuir model 	Liu et al. (2008)
Iron-doped (Fe ^{II}) Activated carbon	14.12 mg·g ⁻¹	<ul style="list-style-type: none"> • Variation of initial concentration • Temperature of 25 °C and initial pH of 6 • Langmuir model 	Wang et al. (2012)
Lanthanum modified platanus ball fiber biochar	124 mg·g ⁻¹	<ul style="list-style-type: none"> • Variation of initial concentration • Temperature of 25 °C • Adsorbent dosage 0.4 g·L⁻¹ • Langmuir model 	Jia et al. (2020)

4.3.4. Fixed bed column study and removal efficiency

Fixed bed columns are a preferable experiment set up to determine the maximum adsorption capacities of green sorption media mixes as it considers axial dispersion, film diffusion resistance and intraparticle diffusion resistance (Patel, 2019). For this study, the sorption process of ZIPGEM was studied in a set of downflow dynamic columns, given its better performance in the isotherm studies in comparison against CPS and BIPGEM. Although the q_m obtained for BIPGEM were almost equivalent to the q_m obtained for ZIPGEM in the isotherm studies it was not selected because ZIPGEM has a lower production cost by excluding the biochar component and by considering the better performance of ZIPGEM at high pHs (pH of 10). The results from the dynamic column study of ZIPGEM are presented in Figure 18. The removal efficiency of phosphate for ZIPGEM ranged between 73% to 92%.

The R^2 obtained from the linear regression curve of the Thomas and Yoon-Nelson model were 0.606 and 0.606, respectively. The K_T constant from the Thomas models calculated from the

linear regression is $2.50E(-6)$ and the calculated q_0 is $7.56 \text{ mg}\cdot\text{g}^{-1}$. While the calculated K_{YN} obtained from the linear regression of the data is $1E(-05) \text{ min}^{-1}$ and the value of τ is ~ 164 days (23,635 min). By comparison the adsorption capacity of ZIPGEM with other adsorbents (Table 26), it can be concluded that ZIPGEM is more effective to other low-cost adsorbents such as zeolites and sponge iron.

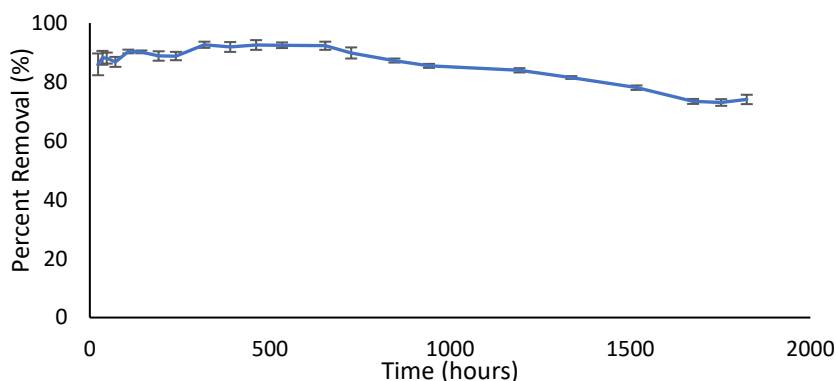


Figure 18. Dynamic phosphate removal efficiency of ZIPGEM via a column study

Table 26. Adsorption capacity of new sorption media in comparison to different adsorbents via column studies in the literature.

Adsorbent	Adsorption Capacity	Conditions	Reference
ZIPGEM	$7.56 \text{ mg}\cdot\text{g}^{-1}$	<ul style="list-style-type: none"> Constant influent rate of $8 \text{ ml}\cdot\text{min}^{-1}$ Influent concentration of $4 \text{ mg}\cdot\text{L}^{-1}$ 	This Study
IFGEM*	$0.76 \text{ mg}\cdot\text{g}^{-1}$	<ul style="list-style-type: none"> Constant influent rate of $3 \text{ ml}\cdot\text{min}^{-1}$ Influent concentration of $2 \text{ mg}\cdot\text{L}^{-1}$ of nitrate and $2 \text{ mg}\cdot\text{L}^{-1}$ of phosphate 	Ordonez et al. (2020a)
AGEM**	$0.74 \text{ mg}\cdot\text{g}^{-1}$		
Sponge iron	$0.087 \text{ mg}\cdot\text{g}^{-1}$	<ul style="list-style-type: none"> Variation of hydraulic retention time Model consistent and Temperature = 25 ± 1 	Cheng et al. (2013)
Zeolite	$0.055 \text{ mg}\cdot\text{g}^{-1}$		
***Fe-LC	$45.88 - 75.85 \text{ mg}\cdot\text{g}^{-1}$	<ul style="list-style-type: none"> Conducted both the Thomas model and BDST model Variation of bed depths 	Wang et al. (2016)
Granulated ferric Hydroxide (GFH)	31,500 BV	<ul style="list-style-type: none"> Variation in influent P concentrations Period of 3 months without interim back flushing At room temperature ($18-25^\circ\text{C}$) 	Genz et al. (2004)
Activated aluminum oxide	21,000 BV		
Ferric Sludge	$18-32.7 \text{ mg}\cdot\text{g}^{-1}$	<ul style="list-style-type: none"> Variation of sludge sample packed in column Variation of bed depth and inlet sample solution Thomas model was used 	Song et al. (2011)

*IFGEM stands for Iron-filings based Green Environmental Media

**AGEM stands for Aluminum based Green Environmental Media

***Fe-LC stands for Fe-loaded ceramic

4.3.5. Media recovery and reuse potential

The growth and production of plant crops require 16 essential elements including the macronutrients: nitrogen (N), phosphorus (P) and potassium (K), the secondary nutrients: calcium (Ca), magnesium (Mg) and sulfur (S) and the micronutrients: boron (B), chloride (Cl), copper (Cu), iron (Fe), manganese (Mn), molybdenum (Mo) and zinc (Zn). Most plant crops required Fe in small quantities of about 0.44 kg to 0.68 kg (1 to 1.5 lb) Fe per 0.405 hectare (1 acre) (Hochmuth et al., 2011). While the application of chemical fertilizer as soil amendment increases crop production it can also cause side effects including water pollution from agricultural runoff, soil acidification, impact to the microbial ecology in the rhizosphere and affect nutritional balance (Lin et al., 2019). Alternatively, the application of organic fertilizers as soil amendment can prevent soil acidification and the long-term application of organic fertilizers can increase total soil organic carbon content (Wang et al., 2019), improve soil nutrients and can regulate and improve the structure of the microbial ecology in different soils (Cui et al., 2018, Lui et al., 2021).

Contemplating the use and reutilization of the exhausted ZIPGEM for local crop fields, instead of final disposal once ZIPGEM reaches saturation, would be more advantageous. Concurrently supporting the realization toward SDGs 2.3. The re-use of the exhausted media as soil amendment is attributed to the sustainability and cost effectiveness of the new sorption media by lowering the cost and environmental impact in circular economy, reducing the ecological effects surrounding phosphorus mining (Koppelaar and Weikard, 2013) for chemical fertilizers and preserving the already limited phosphorus resources (Weikard and Seyhan, 2009). Finally, this would also lie within the scope of the SDG 2.3. to improve soil quality.

4.4. Chapter Conclusion

With the accelerated increase in world population, the United Nations developed an agenda with Sustainable Development Goals to cover areas of concern including the production of clean water and sustainable food under the SDG 2.4 and 6.3. With these goals in mind, this study intends to propose three new green sorption media capable of removing nutrients from different water matrix to prevent eutrophication of aquatic system, while allowing the recycling of the adsorbed nutrients by direct applications of the exhausted media as soil amendment. The major findings of this study include:

- The Langmuir 1 (Equation 3) (C_e/q_e vs. q_e) linear form of the Langmuir isotherm model is preferable for estimating the q_m of the green sorption media (i.e., CPS, ZIPGEM and BIPGEM) given that the simulated data is the most similar to the experimental data. The predicted q_m for CPS ranged from 0.114 to 0.938 $\text{mg}\cdot\text{g}^{-1}$, for ZIPGEM it ranged from 0.947 to 1.832 $\text{mg}\cdot\text{g}^{-1}$ and for BIPGEM it ranged from -0.131 to 1.824 $\text{mg}\cdot\text{g}^{-1}$.
- The sorption media ZIPGEM achieved higher PO_4^{3-} adsorption capacities, and thus, its performance was the most excelled given its little variation on its performance under a wider range of influent water matrix (i.e., pH of 4, 7, and 10 and canal water). This supports its application in different water treatment systems. The maximum adsorption capacity of ZIPGEM estimated in a column study was 4.45 $\text{mg}\cdot\text{g}^{-1}$.
- PO_4^{3-} removals of as high as 99% were attained for ZIPGEM and BIPGEM at initial PO_4^{3-} concentrations below 120 $\text{mg}\cdot\text{L}^{-1}$ regardless of the presence of NO_3^- when using surface water (canal water). Moreover, 90% PO_4^{3-} removals was attained for ZIPGEM at initial PO_4^{3-} concentrations under 60 $\text{mg}\cdot\text{L}^{-1}$ regardless of the initial pH level.

- The sustainable nature of the different ingredients of the media matrix and the high PO_4^{3-} adsorption capacity support the direct application of ZIPGEM, BIPGEM and CPS as soil amendment to aid in sustainable food production while contributing to improving soil quality.
- Higher nitrate removal efficiency was attained by ZIPGEM, followed by BIPGEM, and CPS; however, the biological removal of nitrate was overlooked due to short contact time in this study. Future work may be directed to understand the synthesis of microbiological and -physiochemical nutrient removal mechanisms in the different green sorption media and how the different specialty ingredients of the media can further enhance the growth of microbial ecology (i.e., biochar).

CHAPTER 5: ²CONTINUOUS FIXED-BED COLUMN ADSORPTION OF PERFLUOROOCTANE SULFONIC ACID (PFOS) AND PERFLUOROOCTANOIC ACID (PFOA) FROM CANAL WATER USING ZERO-VALENT IRON-BASED AND PERLITE-ZERO-VALENT IRON-BASED SORPTION MEDIA

5.1. Introduction

Per- and polyfluoroalkyl substances (PFAS) belong to a class of anthropogenic chemicals that have been in the limelight as contaminants of emerging concern for their adverse ecological and human health effects (Kumar et al., 2020; Podder et al., 2021). PFAS have been used widely around the globe since the 1940s (USEPA, 2021) in the manufacturing of water-resistant, stain-resistant, and non-stick commercial products, including coatings on food packaging, carpets, outdoor clothing and textile fabrics, leather goods, cosmetics and personal care products, sport goods, and firefighting foams (Bokkers et al., 2019; Wu et al., 2020; Glüde et al., 2020). With the invention of new forms of PFAS, the current inventory of more than 4,700 PFAS will continue to grow (NIH, 2021). PFAS are persistent in the environment due to their high thermal and chemical stability, attributable to their highly polar and strong carbon-fluorine bonds. As a result, PFAS has been detected in air, water, and soil environments, as well as in effluents of treated wastewater, increasing the potential for human intake via various routes (Besis et al., 2019; Lee et al., 2020). PFAS may pose negative impacts on the endocrine function including thyroid, sex hormone levels (e.g., low testosterone), high estradiol levels, pregnancy-induced hypertension, and birth weight issues (Post et al., 2012; Bruton and Blum, 2017).

² Ordonez, D., Podder, A., Valencia, A., Sadmani, A. H. M., Reinhart, D., and Chang, N. B. (2022): Continuous fixed-bed column adsorption of Perfluorooctane Sulfonic Acid (PFOS) and Perfluorooctanoic Acid (PFOA) from canal water using zero-valent iron-based filtration media, *Separation and Purification Technology*, 299(15), 121800, <https://doi.org/10.1016/j.seppur.2022.121800>.

To mitigate health risks associated with perfluorooctanoic acid (PFOA, $C_8HF_{15}O_2$) and perfluorooctane sulfonic acid (PFOS, $C_8HF_{17}O_3S$)—the most widely used PFAS—the United States Environmental Protection Agency (USEPA) has established a health advisory level of 70 parts per trillion (ppt) for combined PFOA and PFOS in 2016 (USEPA 2016). Some states have adopted stricter regulations than the USEPA advisory limit. For example, California has proposed an interim notification level of 14 ppt and 13 ppt for PFOA and PFOS, respectively for drinking water (OEHHA, 2021). In Florida, about 22 sites, including surface waters near airports and firefighter training sites as well as public water systems, have been reported to be contaminated with PFAS (Scicchitano, 2019). The Florida Department of Environmental Protection (FDEP) has initiated investigations of innovative cost-efficient, environmentally safe, and scalable technologies to mitigate Florida’s water quality issues (FDEP, 2021).

Conventional water treatment processes are not designed to remove PFAS; and thus, the investigation of PFAS removal has been extended to other innovative technologies including oxidation-reduction, volatilization, and microbial and metabolic degradation, in addition to photolytic, electrochemical, and sonochemical methods (Kucharzyk et al., 2017). However, these technologies can be costly. Recent studies on PFAS removal have focused on phase separation processes, including sorption, ion exchange, or sequestration when treating PFAS-laden water (Simon et al., 2019). Membrane processes represent one of the technologies that have effectively treated PFAS in various source waters (Mastropietro et al., 2021; Olimattel et al., 2021). Yet, membrane treatment is energy-intensive and prone to fouling issues that reduce membrane productivity (Jiang et al., 2017; Sadmani et al., 2014). Granular activated carbon (GAC) adsorption is an effective technology to treat PFAS in drinking water sources. A recent study compared the

removal of PFAS via 44 organic and inorganic sorbents, concluding that GAC or powdered activated carbon (PAC) are the best sorbents for removing PFAS (Söregård et al., 2020). GAC is more efficient in treating long-chain PFAS compared to short chain PFAS (Murray et al., 2019), and PAC is more efficient than GAC in PFAS removal because of its higher surface area. The other drawbacks of GAC/PAC include the high cost of treatment, especially the expense of media regeneration upon exhaustion, and the disposal of PFAS-rich regenerant waste and spent media (Belkouteb et al., 2020; Dixit et al., 2021).

Filtration media are cost-effective, sustainable, adaptable, and scalable and have demonstrated efficiency in removing nutrients and metals from various water matrices (Chang et al., 2010; Chang et al., 2018; Jones and Knocke 2017; O'Reilly et al., 2012; Verma et al., 2017). However, limited studies have assessed the ability of such media to remove PFAS from aqueous solutions. Additionally, there is a lack of studies focusing on the efficiency and mechanisms of PFAS removal in natural water matrices when using filtration media comprised of recycled and natural materials. Hence, the novelty of this study lies on investigating the efficiency and mechanisms of removals of selected PFAS using two cost-effective, sustainable filtration media when treating canal water. The selected sorption media were iron-sand-based filtration media, denoted as iron filings-based green environmental media (IFGEM) and sand-based filtration media, denoted as clay, tire crumb, and sand (CTS).

Thus, this novel study investigates the efficiency, adsorption capacity, and removal mechanism of PFOA and PFOS by the two green filtration media (i.e., CTS and IFGEM) via a dynamic column study with surface water from a canal (C-23) located in St. Lucie County, FL as the influent. The C-23 canal (the column influent) is connected to the St. Lucie River estuary—a

drainage area with more than 1,800 square kilometers (700 square miles) throughout the Treasure Coast of Florida (FL), close to the Indian River Lagoon, an ecologically sensitive area. The selected test site, C-23, is a constructed canal draining farmland in northwest Martin County and southwest St. Lucie County, FL collecting both agricultural discharge and urban stormwater runoff. The media performances were assessed via the bench-scale study simulating field conditions before large-scale pilot applications of the filtration media in removing PFAS from surface waters. The filtration media CTS served as a “control” to facilitate determination of the effectiveness of the inclusion of zero-valent iron (ZVI) on PFOS and PFOA removal.

The removals of PFOS and PFOA by the filtration media were hypothesized to be driven by a combination of electrostatic, hydrophobic, and hydrophilic interactions of PFOS and PFOA with the media constituents. Moreover, we hypothesized that the filtration media IFGEM would exhibit a better adsorption capacity because of the inclusion of ZVI, which can further remove PFAS by chemical oxidation and adsorption. Therefore, this study aims to answer the following research questions: (a) What are the removal mechanisms of PFOS and PFOA via filtration media (i.e., CTS and IFGEM)? (b) Does the removal efficiency of PFOS and PFOA differ significantly between CTS (the control) and IFGEM? (c) Can the surface characteristics of the filtration media be related to the removal mechanisms of PFOS and PFOA? (d) How do the interactions of PFOS and PFOA with the filtration media constituents affect PFAS adsorption and breakthrough of the media? (e) How would the adsorption capacity of the filtration media be affected by calcium ions in the natural water matrix in a karst environment when treating the canal-23 water?

5.2. Material and Methods

5.2.1. Study sites and water quality analysis

Fixed-bed column testing of filtration media in removing PFOA and PFOS from water samples collected from different locations within the C-23 canal was conducted in this study. The water from C-23 was selected as it is in Martin County within the St. Johns River watershed in Florida; and prolonged contamination of PFOA and PFOS, even at trace levels, may impact the sensitive Indian River Lagoon ecosystem. In an adjacent location, the presence of PFAS in Stuart, Martin County, Florida was first targeted in 2014 in three public supply wells; moreover in 2016 these wells exceeded the EPA drinking water standards, obligating its shut down (Daprile, 2017). For this study, water collected from C-23 canal Location 3 (shown in Figure 19) during the dry season was used as the influent condition. In addition to the assessment of basic water quality parameters, the water samples were analyzed for PFOS and PFOA at Eurofins Lancaster Environmental Laboratory (Lancaster, PA) following the modified EPA 537.1 method, and for nutrients and algal toxins at Flowers Chemical Laboratories (Altamonte Springs, Florida). In the modified EPA 537.1 method, an aliquot of 250 mL water sample containing analytes and isotopically labeled internal standards is extracted through a weak anion exchange solid phase extraction cartridge. The analytes and internal standards are eluted from the solid phase with a small quantity of extraction solvent. The extract is evaporated and then mixed with a buffer solution. The reconstituted extract is injected to a C18 liquid chromatography column, and the analytes are separated using a gradient composition of methanol and 20 mM ammonium acetate in reagent water as the mobile phase. After elution from the column, the analyte concentrations are measured by electrospray ionization-tandem mass spectrometry.

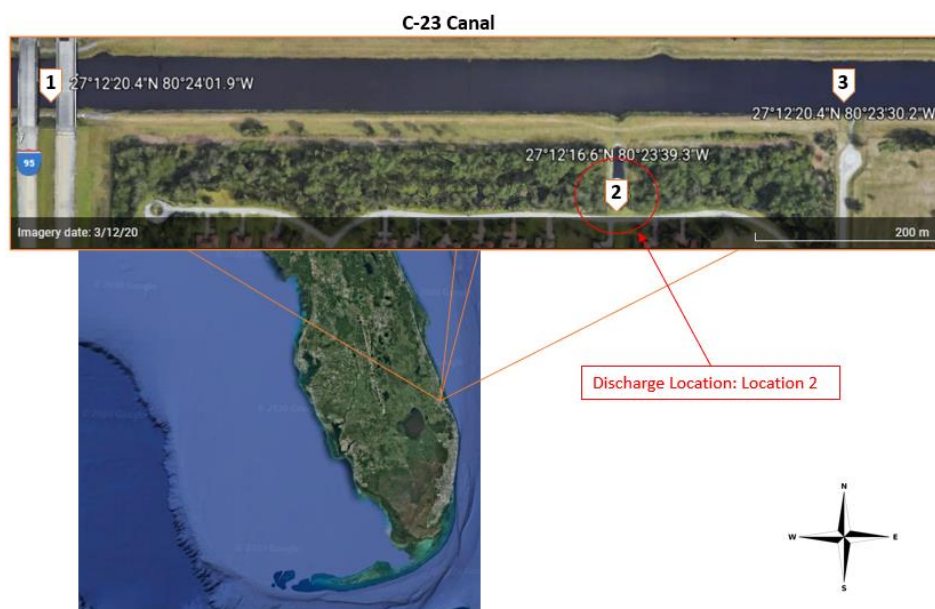


Figure 19. Location of C-23 and water sample collection points for PFAS background study for determining removal using filtration media (Source: Google Earth – Canal 23, 2021).

5.2.2. Media matrix and characteristics

Two filtration media mixes were selected to assess their potential to remove PFAS from water. The media CTS, comprised of 5% clay, 10% tire crumb, and 85% sand (Wen et al., 2020b, Ordonez et al., 2020b) was selected as a control and compared to the ZVI-based media IFGEM, comprised of 5% ZVI, 4% clay, and 91% sand. In a previous study by Valencia et al. 2020, CTS exhibited removals of up to 92.81% for total phosphorus and 70.70% for total nitrogen demonstrating nutrient removal potential. CTS was selected as a control in the current study given the absence of ZVI as component of the media matrix aiding to understand the role ZVI plays in the filtration media. The surface area and density of both CTS and IFGEM were measured based on the BET surface area method and using a pycnometer, respectively, at the certified laboratory EMSL Analytical Inc. located at Cinnaminson, New Jersey. Porosity and hydraulic conductivity of the media were measured at the Geotechnical Engineering Laboratory at University of Central

Florida (UCF). The elemental composition of the raw media samples was determined using an X-ray fluorescence (XRF) spectroscopy and media samples were examined by scanning electron microscopy (SEM) (JEOL JSM-6480) at UCF Advanced Material Processing and Analysis Center (AMPAC). XRF has been employed previously for the analyses of Al and Fe compounds (Bell et al., 2020; Ghorbani and Fakhariyan 2013; Keselj et al., 2012), oxides contained in mining rocks and sand (Sari, 2019), and for the determination of thickness and elemental composition of oxide nanoscale films (Abdel-Fattah et al. 2017). The elemental composition of the filtration media was also evaluated at AMPAC using an X-ray Photoelectron Spectroscopy (XPS) (physical electronics 5400 ESCA) (Fiorita et al. 2022).

The point of zero charge (pH_{ZPC}) for CTS and IFGEM was determined following the salt addition method (Mahmood et al. 2011) in triplicate. In this method, an aliquot of 40 ml of 0.2 M NaNO_3 was first prepared, and the pH solution on each flask was adjusted to 3.5, 4.5, 5.5, 6.5, 7.5, 8.5, 9.5 and 10.5, denoted as initial pH (pH_i), by adding either NaOH (0.1 M) or HNO_3 (0.1M). Then, 5 grams of media were added to each of the solutions and shaken for 24 hours on a shaking platform at a speed of 150 rpm and room temperature (22-23 $^\circ\text{C}$). The samples were then filtered by a 0.45 μm membrane filter and the pH was measured to obtain the final pH value (pH_f), followed by calculating ΔpH by subtracting pH_f from pH_i . The pH_{ZPC} was determined by locating the point where the ΔpH is equal to zero. The measurement of this parameter is important as it provides information on the surface charge and can aid in the understanding of electrostatic interaction between the filtration media and the sorbent (i.e., PFOS and PFOA).

5.2.3. *Experimental set-up*

The column experimental setup consisted of polyvinyl chloride (PVC) columns of 91.5 cm depth and 10.2 cm diameter (Figure 20), containing approximately 13.3 kg of CTS or 14.0 kg of IFGEM. Each PVC column was sectioned into three equal parts (30 cm) to minimize media clogging. The column sections were equally spaced and stacked vertically by attaching them to a headboard. The columns were wrapped with parafilm between each section to prevent air intrusion. Each section of the CTS and IFGEM columns was filled with CTS and IFGEM media, respectively, after slight compaction to minimize short circuiting. A layer of aquarium pebbles and a fabric weed barrier were placed at the bottom of each column section. A layer of aquarium pebbles was also placed at the top of each column section to prevent clogging and aid in distribution of the influent. The column experiments were conducted in triplicate (Figure 20). Before the column experiments were conducted, the columns were flushed with two bed volumes of distilled water to remove any background contamination of the media and left to drain for about 8 h, or until any dripping of water from the column stopped, to avoid dilution of the effluent. Canal water utilized as the influent was collected in 23 liters (5 gallon) plastic carboys and stored at 0 °C in a walk-in refrigerator at UCF Environmental Engineering laboratory. The column influent water was spiked with 70 ng·L⁻¹ each of PFOS and PFOA and administered to each column in a downflow mode with a constant flow rate of 14 mL·min⁻¹. This influent concentration was selected to represent the range of concentrations previously measured in the C-23 canal and those reported in various studies of aquatic systems around the globe. Effluent samples were collected over 12 and 40-h periods and analyzed for PFOS and PFOA at Eurofins Lancaster Laboratory following the modified EPA method 537.1 as described in Section 5.2.1.

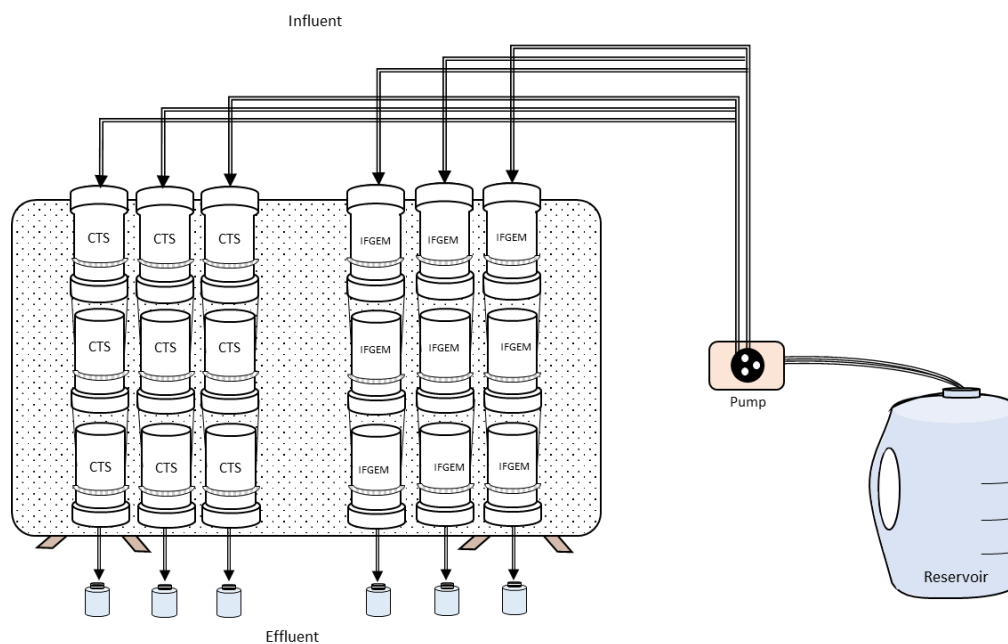


Figure 20. Experimental set up of the fixed-bed column study (in triplicate).

5.2.4. Dynamic adsorption models

Data obtained from the column studies were analyzed using selected dynamic adsorption models to determine PFOS/PFOA breakthrough. This would facilitate the determination of the suitability of the media for future field-scale design and implementation. These models are commonly applied to prove dynamic adsorption mechanisms by filtration media with real world applications. The Thomas model has been used to account for the dynamic adsorption mechanism during phosphorus removal (Jones et al., 2015) and to investigate oil and grease adsorption from refinery desalter effluent (Umembamalu et al., 2020). The Modified Dose Response (MDR), and Yoon Nelson models have been used for biosorbent application for heavy metal removal in wastewater and to estimate the scale-up parameters for adsorption columns (Abdolali et al., 2017).

The Thomas model is one of the most common and widely utilized dynamic models (Patel, 2019). The Thomas model follows second-order reversible reaction kinetics assuming Langmuir

kinetics (Thomas, 1944). It is a simple model used to analyze fixed-bed adsorption columns such as those in the current study. The linear form of the Thomas model is presented by Eq. (37), where the constant k_{TH} is the Thomas rate constant (in $L \cdot \min^{-1} \cdot \text{ng}^{-1}$), m is the mass (in g), Q is the influent flow rate (in $L \cdot \min^{-1}$), t is time (in min) and q_0 is the maximum adsorption capacity of the media (in $\text{ng} \cdot \text{g}^{-1}$). The maximum adsorption capacity, q_0 can be determined from the linear regression of $\ln\left(\frac{C_0}{C_t} - 1\right)$ vs. t plot.

$$\ln\left(\frac{C_0}{C_t} - 1\right) = \frac{k_{TH}q_0m}{Q} - k_{TH}C_0t \quad (37)$$

The MDR is an empirical numerical model (Yan et al., 2001), which can minimize errors from the Thomas model at lower and higher time points of the breakthrough curves (Recepoglu et al., 2018). The variable q_0 (in $\text{ng} \cdot \text{g}^{-1}$) is derived from the intercept and slope from the plot of $\ln\left(\frac{C_t}{C_0 - C_t}\right)$ vs. $\ln(C_0Qt)$, where a_{mdr} is the MDR rate constant (dimensionless) and the variables Q (in $L \cdot \min^{-1}$), m (in grams), and C_0 (in $\text{ng} \cdot L^{-1}$) were previously defined.

$$\ln\left(\frac{C_t}{C_0 - C_t}\right) = a_{mdr} \ln(C_0Qt) - a_{mdr} \ln(q_0m) \quad (38)$$

The Yoon Nelson model was developed to model gas and vapor adsorption by activated carbon. The linear form of the model is represented by Eq. (39) (Yoon and Nelson, 1984), where k_{YN} is the Yoon Nelson rate constant (in \min^{-1}) and τ is time required for 50% of adsorbate breakthrough (in min). The linear form of the Yoon Nelson model is obtained from the linear regression of the plot $\ln\left(\frac{C_t}{C_0} - 1\right)$ vs. t .

$$\ln\left(\frac{C_t}{C_0} - 1\right) = k_{YN}t - \tau k_{YN} \quad (39)$$

5.2.5. Statistical Analysis

Statistical analysis of variance (ANOVA) was utilized to compare the means based on the triplicate column runs and determine if there was a significant difference in the removals of PFOS and PFOA when using CTS and IFGEM. Furthermore, Kolmogorov-Smirnov (K-S) goodness of fit test was applied to PFOA adsorption (effluent concentration with respect to time) by CTS and IFGEM to determine if there was any significant difference among the data distributions for individual breakthrough curves.

The reason for choosing the K-S test instead of the ANOVA test herein is the unequal number of samples being collected across CTS and IFGEM for PFOA breakthrough curve analysis due to budget constraints. The K-S test has been employed for statistical data analyses in a variety of applications including the comparison of greenhouse gas emissions (i.e., CH₄) in rice crop cycle (Luiz, 2021), machine learning survival models (Kovalev and Utkin, 2020), data analysis of RNA sequencing (Yang et al., 2020), and stormwater quality model evaluation (Leutnant et al., 2018). The K-S test, developed by Kolmogorov (Kolmogorov, 1933) and Smirnov (Smirnov, 1948), is a non-parametric test that utilizes cumulative distribution (Aslam, 2019) based on the empirical cumulative distribution function. This approach calculates the maximum distance between two empirical cumulative distribution functions and makes no assumptions regarding the distributions of the data (Lanzante, 2021). The K-S test for a cumulative distribution function is represented by Eq. 40 (Lopes et al., 2007). The two-sample K-S test is helpful in the comparison of two samples to determine if they are from the same distribution (Luiz, 2021). For the comparison of two different data sets corresponding to cumulative distribution functions $F_n(x)$ and $F(x)$, the K-S statistic is given by Eq. (41). The empirical distribution function F_n for n independent and

identically distributed X_i observations is given by Eq. 42, where the term $I_{[-\infty, x]}(X_i)$ represents the indication function where it is 1 if $X_i \leq x$ or else 0 (Luiz, 2021).

$$KS_n = \max|F_n(x) - F(x)| \quad (40)$$

$$KS_{n,m} = \max|F_{1,n}(x) - F_{1,m}(x)| \quad (41)$$

$$F_n(x) = \frac{1}{n} + \sum_{i=1}^n I_{[-\infty, x]}(X_i) \quad (42)$$

Here, KS is the K-S statistic, $F_{1,n}(x)$ and $F_{1,m}(x)$ are the empirical distribution functions of the first and the second samples, respectively. The hypothesis statements are represented by Eqs. 43 and 44. Here, the null hypothesis (H_0) is rejected if $KS_{n,m}$ fulfills the condition in Eq. 45 at a confidence level α , meaning it is greater than the p-value from the statistical analysis.

$$H_o = F_n(x) = F(x) \quad (43)$$

$$H_A = F_n(x) \neq F(x) \quad (44)$$

$$KS_{n,m} \leq c(\alpha) \sqrt{\frac{n+m}{nm}} \quad (45)$$

5.3. Results and Discussion

5.3.1. Background PFOS and PFOA concentrations and water quality parameters

The concentrations of PFOS and PFOA and other water quality parameters including oxidation-reduction potential (ORP), pH, temperature, and nutrients [total nitrogen (TN), total phosphorous (TP)] at different locations within C-23 are listed in Tables B1, B2 and B3 in Appendix B. Two sampling campaigns were performed, one during the dry season and the other during the wet season. The concentrations of PFOA ranged from 3.4 ng·L⁻¹ (dry season) to 14 ng·L⁻¹ (wet season) and those for PFOS ranged from 4.5 ng·L⁻¹ (dry season) to 19 ng·L⁻¹ (wet season). Higher PFAS concentrations (9.7–14 ng·L⁻¹ for PFOA and 14–19 ng·L⁻¹ for PFOS) were

found at locations 1 and 3 (in the canal), in comparison to location 2 (3.4–3.6 ng·L⁻¹ for PFOA and 4.5–5.5 ng·L⁻¹ for PFOS) (discharge location). While location 2 is a discharge point reflecting PFAS carried by the stormwater runoff of the surrounding area (i.e., the subwatershed); locations 1 and 3 (canal) exhibited higher concentrations PFOS and PFOA as these locations represent the receiving water body (i.e., canal), and indicate the accumulation of PFAS over time (Chen et al., 2017). These concentrations are comparable to those observed in other sites in Florida including the Ocala Readiness Center, Marianna Readiness Center and Indian River Lagoon and Atlantic coast (Table B4 in Appendix B). However, other aquatic systems on different sites in the US exhibit higher PFOA and PFOS concentrations, driving interest in the investigation of the media removal efficiency when treating waters with higher concentrations of PFAS than those found in C-23 (Table B1 in Appendix B) (Hansen et al., 2020; Knwich et al., 2009; Sinclair et al., 2004).

The ORP levels in the canal ranged from 127.2 to 142.6 mV during the dry season and from 133.1 to 148.1 mV in the wet season, indicating that the C-23 canal water has an oxidizing environment. The average pH in the canal was 8.4 and 8.6 in the dry and wet seasons, respectively. An increase in TP concentration in the wet season, from 0.048, 0.019, and 0.057 mg·L⁻¹ as P (dry season) to 0.081, 0.048, and 0.082 mg·L⁻¹ as P (wet season) at locations 1, 2, and 3, respectively was observed. TN concentrations remained constant during the two different seasons with concentrations ranging between 1.01 and 1.06 mg·L⁻¹ as N during the dry season, and between 0.94 and 1.33 mg·L⁻¹ as N during the wet season. Finally, the concentration of calcium ion (Ca²⁺) in the C-23 ranged from 39.9 to 99.3 mg·L⁻¹, likely resulting from the weathering of minerals.

5.3.2. Media characterization

The media matrix and characteristics are presented in Table 27. When comparing CTS and IFGEM, IFGEM has a higher surface area and density than CTS. The higher surface area and density of IFGEM, in comparison with CTS can be attributed to the inclusion of ZVI. Moreover, the higher saturated hydraulic conductivity, and porosity values of CTS in comparison with IFGEM indicate that CTS is more permeable than IFGEM.

Table 27. Media matrix and characterization of filtration media.

Name	Media Matrix	BET Surface Area (m ² ·g ⁻¹)	Density (g·cm ⁻³)	Porosity (%)	Saturated Hydraulic conductivity (cm s ⁻¹)	Reference
CTS	85% sand, 10% tire crumb and 5% clay	0.86	2.40	40.10	0.026	Wen et al. (2020a)
IFGEM	91% sand, 5% ZVI and 4% clay	3.11	2.72	29.19	0.013	This study

To further characterize the removal mechanism, the pH_{PZC} of the filtration media was measured (Figure 21). The pH_{PZC} for CTS (Figure 21 (a)) and IFGEM (Figure 21 (b)) were found to be at pH of 5.6 (± 0.08) and 8.5 (± 0.08), respectively. Hence, the surface of CTS is positively charged at $pH < 5.6$ but negatively charged at $pH > 5.6$. For IFGEM, the pH_{PZC} was found at 8.5, stipulating that at any $pH < 8.5$ the surface of IFGEM is positively charged, while at $pH > 8.5$, the surface of IFGEM is negatively charged. A study conducted by Wang et al., (2018) reported that the pH_{PZC} for iron oxides ranged between 6-9.2, supporting the pH_{PZC} of IFGEM to be at a higher pH than for CTS.

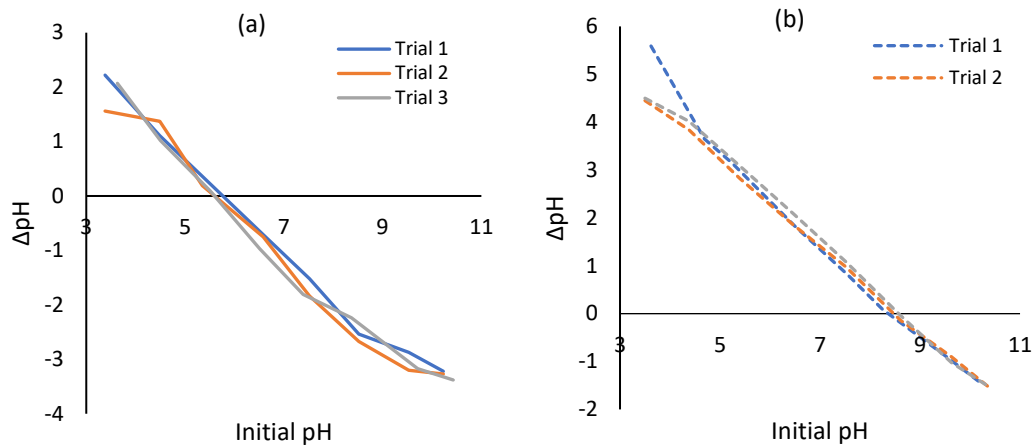


Figure 21. Initial pH vs. ΔpH plots for determining the pH_{PZC} for (a) CTS and (b) IFGEM (Color lines represent triplicates).

The chemical element, oxides composition, and surface chemical analysis for raw CTS and IFGEM filtration media were performed using XRF and XPS as summarized in Table 28 and Table 29 and Figure 22 and Figure 23, respectively. To verify the homogeneity of the media mixing process, triplicate samples of the raw filtration media were collected and analyzed using XRF, and the standard deviation of the constituents was calculated (Kempnaers, 2020). As expected, the main components of the media are SiO_2 (silica) followed by Al_2O_3 (alumina), making up to 83.59% (± 0.95) and 9.57% (± 0.61) of CTS, respectively, and 80.93% (± 3.63) and 8.37% (± 2.79) for IFGEM, respectively. The chemical oxide Fe_2O_3 was detected at lower concentrations in CTS ($0.14\% \pm 0.02$) in comparison to IFGEM ($1.80\% \pm 0.71$).

Table 28. Elemental composition of raw filtration media CTS and IFGEM based on XRF analysis.

CTS		IFGEM	
Compound	Concentration (%)	Compound	Concentration (%)
Al	8.57(±0.61)	Al	8.37(±2.79)
Si	83.59(±0.95)	Si	80.93(±3.63)
P	1.86(±0.14)	P	1.69(±0.15)
S	0.51(±0.22)	S	0.21(±0.29)
Cl	1.29(±0.76)	Cl	1.34(±0.45)
K	2.32(±0.16)	K	1.70(±0.74)
Ca	1.03(±0.05)	Ca	0.74(±0.15)
Ti	0.38(±0.13)	Ti	1.18(±1.33)
Fe	0.31(±0.05)	Fe	3.88(±1.18)

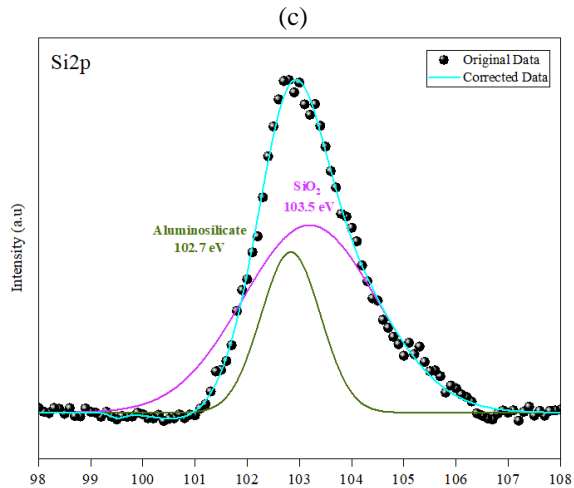
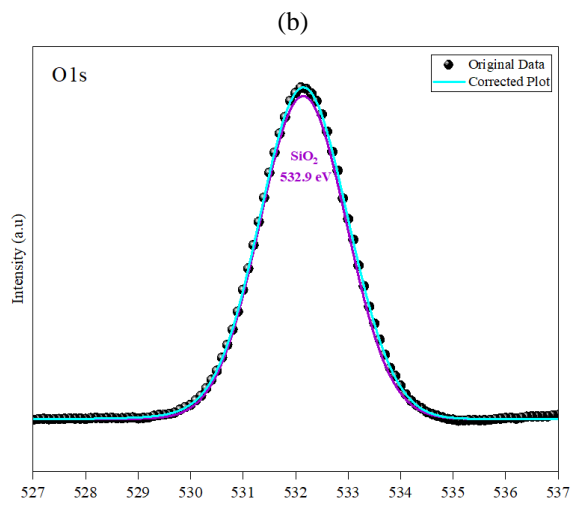
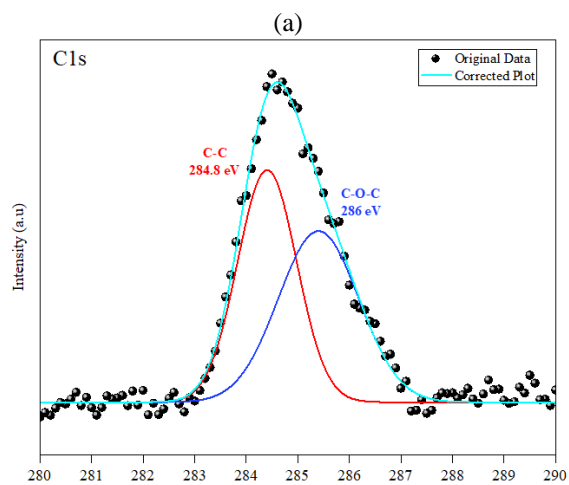
* Values in parentheses correspond to the standard deviation of 3 samples.

Table 29. Chemical oxide composition of raw filtration media CTS and IFGEM based on XRF analysis.

CTS		IFGEM	
Compound	Concentration (%)	Compound	Concentration (%)
Al ₂ O ₃	10.14(±0.56)	Al ₂ O ₃	9.96(±3.82)
SiO ₂	86.39(±1.08)	SiO ₂	83.84(±4.21)
P ₂ O ₅	1.42(±0.14)	P ₂ O ₅	1.41(±0.35)
SO ₃	0.42(±0.18)	SO ₃	0.22(±0.32)
Cl	0.42(±0.27)	Cl	0.47(±0.29)
K ₂ O	0.93(±0.02)	K ₂ O	0.84(±0.36)
CaO	0.46(±0.05)	CaO	0.38(±0.14)
TiO ₂	0.22(±0.08)	TiO ₂	0.88(±0.94)
Cr ₂ O ₃	0.01(±0.01)	MnO	0.02(±0.01)
Fe ₂ O ₃	0.14(±0.02)	Fe ₂ O ₃	1.80(±0.71)
ZnO	0.04(±0.01)	CuO	0.01(±0.00)
Br	0.01(±0.01)	SrO	0.01(±0.00)
SrO	0.01(±0.00)	Cr ₂ O ₃	0.01(±0.01)
SnO ₂	0.01(±0.00)		

* Values in parentheses correspond to the standard deviation of 2 samples.

To characterize the surface of the filtration media, an XPS analysis was conducted for both raw media (i.e, CTS and IFGEM). A survey XPS run was performed for CTS and IFGEM, and the results are presented in Figure B1(a) and (b) in Appendix B, respectively. The survey indicated that the main difference between the two selected filtration media was the presence of Fe, which was not detected in CTS. Additionally, the XPS spectra of C1, O1s, Si2p and Al2p for CTS and the XPS spectra of C1, O1s, Si2p, Al2p and Fe2p for IFGEM are presented in Figure 22 and Figure 23. From the analysis of the peak location in the spectrum, it was determined that the main components available on the surface for both media were SiO₂, Al₂O₃ and Al₂O₅Si. Moreover, in IFGEM, the forms of the Fe oxides targeted at the surface of the media were FeO and Fe₂O₃.



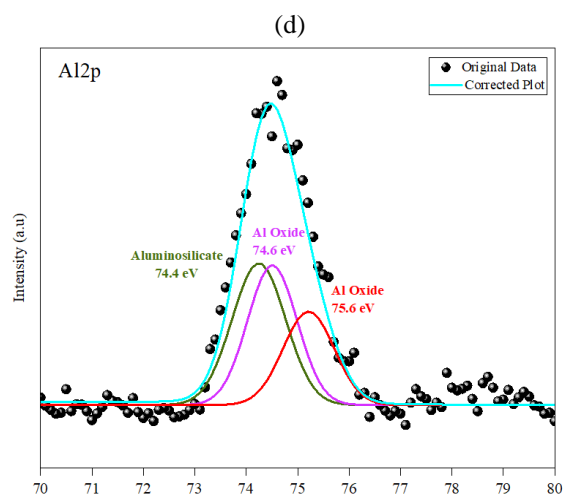
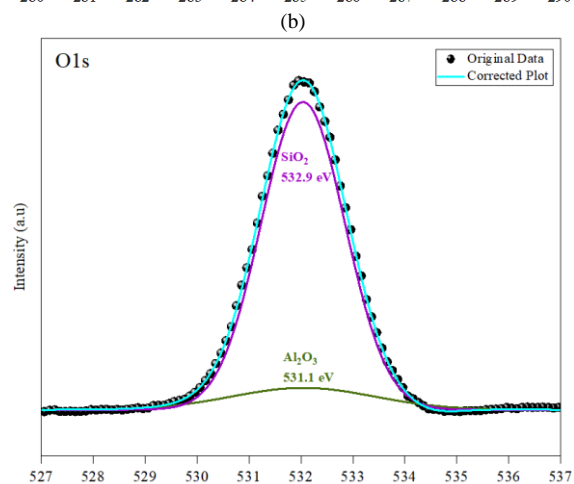
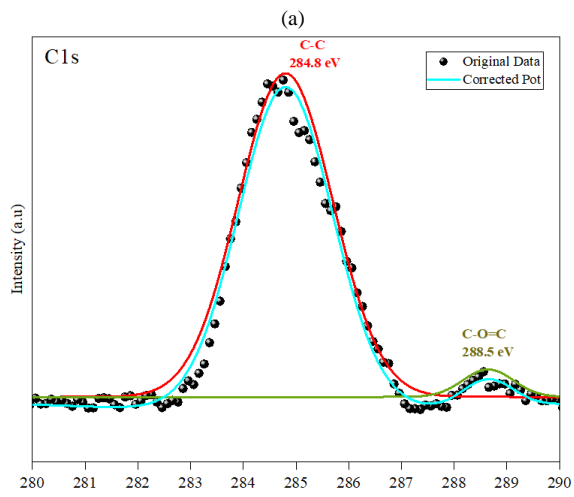
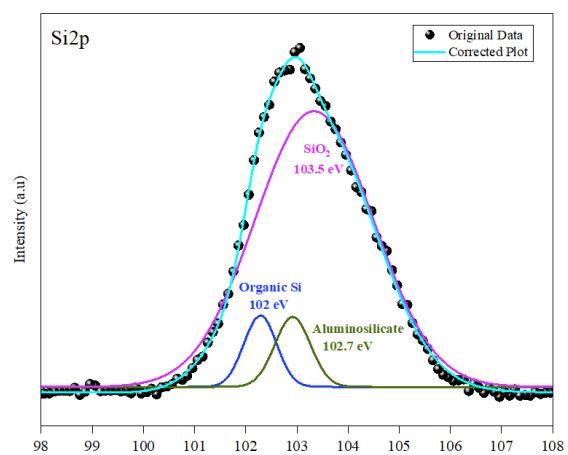


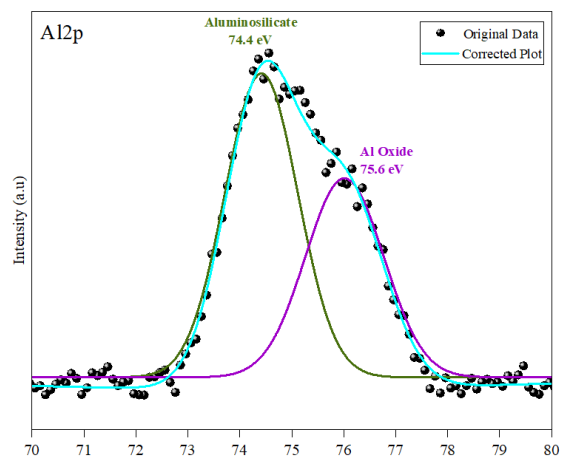
Figure 22. XPS spectra of (a) C1s, (b) O1s, (c) Si2p and (d) Al2p for filtration media CTS [x-axis for all figures correspond to the binding energy (eV)]



(c)



(d)



(e)

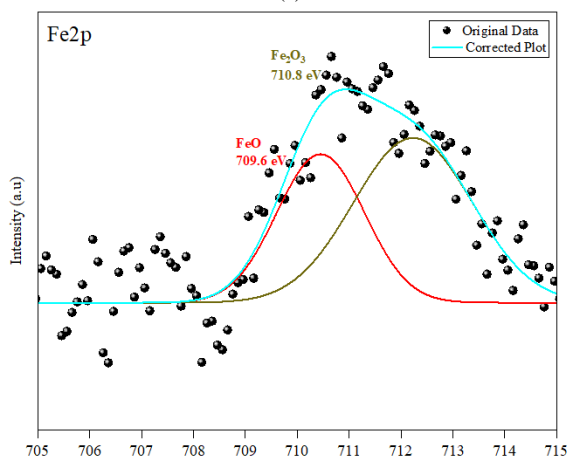


Figure 23. XPS spectra of (a) C1s, (b) O1s, (c) Si2p, (d) Al2p (e) Fe2p for filtration media IFGEM [x-axis for all figures correspond to the binding energy (eV)].

5.3.3. PFOS and PFOA removals by the filtration media

The removal of PFOA and PFOS from aqueous solutions is challenging because of the complex chemical structure of the compounds comprised of hydrophilic functional groups and a hydrophobic fluorine-saturated carbon-chain. The removal efficiencies of PFOS and PFOA by IFGEM and CTS filtration media in fixed-bed columns based on a spiked concentration of $70 \text{ ng}\cdot\text{L}^{-1}$ of PFOA and PFOS are presented in Figure 24 (a) and (b). Both media (i.e., CTS and IFGEM) exhibited removal rates above 97% for PFOS throughout the duration of the column runs. The removal of PFOA by CTS exceeded 96% during the first 6 h of the column operation but decreased during the subsequent hour to 23%. Finally, after 8–12 h of filtration, PFOA removals by CTS were negative (-36 to -50%), suggesting that the desorption may have occurred. IFGEM demonstrated PFOA removal rate above 95% during the first 9 h of column operation; however, after 12 h, the removal efficiency decreased to 72%. Then, during the following hours (18–33 h), PFOA removal by IFGEM decreased to the range of 4–18%; finally, the column reached exhaustion at around 36 h. IFGEM also exhibited negative removal (-0.5 to -1.4%) after the media reached its capacity.

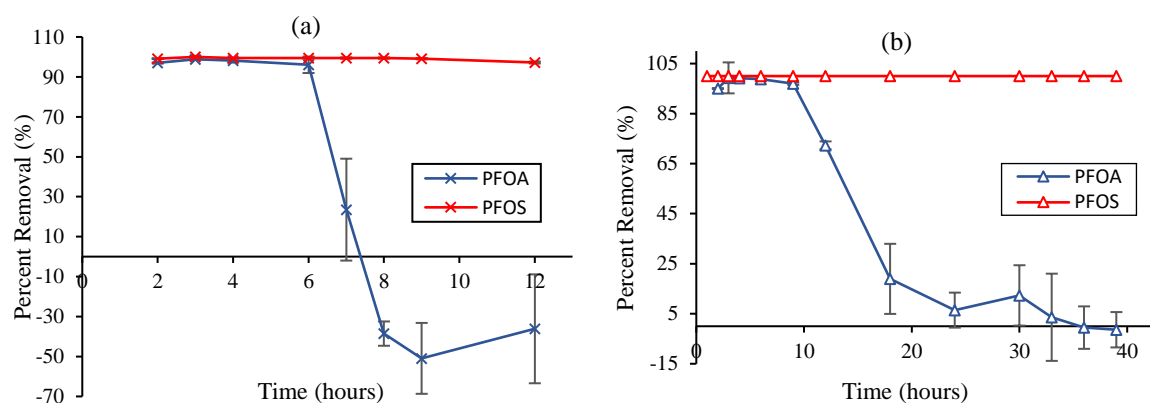


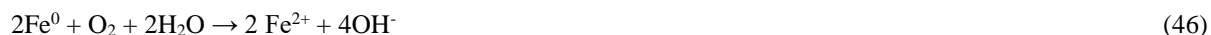
Figure 24. Media performances based on samples collected from the columns in triplicate: (a) PFOS and PFOA percentage removals when using CTS and (b) when using IFGEM [Error bars represent standard deviations of the column runs in triplicate]

5.3.4. Removal mechanisms of PFOS and PFOA using filtration media

The main component of both CTS and IFGEM media is sand, which is commonly used for soil amendment because it can hold water for prolonged times (Davis and Whiting, 2000). Sand has also been utilized in different adsorption-based technologies to remove nutrients (Achak et al., 2009), metals (Diels et al., 2003), and other pollutants (Matamoros et al., 2007). Rostvall et al. (2018) reported an average PFAS removal of 28% by sand and suggested that the sorption mechanism was governed by hydrophobic interactions. However, Helling et al. (2016) observed no adsorption of PFOA and PFOS onto silica surface due to its negative charge, yet these compounds were adsorbed onto the positively charged alumina surface. Ochoa-Herrera and Sierra-Alvarez (2008) also suggested that aluminum may drive the adsorption process of both PFOA and PFOS onto zeolites and suggested that hydrophobic interactions play a major role in PFOS adsorption. This can be related to the current study results as it supports the higher removal of PFOS by the media that both contain aluminum oxides compared to PFOA as observed in this study, attributable to the higher degree of affinity between alumina (Al_2O_3) and the functional groups of PFOS (Wang and Shih, 2011).

In IFGEM filtration media, the inclusion of ZVI likely contributed to the overall adsorption capacity of the media as ZVI oxides can aid in the breaking down of PFOS and PFOA into shorter chain PFAS and subsequently participate in their adsorption onto the media (Hori et al., 2004; 2005; 2007). While investigating the potential of ZVI along with common oxidants to remove PFOS, Parenky et al. (2020) suggested that PFOS could be removed from water through adsorption to and/or complexation with iron (Fe) oxides and dissolved Fe ions originating from ZVI. As demonstrated by XPS, the Fe oxide forms of FeO and Fe_2O_3 are present in the IFGEM media

(Figure 23). Parenky et al. (2020) reported that the adsorption of PFOS to Fe oxides and Fe hydroxides was higher than that of ZVI. ZVI may not directly interact with PFAS as ZVI inherently oxidizes when in contact with oxygen and water, and the media particles become coated with the oxides of iron (Greenlee et al., 2012; Keenan and Sedlak, 2008; Joo et al., 2004). ZVI can be oxidized to Fe^{2+} as per Eqs. 46 and 47 and further to Fe^{3+} (Eq. 48). Furthermore, carbon dioxide and alkyl radicals (R is $\text{C}_7\text{F}_{15}\text{COOH}$) result from the chemical oxidation of PFAS by oxidized iron, resembling the photoirradiation of oxidized carboxylate (Hori et al., 2007). Here, R is perfluorinated and can react in water resulting in an unstable alcohol, which can then hydrolyze, yielding a CF_2 unit and a shorter chain PFAS as per Eq. 49. The process proceeds as the resulting shorter chain PFAS continues to react until their complete mineralization to CO_2 and F^- (Hori et al., 2007).



As such, this process is crucial given that complete mineralization of PFAS may not occur in natural environments without the aid of a photocatalyst or photochemical oxidant (Hori et al., 2004; 2005). The confirmation of PFAS degradation was, however, beyond the scope of our current study.

Furthermore, PFOS and PFOA removals were likely facilitated by their electrostatic interactions with clay and iron coupled with the adsorption promoted by the hydrophilic layer surrounding the iron particles (Le et al., 2021) in IFGEM. This is because PFAS are amphiphilic, comprising hydrophobic fluorocarbon chains and hydrophilic head-groups. Hence, the synergies

among sand, clay, and ZVI in IFGEM may facilitate the removal of PFOS and PFOA through multiple pathways. The adsorption of PFAS onto montmorillonite clay was studied by Wang et al. (2021a), who suggested that the sorption of PFOA and PFOS to clay could be attributed to hydrophobic/electrostatic interactions and hydrogen bonding. Moreover, the surface charge of IFGEM as a function of pH (Figure 21 (a)), should be positive at $\text{pHs} < 8.5$ and negative at pHs greater than 8.5. Given that the pH of the influent (canal water) in location 3 was 8.4 (Table S2), the IFGEM media surface is expected to exhibit a positive charge, and hence, electrostatic interactions with the negatively charged sulfonic and carboxylic acid heads of PFOS and PFOA, respectively, within the typical range of pH of natural waters. ZVI may further remove PFOS and PFOA through reductive degradation and complex formation (Park et al., 2018). On the other hand, the point of zero charge for CTS was found to lay at pH 5.6 (Figure 21 (b)), suggesting that no or limited electrostatic interaction occurred on the surface of CTS filtration media when the pH of the canal water in location 3 was 8.4, further supporting the lower removal efficiency of CTS. The adsorption of PFAS by the filtration media can be studied by SEM examination of the raw and exhausted filtration media IFGEM and CTS (Figure 25). Figure 25 (a) and 21 (b) show the SEM images of CTS raw and exhausted media, respectively. Figure 25 (c) and 21 (d) show the SEM images of IFGEM raw and exhausted media, respectively. Noting that the discrete media particles (Figure 25 (a) and 21 (c)) became “clustered” upon exhaustion (Figure 25 (b) and 21(d)).

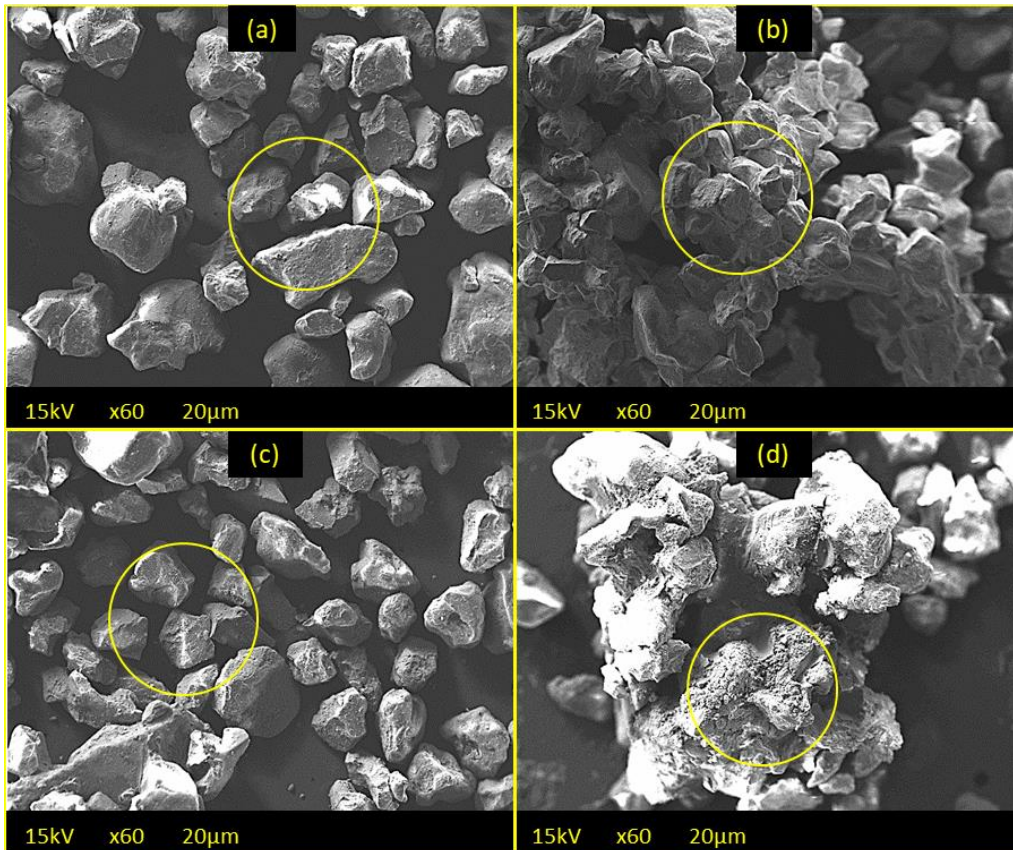


Figure 25. SEM images for (a) CTS raw media, (b) CTS exhausted media, (c) IFGEM raw media, and (d) IFGEM exhausted media (yellow circles highlight the “clustering” of media particles upon exhaustion).

5.3.5. PFOA breakthrough

Typically, breakthrough curves can be characterized by four points including the breakpoint, mass transfer point, operating limit of the column point, and complete exhaustion point (Chowdhury et al., 2015). At the breakpoint, the ratio of C_t and C_o is equal to 0.05 ($C_t/C_o=0.05=t_b$). The point when the ratio of C_t and C_o is equal to 0.5 ($C_t/C_o=0.5=t_{0.5}$) is known as the mass transfer zone and at this point, the media reaches half of its adsorption capacity. The exhaustion point is the point when the value of C_t/C_o is equal to 1, when the media reaches its equilibrium capacity of adsorption (t_e). However, the operating limit of the column is defined by 90% of media

adsorption capacity, i.e., the point at the breakthrough curve when the C_t/C_0 is equal to 0.9 ($C_t/C_0 = 0.9$).

For CTS, t_b , $t_{0.5}$, $t_{0.9}$, and t_e were 6.2, 6.7, 7.2, and 7.3 h, respectively, whereas for IFGEM, t_b , $t_{0.5}$, $t_{0.9}$, and t_e were 9.5, 14.4, 20.5, and 35 h, respectively. Hence, IFGEM took longer to reach the exhaustion point (Figure 24 (a)) than CTS (Figure 24 (b)). Nevertheless, after the media reached exhaustion, some “leaching” of PFAS was observed (i.e., $C_t/C_0 > 1$ and negative removal efficiency); this was more pronounced in the case of CTS. The PFAS leaching from CTS after about 9 h could be related to the presence of tire crumbs. Previous studies have reported the leaching of PFAS from artificial turf fields, which were made of recycled tires (Glüge et al., 2020). Both iron filings and tire crumbs are recycled materials. On the other hand, breakthrough was not observed for PFOS given the prolonged and almost complete removals (~ 100%) during the column operation.

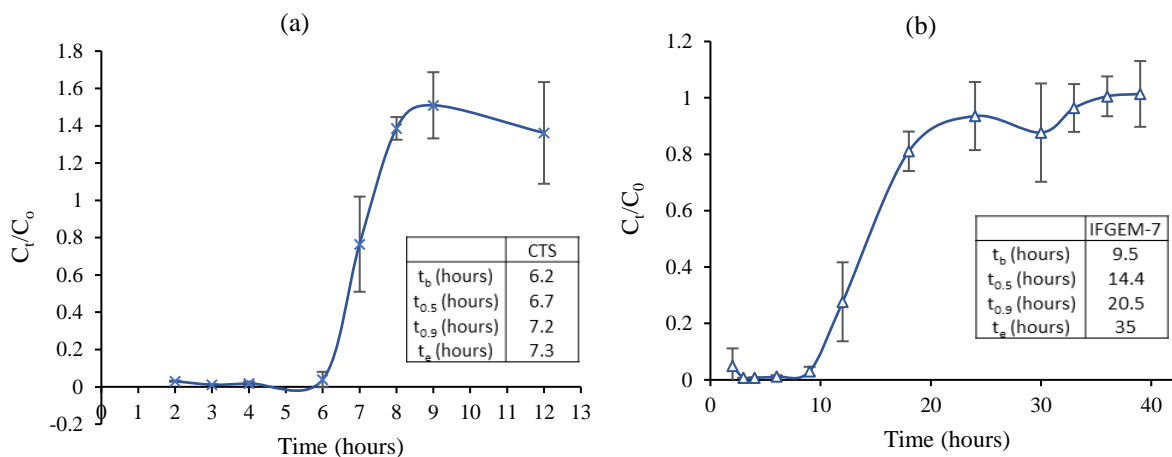


Figure 26. PFOA breakthrough curve for (a) CTS and (b) IFGEM [Error bars represent standard deviations of the column runs in triplicate]

5.3.6. PFOA dynamic adsorption analysis

The filtration media used in this study has not been previously tested for PFAS removal from a surface water matrix. Therefore, to understand the adsorption process and determine the most suitable dynamic model, three different dynamic models were evaluated for both types of media using PFOA adsorption data only since PFOS did not demonstrate a breakthrough. For CTS, the Thomas and Yoon Nelson models presented the highest correlation values with $R^2 = 0.56$ for each case (Table 30), whereas the lowest correlation for CTS was the MDR models ($R^2 = 0.42$). Similarly, for IFGEM, the Thomas and Yoon Nelson models obtained strong correlations with $R^2 = 0.86$, followed by MDR ($R^2 = 0.67$). The higher performance and correlation exhibited by Thomas model for both types of media suggest that the dynamic behavior of the breakthrough curves can be described by Langmuir kinetics of adsorption and second-order reversible reaction kinetics, which the Thomas model is based upon (Liu et al., 2019). Accordingly, PFOA adsorption may be limited to a single molecular layer onto the media for the fixed-bed column process. Hence, the Thomas model was considered the most suitable model for the current study to describe the adsorption behavior by both media. The Thomas model is simplified where the external and internal diffusion are not included and disregards intraparticle mass transfer and external resistance in a liquid phase (Shanmugam et al., 2016; Thomas, 1944).

The time difference between the breakthrough and the exhaustion points for CTS was much shorter (Figure 24) than that for IFGEM, which is supported by the larger K_{TH} constant and the smaller τ value for CTS compared to IFGEM. The time required for 50% breakthrough (τ) was approached earlier (477 min) for CTS. This was about half of the τ of IFGEM (1,110 min) when removing PFOA. Additionally, the longer time for IFGEM to reach equilibrium can be attributed to the larger surface area of IFGEM ($3.11 \text{ m}^2 \cdot \text{g}^{-1}$) compared to CTS ($0.86 \text{ m}^2 \cdot \text{g}^{-1}$), providing more sites

available for adsorption (Gong et al., 2016). The plots from the Thomas model linear regression curves of CTS and IFGEM are presented in Figure 27 to demonstrate the goodness of fit of the dynamic adsorption model with 95% confidence interval. The benefit of employing nonlinear regression of dynamic models was also expressed by Iheanacho et al. (2021) after the comparison of adsorption capacities with linear and non-linear regression.

Table 30. Correlation coefficient and model parameters in dynamic PFOA adsorption modeling analyses.

Model	CTS		IFGEM	
Thomas	R^2	0.56	R^2	0.87
	k_{TH} ($L \cdot ng^{-1} \cdot min^{-1}$)	$1.7(10)^{-4}$	k_{TH} ($L \cdot ng^{-1} \cdot min^{-1}$)	$5.7(10)^{-5}$
	q_0 ($ng \cdot g^{-1}$)	0.04	q_0 ($ng \cdot g^{-1}$)	0.09
MDR	R^2	0.42	R^2	0.79
	a_{mdr}	2.79	a_{mdr}	2.94
	q_0 ($ng \cdot g^{-1}$)	0.05	q_0 ($ng \cdot g^{-1}$)	0.10
Yoon Nelson	R^2	0.56	R^2	0.87
	k_{YN} (min^{-1})	$13.2(10)^{-3}$	k_{YN} (min^{-1})	$4.5(10)^{-3}$
	τ (min)	477	τ (min)	1,110

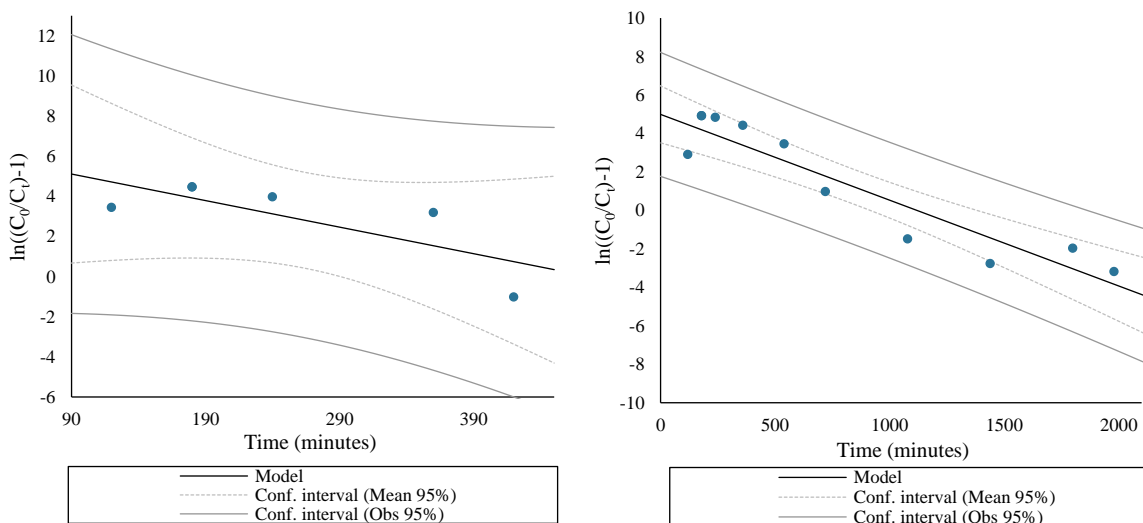


Figure 27. Thomas model liner regression for (a) CTS and (b) IFGEM.

5.3.7. Statistical analysis

The ANOVA test confirmed that there was a significant difference between the removal efficiencies with respect to time of PFOS and PFOA for CTS [F-value (6.64) > F-critical (4.60)]

and IFGEM (F-value (13.94) > F-critical (4.30)]. Furthermore, a two-tailed KS test was applied to the PFOA breakthrough distribution for CTS and IFGEM [shown in Figure 27 (a) and 23(b)]. The D value and the p-value (for $\alpha = 0.05$) were 1 and 0.028, respectively, and hence, one should reject the null hypothesis confirming that the distribution of the two breakthrough curves are significantly different. As a result, the PFOA breakthrough curves for CTS and IFGEM are significantly different at a 95% confidence level.

5.3.8. Influence of water matrix on PFOS and PFOA adsorption by the media

The functional groups of natural organic matter can interact with PFAS via electrostatic or hydrophobic interactions affecting the overall adsorption of PFAS onto the filtration media (Gagliano et al., 2020). Moreover, the presence of inorganic anions can negatively impact PFAS adsorption as it may compete for available adsorption sites (Deng et al., 2010). However, several studies concerning the adsorption of PFAS onto different sorbents including activated carbon (Du et al., 2015) and kaolinite (Xiao et al., 2011) have suggested that the monovalent and divalent cations (i.e., Ca^{2+} and Na^+) could enhance PFAS adsorption. Wang et al. (2015) and Zhao et al. (2013) demonstrated that higher concentration of Ca^{2+} at alkaline pH resulted in an increase in the rejection of PFOS via nanofiltration membranes, owing to PFOS calcium bridging. The interaction between Ca^{2+} and the sulfonate group of the PFOS resulted in enhanced molecular polarity and size of PFOS. Tang et al. (2010) reported that the sorption of PFOS to goethite increased with the increase in concentrations of H^+ and Ca^{2+} , given that Ca^{2+} promotes electrostatic adsorption between PFOS and surface of filtration media. The sorption of PFOS through electrostatic attraction will also potentially increase with the increase in the concentration of Ca^{2+} . You et al. (2010) showed that the sorption of PFOS to sediment increased with increasing concentrations of

Ca^{2+} in the water. However, if the adsorptive interaction is not influenced by electrostatic interaction, then Ca^{2+} and pH would have limited effects on adsorption. This suggests that the presence of Ca^{+2} in water can further enhance the removal of PFAS via IFGEM, unlike CTS where the effect on adsorption will be limited.

5.3.9. Recycle and disposal of filtration media

Proper treatment technologies for PFAS chemicals are necessary for PFAS, which are referred to as forever chemicals; most desirably, these technologies should guarantee the complete destruction of PFAS. Currently, the EPA proposes three technologies that can effectively destroy isolated PFAS-contaminated materials, including thermal treatment, landfill, and underground injection technologies. Thermal desorption can be an option for recovery of PFAS and reuse of the sorbing media. Sorengård et al. (2020a and 2020b), studied the thermal desorption of PFAS from soils and found that at increasing temperature the removal of PFAS from soil increases with removals ranged from 71% to 99% at 450 °C. Horst et al. (2020) discussed undesirable by-products from the treatment of PFAS-contaminated media. At present, the disposal of the spent media to a landfill with zero leachate discharge (RCRA type C) could be the most acceptable alternative; however, further investigation is required.

5.4. Chapter Conclusion

This study investigated the efficiency and mechanisms of removal of PFOS and PFOA from surface waters when using two filtration media CTS and IFGEM (CTS serving as a control) and through a dynamic fixed-bed column study. IFGEM exhibited better performance in removing PFOA and PFOS from C-23 canal water in comparison with CTS. The better performance of

IFGEM was attributed to the larger surface area of IFGEM, the positive surface charge (at pH < 8.5), higher K_{TH} constant, and higher adsorption capacity (q_0) when compared with CTS. The Thomas model serves as the most suitable dynamic model for representing the PFOA adsorption data onto IFGEM and enabled the estimation of q_0 . The larger surface area of IFGEM provides more available sites for adsorption, while the positive surface charge at pH < 8.5 of IFGEM results in electrostatic interactions facilitating PFAS removal. PFOS removal efficiency was higher than PFOA for both the media, attributable to the greater affinity of alumina (Al_2O_3) for PFOS functional groups. The chemical composition of the media, as demonstrated through XRF and XPS, further suggested that Al_2O_3 , as a component of the raw media, may also contribute to the adsorption potential of the media given its positively charged surface. Also, the higher Fe content of IFGEM may have caused greater adsorption of PFOS/A. It is acknowledged that the spent filtration media would require final disposal because such sorption processes may not destroy PFAS. Given that the presence of aluminum in the sand could contribute to PFAS removal, further research on the development of new filtration media with high aluminum content should be pursued to enhance the adsorption of PFAS. Future studies should also investigate the competing effects of nutrients on PFAS adsorption and removal mechanisms.

CHAPTER 6: COMPARING FATE AND TRANSFORMATION OF LONG AND SHORT CHAIN PER- AND POLYFLUOROALKYL SUBSTANCES (PFAS) VIA TWO SPECIALTY ADSORBENTS

6.1. Introduction

Urbanization, population growth, and anthropogenic activities have substantially contributed to the newer and previously unrecognized contaminants of emerging concerns (CECs) (Tang et al., 2021; Valsecchi et al., 2021). Per- and polyfluoroalkyl substances (PFAS) are a class of anthropogenic CECs comprised of over 9,000 identified species that are present and persistent in the environment (Ateia et al., 2019; Naidu et al., 2020; Sima and Jaffé, 2021). The oleophobic and hydrophobic properties of PFAS benefiting industrial applications (i.e., food packaging, fire-resistant fabric, insecticide, and aqueous film forming foams) (Kärman et al., 2011; Simon et al., 2019); however, the widespread occurrence of PFAS is of global concern owing to the persistence, transport, transformation, and accumulation of PFAS in the environmental matrices (Yang et al., 2019). Since the middle of the last century, their ubiquity in natural and the built environment has also raised significant public health concerns. PFAS can increase the cholesterol levels in humans, affect liver enzymes, and cause increased risk of kidney and testicular cancer, high blood pressure or preeclampsia in pregnant women, weight gain of newborn, and decreased vaccine effectiveness in children (Grandjean et al., 2017; Roth et al., 2021; Steenland and Winquist, 2021; Varsi et al., 2022). The most extensively researched long-chain PFAS (i.e., Perfluorocarboxylic acids (PFCAs) and Perfluorosulfonic acids (PFSAs) compounds that have 8 or 6 more carbons, respectively) include perfluorooctane sulfonic acid (PFOS) and perfluorooctanoic acid (PFOA), which are typically found at higher concentrations in surface and ground water than the other PFAS species (Crone et al., 2019; Kleiner et al., 2021). The frequently analyzed short-chain PFAS include

perfluorobutane sulfonic acid (PFBS), perfluorobutanoic acid (PFBA) and perfluorohexanoic acid (PFHxA), which demonstrate low adsorption potential in aqueous solutions relative to long-chain PFAS with log K_{ow} ranges of 2.8-4.6, and high persistence in the environment (Brendel et al., 2018).

Based on peer-reviewed toxicological and epidemiological studies, the EPA established health advisory levels being non-enforceable and non-regulator drinking water concentrations levels for combined PFOA and PFOS concentrations of 70 ppt in 2016 (EPA, 2016). However, due to ever-increasing human health concerns associated with PFAS exposure, in 2022, the EPA updated the health advisory levels for PFOA and PFOS concentrations to 0.004 and 0.02 ppt, respectively (EPA, 2022). Nonetheless, in early 2023 the EPA proposed a National Primary Drinking Water Regulation (NPDWR) and maximum contaminant levels (MCLs) for PFAS compounds as 4 ppt for each PFOA and PFOS, and a Hazard Index of 1 (unitless) for each PFHxS, and PFBS being legally enforceable levels (EPA, 2023b). Congruently, the World Health Organization (WHO) drafted a guidance recommending a limit of 100 ppt of either PFOA or PFOS in drinking water with a total maximum concentration of 500 ppt for combinations of up to 30 PFAS (WHO, 2022). Internationally, the regulations concerning PFAS primarily follow the Stockholm Convention Regulation (EU) No. 2019/1021 (European Union, 2020). In the Stockholm Convention of 2009, a consensus on the elimination of PFOS production and use was established with the inclusion of Persistent Organic Pollutants (POPs) on the list of discontinued compounds (Stockholm Convention, 2009; Brennan et al., 2021). While the regulations prompted the restriction of long-chain PFAS (Zushi et al., 2012), the industry has been replacing the long-chain PFAS with short-chain alternatives (Westreich et al., 2018; Knutsen et al., 2019) including

PFBS, PFBA, PFHxS, PFHxA, PFHpA, and PFPeA. Currently, there are no restrictions for the use of these short-chain PFAS although some have been recommended for voluntary phase-out (Liu et al., 2020). A further amendment to the list of POPs was conducted in the 2022 Conference of the Parties (COP) where salts and PFHxS-related compounds were included in the list (Stockhol Convention, 2022). The EPA also stipulates the final health advisory levels of PFBS at 2,000 ppt (2,000 ng·L⁻¹) (EPA, 2022). Additional drinking water guidelines for PFAS are set by individual US states with relevance to long and short-chain PFAS (Post, 2021). For instance, the guidance health advisory level in Minnesota for PFBA is 7,000 ppt (7,000 ng·L⁻¹) (Minnesota Department of Health, 2022). In addition to regulatory entities, in the US, the PFAS Regulatory Coalition comprised of non-PFAS manufacturing industrial, agricultural, trade associations and municipal entities also support state PFAS regulations and provide recommendations for health based PFAS limits (The PFAS Regulatory Coalition, 2021).

Although lower acute toxicity and bioaccumulation potential have been attributed to short-chain PFAS (Brendel et al., 2018; Li et al., 2020), the short-chain PFAS and their homologues are thought to be even more mobile and persistent when compared to the long-chain PFAS (Gagliano et al., 2020). Additionally, the half-life of short-chain PFAS such as PFHxS (average half-life in drinking water is 5.3 years) is longer than PFOS and PFOA (Li et al., 2018). The treatment of PFAS-contaminated water poses unique challenges due to PFAS physiochemical characteristics. The sulfonate and carboxyl functional groups in PFAS can contribute to their adsorption capacity as well as their mobility and solubility in aqueous solutions (Du et al., 2014; Zhang et al., 2019). However, PFBS and PFBA are the most detected short-chain PFAS in environmental samples and

it is crucial to develop more cost-effective treatment technologies focused on short-chain PFAS removal (Li et al., 2020).

The current technologies for removing PFAS from source waters include ion exchange (Dixit et al., 2021), membrane filtration including reverse osmosis and nanofiltration (Mastropietro et al., 2021), and activated carbon adsorption (Pauletto and Bandosz, 2022). While demonstrating effective PFAS removal from various water matrices, these technologies face some limitations including difficulty in handling the generated byproducts, high capital and/or operating costs, and challenges in recovery and/or regeneration of treatment media (e.g., resins, membranes, adsorbents). In addition, some degradation technologies including electrochemical treatment, chemical oxidation (Dombrowski et al., 2018), photodegradation (Esfahani et al., 2022), and reduction mineralization (Trang et al., 2022) are limited by their high cost and the potential hazard posed by intermediate transformation products that may form during degradation processes. Moreover, in the presence of other co-contaminants in the source water, the control over the treatment of targeted PFAS is difficult.

Specialty adsorbents are innovative media that have gained significant attention due to their low cost, stability, simpler maintenance, and prolonged service life. These adsorption media treat a variety of pollutants including nutrients, metals, algal toxins, organic acids, pharmaceuticals, and other emerging contaminants simultaneously. In this study, the efficiencies of two recently developed adsorption media in removing PFAS were evaluated, and the removal mechanisms were investigated. The two new specialty adsorbents used in this study are Zero-Valent-Iron and Perlite based Green Environmental Media (ZIPGEM) and Clay-Perlite and Sand sorption media (CPS). While the ZIPGEM media is comprised of sand, clay, perlite, and zero-valent-iron (ZVI), CPS

contains sand, clay, and perlite, mixed at specific ratios. Both the media (ZIPGEM and CPS) have been recently evaluated for tannic acid removal from river water (Ordonez et al., 2022b), both exhibiting color removal of ~77%. Based on the common components of sand, clay, and ZVI the effectiveness of the two specialty adsorbents for PFAS removal also compare favorably with that of previously developed green sorption media of Iron-Filings-based Green Environmental Media (IFGEM-7) (Ordonez et al., 2022b).

When investigating another specialty media (IFGEM-7), in a recent study (Ordonez, et al. 2022c), we demonstrated the contribution of ZVI included in the media in adsorbing 99% of PFOS and 28% of PFOA. In another recent study (Ordonez et al. 2022a), we observed high removal of PFOS by IFGEM-7 (97%) and another media comprised of clay, tire crumb, and sand (CTS) (96%). However, CTS reached exhaustion much quicker than IFGEM-7, raising the concern of PFOS desorption possibly from the tire crumb. Based on the observations from the previous studies that included some media constituents (sand, clay, and ZVI) common to those used in the current study, the aim of this study was to mitigate the limitations such as considering effect of pH and estimation of service life as reported in the previous studies while attaining optimal removal efficiencies for selected PFAS. In addition to modifying the matrices of the specialty adsorbents, their efficiencies in removing selected short-chain PFAS were evaluated, considering multi-pollutant remediation scenarios for practical applications.

ZIPGEM and CPS are a new suite of green sorption media which include perlite specifically to interact with clay and ZVI in the media matrix, leading to contribute to PFAS removal from water. Based on the components of perlite, clay, or ZVI, the effectiveness of the two new specialty adsorbents can then be compared in terms of both long and short-chain PFAS

removal. The research questions answered in this study include: (1) How can morphology in these material matrixes of the two specialty adsorbents support PFAS adsorption? (2) What are the possible synergistic interactions of the constituents of CPS (i.e., sand, clay, perlite) and ZIPGEM (i.e., sand, clay, perlite, and ZVI) that may cause differences in PFAS removal efficiencies? (3) Does adsorption by CPS or ZIPGEM favor long-chain vs. short-chain PFAS? (4) Will the inclusion of ZVI in ZIPGEM produce more short-chain PFAS after adsorption? (5) Can a breakthrough curve (using column studies) provide adequate information regarding the media behavior and treatment capacity for full-scale implementation? (6) Can the two specialty adsorbents effectively treat PFAS in surface water and meet the health advisory or regulatory thresholds for both long-chain and short-chain PFAS?

6.2. Material and Methods

6.2.1. Preparation and characterization of specialty adsorbents

The proposed media matrix was designed to enhance PFAS removal by systematically selecting materials that promote electrostatic and hydrophobic interactions. The common constituents of both the media used in this study are sand, clay, and perlite, whereas ZIPGEM also contains ZVI. The media components in percent by volume (% by weight) of ZIPGEM are 85% sand (81.3% sand by weight), 5% clay (2.2 % clay by weight), 5% ZVI (1.5% ZVI by weight), and 5% perlite (15% by weight), whereas CPS is comprised of 92% sand (96.5% sand by weight), 5% clay (2.5% clay by weight), and 3% perlite (1% perlite by weight). The saturated hydraulic conductivity and porosity of ZIPGEM were analyzed at the geotechnical laboratory at the University of Central Florida. Moreover, the BET surface area and bulk density were measured by EMSL, an external laboratory. The hydraulic conductivity, BET surface area, porosity, bulk

density, and chemical composition were previously evaluated for CPS as described in Ordonez, et al. (2022b).

Additional media characterization was conducted using an Empyrean x-ray diffraction (XRD) (PANalytical B.V.) to examine the crystalline phases and surface chemical elemental composition of both CPS and ZIPGEM before and after exhaustion. The XRD analysis was performed using Copper K_{α} radiation wavelength of 1.54 at 45 kV and 40 mA and the XRD patterns scanned at 0° to 80° (2θ) were visualized with the software HighScore (Plus) utilizing the Joint Committee on Power Diffraction Standards (JCPDS) database for phase identification of unknown samples. Furthermore, the Point of Zero Charge (PZC), i.e., the pH when the net charge of the adsorbent surface is zero (pH_{PZC}) can further explain adsorption as it explains surface charge of the adsorbent (i.e., CPS and ZIPGEM). The pH_{PZC} for CPS and ZIPGEM was determined following the protocol outlined in Ordonez et al. (2022a).

6.2.2. Isotherm Kinetic Study

Prior to conducting the column studies, adsorption kinetic testing for PFOS and PFOA was conducted and adsorption capacity of ZIPGEM and CPS was determined. A series of kinetic isotherm studies were conducted in 500 mL polypropylene beakers in duplicate. The beakers were first washed with methanol and a mass of 50 g of media was added to 400 mL aqueous solution spiked at initial PFAS concentration of $10 \mu\text{g}\cdot\text{L}^{-1}$ ($5 \mu\text{g}\cdot\text{L}^{-1}$ of PFOS and $5 \mu\text{g}\cdot\text{L}^{-1}$ of PFOA). The samples were agitated at 160 rpm on a benchtop orbital shaker and collected at seven different times, including after 2, 5, 10, 20, 30 h for ZIPGEM with additional 36 and 42 h of mixing for CPS. Samples were collected and left for 60 minutes to allow the media to settle before filtration

using a 0.8- μm pore size polypropene membrane filter. The water samples were stored and delivered to Eurofins Lancaster Laboratory for analysis of PFOS and PFAS.

The primarily employed kinetic models are the pseudo-first order (PFO), pseudo-second order (PSO) models, intraparticle diffusion model, and Elovich model. The PFO is based on the assumption of proportionality between the adsorbent and the liquid phase adsorbate (Chowdhury and Saha, 2011). The PSO assumes that the rate limiting step is chemical adsorption (Saleh et al., 2017). The PFO and PSO can be used to determine the adsorption capacity of the media and are described in Eq. 51 and Eq. 52, respectively.

$$q_t = q_e(1 - e^{-k_1 t}) \quad (50)$$

$$\log(q_e - q_t) = -k_1 t + \log q_e \quad (51)$$

$$\frac{t}{q_t} = \frac{t}{q_e} + \frac{1}{k_2 q_e^2} \quad (52)$$

where q_e is the equilibrium adsorption capacity ($\text{ng}\cdot\text{g}^{-1}$), q_t is the adsorption capacity at any time t ($\text{ng}\cdot\text{g}^{-1}$) and k_1 and k_2 are the pseudo-first ($\text{L}\cdot\text{min}^{-1}$) and pseudo-second order ($\text{g}\cdot\text{ng}^{-1}\cdot\text{min}^{-1}$) constants, respectively (Syamsu et al., 2022).

Intraparticle diffusion (IPD) model (Eq. 53) is an empirical model based on Fick's second law (Rosa et al., 2019), where k_{id} is the intraparticle diffusion rate constant ($\text{ng}\cdot\text{g}^{-1}\cdot\text{min}^{-1/2}$) and C is the intercept where it can provide information about the boundary thickness ($\text{ng}\cdot\text{g}^{-1}$) (Mahmoud et al., 2017). Hence the larger the C value, the greater the boundary layer effect, with a positive value indicating fast adsorption (McKay et al., 1980; Wu et al., 2009) as this value can be related to the resistance to external mass transfer (Santhi et al., 2010).

$$q_t = k_{id}t^{1/2} + C \quad (53)$$

Elovich model, as given by Eq. 54, best represents chemical adsorption onto heterogenous surfaces (Wei et al., 2021). In Eq. 54, α_e is the initial adsorption rate ($\text{ng}\cdot\text{g}^{-1}\cdot\text{min}^{-1}$) and β is the desorption constant ($\text{g}\cdot\text{ng}^{-1}$) (Najim et al., 2010).

$$q_t = \frac{1}{\beta} \ln(\alpha_e \beta) + \frac{1}{\beta} \ln(t) \quad (54)$$

6.2.3. Fixed-Bed Column Study and Dynamic Models

The fixed-bed column study was aimed to provide appropriate data that can be translated into real-world applications. A fixed-bed column study in triplicate (for each media) was conducted to assess PFAS removal by ZIPGEM and CPS under a scenario close to the real case applications following the experimental protocol outlined in Ordonez et al. 2022a. PVC columns with a total length of 91.5 cm (3 ft) and an inner diameter of 10.2 cm (4 in) were used. Each column, containing ~2600 mL of filtration media, was divided into three sections, each 30.5 cm (12 in) in length. The three column sections were sealed with parafilm and water-resistant tape forming a single column to prevent outside disturbances such as air intrusion. Before the columns were filled with ZIPGEM or CPS, a filter and layer of pebbles were placed at the bottom of the column to prevent clogging of the effluent port. Additionally, a layer of pebbles was included at the top of the media to aid in water distribution. Before commencing the experiment, the columns were flushed with DI water for approximately two bed volumes and left to drain for approximately 8–10 h to remove any impurities present in the media. The influent was prepared by spiking canal water with PFOA and PFOS at a concentration of $70 \text{ ng}\cdot\text{L}^{-1}$ of each of PFOA and PFOS ($140 \text{ ng}\cdot\text{L}^{-1}$ total PFAS) to be introduced in a downflow mode. The influent water characteristics used in this

study are comparable to the concentrations found in the US for groundwater, surface water and some landfill leachates as summarized in Table C1 (in Appendix C). A peristaltic pump was used to deliver the influent to the columns at a constant flowrate of $14 \text{ mL}\cdot\text{min}^{-1}$ until media saturation upon which the delivery of the influent was stopped. The effluent samples were collected at specific time intervals viz. 2, 4, 6, 9, 12, 16, 21, 24, and 32 h for CPS, and 2, 3, 6, 9, 12, 18, 21, 24, 32, 36, 39, 42, and 48 h for ZIPGEM when the media reached exhaustion. The effluent samples were then delivered to Eurofins Lancaster Laboratory for the analysis of PFOS, PFOA, PFHpA, PFHxA, PFHxS, PFPeA, PFBA, and PFBS following the modified EPA method 537.1 (Shoemaker and Tettenhorst, 2020). Following the column study, the experimental data were further evaluated using dynamic adsorption models to estimate the adsorption capacity of the filtration media. For comparison the three commonly utilized dynamic adsorption models, including Thomas, Modified Dose Response (MDR), and the Yoon-Nelson models, were explored (Ordonez et al., 2022a).

The results from the column study pertaining to the breakthrough curve can be further analyzed for real-world implementation to obtain more accurate information of the treatment capacity and service life of the sorption media. Two parameters that can be determined are the length of unused bed at equilibrium (*LUB*) and bed capacity (*BC*) calculated using Eq. 51 and Eq. 52, respectively (Karunaratne and Amarasinghe, 2013). The *LUB* represents the mass transfer zone of the column and is essential for scale-up of the treatment process (Harripersadth and Musonge, 2022). Here, *LUB* is in cm, *Z* is the bed height (cm), T_S is the time corresponding to bed exhaustion (min), T_b is the breakthrough time (min), *BC* is the bed capacity (cm), *Q* is the flow rate ($\text{L}\cdot\text{min}^{-1}$), C_0 is the initial concentration ($\text{ng}\cdot\text{L}^{-1}$), and C_e is the concentration at equilibrium

($\text{ng}\cdot\text{g}^{-1}$). The breakthrough time is dependent on the breakthrough concentration C_b where the allowable breakthrough concentration is assumed to be 5% of C_0 .

$$LUB = \frac{z}{T_S}(T_S - T_b) \quad (55)$$

$$BC = Q(C_0 - C_e)T_S \quad (56)$$

6.2.4. Water Characterization

PFAS can be found in soil, air, and water; for instance, an analysis of the PFAS concentrations at different locations in Switzerland (502 water samples) was performed by Ahrens et al. (2016) concluding that the average total PFAS concentration for 26 PFAS compounds including PFOS, PFOA, PFPeA (Perfluoropentanoic acid), PFHxA, PFHpA (Perfluoroheptanoic acid), PFBS, and PFHxS (Perfluorohexanesulfonate) in drinking water sources was $8.4 \text{ ng}\cdot\text{L}^{-1}$, in surface water the average concentration was $112 \text{ ng}\cdot\text{L}^{-1}$, in groundwater the average concentration was $49 \text{ ng}\cdot\text{L}^{-1}$, landfill leachates was $487 \text{ ng}\cdot\text{L}^{-1}$, and background screening lakes was $3.4 \text{ ng}\cdot\text{L}^{-1}$. Moreover, Liu et al. (2021) concluded that East China and the Southwest regions posed the highest risk associated with high concentrations of PFAS in drinking water, and the mean concentration in different drinking water samples (526 water samples) ranged from $0.1\text{--}502.9 \text{ ng}\cdot\text{L}^{-1}$. In Porto Alegre, Brazil, a very populated and urbanized state capital, between 11 and 10 species of PFAS were found in groundwater and surface water (Stefano et al., 2022).

Surface waters collected from C-23 Canal in Port St. Lucie, Florida, USA were found to contain PFOA and PFOS in the concentrations ranges of $3.4\text{--}15 \text{ ng}\cdot\text{L}^{-1}$ and $4.5\text{--}19 \text{ ng}\cdot\text{L}^{-1}$, respectively (Table 31). The short-chain PFAS including PFHpA, PFHxA, PFHxS, PFPeA, PFBA, and PFBS were also detected at concentrations ranging from 5.7 to $10.27 \text{ ng}\cdot\text{L}^{-1}$ with PFHxS

exhibiting the highest concentration among the short-chain PFAS. The concentrations of other water quality parameters including total nitrogen, organic nitrogen, and total phosphorus ranged from 0.94 to 1.33 mg·L⁻¹ as N, 0.88 to 1.22 mg·L⁻¹ as N, and 0.019-0.082 mg·L⁻¹ as P, respectively (Ordonez et al., 2022a). The concentration of calcium, which can contribute to PFAS adsorption, ranged from 39.93 to 99.33 mg·L⁻¹.

Table 31. Selected properties and background concentrations of selected PFAS in C-23 surface water.

PFAS	Acronym	Classification*	Molecular Weight (g·mol ⁻¹)	Chemical Formula	Concentration Range (ng·L ⁻¹)
Perfluorooctanesulfonic acid	PFOS	PFSA	500.13	C ₈ F ₁₇ SO ₃ H	4.5-19
Perfluorooctanoic acid	PFOA	PFCA	414.07	C ₇ F ₁₅ COOH	3.4-15
Perfluorohexanesulfonic acid	PFHxS	PFSA	400.12	C ₆ F ₁₃ SO ₃ H	9.8-11
Perfluoroheptanoic acid	PFHpA	PFCA	364.06	C ₆ F ₁₃ COOH	5.1-6.2
Perfluorohexanoic acid	PFHxA	PFCA	314.05	C ₅ F ₁₁ COOH	5.5-6.1
Perfluorobutanesulfonic acid	PFBS	PFSA	300.1	C ₄ F ₉ SO ₃ H	6.4-7.9
Perfluoropentanoic acid	PFPeA	PFCA	264.05	C ₄ F ₉ COOH	5.6-7.3
Perfluorobutanoic acid	PFBA	PFCA	212.08	C ₃ F ₇ COOH	7.3-7.9

* Perfluorocarboxylic acids (PFCA), Perfluorosulfonic acids (PFSA)

6.3. Results and Discussion

6.3.1. Specialty adsorbents and water characteristics

The physical properties of CPS including bulk density (g·cm⁻³), porosity (%), hydraulic conductivity (m·sec⁻¹), BET surface area (m²·g⁻¹) analyzed in a recent study by Ordonez et al. (2022b), are summarized in Table 32 for comparison with the physical characteristics of ZIPGEM used in the current study. ZIPGEM has a higher density, BET surface area, saturated conductivity, and porosity when compared to CPS, attributable to the inclusion of ZVI in ZIPGEM.

Table 32. Media characterization

Name	Density (g·cm ³)	BET Surface Area (m ² ·g ⁻¹)	Saturated Hydraulic Conductivity (m·sec ⁻¹)	Porosity (%)	Reference
CPS	2.61	1.08	1.7·(10 ⁻⁴)	26	Ordonez, et al. (2022b)
ZIPGEM	2.78	1.50	2.8 (10 ⁻⁴)	33	This study

In general, PFAS adsorption is governed by surface chemistry and surface charge of the adsorbent material (Campos-Pereira et al., 2020; Pauletto and Bandosz, 2022). The pH_{PZC} is an important parameter that can be linked to the adsorptive interactions driven by the surface charge of the adsorbent. The pH_{PZC} of ZIPGEM (9.2) was higher than CPS (5.6) (Figure 28), indicating that the media possess predominantly positive surface charges in aqueous solutions below pHs of 9.2 and 5.6, respectively. Hence, covering greater pH range in water, ZIPGEM may be more advantageous for implementation of PFAS removal in various water matrices. When investigating PFAS adsorption of 12 PFAS compounds onto ferrihydrite, Carlos-Pereira, et al. (Campos-Pereira et al., 2020) demonstrated that PFAS adsorption was inversely related to pH, attributed to the pH-dependent surface charge of ferrihydrite with lower pH contributing to positive surface charge of the particle.

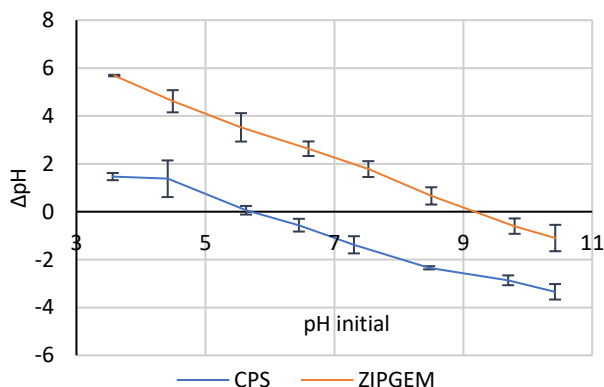


Figure 28. Point of Zero Charge for ZIPGEM and CPS (Each error bar represents one standard deviation above or below the mean of triplicate analyses).

The chemical-state surface characterizations of the raw filtration media CPS and ZIPGEM, analyzed via the x-ray diffraction (XRD), are presented in Figure 29 (a) and 25 (b), respectively. Comparing the spectrum of the raw and exhausted CPS and ZIPGEM media can help address research question 1. While the main difference between CPS and ZIPGEM, as exhibited by the XRD pattern, was the absence of Fe in CPS, after carefully examining the spectrum for the different elements, it can be observed that the main media constituents include SiO₂, Al₂O₅ and Al₂O₃ for CPS and SiO₂, Al₂O₃, and Fe₂O₃ for ZIPGEM (Figure 29 (a) and 25 (b)). Moreover, the crystalline phase difference between the raw and exhausted media is confirmed from the intensities and position of the diffraction peaks. The spectrum was used to evaluate the compounds that are predominant in both media based on the peaks. In this context, the XRD pattern shows sharp peaks associated with crystalline phase identified as SiO₂ between position 26-27 (2θ) for both raw and exhausted CPS and ZIPGEM. Other peaks representative of Al₂O₃ and AlF₃ are present for CPS raw and exhausted media, respectively. The presence of the fluorine in the AlF₃ can suggest and point to the adsorption of PFAS compounds and complexation with ZVI. In addition, peaks corresponding to Fe₃O₃ and FeS₂ were found in ZIPGEM raw and exhausted media, respectively. Similarly, the presence of sulfur in the exhausted media peaks corresponding to FeS₂ can suggest PFAS adsorption onto the media. Hence, by seeing the appearance of AlF₃ in CPS exhausted media we attributed this presence to the interaction between aluminum and fluorine possibly from PFAS compounds. Similarly, the appearance of FeS₂ in ZIPGEM exhausted media was attributed to the interaction between iron and sulfur possible from PFAS compounds.

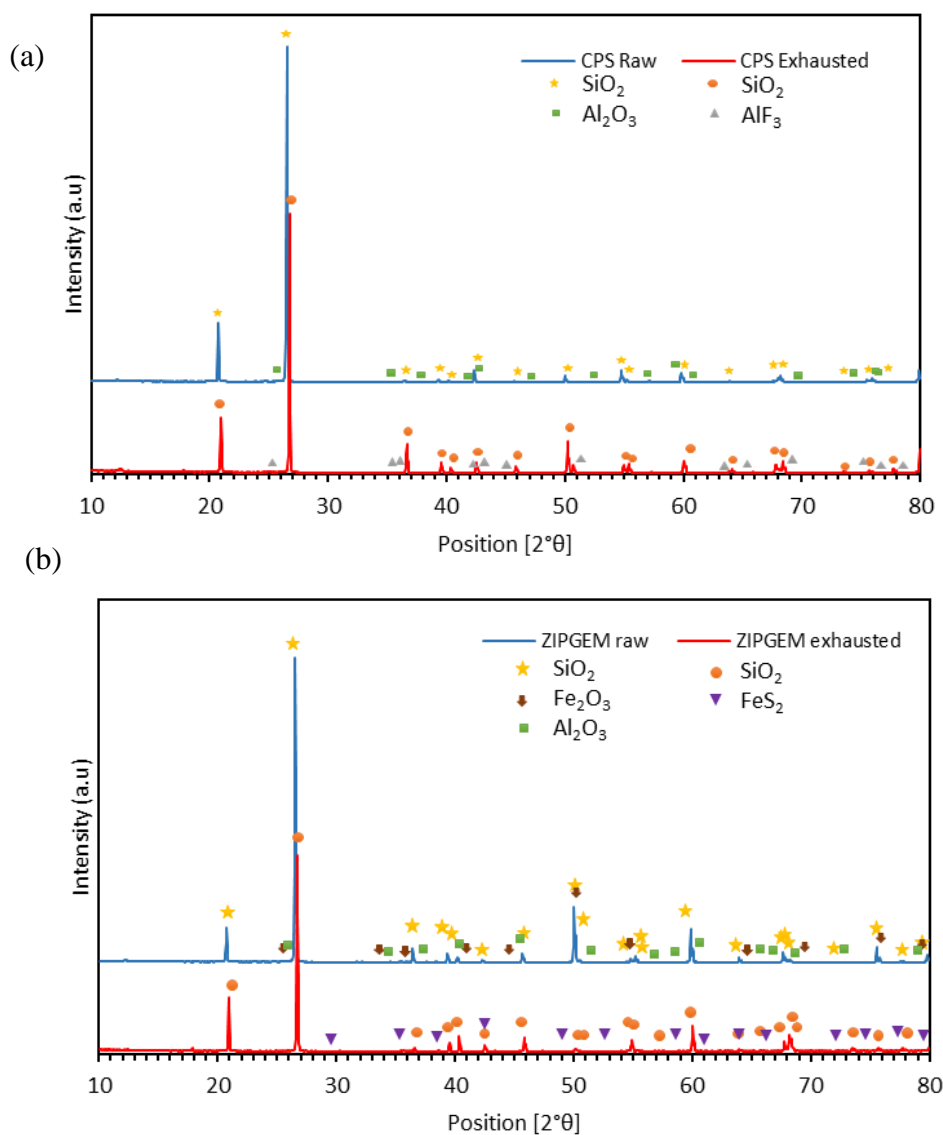


Figure 29. XRD spectra for raw and exhausted CPS (a) and ZIPGEM (b) collected from the top section of the column.

6.3.2. Performance of PFOS and PFOA Removal

6.3.2.1. Adsorption kinetics and isotherms

When considering individual PFOA or PFOS adsorption, it was observed that the media tends to favor either PFOA or PFOS removal at each of the contact times. Some removal (up to 7%) of PFOS by CPS was observed during the first 10 h, followed by a gradual decline in removal.

While PFOS removal of up to 11% by ZIPGEM was observed during the first 10 h, with removal efficiencies remaining positive through the kinetic study ranging from 3 to 11%. However, PFOA removal for both CPS and ZIPGEM was minimal or even negligible, with an observable PFOA removal of 1.3% by ZIPGEM at 30 h. When comparing CPS and ZIPGEM, more PFAS removal was achieved by ZIPGEM at the end of the isotherm kinetic study upon equilibrium with a total run time of 30-h for ZIPGEM and 44-h for CPS.

Furthermore, the kinetic data was fitted to four rate equations where the pseudo-second order rate model had a higher correlation coefficient for PFOS adsorption by ZIPGEM (i.e., the values of R^2 are bolded in Table C2 in Appendix C). This indicates the primary type of PFOS adsorption to be chemisorption processes for ZIPGEM. It should be noted that the PFO and PSO assume surface reaction is the rate-limiting step (Zhou et al., 2021a). The intraparticle diffusion model exhibited the highest R^2 value for PFOS removal by CPS (i.e., 0.762), and PFOA removal by both CPS and ZIPGEM (i.e., 0.398, 0.917, respectively). However, the R^2 value corresponding to PFOA removal by CPS was less than 0.4 indication of the inadequacy of the model to fit the data. When comparing the intraparticle diffusion model for PFOA, a negative C value found for CPS and ZIPGEM could possibly indicate slower adsorption and external mass transfer favoring film diffusion (Yao and Chen, 2017). This further supported since the ZIPGEM kinetic data passed through the origin of the plot, suggesting that intraparticle film diffusion was the rate-limiting step. The large and positive C value for CPS in PFOS removal indicates faster adsorption and a thicker boundary layer for CPS with lower external mass transfer, suggesting a predominant internal mass transfer or, more specifically, pore diffusion. Previous studies have reported rate limiting PFAS

adsorption, and since the kinetics exhibit randomness, it is likely that the adsorption process constantly competes with desorption (Zhou et al., 2021a).

The comparison between the filtration media explored in this study and the one investigated by Ordonez et al. (2022c) indicates that the PSO kinetic model generally best fits PFOS adsorption. The equilibrium adsorption capacities (q_e) for PFOS of ZIPGEM ($2.12 \text{ ng}\cdot\text{g}^{-1}$), Advanced Green Environmental Media (AGEM-2) ($2.30 \text{ ng}\cdot\text{g}^{-1}$), CPS ($0.87 \text{ ng}\cdot\text{g}^{-1}$), and IFGEM-7 ($0.80 \text{ ng}\cdot\text{g}^{-1}$) were similar in range (Table C2 in Appendix C). However, for PFOA adsorption there was no kinetic model that general best fit the data for all media, yet when comparing the performance of the media using PSO for describing PFOA removal only ZIPGEM obtains a positive equilibrium adsorption capacity between both media investigated in this study (Table 33). It should be noted that the negative adsorption capacity determined for CPS corresponds to the PSO and shows its lack of fit to the experimental data as observed by the low R^2 . However, the influent PFAS concentrations should be considered as a factor influencing the adsorption capacity and the fit of the kinetic models when comparing the four media as they are different for both studies.

Table 33. Summary of rate model results for green sorption media investigated for PFAS removal.

Kinetic Parameters and Variables	AGEM-2*	IFGEM-7*	CPS	ZIPGEM
	Pseudo-Second Order	Pseudo-Second Order	Pseudo-Second Order	Pseudo-Second Order
PFOS				
q_e (ng·g ⁻¹)	2.30	0.80	-1.28	2.12
k_1 (·min ⁻¹)	--	--	--	--
k_2 (g·ng ⁻¹ ·min ⁻¹)	-2.31	-16.54	9.06(10) ⁻⁴	-0.004
C	--	--	--	--
k_{id} (g·ng ⁻¹ ·min ⁻¹)	--	--	--	--
R ²	0.958	0.904	0.426	0.904
	Pseudo-Second Order	Pseudo-Second Order	Pseudo-Second Order	Pseudo-Second Order
PFOA				
q_e (ng·g ⁻¹)	1.50	0.900	-4.623	0.447
k_1 (·min ⁻¹)	--	--	--	--
k_2 (g·ng ⁻¹ ·min ⁻¹)	-17.12	0.693	-1.87(10) ⁻⁴	-0.004
C	--	--	--	--
k_{id} (g·ng ⁻¹ ·min ⁻¹)	--	--	--	--
R ²	0.935	0.908	0.161	0.480

*Ordóñez, et al (2022c) influent spiked with 0.7 µg·L⁻¹ of PFOS and 1.62 µg·L⁻¹ of PFOA

6.3.2.2. Long-Chain vs. Short-Chain PFAS Removal

The removals of the long-chain and short-chain PFAS by CPS and ZIPGEM were compared following the fixed-bed column study to answer research question 2. One of the causes for the higher removal efficiency of the columns in comparison to the isotherms is that the isotherm study utilized a much higher PFAS concentration (dosed as ~5,000 ng/L of both PFOS and PFOA) in comparison to the column study concentration (dosed as ~70 ng/L of each PFOA and PFOS). The adsorption of PFOS by both CPS and ZIPGEM was the highest among the PFAS tested in this study. PFOS was found to be below the method detection limits (MDL) of 0.90 ng·L⁻¹ during most

of the sampling times (Figure 30). However, PFOS was detected at the effluent of the ZIPGEM columns at 32, 36 and 42 h and the removal rate varied between 98 and 94%. CPS exhibited a higher initial removal of PFOA (approximately 91%) in comparison to that by ZIPGEM (approximately 84%). Between 2 h and 9 h run time, the removal of PFOA by CPS decreased from 91% to 67% in contrast to the decrease from 88% to 67% by ZIPGEM. Despite CPS commencing with a higher initial PFOA removal, the breakthrough was reached between 16 h and 21 h (Figure 31). ZIPGEM reached a breakthrough a few hours later, i.e., between 24 h and 32 h. These results were anticipated as PFOS is more electronegative than PFOA due to its sulfonate head group, hence there is better adsorption given the stronger hydrophobicity correlated to the $\log K_{ow}$ (log of octanol-water partition coefficient) with a PFOA $\log K_{ow}$ of 6.44 and PFOS $\log K_{ow}$ of 4.51 (Rodea-Palomares et al., 2012). The differences in adsorption between compounds with different fluorocarbon chain length can be related to hydrophobicity (Zhang et al., 2016) where adsorption of PFASs is preferred. Additionally, hydrophobic interactions promote the formation of molecular aggregate on the adsorbent's active surface after the concentration of PFAS on the surface exceeds the critical micelle concentration (Zaggia et al., 2016). As such, the media aggregates such as ZVI and perlite, which are normally hydrophobic, will promote hydrophobic interactions.

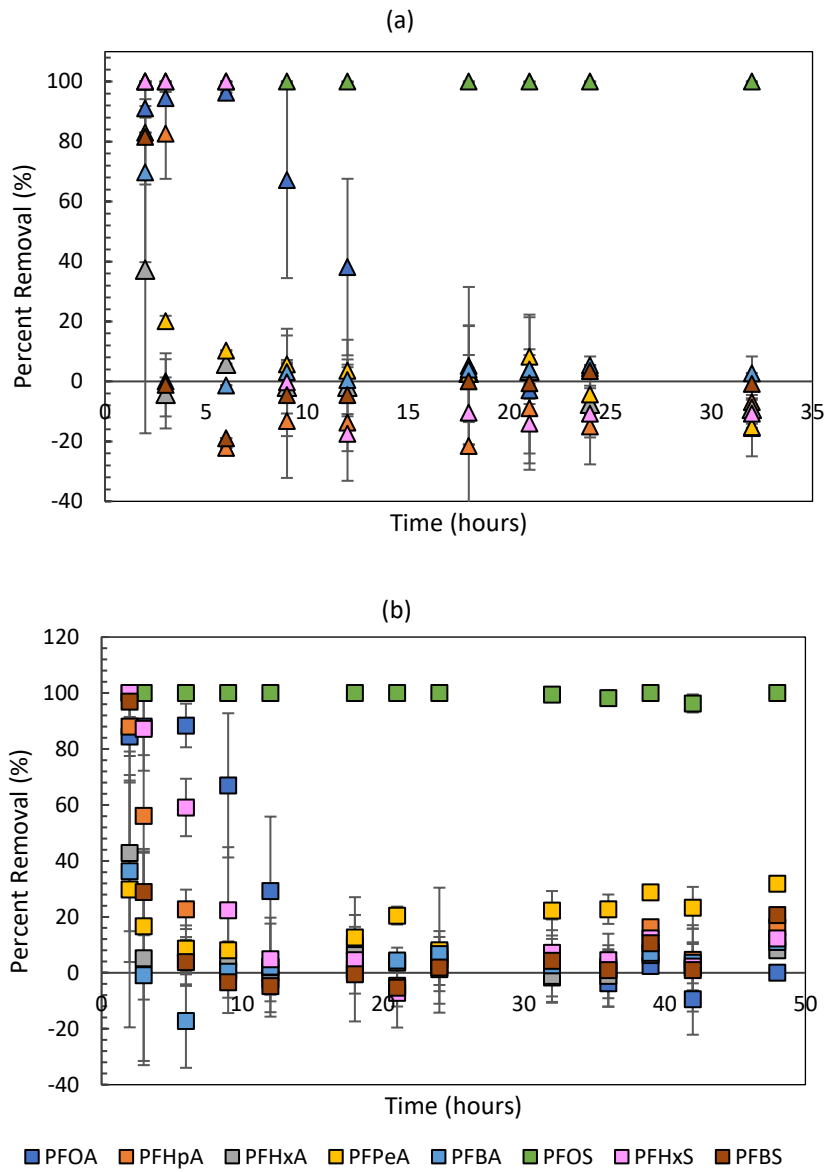


Figure 30. Long-chain and short-chain PFAS removal by (a) CPS and (b) ZIPGEM based on column study.

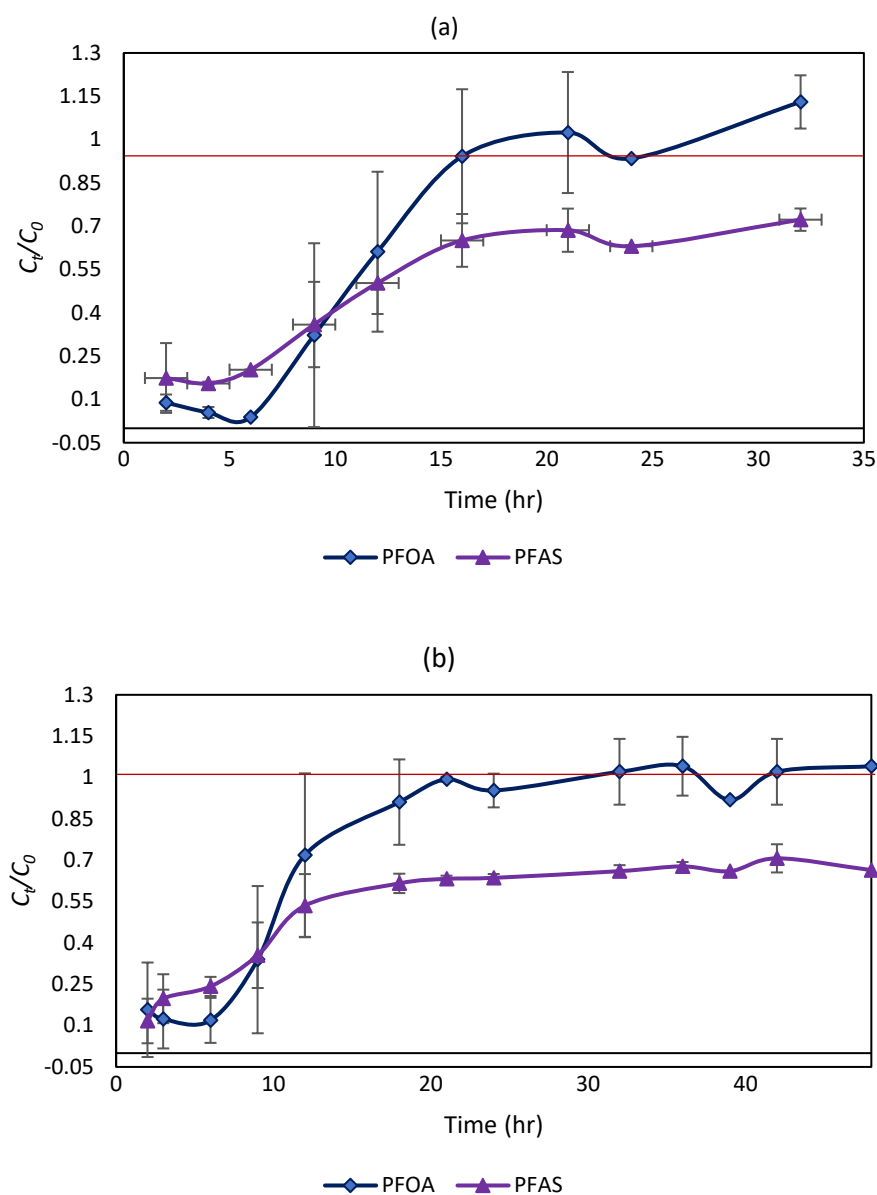


Figure 31. Breakthrough curve for PFOA and PFAS adsorption by (a) CPS and (b) ZIPGEM. (Red line signifies the equilibrium point where $C_t/C_0=1$)

After around 24 h of runtime, when the PFOA removal efficiency of ZIPGEM was approximately 5%, the increase in the removal efficiency of the short-chain PFAS compounds (i.e., PFHpA, PFPeA, and PFBS) was more noticeable. This could be due to the competition between the long versus short-chain PFAS for adsorption on to the media. Here, research question 3 is answered, i.e., the media generally favors the adsorption of long-chain PFAS (PFOS and PFOA). This also

reveals that the specific removal mechanisms by adsorption are governed by electrostatic interactions for the short-chain PFAS as opposed to the hydrophobic interactions for the long-chain PFAS (Gagliano et al., 2020). Moreover, when observing the adsorption of short-chain PFAS, PFHxS was not detected (below the MDL of $0.45 \text{ ng}\cdot\text{L}^{-1}$) for the first 6 h of run time when using CPS, and no removal was achieved after 9 h (Table 34). For ZIPGEM, on average, no PFHxS was detected for the first 2 h of run time, while in general ZIPGEM continued to exhibit positive PFHxS removal up to 12% at 48 h run time. The other short-chain PFAS that was not detected during the initial stage of the CPS column study was PFHpA (below the MDL of $0.45 \text{ ng}\cdot\text{L}^{-1}$) till 2 h, and no removal was observed at 6 h. Although the influent was not spiked with PFHpA there was an initial concentration in the canal water therefore we were able to determine the removal. Additionally, PFHpA was detected after 2 h when using ZIPGEM leading to 81.9% removal, and over all the adsorption capacity of ZIPGEM continued up to 16% at 48 h run time. Furthermore, higher removal obtained for PFHxS when compared to PFBS can be attributed to the molecular sizes of the compounds such that a higher molecular weight was preferred in the adsorption process (Deng et al., 2012a). In general, the order of adsorption by CPS and ZIPGEM was PFOS > PFOA > PFHxS > PFHpA > PFHxA > PFPeA > PFBS > PFBA. The preference of adsorption generally follows the media affinity initially by adsorbing larger molecules with higher molecular weights, followed by short-chain PFCAs (as defined in Table 31) and PFASs (Table 31).

Table 34. PFAS removal efficiencies during the first 9 h column run time (unit: %).

Run Time (hr)	PFOA removal	PFHpA removal	PFHxA removal	PFPeA removal	PFBA removal	PFOS removal	PFHxS removal	PFBS removal	PFAS removal
CPS									
2	91.1	--	5.9	61.6	54.7	--*	--*	72.4	81.9
3	94.5	74.0	-4.1	20.1	0.0	--*	--*	-1.1	84.4
6	96.3	-22.2	5.9	10.3	-1.3	--*	--*	-19.0	81.7
9	67.2	-13.2	-1.8	5.7	3.1	--*	-0.3	-4.6	63.6
ZIPGEM									
2	84.5	81.9	42.8	29.8	36.3	--*	--*	90.6	80.6
3	88.0	56.0	5.2	16.7	-0.9	--*	80.7	28.8	80.0
6	88.4	22.7	4.0	8.6	-17.3	--*	59.1	3.8	75.7
9	67.0	1.2	5.2	8.1	0.4	--*	22.4	-3.4	64.1

* Not detected as value were below MDL

To understand the possible effect of individual media components such as perlite on PFAS removal efficiency, the specialty media sorption capacities were compared. The dynamic models provide a more realistic estimation of the media adsorption capacity in comparison to the kinetic models. Based on the experimental column study data, the Thomas model obtained the highest correlation coefficient for PFOA adsorption by both ZIPGEM and CPS, demonstrating adsorption capacities (q_0) of $0.07 \text{ ng}\cdot\text{g}^{-1}$ and $0.08 \text{ ng}\cdot\text{g}^{-1}$, respectively. When comparing our previous sorption media CTS and IFGEM-7 exhibiting PFOA adsorption capacity of $0.04 \text{ ng}\cdot\text{g}^{-1}$ and $0.09 \text{ ng}\cdot\text{g}^{-1}$, respectively (Ordonez et al., 2022a), it can be deduced that the substitution of tire crumb (due to the concern of desorption) by perlite resulted in an increase in adsorption capacity of CPS. However, the inclusion of perlite in ZIPGEM did not notably contribute to an increase in adsorption capacity compared to IFGEM-7. Therefore, from the suite of sorption media evaluated for PFAS removal, IFGEM-7 can be suggested as the preferable media for application based on its higher PFOA adsorption capacity, while being less costly than ZIPGEM as the media matrix requires one less aggregate.

Coupled with the other media aggregates, the synergistic interactions of PFAS attributed to each media matrix can be accessed. As the behavior and performance of PFAS introduced to various minerals have been widely explored in previous studies which depend on the properties of the mineral (Mukhopadhyay et al., 2021; Vu and Wu, 2022). Some studies suggest that the capacities for PFAS adsorption by minerals (e.g., zeolite, kaolinite, silica, alumina) is limited as minerals do not favor diffusion and display large resistance to mass transfer (Li et al., 2015; Zhang et al., 2019). For instance, it was reported that the adsorption of perfluoroalkyl sulfonic acids (PFSA) (i.e., PFOS, PFBS, and PFHxS) onto the hydroxyl surface of kaolinite is mainly due to electrostatic attraction since the negative charged terminal sulfonate group of PFSA attracts and forms a bond with the positive hydrogen atoms of the hydroxyl surface, whereas the adsorption of the siloxane surface of kaolinite is entropy-driven hydrophobic interaction (Ke et al., 2023). Thus, concluding that the adsorption stability of PFSA on siloxane surface is higher than the hydroxyl surface with long-chain PFSA having higher adsorption stability in comparison to short-chain PFSA. The high PFOS removal efficiency also supports previous findings pertaining to the ease of adsorption of PFOS on mineral surfaces than PFOA (Zhao et al., 2014). This further corroborates the preference of CPS and ZIPGEM in PFAS removal considering the relative contribution between sand, clay, and perlite for CPS, as well as ZVI for ZIPGEM.

Furthermore, the removal of short-chain PFAS can be attributed to their complexations with Fe(III). For instance, the analysis of potential complex formation between PFHxS, PFBS and PFOS demonstrated that the complexation increased with increasing chain length for carboxylic and sulfonate head containing compounds (Park et al., 2018). However, in the same study no differences were observed for the complexation between PFPeA vs. PFBS and PFHpA vs. PFHxS.

In the current study, the range of concentrations of the long-chain and short-chain PFAS compounds that make up the total PFAS at each sampling time from the column study aids in understanding the presence and transformation of the PFAS compounds during the filtration process as well as the possible influence of ZVI on PFAS removal (Figure 32). When the concentration of PFOA decreases as in the case between 2 and 6 h, the concentration of short-chain compounds such as PFPeA, PFHxA, PFHpA, PFHxS and PFBA become more prominent in the column effluent pointing to possible degradation or transformation from long-chain PFAS to short-chain PFAS. However, the concentrations of short-chain PFAS begin to decrease once the concentration of PFOA increases.

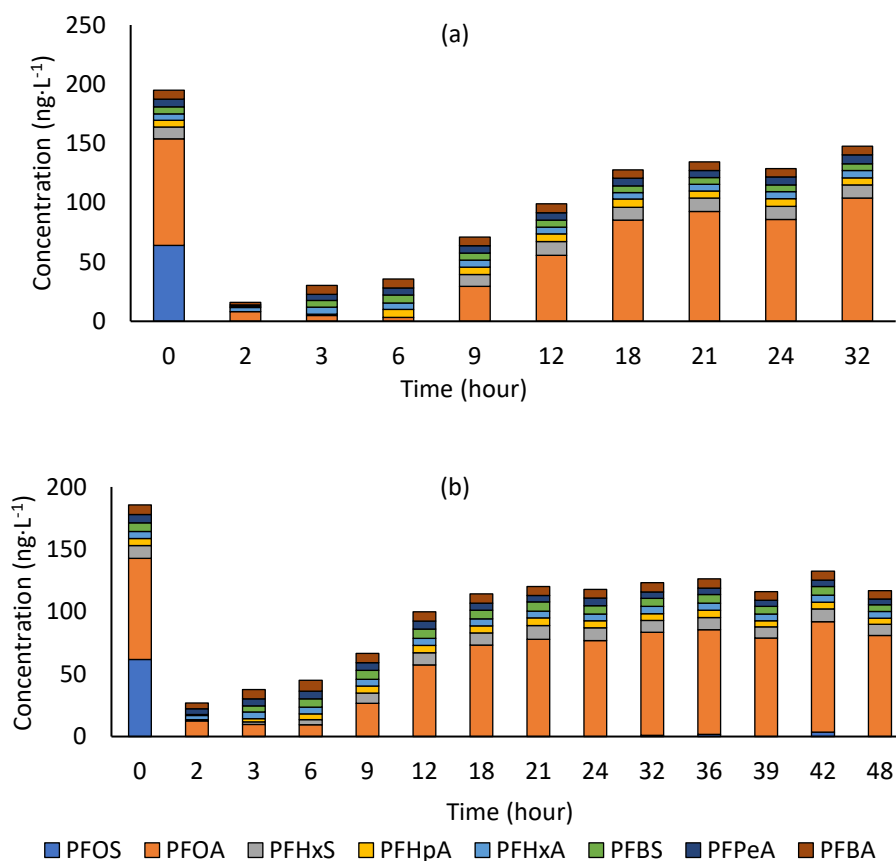


Figure 32. Total concentrations of long and short-chain PFAS for (a) CPS and (b) ZIPGEM based on column study.

Overall, after 18 h of filtration, the proportions of the 8 PFAS compounds remained relatively unchanged for CPS and ZIPGEM. This suggests that the degradation and transformation of long-chain PFAS to short-chain PFAS compounds due to ZVI oxidation contributed to defluorination (Roesch et al., 2020) that occurred during the initial stage of the column study and stabilized as the overall media removal efficiency decreased. Hence, the removal of PFAS by CPS and ZIPGEM is governed by adsorption with the aid of long-chain degradation. Since this treatment approach does not interfere with the formation of new short-chain PFAS compounds, it can be applied as a cost-effective alternative treatment. Addressing research question 4, it can be proposed that ZVI does not affect the transformation of short-chain PFAS.

6.3.3. Real-World Applications and Limitations

The major concerns in PFAS removal include potential PFAS desorption from media and transport and mobility in the environment, which greatly affects water bodies and soil. The concerns pertaining to the current analysis of PFAS adsorption in the literature have mainly focused on PFAS removal efficiencies and mechanisms (Sima and Jaffé, 2021). Most studies on PFAS desorption focus on the effect of PFAS desorption from sediments and adsorptive membranes. For instance, Balgooyen and Remucal (2022) investigated how desorption from riverbed sediments contribute to PFAS transport and mobility. The desorption of PFOS from estuarine sediments was found to be lower than that of PFOA and PFHxS (Navarro et al., 2022). Although, the results suggest some transformation or degradation from long-chain to short-chain PFAS, this finding serves as another possible explanation for the prolonged high removal of PFOS from CPS and ZIPGEM. Yet, further investigation is required to determine if the short-chain PFAS would show higher desorption than its counterpart long chain PFAS.

There are various mechanisms contributing to PFAS removal and adsorption as suggested in the literature including hydrophobic interactions, hydrogen bonding, electrostatic interactions and van der Waals forces. Despite the analysis of PFAS removal in both sorption media, this study was limited to only exploring the physicochemical removal mechanisms. Future work can enhance the understanding of the removal processes considering both physicochemical as well as biological processes that may lead to PFAS transformation or degradation driven by microbial interactions with PFAS. For instance, defluorination of PFAS in the presence of microorganisms was investigated in wetland sediments, where PFOA and PFOS removal increased with iron reduction (Kang et al., 2022). The exploration of the impact of biological removal with iron reduction may be fitting given our filtration media contains ZVI. Moreover, investigating the impact of biodegradation and transformation pathways is a crucial area of future exploration since it has been shown to be responsible for PFAS precursor transformation in wastewater treatment (Lenka et al., 2021; O'Connor et al., 2022).

Due to the potential for our specialty sorption media to be scalable and versatile, the media may find their niche in full-scale PFAS removal application including remediation of contaminated surface waters, groundwaters, and landfill leachate. This is demonstrated by the treatment capacity and lifespan of the media, specifically for PFOA recalling that it reached exhaustion in comparison to PFOS. For instance, the LUB and BC of CPS were 68.63 cm and 53.76 cm, respectively, indicating that 75% of the bed capacity was unused at the time of breakthrough with a C_b of 5.0 $\text{ng}\cdot\text{g}^{-1}$. For ZIPGEM, the LUB and BC were 78.4 cm and 70.6 cm, respectively, signifying that 86% of the bed capacity was unused at the time of breakthrough with a C_b of 9.7 $\text{ng}\cdot\text{g}^{-1}$. This provides insight into the behavior of the mass transfer zone for PFOA adsorption for both CPS and

ZIPGEM, answering research question 5 and revealing the applicability for scale-up even if the adsorption process is continued past the breakthrough point until media exhaustion. Additionally, the length of the column or reactor affects the mass transfer zone, and hence, this is an important parameter to consider for achieving optimal removal.

Due to the recent shift in manufacturing short-chain PFAS from the long-chain ones, the analysis of other short-chain substances like PFBS and PFBA has gained more attention (Zhang et al., 2019). The current study provides insight into the transformation of PFAS when using our specialty sorbents by demonstrating that long-chain PFAS removal may degrade and/or transform into short-chain PFAS. However, in accordance with the EPA advisory levels of PFBS, the final concentrations in the effluent when using both CPS and ZIPGEM ranged from 5.5 to 5.9 ng·L⁻¹—far below 2,000 ng·L⁻¹ when taking into consideration that the influent concentration was below this value. Although the influent concentration for short-chain PFAS was not significant (5.8–6.9 ng·L⁻¹), the concentration of short-chain PFAS at the end of the column study did not alter significantly between the initial and final effluents. Therefore, considering PFAS removal performances of both CPS and ZIPGEM, and the energy consumption and cost of treatment via other alternatives such as membrane filtration, the implementation of the specialty media as a pretreatment technology for other advanced physicochemical treatment methods can prolong their life expectancies. This observation addresses research question 6. Yet, the treatment used is dependent on the water quality desired for treatment (Vu and Wu, 2022); thus, the relevant design parameters such as desired treatment and removal efficiency should also be considered as well as the possibility of the presence of PFAS precursor in the effluent resultant from PFAS transformation during treatment.

6.4. Chapter Conclusion

In this study, fixed-bed column studies were performed to evaluate the physicochemical interactions and removal mechanisms of long and short-chain PFAS using specialty sorbents ZIPGEM and CPS. In general, PFOS adsorption by ZIPGEM was found to be explained by the PSO kinetic model, whereas PFOA and PFOA adsorption by both CPS and ZIPGEM were represented by the intraparticle diffusion model. The comparison of equilibrium adsorption capacities of the media evaluated in this study and our previous work showed that q_e for PFOS was comparable with ZIPGEM ($2.12 \text{ ng}\cdot\text{g}^{-1}$) and AGEM-2 ($2.30 \text{ ng}\cdot\text{g}^{-1}$), and CPS ($0.83 \text{ ng}\cdot\text{g}^{-1}$) and IFGEM-7 ($0.80 \text{ ng}\cdot\text{g}^{-1}$). The higher PFOS removal efficiency compared to PFOA supports the previous findings pertaining to the preference of adsorption of PFOS on mineral surfaces to that of PFOA. This corroborates the preference of CPS and ZIPGEM in PFAS removal considering the contribution of the interactions between sand, clay, perlite for CPS, as well as ZVI for ZIPGEM. However, for PFOA adsorption, ZIPGEM exhibited the largest equilibrium adsorption capacity of $5.72 \text{ ng}\cdot\text{g}^{-1}$ compared to $-4.62 \text{ ng}\cdot\text{g}^{-1}$ for CPS, $1.50 \text{ ng}\cdot\text{g}^{-1}$ for AGEM-2, and $0.90 \text{ ng}\cdot\text{g}^{-1}$ for IFGEM-7. The fixed-bed column study demonstrated that the adsorption of PFOS by both CPS and ZIPGEM was the highest among the PFAS tested in this study, although PFOS was found to be below MDL during most of the sampling times.

CPS exhibited a higher initial removal of PFOA (approximately 91%) compared to that by ZIPGEM (approximately 84%). Thomas model exhibited the highest correlation coefficient for PFOA adsorption by both ZIPGEM and CPS, demonstrating adsorption capacities (q_0) of $0.07 \text{ ng}\cdot\text{g}^{-1}$ and $0.08 \text{ ng}\cdot\text{g}^{-1}$, respectively. When comparing the concentrations of long-chain and short-chain PFAS, the proportions of the 8 PFAS compounds stabilized after the initial run of the column

study for CPS and ZIPGEM, suggesting that along with adsorption there was some degradation and transformation of long-chain PFAS to short-chain PFAS compounds during the run times. The differences in adsorption between compounds with different fluorocarbon chain lengths can be related to the preference of adsorption between sulfonate and carboxylic functional groups. Higher molecular weights and hydrophobic interactions could be associated with the general preference of adsorption for long-chain PFAS over short-chain PFAS.

CHAPTER 7: CONCLUSION

A wide variety of specialty adsorbents can be found in literature given the importance of their roles for cost-effective water treatment in the field scale. The overarching goal of this study is to investigate the removal efficiency and the mechanism of removal of some critical water matrix constituents (i.e., nitrate, phosphate, TOC, and tannic acid), and contaminants of emerging concerns (i.e., MC-LR and PFAS) via a series of specialty adsorbents (sorption media). These specialty adsorbents with chemical, molecular, and even microbial insights fall within the sustainable nature of specialty ingredients and wide availability tailored for scalable applications in any landscape.

For instance, the increasing needs of drinking water due to population growth requires seeking for new tap water sources. However, these large-scale tap water sources are oftentimes abundant with dissolved natural organic matter (NOM), such as tannic acid issue causing color in water. If not removed at the source locations beforehand, NOM would impact coagulation and flocculation unit, and/or become precursors to prompt the production of DPB after chlorination in drinking water treatment. Chapter 2 focuses on developing and testing a suite of cost-effective, scalable, adaptable, and sustainable sorption media that can be implemented near the source locations of tap water as a pretreatment option to remove color for a long-distance interbasin transfer. Within the five tested sorption media, a media recipe of Zero-valent-Iron and Perlite Based Green Sorption Media (ZIPGEM) with ingredients of 85% sand, 5% clay, 6% zero-valent-iron (ZVI) and 4% perlite by volume stood out as the best option for color removal. Findings showed that ZIPGEM can maintain a color removal of ~77% for about 14,080 minutes, maintaining the effluent concentration below 40 Pt-Co units given the influent condition of 175 ± 10

Pt-Co units. A recovery on the adsorption capacity of ZIPGEM was observed around 40,000 minutes due to synergetic effects among several different ingredients of recycled ZVI, clay, sand, and perlites. ZIPGEM can be applied to industrial wastewater treatment for dye removal as well. Moreover, the removal of color (i.e., tannic acid) by the sorption media can be affected by MC-LR, and vice versa, due the similitude on it chemical structure, this influences on the development of Chapter 3.

The recurrent events of harmful algal blooms due to an increase of nutrients in eutrophic water bodies have augmented concerns over the presence of cyanobacterial toxins, especially *Microcystis*. Microcystin-LR (MC-LR) is the most common microcystin toxin, gaining focus in the literature for its effect on human health. Chapter 3 investigates the simultaneous removal of MC-LR and phosphate via 3 green sorption media in the presence of calcium ions in a karst environment. The 3 green sorption media are known as: (1) CPS (clay, perlite, and sand), (2) ZIPGEM (Zero-valent-Iron and Perlite Based Green Environmental Media), and (3) BIPGEM (Biochar-Zero-valent-Iron and Perlite Based Green Environmental Media). Based on the MC-LR removal efficiency, BIPGEM had the best performance, followed by ZIPGEM and CPS. In terms of simultaneous removal of phosphate ions and MC-LR when calcium and phosphate ions are present, ZIPGEM achieved higher removal rate followed by BIPGEM and CPS, respectively. The MC-LR adsorption capacity of BIPGEM in a dynamic environment is $1.19 \mu\text{g}\cdot\text{g}^{-1}$ based on the Modified Dose Response model, while the adsorption capacity is $4.63 \mu\text{g}\cdot\text{g}^{-1}$ based on the Langmuir isotherm model. The decrease in the adsorption capacity of BIPGEM in a dynamic environment can be attributed to the presence of dissolved organic matter and inorganic ions (investigated in Chapter 2), present in the influent water matrix. The influence of the water matrix

was also observed in the isotherm studies, as the presence of PO_4^{3-} negatively impacted the removal efficiencies of MC-LR, while Ca^{2+} positively impacted the removal efficiencies of MC-LR. On the contrary, the removal of PO_4^{3-} was not affected by the presence of MC-LR. The PO_4^{3-} adsorption capacity and nutrient removal efficiency of the specialty sorption media CPS, ZIPGEM and BIPGEM was further investigated in Chapter 4.

Phosphorus is one of the main elements needed for food production. However, it is regarded as a nuisance if found at higher concentrations in an aquatic system. In Chapter 4, three specialty adsorbents (i.e., green sorption media) including Clay-Perlite and Sand (denoted as CPS), Zero-Valent Iron and Perlite-based Green Environmental Media (denoted as ZIPGEM), as well as Biochar, Zero-Valent Iron, and Perlite-based Green Environmental Media (denoted as BIPGEM) were studied for phosphate maximum adsorption capacity (q_m) and their performance under different water matrices (i.e., pH of 4, 7, 10 and canal water). The ZIPGEM media mix outperforms BIPGEM and CPS in terms of phosphate adsorption capacity and nitrate removal. According to the Langmuir isotherm model, the q_m of ZIPGEM is 1.83, 1.80, 0.947 and 1.78 $\text{mg}\cdot\text{g}^{-1}$ at a water matrix of pH at 4, 7, 10 and the natural condition when using canal water spiked with nitrate to explore the competing effect, respectively. Moreover, PO_4^{3-} removal efficiencies up to 99% by ZIPGEM and BIPGEM were observed regardless of the initial water matrix (pH variance and concurrent elements). The predicted maximum adsorption capacity of ZIPGEM by a fixed bed column study was estimated as 7.56 $\text{mg}\cdot\text{g}^{-1}$. Overall, the sustainable and scalable nature of the proposed specialty adsorbent, ZIPGEM, with high phosphate adsorption capacity can be integrated in various water treatment processes and supports the potential utilization of the media mix as soil amendment for food production in circular economy. Within this chapter, the investigation of the

removal efficiency of traditional constituents by the different specialty adsorbents was concluded. However, the emergence of new constituents known as PFAS which can affect human health and ecosystems motivated the research with the in-depth analysis in chapter 5 and 6.

The oleophobic and hydrophobic properties of per- and polyfluoroalkyl substances (PFAS) benefiting their industrial applications have resulted in the persistence, transport, transformation, and accumulation of PFAS in the environmental matrices around the globe. In Chapter 5 the efficiency and mechanisms of removal of PFOS and PFOA from surface waters was investigated when using two sorption media CTS and IFGEM (CTS serving as a control), and through a dynamic fixed-bed column study. IFGEM exhibited better performance in removing PFOA and PFOS from C-23 canal water in comparison with CTS. The better performance of IFGEM was attributed to the larger surface area of IFGEM, the positive surface charge (at $\text{pH} < 8.5$), higher K_{TH} constant, and higher adsorption capacity (q_0) when compared to CTS. The Thomas model serves as the most suitable dynamic model for representing the PFOA adsorption data onto IFGEM and enabled the estimation of q_0 . The larger surface area of IFGEM provides more available sites for adsorption, while the positive surface charge at $\text{pH} < 8.5$ of IFGEM results in electrostatic interactions facilitating PFAS removal. PFOS removal efficiency was higher than PFOA for both the media, attributable to the greater affinity of alumina (Al_2O_3) for PFOS functional groups. The chemical composition of the media, as demonstrated through XRF and XPS, further suggested that Al_2O_3 , being a component of the raw media, may also contribute to the adsorption potential of the media due to its positively charged surface. Also, the higher Fe content of IFGEM may have caused greater adsorption of PFOS/A. It is acknowledged that the spent sorption media would require final disposal because such sorption processes may not destroy PFAS. Moreover, the investigation

of PFAS degradation by mineralization was beyond the objective of this study. However, given that the presence of short chain PFAS is worrisome due to their higher mobility and the interest in further determining the mechanism of PFAS removal via the sorption media this investigation was extended for exploring the fate and transformation of short chain PFAS in Chapter 6.

Chapter 6 investigated two specialty adsorbents, including Zero-Valent-Iron and Perlite based Green Environmental Media (ZIPGEM) and Clay-Perlite and Sand sorption media (CPS) in removing long-chain and short-chain PFAS via a fixed-bed column study to improve our understanding of PFAS fate and transformation. The adsorption of perfluorooctane sulfonic acid (PFOS) by ZIPGEM was best explained by Pseudo-Second order kinetics. The intraparticle diffusion model was a better fit for adsorption of perfluorooctanoic acid (PFOA) by both CPS and ZIPGEM. CPS exhibited a higher initial removal of PFOA (approximately 91%) compared to that by ZIPGEM (approximately 84%). During the initial 2-h run, the removals of perfluoropentanoic acid (PFPeA), perfluorobutanesulfonic acid (PFBS) and perfluorobutanoic acid (PFBA) by CPS were approximately 82%, 72%, and 54%, respectively. The removals of PFPeA, PFBS and PFBA by ZIPGEM were approximately 42%, 90%, and 36%, respectively. In general, the order of adsorption by CPS and ZIPGEM was PFOS > PFOA > PFHxS > PFHpA > PFHxA > PFPeA > PFBS > PFBA. The preference of adsorption generally follows the media affinity initially by adsorbing larger molecules with higher molecular weights, followed by short chain perfluorocarboxylic acids (PFCA) and perfluorosulfonic acids (PFSA). Overall, adsorption coupled with some degradation and transformation of long-chain PFAS to short-chain PFAS compounds aided in PFAS removal mechanism when using CPS and ZIPGEM.

Finally, methods of disposal of the sorption media or recycling potential were discussed in each chapter. The limitations, challenges, and future orientation of this study with respect to each constituent and sorption media was mentioned as well. Moreover, the adsorption capacity exhibited by the different specialty adsorbents presented in this study supports its application potential at a field scale. This future work is imperative given that the even though we try to mimic field condition in the lab, they may not fully resemble field conditions given that non-controllable factor in the environment (i.e., animals, climate, daily variation of water matrix).

APPENDIX A: COMPLEMENTARY INFORMATION ON CHAPTER 4

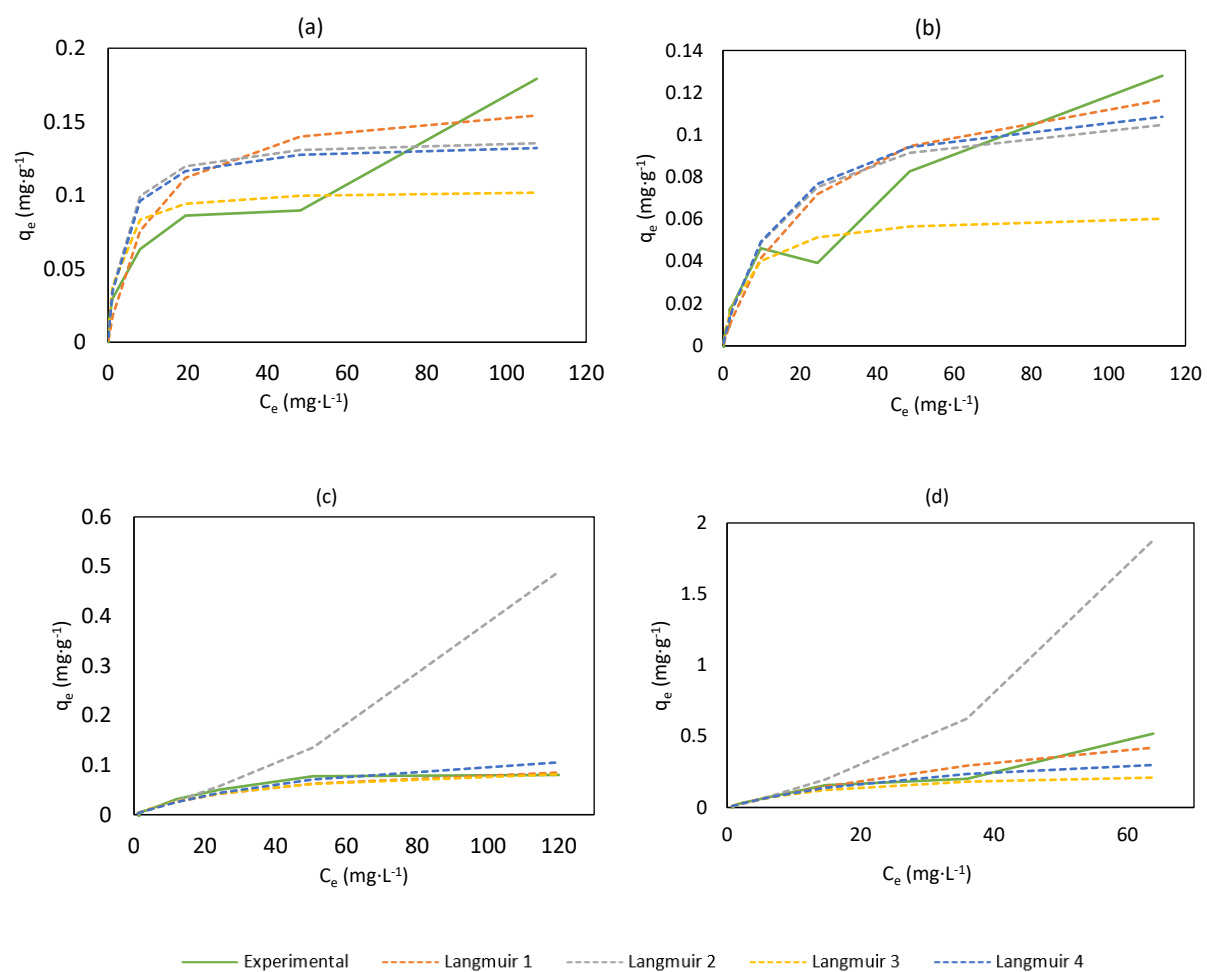


Figure A1. Comparison of CPS PO_4^{3-} adsorption experimental data and the different linear fittings of the Langmuir isotherm model at (a) pH of 4, (b) pH of 7, (c) pH of 10 and (d) Canal water.

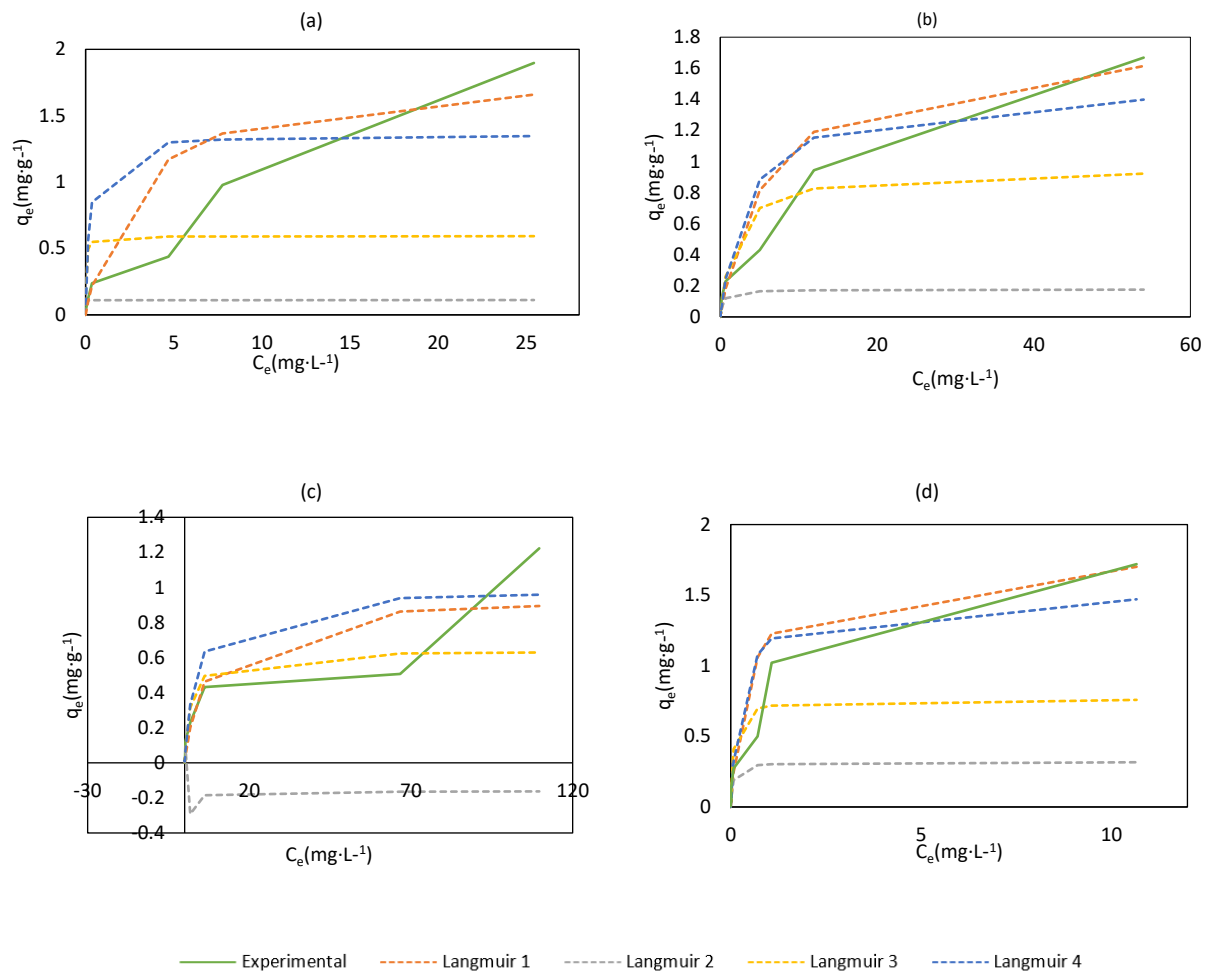


Figure A2. Comparison of ZIPGEM PO_4^{3-} adsorption experimental data and the different linear fittings of the Langmuir isotherm model at (a) pH of 4, (b) pH of 7, (c) pH of 10 and (d) Canal water.

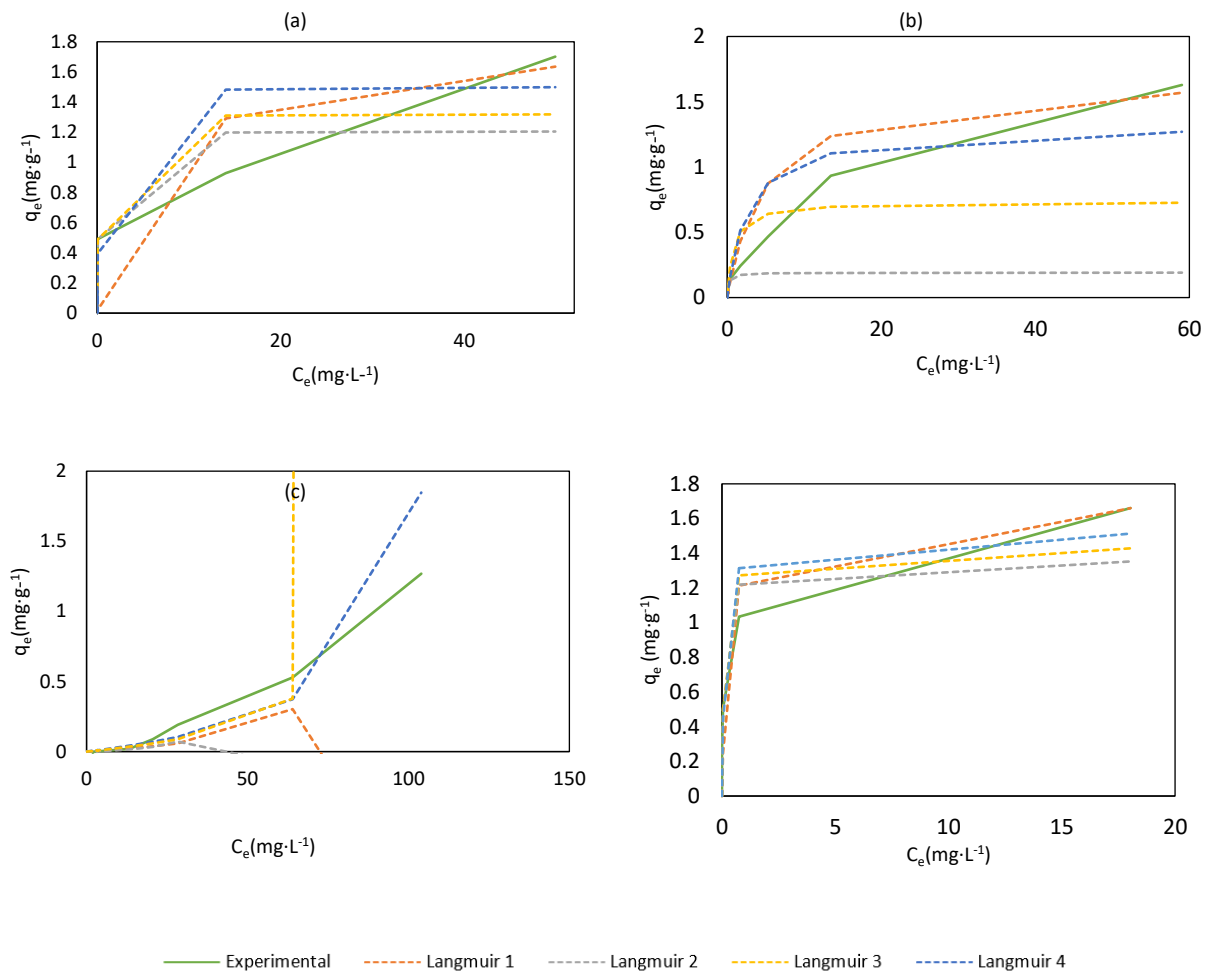


Figure A3. Comparison of BIPGEM PO_4^{3-} adsorption experimental data and the different linear fittings of the Langmuir isotherm model at (a) pH of 4, (b) pH of 7, (c) pH of 10 and (d) Canal water.

APPENDIX B: COMPLEMENTARY INFORMATION ON CHAPTER 5

Table B1. PFAS background concentrations at sampling locations Canal-23.

Sample ID	Dry season (January 27, 2021)		Wet season (June 2, 2021)	
	PFOA (ng·L ⁻¹)	PFOS (ng·L ⁻¹)	PFOA (ng·L ⁻¹)	PFOS (ng·L ⁻¹)
Location 1	15	16	14	19
Location 2	3.4	4.5	3.6	5.5
Location 3	14	14	9.7	14

Table B2. Basic description of sampling locations with water quality.

Dry Season (January 27, 2021)					
Sample ID	Latitude	Longitude	pH	Temp (°C)	ORP (mV)
Location 1	27.205676	-80.400518	8.7	26.9	127.2
Location 2	27.204614	-80.39424	8.2	24.8	139.3
Location 3	27.205674	-80.391727	8.4	27.9	142.6
Wet Season (June 2, 2021)					
Sample ID	Latitude	Longitude	pH	Temp (°C)	ORP (mV)
Location 1	27.205676	-80.400518	8.6	28.9	133.1
Location 2	27.204614	-80.39424	8.7	29.9	141
Location 3	27.205674	-80.391727	8.5	--	148.1

* U stands for that the compound was analyzed for but not detected.

Table B3. Nutrient concentrations at sampling locations around C-23.

Dry Season (January 27, 2021)				
Sample ID	Organic Nitrogen (mg·L ⁻¹)	TN (mg·L ⁻¹ as N)	TP (mg·L ⁻¹ as P)	Ca ²⁺ (mg·L ⁻¹)
Location 1	0.980	1.010	0.048	--
Location 2	0.912	1.020	0.019	--
Location 3	1.040	1.060	0.057	96.03
Wet Season (June 2, 2021)				
Sample ID	Organic Nitrogen (mg·L ⁻¹)	TN (mg·L ⁻¹ as N)	TP (mg·L ⁻¹ as P)	Ca ²⁺ (mg·L ⁻¹)
Location 1	1.220	1.330	0.081	99.33
Location 2	0.881	0.942	0.048	39.93
Location 3	1.030	1.070	0.082	93.93

* U stands for under detection limits with reading

**I signifies that the reported value is between the laboratory method detection limit and the laboratory quantitation limit.

***Sample held beyond the accepted holding time

Table B4. PFAS concentrations at different locations in the US.

Site	PFOA (ng·L ⁻¹)	PFOS (ng·L ⁻¹)	Sample date	Reference
Tennessee River, TN, US	<25-513	55.03	2000	Hansen et al (2002)
Wilson Dam, TN, US	105-144	275-598	2000	Hansen et al (2002)
Conasauga River (CR 3), GA, US	480	318	3/2006	Konwick et al (2009)
Dalton, GA, US	293-299	119-120	3/2006	Konwick et al (2009)
Saginaw Bay Region, MI, US	3.10-12.69	<8-24.08	2001	Sinclair et al (2004)
Southwestern Michigan, MI, US	7.22-29.26	8.74-35.86	2001	Sinclair et al (2004)
Little Pine Lake, NJ, US	25.9	100	7/2015-11/2016	Goodrow et al (2020)
Pine Lake, NJ, US	13.6	102	7/2015-11/2016	Goodrow et al (2020)
Cooley Landing, CA, US	75.6	44.3	2009	Sedlak, Meg, et al (2018)
Ocala Readiness Center, FL, US	7	9.7	2018	Cui et al. (2020)
Marianna Readiness Center, FL, US	1.6	16	2018	Cui et al. (2020)
Indian River lagoon and Atlantic Coast, FL, US	6.6	23	2019, 2021	Griffin et al (2022)

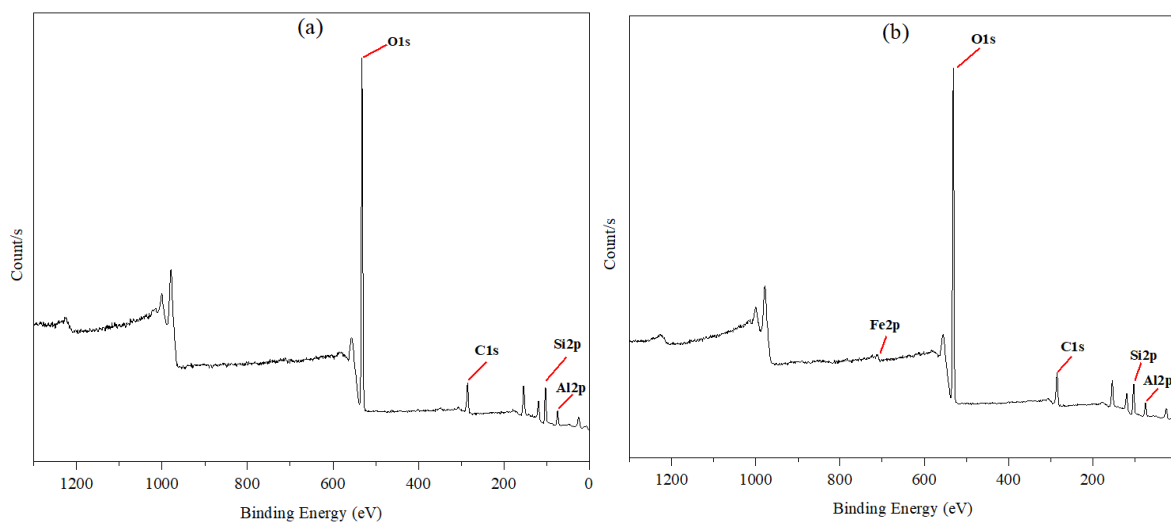


Figure B5. XPS survey analysis for (a) CTS and (b) IFGEM.

APPENDIX C: COMPLEMENTARY INFORMATION ON CHAPTER 6

Table C1. Comparison of Groundwater, Surface Water PFAS Concentrations

PFAS Compounds	Source	Concentration (ng·L⁻¹)	Reference
PFOS	Groundwater- Cape Cod MA, USA	50	Tokranov et al. (2021)
	Groundwater- military base PA	42,600	Lassalle et al. (2021)
	Surface water – Truckee River NV, USA	17.4	Bai and Son. (2021)
	Surface water – Las Vegas Wash NV, USA	38	Bai and Son (2021)
	Surface water- Great Lakes. MI, USA	13-51	Schwichtenberg et al. (2020)
	Surface water- Dunabe River Basin, Australia	37	Clara et al. (2009)
	Surface water- Tangxun Lake, China	73.4-1,650	Zhou et al. (2013)
	Wastewater effluent- Tangxun River, China	1,130-2,130	Zhou et al. (2013)
	Landfill leachate	270	Singh et al. (2021)
Landfill leachate	11	Zhang et al. (2022)	
PFAS	Groundwater- Cape Cod MA, USA	29	Tokranov et al. (2021)
	Groundwater- military base PA	870	Lasalle et al. (2021)
	Surface water – Truckee River NV, USA	1.6-19.2	Bai and Son (2021)
	Surface water – Las Vegas Wash NV, USA	65.5	Bai and Son (2021)
	Surface water- Great Lakes. MI, USA	13-18	Schwichtenberg et al. (2020)
	Surface water- Dunabe River Basin, Australia	21	Clara et al. (2009)
	Landfill leachate	2,400	Singh et al. (2021)
	Landfill leachate	0.93	Zhang et al. (2022)
PFHpA	Surface water- Tangxun Lake, China	23.8-478	Zhou et al. (2013)
	Drinking water intake- Cape Fear River, NC, USA	10-324	Sun et al. (2016)
	Landfill leachate	1435	Zhang et al. (2018)
PFHxA	Surface water- Tangxun Lake, China	27.8-462	Zhou et al. (2013)
	Drinking water intake- Cape Fear River, NC, USA	10-318	Sun et al. (2016)
	Landfill leachate	423	Zhang et al. (2018)
PFHxS	Surface water- Tangxun Lake, China	286-578	Zhou et al. (2013)
	Drinking water intake- Cape Fear River, NC, USA	10-193	Sun et al. (2016)
PFPeA	Surface water- Tangxun Lake, China	26.4-254	Zhou et al. (2013)
	Drinking water intake- Cape Fear River, NC, USA	10-191	Sun et al. (2016)
	Landfill leachate	0.01–0.78	Hale et al. (2017)
PFBA	Surface water- Tangxun Lake, China	1,820-6,280	Zhou et al. (2013)
	Drinking water intake- Cape Fear River, NC, USA	10-104	Sun et al. (2016)
PFBS	Surface water- Tangxun Lake, China	2,240-4,520	Zhou et al. (2013)
	Drinking water intake- Cape Fear River, NC, USA	10-80	Sun et al. (2016)
	Landfill leachate	0.015-0.4	Hale et al. (2017)

Table C2. Summary of Pseudo-first order, Pseudo-second order and intraparticle diffusion model kinetics of PFOS and PFAS for media

	ZIPGEM				CPS			
	Pseudo-First Order	Pseudo-Second Order	Intraparticle Diffusion	Elovich	Pseudo-First Order	Pseudo-Second Order	Intraparticle Diffusion	Elovich
<i>PFOS</i>								
q_e (ng·g ⁻¹)	--	2.12	--	--	0.87	-1.28	--	--
k_1 (·min ⁻¹)	--	--	--	--	2.30(10) ⁻⁴	--	--	--
k_2 (g·ng ⁻¹ ·min ⁻¹)	--	-0.004	--	--	--	9.06(10) ⁻⁴	--	--
k_{id} (g·ng ⁻¹ ·min ⁻¹)	--	--	-0.006	--	--	--	-0.124	--
C	--	--	2.95	--	--	--	3.56	--
α_e (ng·g ⁻¹ ·min ⁻¹)	--	--	--	2.22(10) ¹³⁰	--	--	--	1.4(10) ⁻⁷
β (g·ng ⁻¹)	--	--	--	111.11	--	--	--	-11.16
R²	--	0.904	0.013	0.002	0.425	0.426	0.762	0.741
<i>PFOA</i>								
q_e (ng·g ⁻¹)	5.72	0.447	--	--	--	-4.623	--	--
k_1 (·min ⁻¹)	-0.0005	--	--	--	--	--	--	--
k_2 (g·ng ⁻¹ ·min ⁻¹)	--	-0.004	--	--	--	1.87(10) ⁻⁴	--	--
k_{id} (g·ng ⁻¹ ·min ⁻¹)	--	--	0.103	--	--	--	-0.084	--
C	--	--	-4.193	--	--	--	-0.932	--
α_e (ng·g ⁻¹ ·min ⁻¹)	--	--	--	0.0006	--	--	--	-0.017
β (g·ng ⁻¹)	--	--	--	0.834	--	--	--	-0.932
R²	0.900	0.480	0.917	0.904	--	0.161	0.398	0.366

REFERENCES

- Abbaspour N, Hurrell R, Kelishadi R (2014). Review on iron and its importance for human health. *Journal of Research in Medical Sciences: The Official Journal Of Isfahan University Of Medical Sciences* 19, 164.
- Abdel-Fattah TM, Wixtrom A, Arias L, Zhang K, Baumgart H, (2017). Quantitative analysis of X-ray fluorescence absorption and emission for thickness determination of ALD-grown metal and oxide nanoscaled films. *Journal of Nanoscience and Nanotechnology* 17(8), 5745.
- Abdolali A, Ngo HH, Guo W, Zhou JL, Zhang J, Liang S, Chang SW, Nguyen DD, Liu Y (2017). Application of a breakthrough biosorbent for removing heavy metals from synthetic and real wastewaters in a lab-scale continuous fixed-bed column. *Bioresource Technology* 229, 78.
- Abdolmaleki F, Khorshidi N, Azadmehr A, Maghsoudi A (2021). Enhanced adsorptive removal of phosphate from aqueous solution by activated sand/metal layered double hydroxides. *International Journal of Environmental Analytical Chemistry*, 1-29.
- Achak M, Mandi L, Ouazzani N (2009) Removal of organic pollutants and nutrients from olive mill wastewater by a sand filter. *Journal of Environmental Management* 90, 2771.
- Ahamed S, Sperling J, Galford G, Stephens JC, Arent, D (2019). The food-energy-water nexus, regional sustainability, and hydraulic fracturing: An integrated assessment of the Denver region. *Case Studies in the Environment* 2019, 1-21.
- Ahrens L, Hedlund J, Dürig W, Tröger R, Wiberg, K (2016). Screening of PFASs in groundwater and surface water. national environmental monitoring commissioned by the swedish epa, Swedish Environmental Protection Agency.
- Al-Mayouf A, (1997). Corrosion of iron in aqueous solutions containing a chemical cleaning agent. *Desalination* 114, 29-36.
- Albu SP, Ghicov A, Macak JM, Hahn R, Schmuki P (2007). Self-organized, free-standing TiO₂ nanotube membrane for flow-through photocatalytic applications. *Nano letters* 7, 1286-1289.
- Aljeboree AM, Alshirifi AN, Alkaim AF (2017). Kinetics and equilibrium study for the adsorption of textile dyes on coconut shell activated carbon. *Arabian journal of chemistry* 10, S3381-S3393.
- Alkan M, Doğan M (2001). Adsorption of copper (II) onto perlite. *Journal of Colloid and Interface Science* 243, 280-291.
- Almanassra IW, Mckay G, Kochkodan V, Atieh MA, Al-Ansari T (2021). A state of the art review on phosphate removal from water by biochars. *Chemical Engineering Journal* 409, 128211.
- Almeelbi T, Bezbaruah A (2012). Aqueous phosphate removal using nanoscale zero-valent iron. In *Nanotechnology for Sustainable Development Springer*, 197-210.
- Almuhtaram H, Wang C, Hofmann R (2021) The importance of measuring ultraviolet fluence accurately: A review of microcystin-LR removal by direct photolysis. *Environmental Science and Technology Letters* 8(3), 199-205.
- Alshameri A, Yan C, Lei X (2014). Enhancement of phosphate removal from water by TiO₂/Yemeni natural zeolite: preparation, characterization and thermodynamic. *Microporous and mesoporous materials*, 196, 145-157.

- Appel J (1973) Freundlich's adsorption isotherm. *Surface Science* 39(1), 237-244.
- Amari A, Mohammed Alzahrani F, Mohammedsaleh Katubi K, Salem Alsaiari N, Tahoon MA, Ben Rebah F (2021). Clay-polymer nanocomposites: Preparations and utilization for pollutants removal. *Materials* 14, 1365.
- Ampiauw RE, Yaqub M, Lee W (2019). Adsorption of microcystin onto activated carbon: A review. *Membr. Water Treat* 10, 405-415.
- Aslam M (2019) Introducing Kolmogorov–Smirnov tests under uncertainty: an application to radioactive data. *ACS Omega* 5(1), 914.
- Ateia M, Maroli A, Tharayil N, Karanfil T (2019). The overlooked short-and ultrashort-chain poly- and perfluorinated substances: A review. *Chemosphere* 220, 866-882.
- Atikul Islam M, Sakakibara H, Karim MR, Sekine M (2013). Potable water scarcity: options and issues in the coastal areas of Bangladesh. *Journal of water and health* 11, 532-542.
- Awual MR, Shenashen M, Jyo A, Shiwaku H, Yaita T (2014). Preparing of novel fibrous ligand exchange adsorbent for rapid column-mode trace phosphate removal from water. *Journal of Industrial and Engineering Chemistry* 20, 2840-2847.
- Bai X, Son Y (2021). Perfluoroalkyl substances (PFAS) in surface water and sediments from two urban watersheds in Nevada, USA. *Science of the Total Environment* 751, 141622.
- Bakatula EN, Richard D, Neculita CM, Zagury GJ (2018) Determination of point of zero charge of natural organic materials. *Environmental Science and Pollution Research* 25, 7823-7833.
- Baldia SF, Conaco MCG, Nishijima T, Imanishi S, Harada K-I (2003) Microcystin production during algal bloom occurrence in Laguna de Bay, the Philippines. *Fisheries Science* 69(1), 110-116.
- Balگوoyen S, Remucal CK (2022). Tributary Loading and Sediment Desorption as Sources of PFAS to Receiving Waters. *ACS EST Water* 2, 436-445.
- Ball V, Meyer F (2016). Deposition kinetics and electrochemical properties of tannic acid on gold and silica. *Colloids and Surfaces A: Physicochemical and Engineering Aspects* 491, 12-17.
- Barbier EB, Burgess JC (2001). The economics of tropical deforestation. *Journal of Economic Surveys* 15, 413-433.
- Barca C, Gerente C, Meyer D, Chazarenc F, Andres Y (2012). Phosphate removal from synthetic and real wastewater using steel slags produced in Europe. *Water Research*, 46(7), 2376-2384.
- Barry V, Winquist A, Steenland K (2013). Perfluorooctanoic acid (PFOA) exposures and incident cancers among adults living near a chemical plant. *Environmental health perspectives* 121, 1313-1318.
- Beavers C, Ellis R, Hanlon C, MacDonald G, (2013). An overview of phosphate mining and reclamation in Florida. Master's Thesis.
- Becaria A, Campbell A, Bondy SC (2002). Aluminum as a toxicant. *Toxicology and Industrial Health*, 18(7), 309-320.
- Bedan ES, Clausen JC (2009). Stormwater runoff quality and quantity from traditional and low impact development watersheds 1. *Jawra journal of the american water resources association* 45, 998-1008.
- Bektaş T, Uğurluoğlu BK, Tan B (2021). Phosphate removal by Ion exchange in batch mode. *Water Practice and Technology* 16, 1343-1354.

- Belkouteb N, Franke V, McCleaf P, Köhler S, Ahrens L (2020) Removal of per-and polyfluoroalkyl substances (PFASs) in a full-scale drinking water treatment plant: Long-term performance of granular activated carbon (GAC) and influence of flow-rate. *Water Research* 182, 115913.
- Bell AM, Backhouse DJ, Deng W, Eales JD, Kilinc E, Love K, Rautiyal P, Rigby JC, Stone AH, Vaishnav S (2020) X-Ray fluorescence analysis of feldspars and silicate glass: effects of melting time on fused bead consistency and volatilisation. *Minerals* 10(5), 442.
- Bello OS, Bello IA, Adegoke KA (2013). Adsorption of dyes using different types of sand: a review. *South African Journal of Chemistry* 66, 117-129.
- Besis A, Botsaropoulou E, Samara C, Katsoyiannis A, Hanssen L, Huber S (2019) Perfluoroalkyl substances (PFASs) in air-conditioner filter dust of indoor microenvironments in Greece: Implications for exposure. *Ecotoxicology & Environmental Safety* 183, 109559.
- Bharathi KS, Ramesh SPT (2013). Fixed-bed column studies on biosorption of crystal violet from aqueous solution by *Citrullus lanatus* rind and *Cyperus rotundus*. *Applied Water Science* 3, 673-687.
- Bhatnagar A, Jain A (2005) A comparative adsorption study with different industrial wastes as adsorbents for the removal of cationic dyes from water. *Journal of Colloid and Interface Science* 281(1), 49-55.
- Billam M, Tang L, Cai Q, Mukhi S, Guan H, Wang P, Wang Z, Theodorakis CW, Kendall RJ, Wang JS (2006) Seasonal variations in the concentration of microcystin-LR in two lakes in western Texas, USA. *Environmental Toxicology and Chemistry: An International Journal* 25(2), 349-355.
- Bláha L, Babica P, Maršálek B (2009) Toxins produced in cyanobacterial water blooms-toxicity and risks. *Interdisciplinary Toxicology* 2(2), 36-41.
- Bokkers B, Van de Ven B, Janssen P, Bil W, Van Broekhuizen F, Zeilmaker M, Oomen AG (2019) Per-and polyfluoroalkyl substances (PFASs) in food contact materials. Joint Research Center, Brussels, Belgium
- Borrelli P, Robinson DA, Panagos P, Lugato E, Yang JE, Alewell C, Wuepper D, Montanarella L, Ballabio C (2020). Land use and climate change impacts on global soil erosion by water. *Proceedings of the National Academy of Sciences* 117, 21994-22001.
- Bottino A, Capannelli C, Del Borghi A, Colombino M, Conio O (2001). Water treatment for drinking purpose: ceramic microfiltration application. *Desalination* 141, 75-79.
- Bourne DG, Blakeley RL, Riddles P, Jones GJ (2006). Biodegradation of the cyanobacterial toxin microcystin LR in natural water and biologically active slow sand filters. *Water Research* 40, 1294-1302.
- Boyd CE, Boyd CE (2020). Eutrophication. *Water Quality: An Introduction*, 311-322.
- Brendel S, Fetter É, Staude C, Vierke L, Biegel-Engler A (2018). Short-chain perfluoroalkyl acids: environmental concerns and a regulatory strategy under REACH. *Environmental Sciences Europe* 30, 1-11.
- Brennan NM, Evans AT, Fritz MK, Peak SA, von Holst HE (2021). Trends in the regulation of per-and polyfluoroalkyl substances (PFAS): a scoping review. *International journal of environmental research and public health* 18, 10900.
- Brix H, Arias C, Del Bubba M (2001). Media selection for sustainable phosphorus removal in subsurface flow constructed wetlands. *Water science and technology*, 44(11-12), 47-54.

- Bruton TA, Blum A (2017) Proposal for coordinated health research in PFAS-contaminated communities in the United States. *Environmental Health* 16, 1.
- Byl TD, Miller B, Toomey R, Young DE (2021) Harmful Algal Blooms in Karst Terrains. *US Geological Survey Karst Interest Group Proceedings*, 19, 114.
- Campbell LS, Davies B (1995). Soil sorption of caesium modelled by the Langmuir and Freundlich isotherm equations. *Applied Geochemistry* 10, 715-723.
- Campinas M, Rosa MJ (2006) The ionic strength effect on microcystin and natural organic matter surrogate adsorption onto PAC. *Journal of Colloid and Interface Science* 299(2), 520-529.
- Campos-Pereira H, Kleja DB, Sjöstedt C, Ahrens L, Klysubun W, Gustafsson JP (2020). The adsorption of per- and polyfluoroalkyl substances (PFASs) onto ferrihydrite is governed by surface charge. *Environmental science and technology* 54, 15722-15730.
- Cantoni B, Turolla A, Wellmitz J, Ruhl AS, Antonelli M (2021). Perfluoroalkyl substances (PFAS) adsorption in drinking water by granular activated carbon: Influence of activated carbon and PFAS characteristics. *Science of The Total Environment* 795, 148821.
- Cerón-Vivas A, Villamizar León MP, Cajigas AA (2023). Geosmin and 2-methylisoborneol removal in drinking water treatment. *Water Practice and Technology* 18, 159-167.
- Chang MY, Juang RS (2004). Adsorption of tannic acid, humic acid, and dyes from water using the composite of chitosan and activated clay. *Journal of colloid and interface science* 278, 18-25.
- Chang NB, Wanielista MP, Daranpob A, Xuan Z, Hossain F (2010) New performance-based passive septic tank underground drainfield for nutrient and pathogen removal using sorption media. *Environmental Engineering Science* 27, 469.
- Chang NB, Wanielista MP, Makkeasorn A (2014). Innovative design of low impact development in support of green building initiative.
- Chang NB, Wanielista MP, Marimon Z (2015). Comparative evaluation of Floating Treatment Wetlands for nutrient removal and algal toxin control in wet detention ponds. *International Low Impact Development Conference 2015: LID: It Works in All Climates and Soils*, pp. 168-175.
- Chang NB, Houmann C, Wanielista MP (2016). Scaling up adsorption media reactors for copper removal with the aid of dimensionless numbers. *Chemosphere* 144, 1098-1105.
- Chang NB, Wen D, McKenna AM, Wanielista MP (2018). The impact of carbon source as electron donor on composition and concentration of dissolved organic nitrogen in biosorption-activated media for stormwater and groundwater co-treatment. *Environmental Science & Technology* 52, 9380.
- Chang NB, Wen D, Colona W, Wanielista MP (2019a). Comparison of biological nutrient removal via two biosorption-activated media between laboratory-scale and field-scale linear ditch for stormwater and groundwater co-treatment. *Water, Air, & Soil Pollution* 230, 1-19.
- Chang NB, Wen D, Wanielista MP (2019b). Impact of changing environmental factors and species competition on iron filings-based green environmental media for nutrient removal in stormwater treatment. *Environmental Progress & Sustainable Energy* 38, 13087.
- Chassapis K, Roulia M, Vrettou E, Parassiris A (2010). Preparation of bioinorganic fertilizing media by adsorption of humates on glassy aluminosilicates. *Colloids and surfaces B: Biointerfaces* 81, 115-122.

- Chatterjee S, Guha N, Krishnan S, Singh AK, Mathur P, Rai DK (2020). Selective and recyclable Congo red dye adsorption by spherical Fe₃O₄ nanoparticles functionalized with 1, 2, 4, 5-benzenetetracarboxylic acid. *Scientific reports* 10, 111.
- Chaudhry FN, Malik M (2017). Factors affecting water pollution: a review. *J Ecosyst Ecography* 7, 1-3.
- Chen H, Reinhard M, Nguyen TV, You L, He Y, Gin KYH (2017) Characterization of occurrence, sources and sinks of perfluoroalkyl and polyfluoroalkyl substances (PFASs) in a tropical urban catchment. *Environmental Pollution* 227, 397.
- Chowdhury S, Saha P (2011). Adsorption kinetic modeling of safranin onto rice husk biomatrix using pseudo-first-and pseudo-second-order kinetic models: Comparison of linear and non-linear methods. *Clean Soil, Air, Water* 39, 274-282.
- Chowdhury ZZ, Abd Hamid SB, Zain SM (2015) Evaluating design parameters for breakthrough curve analysis and kinetics of fixed bed columns for Cu (II) cations using lignocellulosic wastes. *BioResources* 10,732.
- Clara M, Gans O, Weiss S, Sanz-Escribano D, Scharf S, Scheffknecht C (2009). Perfluorinated alkylated substances in the aquatic environment: an Austrian case study. *Water Research* 43, 4760-4768.
- Colomina MT, Peris-Sampedro F (2017). Aluminum and Alzheimer's disease. *Neurotoxicity of Metals*, 183-197.
- Cordner A, De La Rosa VY, Schaidler LA, Rudel RA, Richter L, Brown P (2019). Guideline levels for PFOA and PFOS in drinking water: the role of scientific uncertainty, risk assessment decisions, and social factors. *Journal of Exposure Science and Environmental Epidemiology* 29, 157-171.
- Crini G, Lichtfouse E, Wilson LD, Morin-Crini N (2018). Adsorption-oriented processes using conventional and non-conventional adsorbents for wastewater treatment. *Green Adsorbents for Pollutant Removal: Fundamentals and Design*, 23-71.
- Crittenden JC, Hutzler NJ, Geyer DG, Oravitz JL, Friedman G (1986). Transport of organic compounds with saturated groundwater flow: Model development and parameter sensitivity. *Water Resources Research* 22, 271-284.
- Crone BC, Speth TF, Wahman DG, Smith SJ, Abulikemu G, Kleiner EJ, Pressman JG (2019). Occurrence of per-and polyfluoroalkyl substances (PFAS) in source water and their treatment in drinking water. *Critical Reviews in Environmental Science and Technology* 49, 2359-2396.
- Cui X, Zhang Y, Gao J, Peng F, Gao P (2018). Long-term combined application of manure and chemical fertilizer sustained higher nutrient status and rhizospheric bacterial diversity in reddish paddy soil of Central South China. *Scientific reports*, 8(1), 1-11.
- Dada A, Olalekan A, Olatunya A, Dada O (2012). Langmuir, Freundlich, Temkin and Dubinin–Radushkevich isotherms studies of equilibrium sorption of Zn²⁺ unto phosphoric acid modified rice husk. *IOSR Journal of Applied Chemistry* 3, 38-45.
- Daprile L (2017) Stuart replaced wells after EPA found too much PFOS and PFOA in drinking water. *Treasure Coast Newspaper*.
- Darko B, Jiang JQ, Kim H, Machala L, Zboril R, Sharma VK (2014). Advances made in understanding the interaction of ferrate (VI) with natural organic matter in water. *Water Reclamation and Sustainability*. Elsevier, pp. 183-197.

- Darlington R, Barth E, McKernan J (2018). The challenges of PFAS remediation. *The Military Engineer* 110, 58.
- Das TK, Scott Q, Bezbaruah AN (2021). Montmorillonite-iron crosslinked alginate beads for aqueous phosphate removal. *Chemosphere* 281, 130837.
- Davis AP (2005). *Green engineering principles promote low-impact development*. ACS Publications
- Davis JG, Whiting D (2000) *Choosing a soil amendment*. Colorado State University. Libraries.
- Davis TW, Bullerjahn GS, Tuttle T, McKay RM, Watson SB (2015). Effects of increasing nitrogen and phosphorus concentrations on phytoplankton community growth and toxicity during *Planktothrix* blooms in Sandusky Bay, Lake Erie. *Environmental science and technology* 49, 7197-7207.
- de Maagd PGJ, Hendriks AJ, Seinen W, Sijm DT (1999) pH-dependent hydrophobicity of the cyanobacteria toxin microcystin-LR. *Water Research* 33(3), 677-680.
- Deng S, Yu Q, Huang J, Yu G (2010) Removal of perfluorooctane sulfonate from wastewater by anion exchange resins: Effects of resin properties and solution chemistry. *Water Research* 44, 5188.
- Deng S, Zhang Q, Nie Y, Wei H, Wang B, Huang J, Yu G, Xing B (2012a). Sorption mechanisms of perfluorinated compounds on carbon nanotubes. *Environmental pollution* 168, 138-144.
- Deng Y, Wang L, Hu X, Liu B, Wei Z, Yang S, Sun C (2012b). Highly efficient removal of tannic acid from aqueous solution by chitosan-coated attapulgite. *Chemical Engineering Journal* 181, 300-306.
- Deng Y, Li Y, Li X, Sun Y, Ma J, Lei M, Weng L (2018). Influence of calcium and phosphate on pH dependency of arsenite and arsenate adsorption to goethite. *Chemosphere* 199, 617-624.
- Desta MB (2013). Batch sorption experiments: Langmuir and Freundlich isotherm studies for the adsorption of textile metal ions onto teff straw (*Eragrostis tef*) agricultural waste. *Journal of thermodynamics* 2013.
- Dewi R, Agusnar H, Alfian Z (2018). Characterization of technical kaolin using XRF, SEM, XRD, FTIR and its potentials as industrial raw materials. *Journal of Physics: Conference Series*. IOP Publishing, p. 042010.
- Diana M, Felipe-Sotelo M, Bond T (2019). Disinfection byproducts potentially responsible for the association between chlorinated drinking water and bladder cancer: a review. *Water research* 162, 492-504.
- Dietrich AM, Burlingame GA (2015). Critical review and rethinking of USEPA secondary standards for maintaining organoleptic quality of drinking water. *Environmental science & technology* 49, 708-720.
- Diels L, Spaans P, Van Roy S, Hooyberghs L, Ryngaert A, Wouters H, Waltert E, Macaskie L, Finlay J, Pernfuss B (2003) Heavy metals removal by sand filters inoculated with metal sorbing and precipitating bacteria. *Hydrometallurgy* 71, 235.
- Dietz ME (2007). Low impact development practices: A review of current research and recommendations for future directions. *Water, air, and soil pollution*, 186(1), 351-363.
- Din ATM, Hameed B, Ahmad AL (2009). Batch adsorption of phenol onto physiochemical-activated coconut shell. *Journal of Hazardous Materials* 161, 1522-1529.
- Dixit F, Barbeau B, Mohseni M (2019) Microcystin-LR removal by ion exchange: investigating multicomponent interactions in natural waters. *Environmental Pollution* 253, 790-799.

- Dixit F, Dutta R, Barbeau B, Berube P, Mohseni M (2021). PFAS removal by ion exchange resins: A review. *Chemosphere* 272, 129777.
- Doğan M, Alkan M, Onganer Y (2000). Adsorption of methylene blue from aqueous solution onto perlite. *Water, Air, and Soil Pollution* 120, 229-248.
- Doğan M, Alkan M, (2003). Removal of methyl violet from aqueous solution by perlite. *Journal of colloid and interface science* 267, 32-41.
- Dombrowski PM, Kakarla P, Caldicott W, Chin Y, Sadeghi V, Bogdan D, Barajas-Rodriguez F, Chiang SY (2018). Technology review and evaluation of different chemical oxidation conditions on treatability of PFAS. *Remediation Journal* 28, 135-150.
- Dorgham MM (2014). Effects of eutrophication. *Eutrophication: Causes, Consequences and Control: Volume 2*, 29-44.
- Du Z, Deng S, Bei Y, Huang Q, Wang B, Huang J, Yu G (2014). Adsorption behavior and mechanism of perfluorinated compounds on various adsorbents—A review. *Journal of hazardous materials* 274, 443-454.
- Du Z, Deng S, Chen Y, Wang B, Huang J, Wang Y, Yu G (2015) Removal of perfluorinated carboxylates from washing wastewater of perfluorooctanesulfonyl fluoride using activated carbons and resins. *Journal of Hazardous Materials* 286, 136.
- Dziga D, Wasylewski M, Wladyka B, Nybom S, Meriluoto J (2013) Microbial degradation of microcystins. *Chemical Research in Toxicology* 26(6), 841-852.
- Eckart K, McPhee Z, Bolisetti T (2017). Performance and implementation of low impact development—A review. *Science of the Total Environment* 607, 413-432.
- Edzwald JK, Toensing DC, Leung MCY (1976). Phosphate adsorption reactions with clay minerals. *Environmental Science and Technology*, 10(5), 485-490.
- Elanchezhyan SS, Preethi J, Rathinam K, Njaramba LK, Park CM (2021) Synthesis of magnetic chitosan biopolymeric spheres and their adsorption performances for PFOA and PFOS from aqueous environment. *Carbohydrate Polymers* 267, 118165.
- El-Sayed GO (2011). Removal of methylene blue and crystal violet from aqueous solutions by palm kernel fiber. *Desalination* 272, 225-232.
- Emerson CH, Welty C, Traver RG (2005). Watershed-scale evaluation of a system of storm water detention basins. *Journal of Hydrologic Engineering* 10, 237-242
- EPA (1986). Quality criteria for water 1986: U.S. Environmental Protection Agency Report 440/5-86-001. Office of Water. Washington, D.C.
- EPA (2002). National Recommended Water Quality Criteria; EPA-822-R-02-047. Washington DC.
- EPA (2008). National secondary drinking water regulations. USEPA Agency. Washington DC.
- EPA (2012). EPA drinking water guidance on disinfection by-products. No. 4 Advice Note. Washington DC.
- EPA (2015). Drinking Water Health Advisory for the Cyanobacterial Microcystin Toxins Agency, USEPA, Washington DC.
- EPA (2016). FACT SHEET PFOA & PFOS Drinking Water Health Advisories. in: Agency, USEPA. (Ed.), p. 5., Washington DC.
- EPA (2017a). Basic Information on Nitrate in Drinking Water. Washington DC.
- EPA (2017b). Basic Information on Nitrite in Drinking Water. Washington DC.
- EPA (2018). Final aquatic life ambient water quality criteria for aluminum, USEPA Agency (Ed.). Washington DC.

- EPA (2021). Health Effects from Cyanotoxins. Agency, USEPA. (ed) Washington DC.
- EPA (2022). Drinking Water Health Advisories for PFAS Fact Sheet for Communities. in: Agency, U.E.P. (Ed.). Washington DC.
- EPA (2023a). Drinking Water Health Advisories for PFOA, PFOS, GenX Chemicals and PFBS. in: Advisor, W.H. (Ed.). Washington DC.
- EPA (2023b). PFAS National Primary Drinking Water Regulation Relemaking. EPA.
- EPA (2023c). Secondary Drinking Water Standards: Guidance for Nuisance Chemicals.
- Esfahani EB, Zeidabadi FA, Zhang S, Mohseni M (2022). Photo-chemical/catalytic Oxidative/Reductive Decomposition of Per-and Polyfluoroalkyl Substances (PFAS), Decomposition Mechanisms and Effects of Key Factors: A Review. Environmental Science: Water Research & Technology.
- European Union (2020). Commission Delegated Regulation (EU) 2020/784 of 8 April 2020. Amending Annex I to Regulation (EU) 2019/1021 of the European Parliament and of the Council as regards the listing of perfluorooctanoic acid (PFOA), its salts and PFOA-related compounds, Official Journal of the European Union.
- Falconer IR, Runnegar MT, Beresford AM (1983). Evidence of liver damage by toxin from a bloom of the blue-green alga, *Microcystis aeruginosa*. Medical Journal of Australia, 1(11), 511-514.
- Falconer IR (1998). Algal toxins and human health. Quality and treatment of drinking water II, 53-82.
- Fan AM, Steinberg VE (1996). Health implications of nitrate and nitrite in drinking water: an update on methemoglobinemia occurrence and reproductive and developmental toxicity. Regulatory toxicology and pharmacology 23, 35-43.
- Fang H, Cui Z, He G, Huang L, Chen M (2017). Phosphorus adsorption onto clay minerals and iron oxide with consideration of heterogeneous particle morphology. Science of the Total Environment, 605, 357-367.
- Fawell J, Robinson D, Bull R, Birnbaum L, Boorman G, Butterworth B, Daniel P, Galal-Gorchev H, Hauchman F, Julkunen P (1997). Disinfection by-products in drinking water: critical issues in health effects research. Environmental health perspectives 105, 108-109.
- FDEP (2021) DEP's Efforts to Address PFAS in the Environment.
- Ferguson JF, King T (1977). A model for aluminum phosphate precipitation. Journal (Water Pollution Control Federation), 646-658.
- Filatova D (2021). Origin and release of cyanotoxins in surface water reservoirs. Ph.D. Dissertation, Univeristy of Barcelona, Spain.
- Fiorito E, Porcedda GE, Brundu L, Passiu C, Atzei D, Ennas G, Elsener B, Fantauzzi M, Rossi A (2022) Calcium carbonate as sorbent for lead removal from wastewaters. Chemosphere 296,133897
- Foss AJ, Miles CO, Wilkins AL, Rise F, Trovik KW, Cieslik K, Aubel MT (2020) Analysis of total microcystins and nodularins by oxidative cleavage of their ADMAdda, DMAdda, and Adda moieties. Analytica Chimica Acta: X 6, 100060
- Fujiki H, Suganuma M (2011). Tumor promoters-microcystin-LR, nodularin and TNF- α and human cancer development. Anti-Cancer Agents in Medicinal Chemistry (Formerly Current Medicinal Chemistry-Anti-Cancer Agents) 11, 4-18.
- Gagliano E, Sgroi M, Falciglia PP, Vagliasindi FG, Roccaro P (2020). Removal of poly-and perfluoroalkyl substances (PFAS) from water by adsorption: Role of PFAS chain length,

- effect of organic matter and challenges in adsorbent regeneration. *Water research* 171, 115381.
- Gao M, Deng C, Fan Z, Yao N, Xu X, Yang P, Zhang X (2007). A simple pathway to the synthesis of magnetic nanoparticles with immobilized metal ions for the fast removal of microcystins in water. *Small* 3, 1714-1717.
- Gao YQ, Gao NY, Deng Y, Gu JS, Shen YC, Wang SX (2012) Adsorption of Microcystin-LR from Water with Iron Oxide Nanoparticles. *Water Environment Research* 84(7), 562-568.
- Geertz HH, Rasmussen G (1994). Influence of ochre and acidification on the survival and hatching of brown trout eggs (*Salmo trutta*). Sublethal and chronic effects of pollutants on fresh fish, 10, 196-210
- Georgantas D, Grigoropoulou H (2006). Phosphorus and organic matter removal from synthetic wastewater using alum and aluminum hydroxide. *Global NEST J* (8), 121-130.
- Ghasemi M, Keshtkar AR, Dabbagh R, Safdari SJ (2011). Biosorption of uranium (VI) from aqueous solutions by Ca-pretreated *Cystoseira indica* alga: Breakthrough curves studies and modeling. *Journal of hazardous materials* 189, 141-149.
- Ghisari M, Eiberg H, Long M, Bonefeld-Jørgensen EC (2014). Polymorphisms in Phase I and Phase II genes and breast cancer risk and relations to persistent organic pollutant exposure: a case-control study in Inuit women. *Environmental Health* 13, 19.
- Ghorbani A, Fakhariyan A (2013) Recovery of Al₂O₃, Fe₂O₃ and TiO₂ from bauxite processing waste (red mud) by using combination of different acids. *Journal of Basic and Applied Scientific Research* 3(1), 187.
- Ghribi A, Chlendi M (2011). Modeling of fixed bed adsorption: application to the adsorption of an organic dye. *Asian journal of textile* 1, 161-171.
- Gironás J, Adriasola JM, Fernández B (2008). Experimental analysis and modeling of a stormwater perlite filter. *Water Environment Research*, 80(6), 524-539.
- Glüge J, Scheringer M, Cousins IT, DeWitt JC, Goldenman G, Herzke D, Lohmann R, Ng CA, Trier X, Wang Z (2020) An overview of the uses of per- and polyfluoroalkyl substances (PFAS). *Environmental Science: Processes & Impacts* 22(12), 2345.
- Gong Z, Li S, Ma J, Zhang X (2016) Self-flocculated powdered activated carbon with different oxidation methods and their influence on adsorption behavior. *Journal of Hazardous Materials* 304, 222.
- González-López M, Laureano-Anzaldo C, Pérez-Fonseca A, Arellano M, Robledo-Ortíz J (2021) A discussion on linear and non-linear forms of Thomas equation for fixed-bed adsorption column modeling. *Revista Mexicana de Ingeniería Química* 20(2), 875-884.
- Gora SL, Andrews SA (2017). Adsorption of natural organic matter and disinfection byproduct precursors from surface water onto TiO₂ nanoparticles: pH effects, isotherm modelling and implications for using TiO₂ for drinking water treatment. *Chemosphere* 174, 363-370.
- Govindaraj M, Muthukumar M, Bhaskar Raju G (2010). Electrochemical oxidation of tannic acid contaminated wastewater by RuO₂/IrO₂/TaO₂-coated titanium and graphite anodes. *Environmental technology* 31, 1613-1622.
- Grandjean P, Heilmann C, Weihe P, Nielsen F, Mogensen UB, Timmermann A, Budtz-Jørgensen E (2017). Estimated exposures to perfluorinated compounds in infancy predict attenuated vaccine antibody concentrations at age 5-years. *Journal of immunotoxicology* 14, 188-195.
- Greenlee LF, Torrey JD, Amaro RL, Shaw JM (2012) Kinetics of zero valent iron nanoparticle oxidation in oxygenated water. *Environmental Science and Technology* 46(23),12913.

- Greer FR, Shannon M (2005). Infant methemoglobinemia: The role of dietary nitrate in food and water. *Pediatrics (Evanston)* 116, 784-786.
- Gundersen C, Ziliak JP (2015). Food insecurity and health outcomes. *Health affairs* 34, 1830-1839.
- Guo X, Wang J (2019). Comparison of linearization methods for modeling the Langmuir adsorption isotherm. *Journal of Molecular Liquids* 296, 111850.
- Guo YC, Lee AK, Yates RS, Liang S, Rochelle PA (2017) Analysis of microcystins in drinking water by ELISA and LC/MS/MS. *American Water Works Association* 109(3), 13-25.
- Gupta VK, Kumar R, Nayak A, Saleh TA, Barakat M (2013). Adsorptive removal of dyes from aqueous solution onto carbon nanotubes: a review. *Advances in colloid and interface science* 193, 24-34.
- Hach 2021. Nitrate, Dimethylphenol LR Method 10206 TNTPlus Method
- Hach 2022. Phosphorus, Reactive and Total, Method 10209 and Method 10210 Ascorbic Acid TNTplus Method
- Hale SE, Arp HPH, Slinde GA, Wade EL, Bjørseth K, Breedveld GD, Straith BF, Moe KG, Jartun M, Høisæter Å (2017). Sorbent amendment as a remediation strategy to reduce PFAS mobility and leaching in a contaminated sandy soil from a Norwegian firefighting training facility. *Chemosphere* 171, 9-18.
- Hameed B, Din AM, Ahmad A (2007). Adsorption of methylene blue onto bamboo-based activated carbon: kinetics and equilibrium studies. *Journal of hazardous materials*, 141(3), 819-825.
- Hamdi N, Srasra E (2012). Removal of phosphate ions from aqueous solution using Tunisian clays minerals and synthetic zeolite. *Journal of Environmental Sciences*, 24(4), 617-623.
- Harripersadth C, Musonge P (2022). The Dynamic Behaviour of a Binary Adsorbent in a Fixed Bed Column for the Removal of Pb^{2+} Ions from Contaminated Water Bodies. *Sustainability* 14, 7662.
- Hansen KJ, Johnson HO, Eldridge JS, Butenhoff JL, Dick LA (2002) Quantitative characterization of trace levels of PFOS and PFOA in the Tennessee River. *Environmental Science and Technology* 36(8), 1681-1685.
- Heath M, Wood SA, Young RG, Ryan KG (2016). The role of nitrogen and phosphorus in regulating *Phormidium* sp.(cyanobacteria) growth and anatoxin production. *FEMS Microbiology Ecology* 92, 021.
- Helling MS, Josefsson S, Hughes AV, Ahrens L (2016) Sorption of perfluoroalkyl substances to two types of minerals. *Chemosphere* 159, 385.
- Ho Y, Chiang C, (2001) Sorption studies of acid dye by mixed sorbents. *Adsorption* 7(2), 139-147.
- Hochmuth G (2011). Iron (Fe) nutrition of plants. University of Florida If as Extension. SI, 353, 1-8.
- Hooth MJ, McDorman KS, Hester SD, George MH, Brooks LR, Swank AE, Wolf DC (2002). The carcinogenic response of Tsc2 mutant Long-Evans (Eker) rats to a mixture of drinking water disinfection by-products was less than additive. *Toxicological Sciences* 69, 322-331.
- Hori H, Hayakawa E, Einaga H, Kutsuna S, Koike K, Ibusuki T, Kiatagawa H, Arakawa R (2004) Decomposition of environmentally persistent perfluorooctanoic acid in water by photochemical approaches. *Environmental Science and Technology* 8(22), 6118.

- Hori H, Yamamoto A, Hayakawa E, Taniyasu S, Yamashita N, Kutsuna S, Kiatagawa H, Arakawa R (2005) Efficient decomposition of environmentally persistent perfluorocarboxylic acids by use of persulfate as a photochemical oxidant. *Environmental Science & Technology* 39(7), 2383.
- Hori H, Yamamoto A, Koike K, Kutsuna S, Osaka I, Arakawa R (2007). Photochemical decomposition of environmentally persistent short-chain perfluorocarboxylic acids in water mediated by iron (II)/(III) redox reactions. *Chemosphere* 68, 572-578.
- Horst J, McDonough J, Ross I, Houtz E (2020). Understanding and managing the potential by-products of PFAS destruction. *Groundwater Monitoring & Remediation*, 40(2), 17-2
- Hosseini SA, Toghroli A (2021). Effect of mixing Nano-silica and Perlite with pervious concrete for nitrate removal from the contaminated water. *Advances in concrete construction* 11, 531-544.
- Hu J, Wang Z, Ng W, Ong S (1999) Disinfection by-products in water produced by ozonation and chlorination. *Environmental Monitoring and Assessment* 59(1), 81-93.
- Huang WJ, Cheng BL, Cheng YL (2007). Adsorption of microcystin-LR by three types of activated carbon. *Journal of Hazardous Materials* 141, 115-122.
- Huang Y, Yang JK, Keller AA (2014). Removal of arsenic and phosphate from aqueous solution by metal (hydr-) oxide coated sand. *ACS Sustainable Chemistry & Engineering*, 2(5), 1128-1138.
- Iheanacho OC, Nwabanne JT, Obi CC, Onu CE (2021). Packed bed column adsorption of phenol onto corn cob activated carbon: linear and nonlinear kinetics modeling. *South African Journal of Chemical Engineering* 36, 80-93.
- Jain A, Singh BN, Singh S, Singh H, Singh S (2010). Exploring biodiversity as bioindicators for water pollution. *National Conference on Biodiversity, Development and Poverty Alleviation*, 50-56.
- Jawad AH, Mamat NH., Abdullah MF, Ismail K (2017). Adsorption of methylene blue onto acid-treated mango peels: kinetic, equilibrium and thermodynamic study. *Desal Wat Treat* 59, 210-219.
- Jedla MR, Koneru B, Franco A, Rangappa D, Banerjee P (2022). Recent developments in nanomaterials based adsorbents for water purification techniques. *Biointerface Res. Appl. Chemistry* 12, 5821-5835.
- Jia Z, Zeng W, Xu H, Li S, Peng Y (2020). Adsorption removal and reuse of phosphate from wastewater using a novel adsorbent of lanthanum-modified platanus biochar. *Process Safety and Environmental Protection*, 140, 221-232.
- Jiang C, Jia L, He Y, Zhang B, Kirumba G, Xie J. (2013). Adsorptive removal of phosphorus from aqueous solution using sponge iron and zeolite. *Journal of colloid and interface science*, 402, 246-252.
- Jiang S, Li Y, Ladewig BP (2017). A review of reverse osmosis membrane fouling and control strategies. *Science of the Total Environment* 595, 567.
- Johnson RL, Anschutz AJ, Smolen JM, Simcik MF, Penn RL (2007) The adsorption of perfluorooctane sulfonate onto sand, clay, and iron oxide surfaces. *Journal of Chemical & Engineering Data* 52(4), 1165.
- Jones J, Chang NB, Wanielista M (2015). Reliability analysis of phosphorus removal efficiencies of stormwater runoff with green sorption media under varying influent conditions. *Science of the Total Environment* 502(1), 434.

- Jones A, Knocke W (2017). Evaluating the role of soluble aluminum in manganese removal via MnOx (s)-coated filtration media in drinking water treatment. *Water Research* 111, 595.
- Joo SH, Feitz AJ, Waite TD (2004). Oxidative degradation of the carbothioate herbicide, molinate, using nanoscale zero-valent iron. *Environmental Science & Technology* 38(7), 2242.
- Kaal J, Nierop K, Verstraten J (2005). Retention of tannic acid and condensed tannin by Fe-oxide-coated quartz sand. *Journal of Colloid and Interface Science* 287, 72-79.
- Kadlec RH (2016). Large constructed wetlands for phosphorus control: A review. *Water* 8, 243.
- Kang Y, Li M, Guo Z, Zhang Y, Li W, Wu H, Zhang J (2022). Effect of electron shuttles on typical perfluoroalkyl substance removal via iron oxide reduction in wetland sediment. *Journal of Cleaner Production* 365, 132821.
- Kärman A, Elgh-Dalgren K, Lafossas C, Møskeland T (2011). Environmental levels and distribution of structural isomers of perfluoroalkyl acids after aqueous fire-fighting foam (AFFF) contamination. *Environmental chemistry* 8, 372-380.
- Karunarathne H, Amarasinghe B (2013). Fixed bed adsorption column studies for the removal of aqueous phenol from activated carbon prepared from sugarcane bagasse. *Energy Procedia* 34, 83-90.
- Katz BG (1992). Hydrochemistry of the upper Floridan aquifer, Florida. *Water-Resources Investigations Report* 91, 4196.
- Kayranli B (2011). Adsorption of textile dyes onto iron based waterworks sludge from aqueous solution; isotherm, kinetic and thermodynamic study. *Chemical engineering journal* 173, 782-791.
- Ke ZW, Wei SJ, Shen P, Chen YM, Li YC (2023). Mechanism for the adsorption of Per- and polyfluoroalkyl substances on kaolinite: Molecular dynamics modeling. *Applied Clay Science* 232, 106804.
- Keenan CR, Sedlak DL (2008). Factors affecting the yield of oxidants from the reaction of nanoparticulate zero-valent iron and oxygen. *Environmental Science & Technology* 42(4), 1262.
- Keselj D, Lazic D, Penavin-Skundric J, Sladojevic S, Vasiljevic L (2012). Determination of alumina oxide in bauxites by X-Ray fluorescence analysis. *Global Journal of Science Frontier Research Chemistry* 12.
- Kempnaers L (2020). *The Basics of Elemental Analysis with XRF – Q&A*. Malvern Panalytical.
- Khan MN, Mohammad F (2014). Eutrophication: challenges and solutions. *Eutrophication: Causes, Consequences and Control* 2, 1-15.
- Khuntia BK, Anwar MF, Alam T, Samim M, Kumari M, Arora I (2019). Synthesis and characterization of zero-valent iron nanoparticles, and the study of their effect against the degradation of DDT in soil and assessment of their toxicity against collembola and ostracods. *ACS omega* 4, 18502-18509.
- Kinnear S (2010). Cyindrospermopsin: a decade of progress on bioaccumulation research. *Marine drugs* 8, 542-564.
- Kleiner EJ, Sanan T, Smith SJ, Pressman JG, Abulikemu G, Crone BC, Wahman DG (2021). Practical implications of perfluoroalkyl substances adsorption on bottle materials: Isotherms. *AWWA Water Science* 3, 1243.
- Knežević B, Žmuk B (2021) 2.1. Two-way analysis of variance (ANOVA) without replication. *Experimental design and biometric research. Toward Innovations*, 130.

- Knutsen H, Mæhlum T, Haarstad K, Slinde GA, Arp HPH (2019). Leachate emissions of short- and long-chain per- and polyfluoroalkyl substances (PFASs) from various Norwegian landfills. *Environmental Science: Processes and Impacts* 21, 1970-1979.
- Kolmogorov A (1933) Sulla determinazione empirica di una legge di distribuzione. *Giorn Dell'inst Ital Degli Att* 4, 83.
- Konwick BJ, Tomy GT, Ismail N, Peterson JT, Fauver RJ, Higginbotham D, Fisk AT (2008) Concentrations and patterns of perfluoroalkyl acids in Georgia, USA surface waters near and distant to a major use source. *Environmental Toxicology and Chemistry: An International Journal* 27(10), 2011.
- Koppelaar R, Weikard H (2013). Assessing phosphate rock depletion and phosphorus recycling options. *Global Environmental Change* 23, 1454-1466.
- Kovalev MS, Utkin LV (2020). A robust algorithm for explaining unreliable machine learning survival models using the Kolmogorov–Smirnov bounds. *Neural Networks* 132. 1.
- Krasner SW, McGuire MJ, Jacangelo JG, Patania NL, Reagan KM, Aieta EM (1989). The occurrence of disinfection by-products in US drinking water. *Journal-American Water Works Association* 81, 41-53.
- Kucharzyk KH, Darlington R, Benotti M, Deeb R, Hawley E (2017) Novel treatment technologies for PFAS compounds: A critical review. *Journal of Environmental Management* 204, 757.
- Kulkarni S, Kaware J (2014). Regeneration and recovery in adsorption-a review. *Int. J. Innov. Sci. Eng. Technol* 1, 61-64.
- Kumar M, Borah P, Devi P (2020). Priority and emerging pollutants in water. *Inorganic Pollutants in Water*. Elsevier, 33.
- Kumar P, Pérez JAE, Cledon M, Brar SK, Duy SV, Sauvé S, Knystautas É (2020). Removal of microcystin-LR and other water pollutants using sand coated with bio-optimized carbon submicron particles: Graphene oxide and reduced graphene oxide. *Chemical Engineering Journal* 397, 125398.
- Kutser T, Pierson DC, Tranvik L, Reinart A, Sobek S, Kallio K (2005). Using satellite remote sensing to estimate the colored dissolved organic matter absorption coefficient in lakes. *Ecosystems* 8, 709-720.
- Lambert TW, Holmes CF, Hrudey SE (1996). Adsorption of microcystin-LR by activated carbon and removal in full scale water treatment. *Water Research* 30(6), 1411-1422.
- Landsberg JH (2002). The effects of harmful algal blooms on aquatic organisms. *Reviews in fisheries science* 10, 113-390.
- Lanzante JR (2021). Testing for differences between two distributions in the presence of serial correlation using the Kolmogorov–Smirnov and Kuiper's tests. *International Journal of Climatology* 41(14), 6314
- Lapointe BE, Herren LW, Debortoli DD, Vogel MA (2015). Evidence of sewage-driven eutrophication and harmful algal blooms in Florida's Indian River Lagoon. *Harmful Algae* 43, 82-102.
- Larson JF, Wolf DC, Butterworth BE (1994). Induced cytotoxicity and cell proliferation in the hepatocarcinogenicity of chloroform in female B6C3F1 mice: comparison of administration by gavage in corn oil vs ad libitum in drinking water. *Toxicological Sciences* 22, 90-102.

- Lassalle J, Gao R, Rodi R, Kowald C, Feng M, Sharma VK, Hoelen T, Bireta P, Houtz EF, Staack, D (2021). Degradation of PFOS and PFOA in soil and groundwater samples by high dose Electron Beam Technology. *Radiation Physics and Chemistry* 189, 109705.
- Laureano-Rosario AE, McFarland M, Bradshaw II DJ, Metz J, Brewton RA, Pitts T, Perricone C, Schreiber S, Stockley N, Wang G (2021). Dynamics of microcystins and saxitoxin in the Indian River Lagoon, Florida. *Harmful Algae* 103, 102012.
- Lawton LA, Robertson PK, Cornish BJ, Marr IL, Jaspars M (2003). Processes influencing surface interaction and photocatalytic destruction of microcystins on titanium dioxide photocatalysts. *Journal of Catalysis* 213(1), 109-113.
- Le ST, Kibbey TC, Weber KP, Glamore WC, O'Carroll DM (2021). A group-contribution model for predicting the physicochemical behavior of PFAS components for understanding environmental fate. *Science of The Total Environment* 764, 142882.
- Lee JH, Bang KW (2000). Characterization of urban stormwater runoff. *Water research*, 34(6), 1773-1780.
- Lee J, Jun H, Kubota Y, Kim T (2021). Synthesis of red fluorescent dye with acid gas sensitive optical properties and fabrication of a washable and wearable textile sensor. *Textile Research Journal* 91, 2036-2052.
- Lee J, Walker HW (2006) Effect of process variables and natural organic matter on removal of microcystin-LR by PAC– UF. *Environmental Science & Technology* 40(23), 7336-7342.
- Lee J, Walker HW (2008) Mechanisms and factors influencing the removal of microcystin-LR by ultrafiltration membranes. *Journal of Membrane Science* 320(1-2), 240-247.
- Lee J, Walker HW (2011) Adsorption of microcystin-LR onto iron oxide nanoparticles. *Colloids and Surfaces A: Physicochemical and Engineering Aspects* 373(1-3), 94-100.
- Lei Y, Song B, Saakes M, van der Weijden RD, Buisman CJ (2018). Interaction of calcium, phosphorus and natural organic matter in electrochemical recovery of phosphate. *Water research*, 142, 10-17.
- Lee YM, Lee JY, Kim MK, Yang H, Lee JE, Son Y, Kho Y, Choi K, Zoh KD (2020). Concentration and distribution of per-and polyfluoroalkyl substances (PFAS) in the Asan Lake area of South Korea. *Journal of Hazardous Materials* 381, 120909.
- Leng L, Xiong Q, Yang L, Li H, Zhou Y, Zhang W, Jiang S, Li H, Huang H (2021). An overview on engineering the surface area and porosity of biochar. *Science of the total Environment* 763, 144204
- Lenka SP, Kah M, Padhye LP (2021). A review of the occurrence, transformation, and removal of poly-and perfluoroalkyl substances (PFAS) in wastewater treatment plants. *Water research* 199, 117187.
- Ler A, Stanforth R (2003). Evidence for surface precipitation of phosphate on goethite. *Environmental Science & Technology* 37, 2694-2700.
- Leutnant D, Muschalla D, Uhl M (2018) Distribution-based calibration of a stormwater quality model. *Water* 10(8), 1027.
- Li B, Boiarkina I, Young B, Yu W, Singhal N (2016a). Prediction of future phosphate rock: a demand based model.
- Li F, Duan J, Tian S, Ji H, Zhu Y, Wei Z, Zhao D (2020). Short-chain per-and polyfluoroalkyl substances in aquatic systems: Occurrence, impacts and treatment. *Chemical Engineering Journal* 380, 122506.

- Li J, Hu M, Ma W, Liu Y, Dong F, Zou R, Chen Y (2023). Optimization and multi-uncertainty analysis of best management practices at the watershed scale: A reliability-level based bayesian network approach. *Journal of Environmental Management* 331, 117280.
- Li J, Shimizu K, Maseda H, Lu Z, Utsumi M, Zhang Z, Sugiura N (2012). Investigations into the biodegradation of microcystin-LR mediated by the biofilm in wintertime from a biological treatment facility in a drinking-water treatment plant. *Bioresource Technology* 106, 27-35.
- Li K, Zeng Z, Xiong J, Yan L, Guo H, Liu S, Dai Y, Chen T (2015). Fabrication of mesoporous Fe₃O₄@ SiO₂@ CTAB-SiO₂ magnetic microspheres with a core/shell structure and their efficient adsorption performance for the removal of trace PFOS from water. *Colloids and Surfaces A: Physicochemical and Engineering Aspects* 465, 113-123.
- Li L, Qiu Y, Huang J, Li F, Sheng GD (2014) Mechanisms and factors influencing adsorption of microcystin-LR on biochars. *Water, Air, & Soil Pollution* 225(12), 1-10.
- Li M, Liu J, Xu Y, Qian G (2016). Phosphate adsorption on metal oxides and metal hydroxides: A comparative review. *Environmental Reviews*, 24(3), 319-332.
- Li XF, Mitch WA (2018). Drinking water disinfection byproducts (DBPs) and human health effects: multidisciplinary challenges and opportunities. *Environmental Science & Technology* 52, 1681-1689.
- Li Y, Fletcher T, Mucs D, Scott K, Lindh CH, Tallving P, Jakobsson K (2018). Half-lives of PFOS, PFHxS and PFOA after end of exposure to contaminated drinking water. *Occupational and environmental medicine* 75, 46-51.
- Li Y, Miao X, Wei Z, Cui J, Li S, Han R, Zhang Y, Wei W (2016b). Iron-Tannic Acid Nanocomplexes: Facile Synthesis And Application For Removal Of Methylene Blue From Aqueous Solution. *Digest Journal of Nanomaterials & Biostructures (DJNB)* 11.
- Lin H, Wang Y, Niu J, Yue Z, Huang Q (2015). Efficient sorption and removal of perfluoroalkyl acids (PFAAs) from aqueous solution by metal hydroxides generated in situ by electrocoagulation. *Environmental science & technology* 49, 10562-10569.
- Lin L, Yang H, Xu X (20220). Effects of water pollution on human health and disease heterogeneity: a review. *Frontiers in Environmental Science*, 975.
- Lin L, Wan C, Lee DJ, Lei Z, Liu X (2014). Ammonium assists orthophosphate removal from high-strength wastewaters by natural zeolite. *Separation and Purification Technology*, 133, 351-356.
- Lin W, Lin M, Zhou H, Wu H, Li Z, Lin W (2019). The effects of chemical and organic fertilizer usage on rhizosphere soil in tea orchards. *PloS one*, 14(5), e0217018.
- Litke DW (1999). Review of phosphorus control measures in the United States and their effects on water quality: US Geological Survey Water-Resources Investigations Report 99-4007. US Geological Survey Fact Sheet FS-007-98, South Carolina.
- Liu CJ, Werner D, Bellona C (2019). Removal of per-and polyfluoroalkyl substances (PFASs) from contaminated groundwater using granular activated carbon: a pilot-scale study with breakthrough modeling. *Environmental Science: Water Research and Technology* 5, 1844-1853.
- Liu G, Zheng H, Zhai X, Wang Z (2018). Characteristics and mechanisms of microcystin-LR adsorption by giant reed-derived biochars: role of minerals, pores, and functional groups. *Journal of Cleaner Production* 176, 463-473.

- Liu J, Weinholtz L, Zheng L, Peiravi M, Wu Y, Chen D (2017). Removal of PFOA in groundwater by Fe₀ and MnO₂ nanoparticles under visible light. *Journal of Environmental Science and Health, Part A* 52(11), 1048
- Liu L, Qu Y, Huang J, Weber R (2021). Per- and polyfluoroalkyl substances (PFASs) in Chinese drinking water: risk assessment and geographical distribution. *Environmental Sciences Europe* 33, 1-12.
- Liu L, Luo X B, Ding L, Luo SL (2019). Application of nanotechnology in the removal of heavy metal from water. *Nanomaterials for the removal of pollutants and resource reutilization*. Elsevier, 83.
- Liu S, Yang R, Yin N, Faiola F (2020). The short-chain perfluorinated compounds PFBS, PFHxS, PFBA and PFHxA, disrupt human mesenchymal stem cell self-renewal and adipogenic differentiation. *Journal of Environmental Sciences* 88, 187-199.
- Liu X, Li Y, Chen Z, Yang H, Cai Y, Wang S, Chen J, Hu B, Huang Q, Shen C (2023). Advanced porous nanomaterials as superior adsorbents for environmental pollutants removal from aqueous solutions. *Critical Reviews in Environmental Science and Technology*, 1-21.
- Liu X, Shen F, Qi X (2019). Adsorption recovery of phosphate from aqueous solution by CaO-biochar composites prepared from eggshell and rice straw. *Science of the Total Environment* 666, 694-702.
- Liu YL, Walker HW, Lenhart JJ (2019a). Adsorption of microcystin-LR onto kaolinite, illite and montmorillonite. *Chemosphere* 220, 696-705.
- Liu YL, Walker HW, Lenhart JJJ (2019b). The effect of natural organic matter on the adsorption of microcystin-LR onto clay minerals. *Colloids and Surfaces A: Physicochemical and Engineering Aspects* 583, 123964.
- Loganathan P, Vigneswaran S, Kandasamy J, Bolan NS (2014). Removal and recovery of phosphate from water using sorption. *Critical Reviews in Environmental Science and Technology* 44, 847-907.
- Lone Y, Koiri RK, Bhide M (2015). An overview of the toxic effect of potential human carcinogen Microcystin-LR on testis. *Toxicology Reports* 2, 289-296.
- Lopes RH, Reid I, Hobson PR (2007). The two-dimensional Kolmogorov-Smirnov test. *Proceedings of Science, XI International Workshop on Advanced Computing and Analysis Techniques in Physics Research*, Amsterdam, the Netherlands
- Lopes WS, Buriti JS, Cebalos BS, Sousa JT, Leite VD, Vieira FFS (2017). Removal of microcystin-LR from drinking water using a system involving oxidation and adsorption. *Water, Air, and Soil Pollution* 228(9), 1-14.
- Lopez-Espinosa MJ, Mondal D, Armstrong B, Bloom MS, Fletcher T (2012). Thyroid function and perfluoroalkyl acids in children living near a chemical plant. *Environmental health perspectives* 120, 1036-1041.
- Lowe J, Hossain MM (2008). Application of ultrafiltration membranes for removal of humic acid from drinking water. *Desalination* 218, 343-354.
- Luiz AJB (2021) Application of the Kolmogorov- Smirnov Test to compare greenhouse gas emissions over time. *Revista Brasileira De Biometria* 39, 60-70.
- Ma J, Lenhart JH, Tracy K (2011). Orthophosphate adsorption equilibrium and breakthrough on filtration media for storm-water runoff treatment. *Journal of irrigation and drainage engineering*, 137(4), 244-250.

- Ma J, Wang R, Wang X, Zhang H, Zhu B, Lian L, Lou D (2019). Drinking water treatment by stepwise flocculation using polysilicate aluminum magnesium and cationic polyacrylamide. *Journal of Environmental Chemical Engineering* 7, 103049.
- Mahmood T, Saddique MT, Naeem A, Westerhoff P, Mustafa S, Alum A (2011). Comparison of different methods for the point of zero charge determination of NiO. *Industrial & Engineering Chemistry Research* 50(17), 10017-10023.
- Mahmoud ME, Amira MF, Seleim SM, Mohamed AK (2017). Adsorption isotherm models, kinetics study, and thermodynamic parameters of Ni (II) and Zn (II) removal from water using the LbL technique. *Journal of Chemical and Engineering Data* 62, 839-850.
- Mahmood T, Saddique MT, Naeem A, Westerhoff P, Mustafa S, Alum A (2011). Comparison of different methods for the point of zero charge determination of NiO. *Industrial & Engineering Chemistry Research* 50(17), 10017.
- Mane R, Bhusari V (2012). Removal of colour (dyes) from textile effluent by adsorption using orange and banana peel. *International Journal of Engineering Research and Applications* 2, 1997-2004.
- Manisalidis I, Stavropoulou E, Stavropoulos A, Bezirtzoglou E (2020). Environmental and health impacts of air pollution: a review. *Frontiers in public health*, 14.
- Mashile PP, Mpupa A, Nomngongo PN (2018). Adsorptive removal of microcystin-LR from surface and wastewater using tyre-based powdered activated carbon: Kinetics and isotherms. *Toxicon* 145, 25-31.
- Mastropietro TF, Bruno R, Pardo E, Armentano D (2021). Reverse osmosis and nanofiltration membranes for highly efficient PFASs removal: overview, challenges and future perspectives. *Dalton Transactions* 50, 5398-5410.
- Matamoros V, Arias C, Brix H, Bayona JM (2007). Removal of pharmaceuticals and personal care products (PPCPs) from urban wastewater in a pilot vertical flow constructed wetland and a sand filter. *Environmental Science & Technology* 41, 8171
- Mathialagan T, Viraraghavan T (2002). Adsorption of cadmium from aqueous solutions by perlite. *Journal of Hazardous Materials*, 94(3), 291-303.
- McDowell LA, Kudravalli P, Sticco KL (2022). Iron Overload. *StatPearls* [Internet].
- McGregor R, Zhao Y (2021). The in situ treatment of TCE and PFAS in groundwater within a silty sand aquifer. *Remediation Journal* 31, 7-17.
- McKay G, Otterburn M, Sweeney A (1980). The removal of colour from effluent using various adsorbents—III. Silica: Rate processes. *Water Research* 14, 15-20.
- Meesuk L, Seammai S (2010). The use of perlite to remove dark colour from repeatedly used palm oil. *Sci Asia* 36, 33-39.
- Melillo JM, Richmond T, Yohe G (2014). Climate change impacts in the United States. *Third national climate assessment* 52.
- Minnesota Department of Health (2022). Perfluorobutanoic acid (PFBA) and water. in: Unit, H.R.A. (Ed.).
- Mor S, Chhoden K, Ravindra K (2016). Application of agro-waste rice husk ash for the removal of phosphate from the wastewater. *Journal of Cleaner Production* 129, 673-680.
- Morris RD, Audet AM, Angelillo IF, Chalmers TC, Mosteller F (1992). Chlorination, chlorination by-products, and cancer: a meta-analysis. *American journal of public health* 82, 955-963.
- Morris RJ, Williams DE, Luu HA, Holmes CF, Andersen RJ, Calvert SE (2000) The adsorption of microcystin-LR by natural clay particles. *Toxicon* 38(2), 303-308.

- Moussavi G, Bagheri A (2012). Removal of petroleum hydrocarbons from contaminated groundwater by the combined technique of adsorption onto perlite followed by the O₃/H₂O₂ process. *Environmental technology* 33, 1905-1912.
- Mukhopadhyay R, Sarkar B, Palansooriya KN, Dar JY, Bolan NS, Parikh SJ, Sonne C, Ok YS (2021). Natural and engineered clays and clay minerals for the removal of poly-and perfluoroalkyl substances from water: State-of-the-art and future perspectives. *Advances in Colloid and Interface Science* 297, 102537.
- Murray CC, Vatankhah H, McDonough CA, Nickerson A, Hedtke TT, Cath TY, Higgins CP, Bellona CL (2019). Removal of per-and polyfluoroalkyl substances using super-fine powder activated carbon and ceramic membrane filtration. *Journal of hazardous materials* 366, 160-168.
- Mustafa YA, Ebrahim SE (2010). Utilization of Thomas model to predict the breakthrough curves for adsorption and ion exchange. *J. Eng* 4, 6206-6223.
- Naidu R, Nadebaum P, Fang C, Cousins I, Pennell K, Conder J, Newell C, Longpré D, Warner S, Crosbie N (2020). Per-and poly-fluoroalkyl substances (PFAS): Current status and research needs. in: *Innovation, E.T.a. (Ed.). Elsevier*, p. 100915.
- Najim TS, Yassin SA, Majli AJ (2010). Poly (furfural-Acetone) as new adsorbent for removal of Cu (II) from aqueous solution: Thermodynamic and kinetic studies. *International Journal of Chemistry* 2, 44.
- Navarro DA, Oliver DP, Simpson SL, Kookana RS (2022). Organic carbon and salinity affect desorption of PFAS from estuarine sediments. *Journal of Soils and Sediments* 22, 1302-1314.
- Nayak PS, Sing B (2007). Instrumental characterization of clay by XRF, XRD and FTIR. *Bulletin of materials science* 30.
- Neumann U, Weckesser J (1998). Elimination of microcystin peptide toxins from water by reverse osmosis. *Environmental Toxicology and Water Quality: An International Journal* 13(2), 143-148.
- Nieder R, Benbi DK, Reichl FX, Nieder R, Benbi DK, Reichl FX (2018). Reactive water-soluble forms of nitrogen and phosphorus and their impacts on environment and human health. *Soil components and human health*, 223-255.
- NIH (2021) Perfluoroalkyl and Polyfluoroalkyl Substances (PFAS), National Institute of Environmental Health Sciences. <https://www.niehs.nih.gov/health/topics/agents/pfc/index.cfm> accessed by Oct. 2021
- Nobre MM (1997) Detecção de toxinas (microcistinas) produzidas por cianobactérias (algas azuis) em represas para abastecimento público, pelo método de imunoadsorção ligado à enzima (ELISA).
- Nouri J, Mahvi A, Bazrafshan E (2010). Application of electrocoagulation process in removal of zinc and copper from aqueous solutions by aluminum electrodes. *International Journal of Environmental Research* 4, 201-208.
- Nwabanne JT, Iheanacho OC, Obi CC, Onu CE (2022). Linear and nonlinear kinetics analysis and adsorption characteristics of packed bed column for phenol removal using rice husk-activated carbon. *Applied Water Science*, 12(5), 91.
- Ochoa-Herrera V, Sierra-Alvarez R (2008) Removal of perfluorinated surfactants by sorption onto granular activated carbon, zeolite and sludge. *Chemosphere* 72, 1588

- O'Connor J, Bolan NS, Kumar M, Nitai AS, Ahmed MB, Bolan SS, Vithanage M, Rinklebe J, Mukhopadhyay R, Srivastava P (2022). Distribution, transformation and remediation of poly-and per-fluoroalkyl substances (PFAS) in wastewater sources. *Process Safety and Environmental Protection* 164, 91-108.
- OEHHA (2021). The PFAS Regulatory Coalition, 2021. Comments of the PFAS Regulatory Coalition on California OEHHA's Proposed Public Health Goals for Perfluorooctanoic Acid and Perfluorooctane Sulfonic Acid in Drinking Water. in: Branch, P.a.E.T, Assessment, O.o.E.H.H, Agency, C.E.P. (Eds.), OEHHA, p. 7.
- Omoike A (1999). Removal of phosphorus and organic matter removal by alum during wastewater treatment. *Water Research* 33, 3617-3627.
- O'Reilly AM, Wanielista MP, Chang N-B, Xuan Z, Harris WG (2012). Nutrient removal using biosorption activated media: Preliminary biogeochemical assessment of an innovative stormwater infiltration basin. *Science of the Total Environment* 432, 227.
- Ordonez D, Valencia A, Chang NB, Wanielista MP (2020a). Synergistic effects of aluminum/iron oxides and clay minerals on nutrient removal and recovery in water filtration media. *Journal of Cleaner Production* 275, 122728.
- Ordonez D, Valencia A, Elhakiem H, Chang NB, Wanielista MP (2020b). Adsorption thermodynamics and kinetics of Advanced Green Environmental Media (AGEM) for nutrient removal and recovery in agricultural discharge and stormwater runoff. *Environmental Pollution* 266, 115172.
- Ordonez D, Podder A, Valencia A, Sadmani AA, Reinhart D, Chang NB (2022a). Continuous fixed-bed column adsorption of perfluorooctane sulfonic acid (PFOS) and perfluorooctanoic acid (PFOA) from canal water using zero-valent Iron-based filtration media. *Separation and Purification Technology* 299, 121800.
- Ordonez D, Valencia A, Pereira B, Chang NB (2022b). Color removal for large-scale interbasin water transfer: Experimental comparison of five sorption media. *Environmental Research* 212, 113208.
- Ordonez D, Valencia A, Sadmani AA, Chang NB (2022c). Green sorption media for the removal of perfluorooctanesulfonic acid (PFOS) and perfluorooctanoic acid (PFOA) from water. *Science of the Total Environment* 819, 152886.
- Ozel U, Akdemir A, Ergun ON (2012). Utilization of natural zeolite and perlite as landfill liners for in situ leachate treatment in landfills. *International Journal of Environmental Research and Public Health*, 9(5), 1581-1592.
- Padmakumar K, Menon N, Sanjeevan V (2012). Is occurrence of harmful algal blooms in the exclusive economic zone of India on the rise? *International Journal of Oceanography*.
- Palmstrom NS, Carlson RE, Cooke GD (1988). Potential links between eutrophication and the formation of carcinogens in drinking water. *Lake and Reservoir Management* 4, 1-15.
- Panieri E, Baralic K, Djukic-Cosic D, Buha Djordjevic A, Saso L (2022). PFAS Molecules: A Major Concern for the Human Health and the Environment. *Toxics* 10, 44.
- Parenty AC, Gevaerd de Souza N, Asgari P, Jeon J, Nadagouda MN, Choi H (2020). Removal of perfluorooctanesulfonic acid in water by combining zerovalent iron particles with common oxidants. *Environmental Engineering Science* 37(7), 472.
- Park S, Zenobio JE, Lee LS (2018). Perfluorooctane sulfonate (PFOS) removal with Pd0/nFe0 nanoparticles: adsorption or aqueous Fe-complexation, not transformation? *Journal of hazardous materials* 342, 20-28.

- Patel H (2019) Fixed-bed column adsorption study: a comprehensive review. *Applied Water Science* 9(3),1-17.
- Pauletto PS, Bandosz TJ (2022). Activated carbon versus metal-organic frameworks: A review of their PFAS adsorption performance. *Journal of Hazardous Materials* 425, 127810.
- Pavagadhi S, Tang ALL, Sathishkumar M, Loh KP, Balasubramanian R (2013). Removal of microcystin-LR and microcystin-RR by graphene oxide: adsorption and kinetic experiments. *Water Research* 47(13), 4621-4629.
- Peng Y, Deng S, Kong Z, Yuan Y, Long H, Fang J, Ma H, Shao Z, He Q, Chai H (2022). Biochar and woodchip amended bioreactor extending reactive volume for enhanced denitrification in stormwater runoff. *Journal of Water Process Engineering* 46, 102541.
- Perez-Benito JF (2003). Coagulation of colloidal manganese dioxide by divalent cations. *Colloids and Surfaces A: Physicochemical and Engineering Aspects* 225, 145-152.
- Phlips EJ, Badylak S, Christman M, Wolny J, Brame J, Garland J, Hall L, Hart J, Landsberg J, Lasi M (2011). Scales of temporal and spatial variability in the distribution of harmful algae species in the Indian River Lagoon, Florida, USA. *Harmful Algae* 10(3), 277-290.
- Piyathilaka PC, Manage PM (2017). Microcystin-LR Contamination Status and Physico-Chemical Water Quality Parameters of Five Selected Recreational Water Bodies in Sri Lanka. *Journal of Food and Agriculture* 10 (1-2), 35-42.
- Podder A, Sadmani AA, Reinhart D, Chang N-b, Goel R (2021). Per and poly-fluoroalkyl substances (PFAS) as a contaminant of emerging concern in surface water: A transboundary review of their occurrences and toxicity effects. *Journal of Hazardous Materials*, 126361
- Post GB, Cohn PD, Cooper KR (2012). Perfluorooctanoic acid (PFOA), an emerging drinking water contaminant: a critical review of recent literature. *Environmental Research* 116, 93.
- Post G (2021). Recent US state and federal drinking water guidelines for per-and polyfluoroalkyl substances. *Environmental Toxicology and Chemistry* 40, 550-563.
- Pradhan S, Helal M.I, Al-Ghamdi SG, Mackey HR (2020). Performance evaluation of various individual and mixed media for greywater treatment in vertical nature-based systems. *Chemosphere* 245, 125564.
- Prema P, Thangapandian S, Selvarani M, Subharanjani S, Amutha C (2011). Color removal efficiency of dyes using nanozerovalent iron treatment. *Toxicological & Environmental Chemistry* 93, 1908-1917.
- Qaseem S, Dlamini DS, Zikalala SA, Tesha JM, Husain MD, Wang C, Jiang Y, Wei X, Vilakati GD, Li J (2020). Electro-catalytic membrane anode for dye removal from wastewater. *Colloids and Surfaces A: Physicochemical and Engineering Aspects* 603, 125270.
- Quan X, Zhao X, Chen S, Zhao H, Chen J, Zhao Y (2005). Enhancement of p, p'-DDT photodegradation on soil surfaces using TiO₂ induced by UV-light. *Chemosphere* 60, 266-273.
- Rambabu K, Bharath G, Monash P, Velu S, Banat F, Naushad M, Arthanareeswaran G, Show PL (2019). Effective treatment of dye polluted wastewater using nanoporous CaCl₂ modified polyethersulfone membrane. *Process Safety and Environmental Protection* 124, 266-278.
- Rao K, Rao PL, Bhattacharya R, (1996) The cyanobacterial toxin microcystin-LR induced DNA damage in mouse liver in vivo. *Toxicology* 114(1), 29-36., Krishnaiah, K, 1994. Colour removal from a dyestuff industry effluent using activated carbon.

- Rasko DA, Webster DR, Sahl JW, Bashir A, Boisen N, Scheutz F, Paxinos EE, Sebra R, Chin CS, Iliopoulos D (2011). Origins of the E. coli strain causing an outbreak of hemolytic–uremic syndrome in Germany. *New England Journal of Medicine* 365, 709-717.
- Recepoğlu YK, Kabay N, Ipek IY, Arda M, Yüksel M, Yoshizuka K, Nishihama S (2018) Packed bed column dynamic study for boron removal from geothermal brine by a chelating fiber and breakthrough curve analysis by using mathematical models. *Desalination* 437, 1.
- Reddi L, Inyang HI (2000). *Geoenvironmental engineering: principles and applications*. CRC Press.
- Reddy KR, Xie T, Dastgheibi S (2014). Nutrients removal from urban stormwater by different filter materials. *Water, Air, & Soil Pollution*, 225(1), 1-14.
- Richardson SD, Willson CS, Rusch KA (2004). Use of rhodamine water tracer in the marshland upwelling system. *Groundwater* 42, 678-688.
- Rizzuto P (2022). Global PFAS Guidance Fuels Debate as EPA Tap Water Limits Loom. *Bloomberg Law*.
- Rong J, Zhao Z, Jing Z, Zhang T, Qiu F, Xu, J (2017) High-specific surface area hierarchical Al₂O₃ carbon fiber based on a waste paper fiber template: preparation and adsorption for iodide ions. *Journal of Wood Chemistry and Technology* 37(6), 485-492.
- Rodea-Palomares I, Leganés F, Rosal R, Fernández-Piñas F (2012). Toxicological interactions of perfluorooctane sulfonic acid (PFOS) and perfluorooctanoic acid (PFOA) with selected pollutants. *Journal of Hazardous Material* 201, 209-218.
- Roesch P, Vogel C, Simon FG (2020). Reductive defluorination and mechanochemical decomposition of per- and polyfluoroalkyl substances (PFASs): from present knowledge to future remediation concepts. *International Journal of Environmental Research and Public Health* 17, 7242.
- Rosa M, Egado J, Márquez M (2019). Empirical kinetic models for the electrochemical extraction of arsenic and heavy metals from clay containing tailings. *Applied Clay Science* 182, 105254.
- Rossatto DL, Netto MS, Reis GS, Silva LF, Dotto GL (2021). Volcanic rock powder residues as precursors for the synthesis of adsorbents and potential application in the removal of dyes and metals from water. *Environmental Science and Pollution Research*, 1-9.
- Rostvall A, Zhang W, Dürig W, Renman G, Wiberg K, Ahrens L, Gagi-Ferreri P (2018) Removal of pharmaceuticals, perfluoroalkyl substances and other micropollutants from wastewater using lignite, Xylit, sand, granular activated carbon (GAC) and GAC+ Polonite® in column tests–Role of physicochemical properties. *Water Research* 137, 97
- Roth K, Yang Z, Agarwal M, Liu W, Peng Z, Long Z, Birbeck J, Westrick J, Liu W, Petriello MC (2021). Exposure to a mixture of legacy, alternative, and replacement per- and polyfluoroalkyl substances (PFAS) results in sex-dependent modulation of cholesterol metabolism and liver injury. *Environment International* 157, 106843.
- Sadegh H, Ali GA (2021). Potential applications of nanomaterials in wastewater treatment: nanoadsorbents performance. In *Research Anthology on Synthesis, Characterization, and Applications of Nanomaterials (1230-1240)*: IGI Global.
- Sadmani AA, Andrews RC, Bagley DM (2014) Rejection of pharmaceutically active and endocrine disrupting compounds by nanofiltration as a function of source water humic substances. *Journal of Water Process Engineering* 2(0), 63.

- Saleh TA, Sari A, Tuzen M (2017). Effective adsorption of antimony (III) from aqueous solutions by polyamide-graphene composite as a novel adsorbent. *Chemical Engineering Journal* 307, 230-238.
- Sathishkumar M, Pavagadhi S, Vijayaraghavan K, Balasubramanian R, Ong S (2010). Experimental studies on removal of microcystin-LR by peat. *Journal of hazardous Materials* 184(1-3), 417-424.
- Santhi T, Manonmani S, Smitha T (2010). Kinetics and isotherm studies on cationic dyes adsorption onto annona squamosa seed activated carbon. *International Journal of Engineering Science and Technology* 2, 287-295.
- Santos SC, Vilar VJ, Boaventura RA (2008). Waste metal hydroxide sludge as adsorbent for reactive dye. *Journal of Hazardous Materials* 153, 999-1008.
- Sari RK (2019) Analysis of oxide content in sand and rock found in public mining of west sumatra province using XRF test. *Journal of Physics: Conference Series* 1317(1).
- Sauvé S, Desrosiers M (2014). A review of what is an emerging contaminant. *Chemistry Central Journal* 8, 1-7.
- Scicchitano P (2019) Toxic PFAS Chemical Found In Florida — Here's Where. Patch.
- Schindler DW (1974). Eutrophication and recovery in experimental lakes: implications for lake management. *Science* 184, 897-899.
- Schwichtenberg T, Bogdan D, Carignan CC, Reardon P, Rewerts J, Wanzek T, Field JA (2020). PFAS and dissolved organic carbon enrichment in surface water foams on a northern US freshwater lake. *Environmental Science and Technology* 54, 14455-14464.
- Selezneva A, Seleznev V. Sayriddinov SS (2021). *Nanofiltration to Purify Drinking Water from Cyanobacteria and Microcystins in Water Supply Systems*, p. 022043, IOP Publishing.
- Setoguchi S, Leddin D, Metz G, Omary MB (2022). Climate change, health, and health care systems: a global perspective. *Gastroenterology* 162, 1549-1555.
- Shafique M, Kim R, Rafiq M (2018). Green roof benefits, opportunities and challenges—A review. *Renewable and Sustainable Energy Reviews* 90, 757-773.
- Shanmugam D, Alagappan M, Rajan RK (2016). Bench-scale packed bed sorption of Cibacron blue F3GA using lucrative algal biomass. *Alexandria Engineering Journal* 55(3), 2995.
- Sharma VK, Triantis TM, Antoniou MG, He X, Pelaez M, Han C, Song W, O'Shea KE, Armah A, Kaloudis T (2012). Destruction of microcystins by conventional and advanced oxidation processes: a review. *Separation and Purification Technology* 91, 3-17.
- Shawwa AR, Smith DW (2001). Kinetics of microcystin-LR oxidation by ozone. *Ozone Science & Engineering* 23(2), 161-170.
- Shengguang Y, Daying X, Xiaolong Y, Jun Z (1991). Effect of algae and water on water color shift. *Chinese Journal of Oceanology and Limnology* 9, 49-56.
- Sima MW, Jaffé PR (2021). A critical review of modeling Poly-and Perfluoroalkyl Substances (PFAS) in the soil-water environment. *Science of the Total Environment* 757, 143793.
- Simon JA, Abrams S, Bradburne T, Bryant D, Burns M, Cassidy D, Cherry J, Chiang SY, Cox D, Crimi M (2019). PFAS Experts Symposium: Statements on regulatory policy, chemistry and analytics, toxicology, transport/fate, and remediation for per-and polyfluoroalkyl substances (PFAS) contamination issues. *Remediation Journal* 29, 31-48.
- Simsek EB, Beker U, Senkal BF (2014). Predicting the dynamics and performance of selective polymeric resins in a fixed bed system for boron removal. *Desalination* 349:39-50.

- Sinclair E, Kannan K, Taniyasu S, Yamashita N (2004). Perfluorooctanoic acid and perfluorooctane sulfonate in Michigan and New York waters.
- Singh A, Kumar D, Gaur J (2012). Continuous metal removal from solution and industrial effluents using *Spirogyra* biomass-packed column reactor. *Water Research* 46(3):779-788
- Singh KP, Mohan D, Sinha S, Tondon G, Gosh D (2003). Color removal from wastewater using low-cost activated carbon derived from agricultural waste material. *Industrial & Engineering Chemistry Research* 42, 1965-1976.
- Singh RK, Brown E, Thagard SM, Holsen TM (2021). Treatment of PFAS-containing landfill leachate using an enhanced contact plasma reactor. *Journal of Hazardous Materials* 408, 124452.
- Sivaraj R, Namasivayam C, Kadirvelu K (2001). Orange peel as an adsorbent in the removal of acid violet 17 (acid dye) from aqueous solutions. *Waste management* 21, 105-110.
- SJRWDM (2021). St. Johns River Water Management. Water Supply, Florida's Aquifer. (sjrwmd.com).
- Sokolovic RS, Sokolovic S (1996). New technology for waste water from water-washed paint spray booths. *Environmental technology*, 17(1), 35-43.
- Song J, Zou W, Bian Y, Su F, Han R (2011). Adsorption characteristics of methylene blue by peanut husk in batch and column modes. *Desalination* 265(1-3), 119-125.
- Söregård M, Lindh AS, Ahrens L (2020a). Thermal desorption as a high removal remediation technique for soils contaminated with per-and polyfluoroalkyl substances (PFASs). *PLoS one*. 15(6): 0234476.
- Söregård M, Östblom E, Köhler S, Ahrens L (2020b) Adsorption behavior of per-and polyfluoroalkyl substances (PFASs) to 44 inorganic and organic sorbents and use of dyes as proxies for PFAS sorption. *Journal of Environmental Chemical Engineering* 8,103744
- Soro MP, N'goran KM, Ouattara AA, Yao KM, Diaco T (2023). Nitrogen and phosphorus spatio-temporal distribution and fluxes intensifying eutrophication in three tropical rivers of Côte d'Ivoire (West Africa). *Marine Pollution Bulletin* 186, 114391.
- Steenland K, Winquist A (2021). PFAS and cancer, a scoping review of the epidemiologic evidence. *Environmental Research* 194, 110690.
- Stefano PHP, Roisenberg A, D'Anna Acayaba R, Roque AP, Bandoria DR, Soares A, Montagner CC (2022). Occurrence and distribution of per-and polyfluoroalkyl substances (PFAS) in surface and groundwaters in an urbanized and agricultural area, Southern Brazil. *Environmental Science and Pollution Research*, 1-11.
- Stocker K, Ellersdorfer M (2022). Phosphate Fixation and P Mineralogy on Natural and Ca-Modified Zeolites During Simultaneous Nutrient Removal. *Water, Air, & Soil Pollution* 233, 41.
- Stockholm Convention (2009). Governments unite to step-up reduction on global DDT reliance and add nine new chemicals under international treaty. Geneva.
- Stockholm Convention (2022). The new POPs under the Stockholm Convention. United Nations environment programme.
- Stumm W, Lee GF (1961). Oxygenation of ferrous iron. *Industrial & Engineering Chemistry*, 53(2), 143-146.
- Sultana S, Awal S, Shaika NA, Khan S (2022). Cyanobacterial blooms in earthen aquaculture ponds and their impact on fisheries and human health in Bangladesh. *Aquaculture Research* 53, 5129-5141.

- Su X, Steinman AD, Tang X, Xue Q, Zhao Y, Xie L (2017). Response of bacterial communities to cyanobacterial harmful algal blooms in Lake Taihu, China. *Harmful Algae* 68, 168-177.
- Subramaniam M, Goh P, Abdullah N, Lau W, Ng B, Ismail A (2017). Adsorption and photocatalytic degradation of methylene blue using high surface area titanate nanotubes (TNT) synthesized via hydrothermal method. *Journal of Nanoparticle Research* 19(6), 1-13.
- Sun C, Xiong B, Pan Y, Cui H (2017). Adsorption removal of tannic acid from aqueous solution by polyaniline: Analysis of operating parameters and mechanism. *Journal of colloid and interface science* 487, 175-181.
- Sun G, Xu X (1997). Sunflower stalks as adsorbents for color removal from textile wastewater. *Industrial & engineering chemistry research* 36, 808-812.
- Sun M, Arevalo E, Strynar M, Lindstrom A, Richardson M, Kearns B, Pickett A, Smith C, Knappe DR (2016). Legacy and emerging perfluoroalkyl substances are important drinking water contaminants in the Cape Fear River Watershed of North Carolina. *Environmental science and technology letters* 3, 415-419.
- Sunderland EM, Hu XC, Dassuncao C, Tokranov AK, Wagner CC, Allen JG (2019). A review of the pathways of human exposure to poly-and perfluoroalkyl substances (PFASs) and present understanding of health effects. *Journal of exposure science & environmental epidemiology* 29, 131-147.
- Syamsu K, Fahma F, Pari G (2022). Ethylene Adsorption on Activated Carbon Paper Liner: A Model Kinetic Study. *IOP Conference Series: Earth and Environmental Science*. IOP Publishing, p. 012022.
- Szymczyk P, Filipkowska U, Józwiak T, Kuczajowska-Zadrożna M (2016). Phosphate removal from aqueous solutions by chitin and chitosan in flakes. *Progress on Chemistry and Application of Chitin and its Derivatives*, 21, 192-202
- Tak S, Vellanki BP (2018). Natural organic matter as precursor to disinfection byproducts and its removal using conventional and advanced processes: state of the art review. *Journal of water and health* 16, 681-703.
- Talibi T, Onyeneke C, Eguzouwa C, Natural and Human Impacts of Overpopulation on the Economy.
- Tang CY, Fu QS, Gao D, Criddle CS, Leckie JO (2010). Effect of solution chemistry on the adsorption of perfluorooctane sulfonate onto mineral surfaces. *Water research* 44, 2654.
- Tang L, Liu X, Yang G, Xia J, Zhang N, Wang D, Deng H, Mao M, Li X, Ni BJ (2021). Spatial distribution, sources and risk assessment of perfluoroalkyl substances in surface soils of a representative densely urbanized and industrialized city of China. *Catena* 198, 105059.
- Tara N, Siddiqui SI, Rathi G, Chaudhry SA, Asiri AM (2020). Nano-engineered adsorbent for the removal of dyes from water: A review. *Current Analytical Chemistry* 16, 14-40.
- Team CW (2009). Color of Water Fact Sheet. State Water Resources Control Board.
- Teixeira MR, Rosa MJ (2005). Microcystins removal by nanofiltration membranes. *Separation and Purification Technology* 46(3), 192-201.
- Teng Y, Liu Z, Yao K, Song W, Sun Y, Wang H, Xu Y (2019). Preparation of attapulgite/CoFe₂O₄ magnetic composites for efficient adsorption of tannic acid from aqueous solution. *International Journal of Environmental Research and Public Health* 16, 2187.
- Thomas HC, (1944) Heterogeneous ion exchange in a flowing system. *Journal of the American Chemical Society* 66, 1664.

- Thostrup L, Christoffersen K (1999). Accumulation of microcystin in *Daphnia magna* feeding on toxic *Microcystis*. *Archiv für Hydrobiologie*, 447-467.
- Tokranov AK, LeBlanc DR, Pickard HM, Ruyle BJ, Barber LB, Hull RB, Sunderland EM, Vecitis CD (2021). Surface-water/groundwater boundaries affect seasonal PFAS concentrations and PFAA precursor transformations. *Environmental Science: Processes and Impacts* 23, 1893-1905.
- Toussaint B, Raffael B, Angers-Loustau A, Gilliland D, Kestens V, Petrillo M, Rio-Echevarria I.M, Van den Eede G (2019). Review of micro-and nanoplastic contamination in the food chain. *Food Additives & Contaminants: Part A* 36, 639-673.
- Trang B, Li Y, Xue XS, Ateia M, Houk K, Dichtel WR (2022). Low-temperature mineralization of perfluorocarboxylic acids. *Science* 377, 839-845.
- Trazzi P, Leahy JJ, Hayes MH, Kwapinski W (2016). Adsorption and desorption of phosphate on biochars. *Journal of environmental chemical engineering*, 4(1), 37-46.
- Ukaogo PO, Ewuzie U, Onwuka CV (2020). Environmental pollution: causes, effects, and the remedies. *Microorganisms for sustainable environment and health*. Elsevier, pp. 419-429.
- Umembamalu CJ, Igwegbe CA, Osuagwu EU, Nwabanne JT (2020) Packed bed column adsorption of oil and grease from refinery desalter effluent, using rice husks derived carbon as the adsorbent: Influence of process parameters and Bohart–Adams kinetics study. *World News of Natural Sciences* 31, 155.
- UN (2022). Peace, dignity and equality on a healthy planet. *Global issues Population*. <https://www.un.org/en/global-issues/population>.
- UN (2023a). SDG 2: Zero Hunger. United Nations.
- UN (2023b). SDG 6: Clean water and sanitation. United Nations.
- Urbonas B, Stahre P (1993). Stormwater: Best management practices and detention for water quality, drainage, and CSO management.
- USEPA (2019). EPA Issues Recommendations for Recreational Water Quality Criteria and Swimming Advisories for Cyanotoxins.
- USEPA (2019). Determination of Selected Perfluorinated Alkyl Acids in Drinking Water by Solid Phase Extraction and Liquid Chromatography/Tandem Mass Spectrometry (LC/MS/MS), EPA Method 537. Version 1.1. In: U.S. Environmental Protection Agency, editor.
- USEPA (2016). Drinking Water Health Advisories for PFOA and PFOS. <https://www.epa.gov/ground-water-and-drinking-water/drinking-water-health-advisories-pfoa-and-pfos> Accessed on: March 23, 2022
- USEPA (2021). Research on Per-and Polyfluoroalkyl Substances (PFAS). <https://www.epa.gov/chemical-research/research-and-polyfluoroalkyl-substances-pfas> Accessed on: March 23, 2022
- USGS (2018). Water Color Water Science School.
- Uusipaikka E (2008). Confidence intervals in generalized regression models. Chapman and Hall/CRC.
- Uyak V, Toroz I (2007). Disinfection by-product precursors reduction by various coagulation techniques in Istanbul water supplies. *Journal of hazardous materials* 141, 320-328.
- Vadivelan V, Kumar KV (2005). Equilibrium, kinetics, mechanism, and process design for the sorption of methylene blue onto rice husk. *Journal of colloid and interface science* 286, 90-100.

- Valencia A, Chang NB, Wen D, Ordonez D, Wanielista MP (2019). Optimal recipe assessment of iron filing-based green environmental media for improving nutrient removal in stormwater runoff. *Environmental Engineering Science* 36, 1323-1336.
- Valencia A, Ordonez D, Wen D, McKenna AM, Chang NB, Wanielista MP (2020). The interaction of dissolved organic nitrogen removal and microbial abundance in iron-filings based green environmental media for stormwater treatment. *Environmental Research* (188), 109815
- Valencia A, Zhang W, Chang NB (2021). Integration of machine learning classifiers and higher order tensors for screening the optimal recipe of filter media in stormwater treatment. *Science of The Total Environment* 771, 145423.
- Valsecchi S, Babut M, Mazzoni M, Pascariello S, Ferrario C, De Felice B, Bettinetti R, Veyrand B, Marchand P, Polesello S (2021). Per-and Polyfluoroalkyl Substances (PFAS) in Fish from European Lakes: Current Contamination Status, Sources, and Perspectives for Monitoring. *Environmental Toxicology and Chemistry* 40, 658-676.
- Varsi K, Torsvik IK, Huber S, Averina M, Brox J, Bjørke-Monsen AL (2022). Impaired gross motor development in infants with higher PFAS concentrations. *Environmental Research* 204, 112392.
- Veni DK, Kannan P, Edison TNJI, Senthilkumar A (2017). Biochar from green waste for phosphate removal with subsequent disposal. *Waste Management*, 68, 752-759.
- Verma S, Daverey A, Sharma A (2017) Slow sand filtration for water and wastewater treatment—a review. *Environmental Technology Reviews* 6, 47.
- Vieira JMdS, Azevedo MTdP, de Oliveira Azevedo SMF, Honda RY Corrêa B (2005). Toxic cyanobacteria and microcystin concentrations in a public water supply reservoir in the Brazilian Amazonia region. *Toxicon* 45(7), 901-909.
- Villars K, Huang Y, Lenhart JJ (2020) Removal of the cyanotoxin microcystin-LR from drinking water using granular activated carbon. *Environmental Engineering Science* 37(9), 585-595.
- Vu CT, Wu T (2022). Recent progress in adsorptive removal of per-and poly-fluoroalkyl substances (PFAS) from water/wastewater. *Critical Reviews in Environmental Science and Technology* 52, 90-129.
- Vymazal J (2010). Constructed wetlands for wastewater treatment. *Water* 2, 530-549.
- Wang F, Shih K (2011). Adsorption of perfluorooctanesulfonate (PFOS) and perfluorooctanoate (PFOA) on alumina: Influence of solution pH and cations. *Water Research* 45, 2925.
- Wang, H, Xu, J, Liu, X, Zhang, D, Li, L, Li, W, & Sheng, L. (2019). Effects of long-term application of organic fertilizer on improving organic matter content and retarding acidity in red soil from China. *Soil and Tillage Research*, 195, 104382.
- Wang, J, Zheng, S, Liu, J, Xu, Z, 2010. Tannic acid adsorption on amino-functionalized magnetic mesoporous silica. *Chemical Engineering Journal* 165, 10-16.
- Wang F, Liu C, Shih K (2012) Adsorption behavior of perfluorooctanesulfonate (PFOS) and perfluorooctanoate (PFOA) on boehmite. *Chemosphere* 89(8),1009.
- Wang M, Orr AA, Jakubowski JM, Bird KE, Casey CM, Hearon SE, Tamamis P, Phillips TD (2021a) Enhanced adsorption of per-and polyfluoroalkyl substances (PFAS) by edible, nutrient-amended montmorillonite clays. *Water Research* 188, 116534.
- Wang T, Zhao C, Li P, Li Y, Wang J (2015). Fabrication of novel poly (m-phenylene isophthalamide) hollow fiber nanofiltration membrane for effective removal of trace amount perfluorooctane sulfonate from water. *Journal of Membrane Science* 477, 74.

- Wang Y, He H, Zhang N, Shimizu K, Lei Z, Zhang Z (2018). Efficient capture of phosphate from aqueous solution using acid activated akadama clay and mechanisms analysis. *Water Science and Technology*, 78(7), 1603-1614.
- Wang Y, Shao Q, Huang S, Zhang B, Xu C (2018). High performance and simultaneous sequestration of Cr (VI) and Sb (III) by sulfidated zerovalent iron. *Journal of Cleaner Production* 191, 436.
- Wang Y, Khan N, Huang D, Carroll KC, Brusseau ML (2021b). Transport of PFOS in aquifer sediment: Transport behavior and a distributed-sorption model. *Science of the Total Environment* 779, 146444.
- Wang Z, Nie E, Li J, Yang M, Zhao Y, Luo X, Zheng Z (2012). Equilibrium and kinetics of adsorption of phosphate onto iron-doped activated carbon. *Environmental Science and Pollution Research*, 19(7), 2908-2917.
- Wei W, Zhang X, Zhang Y, Xin M, Run W, Huilan S, Chunli L, Ziwen D, Youming Q (2021). Adsorption of emerging sodium p-perfluorooctanoate (OPF) onto soils: Kinetics, isotherms and mechanisms. *Pedosphere* 31, 596-605.
- Weikard HP, Seyhan D (2009). Distribution of phosphorus resources between rich and poor countries: the effect of recycling. *Ecological Economics* 68, 1749-1755.
- Wen D, Chang NB, Wanielista MP (2018). Comparative copper toxicity impact and enzymatic cascade effect on Biosorption Activated Media and woodchips for nutrient removal in stormwater treatment. *Chemosphere* 213, 403-413.
- Wen D, Chang, N.-B, Wanielista, M.P, 2020a. Assessing nutrient removal in stormwater runoff for urban farming with iron filings-based green environmental media. *Scientific Reports* 10, 9379.
- Wen D, Valencia A, Ordonez D, Chang N B, Wanielista M (2020b). Comparative nitrogen removal via microbial ecology between soil and green sorption media in a rapid infiltration basin for co-disposal of stormwater and wastewater. *Environmental Research* 184, 109338.
- Westreich P, Mimna R, Brewer J, Forrester F (2018). The removal of short-chain and long-chain perfluoroalkyl acids and sulfonates via granular activated carbons: A comparative column study. *Remediation Journal* 29, 19-26.
- Wetzel RG (2001). *Limnology: lake and river ecosystems*: gulf professional publishing.
- WHO (2003). *Guidelines for Safe Recreational Water Environments*. Coastal and Freshwaters. World Health Organization 1, 136-158.
- WHO (2017). *Guidelines for Drinking-water Quality*. Fourth Edition.
- WHO (2020). *Cyanobacterial toxins: microcystins Background document for development of WHO Guidelines for drinking-water quality and Guidelines for safe recreational water environments*. Organization.
- WHO (2022). *Background document for development of WHO guidelines for drinking-water quality. PFOS and PFAS in Drinking-water*. World Health Organization; *Arsenic in Drinking-Water* Geneva.
- Williams KA, Nelson PV, Hesterberg D (2000). Phosphate and potassium retention and release during chrysanthemum production from precharged materials: I. Alumina. *Journal of the American Society for Horticultural Science*, 125(6), 748-756.
- Wigle DT (1998). Safe drinking water: a public health challenge. *Chronic Diseases and Injuries in Canada* 19, 103.

- Winston RJ, Hunt WF, Kennedy SG, Merriman LS, Chandler J, Brown D (2013). Evaluation of floating treatment wetlands as retrofits to existing stormwater retention ponds. *Ecological Engineering* 54, 254-265.
- Wong S, Ghafar NA, Ngadi N, Razmi FA, Inuwa IM, Mat R, Amin NAS (2020). Effective removal of anionic textile dyes using adsorbent synthesized from coffee waste. *Scientific Reports* 10, 2928.
- Wu B, Wan J, Zhang Y, Pan B, Lo IM (2019). Selective phosphate removal from water and wastewater using sorption: process fundamentals and removal mechanisms. *Environmental Science and Technology* 54, 50-66.
- Wu C, Tu J, Liu W, Zhang J, Chu S, Lu G, Lin Z, Dang Z (2017) The double influence mechanism of pH on arsenic removal by nano zero valent iron: electrostatic interactions and the corrosion of FeO. *Environmental Science: Nano* 4(7), 1544-1552.
- Wu FC, Tseng RL, Juang RS (2009). Initial behavior of intraparticle diffusion model used in the description of adsorption kinetics. *Chemical engineering journal* 153, 1-8.
- Wu Y, Romanak K, Bruton T, Blum A, Venier M (2020). Per- and polyfluoroalkyl substances in paired dust and carpets from childcare centers. *Chemosphere* 251, 126771.
- Wurtsbaugh WA, Paerl HW, Dodds WK, (2019). Nutrients, eutrophication and harmful algal blooms along the freshwater to marine continuum. *Wiley Interdisciplinary Reviews: Water* 6, e1373.
- Xiao F, Zhang X, Penn L, Gulliver JS, Simcik MF (2011). Effects of monovalent cations on the competitive adsorption of perfluoroalkyl acids by kaolinite: experimental studies and modeling. *Environmental Science & Technology* 45, 10028.
- Xiao X, Li F, Huang J, Sheng GD, Qiu Y (2012). Reduced adsorption of propanil to black carbon: effect of dissolved organic matter loading mode and molecule size. *Environmental Toxicology and Chemistry* 31(6), 1187-1193.
- Xiao X, Agustí S, Pan Y, Yu Y, Li K, Wu J, Duarte CM (2019). Warming amplifies the frequency of harmful algal blooms with eutrophication in Chinese coastal waters. *Environmental Science & Technology* 53, 13031-13041.
- Xiong J, Hou Y, Wang J, Liu Z, Qu Y, Li Z, Wang X (2021). The rejection of perfluoroalkyl substances by nanofiltration and reverse osmosis: influencing factors and combination processes. *Environmental Science: Water Research and Technology* 7, 1928-1943.
- Yao Y, Gao B, Inyang M, Zimmerman AR, Cao X, Pullammanappallil P, Yang L (2011). Biochar derived from anaerobically digested sugar beet tailings: characterization and phosphate removal potential. *Bioresource Technology*, 102(10), 6273-6278.
- Yan G, Viraraghavan T, Chen M (2001). A new model for heavy metal removal in a biosorption column. *Adsorption Science & Technology* 19, 25.
- Yang C, Lee HK, Zhang Y, Jiang LL, Chen ZF, Chung ACK, Cai Z (2019). In situ detection and imaging of PFOS in mouse kidney by matrix-assisted laser desorption/ionization imaging mass spectrometry. *Analytical chemistry* 91, 8783-8788.
- Yang S, Zhang K, Fang Z (2020). Robust RNA-seq data analysis using an integrated method of ROC curve and Kolmogorov–Smirnov test. *Communications in Statistics-Simulation and Computation* 1-14.
- Yeager N, Carpenter A (2019). State approaches to addressing cyanotoxins in drinking water. *AWWA Water Science* 1, e1121.

- Yoon YH, Nelson JH (1984). Application of gas adsorption kinetics I. A theoretical model for respirator cartridge service life. *American Industrial Hygiene Association Journal* 45, 509.
- You C, Jia C, Pan G (2010). Effect of salinity and sediment characteristics on the sorption and desorption of perfluorooctane sulfonate at sediment-water interface. *Environmental Pollution* 158(5), 1343.
- Yun X, Lewis AJ, Stevens-King G, Sales CM, Spooner DE, Kurz MJ, Suri R, McKenzie ER (2023). Bioaccumulation of per- and polyfluoroalkyl substances by freshwater benthic macroinvertebrates: Impact of species and sediment organic carbon content. *Science of the Total Environment* 866, 161208.
- Zaggia A, Conte L, Falletti L, Fant M, Chiorboli A (2016). Use of strong anion exchange resins for the removal of perfluoroalkylated substances from contaminated drinking water in batch and continuous pilot plants. *Water research* 91, 137-146.
- Zaied B, Rashid M, Nasrullah M, Zularisam A, Pant D, Singh L (2020). A comprehensive review on contaminants removal from pharmaceutical wastewater by electrocoagulation process. *Science of the Total Environment* 726, 138095.
- Zeng S, Kan E (2021). Adsorption and regeneration on iron-activated biochar for removal of microcystin-LR. *Chemosphere* 273, 129649.
- Žegura B, Sedmak B, Filipič M (2003) Microcystin-LR induces oxidative DNA damage in human hepatoma cell line HepG2. *Toxicol* 41(1), 41-48.
- Zhan MM, Hong Y (2022) Recent Advances in Technologies for Removal of Microcystins in Water: a Review. *Current Pollution Reports*, 1-15.
- Zhang C, Jiang S, Tang J, Zhang Y, Cui Y, Su C, Qu Y, Wei L, Cao H, Quan J (2018). Adsorptive performance of coal based magnetic activated carbon for perfluorinated compounds from treated landfill leachate effluents. *Process Safety and Environmental Protection* 117, 383-389.
- Zhang D, Luo Q, Gao B, Chiang SYD, Woodward D, Huang Q (2016). Sorption of perfluorooctanoic acid, perfluorooctane sulfonate and perfluoroheptanoic acid on granular activated carbon. *Chemosphere* 144, 2336-2342.
- Zhang D, Zhang W, Liang Y (2019). Adsorption of perfluoroalkyl and polyfluoroalkyl substances (PFASs) from aqueous solution-A review. *Science of the Total Environment* 694, 133606.
- Zhang J, Huang Z, Gao L, Gray S, Xie Z (2022). Study of MOF incorporated dual layer membrane with enhanced removal of ammonia and per-/poly-fluoroalkyl substances (PFAS) in landfill leachate treatment. *Science of The Total Environment* 806, 151207.
- Zhang L, Jun M, Xin L, Shutao W (2009). Enhanced removal of organics by permanganate preoxidation using tannic acid as a model compound—Role of in situ formed manganese dioxide. *Journal of Environmental Sciences* 21, 872-876.
- Zhang X, He J, Xiao S, Yang X (2019). Elimination kinetics and detoxification mechanisms of microcystin-LR during UV/Chlorine process. *Chemosphere* 214, 702-709.
- Zhang Z, Sarkar D, Datta R, Deng Y (2021). Adsorption of perfluorooctanoic acid (PFOA) and perfluorooctanesulfonic acid (PFOS) by aluminum-based drinking water treatment residuals. *Journal of Hazardous Materials Letters* 2, 100034
- Zhao C, Zhang J, He G, Wang T, Hou D, Luan Z (2013). Perfluorooctane sulfonate removal by nanofiltration membrane: the role of calcium ions. *Chemical Engineering Journal* 233, 224.

- Zhao L, Bian J, Zhang Y, Zhu L, Liu Z (2014). Comparison of the sorption behaviors and mechanisms of perfluorosulfonates and perfluorocarboxylic acids on three kinds of clay minerals. *Chemosphere* 114, 51-58.
- Zhou D, Brusseau ML, Zhang Y, Li S, Wei W, Sun H, Zheng C (2021a). Simulating PFAS adsorption kinetics, adsorption isotherms, and nonideal transport in saturated soil with tempered one-sided stable density (TOSD) based models. *Journal of Hazardous Materials* 411, 125169.
- Zhou XF, Liang JP, Zhao ZL, Yuan H, Qiao JJ, Xu QN, Wang HL, Wang WC, Yang DZ (2021b). Ultra-high synergetic intensity for humic acid removal by coupling bubble discharge with activated carbon. *Journal of Hazardous Materials* 403, 123626.
- Zhou Z, Liang Y, Shi Y, Xu L, Cai Y (2013). Occurrence and transport of perfluoroalkyl acids (PFAAs), including short-chain PFAAs in Tangxun Lake, China. *Environmental science and technology* 47, 9249-9257.
- Zushi Y, Hogarh JN, Masunaga S (2012). Progress and perspective of perfluorinated compound risk assessment and management in various countries and institutes. *Clean Technologies and Environmental Policy* 14, 9-20.